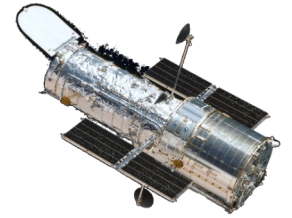


December 2023



Cosmic Origins Spectrograph Instrument Handbook for Cycle 32



STScI | SPACE TELESCOPE
SCIENCE INSTITUTE

3700 San Martin Drive
Baltimore, MD 21218
<https://hsthelp.stsci.edu>

COS Instrument Handbook	4
Acknowledgments	6
References and Additional Information	7
Chapter 1: An Introduction to COS	8
1.1 Overview	9
1.2 Observing with COS	10
1.3 COS Quick Reference Guide	12
1.4 COS FAQ	16
1.5 Purpose of this Handbook	17
Chapter 2: Proposal and Program Considerations	18
2.1 Choosing between COS and STIS	19
2.2 Essential questions for preparing COS observations	22
Chapter 3: Description and Performance of the COS Optics	24
3.1 The Optical Design of COS	25
3.2 Size of a Resolution Element	32
3.3 The COS Line-Spread Function	33
Chapter 4: Description and Performance of the COS Detectors	40
4.1 The FUV XDL Detector	41
4.2 The NUV MAMA Detector	52
Chapter 5: Spectroscopy with COS	57
5.1 The Capabilities of COS	58
5.1.13 COS Observations below 1150 Angstroms	78
5.2 TIME-TAG vs. ACCUM Mode	79
5.3 Valid Exposure Times	82
5.4 Estimating the BUFFER-TIME in TIME-TAG Mode	84
5.5 Spanning the Gap with Multiple CENWAVE Settings	89
5.6 FUV Single-Segment Observations	94
5.7 Internal Wavelength Calibration Exposures	95
5.8 Fixed-Pattern Noise	99
5.9 COS Spectroscopy of Extended Sources	107
5.10 Wavelength Settings and Ranges	109
5.11 Spectroscopy with Available-but-Unsupported Settings	110
5.12 FUV Detector Lifetime Positions	111
5.13 Spectroscopic Use of the Bright Object Aperture	116
Chapter 6: Imaging with COS	117
6.1 Introduction to COS Imaging	118
6.2 Sensitivity	121
6.3 Image Characteristics	123
Chapter 7: Exposure-Time Calculator - ETC	126
7.1 The COS Exposure Time Calculators	127
7.2 Imaging Observations of Red Objects	128
7.3 Sensitivity, Count Rate, and Signal-to-Noise	129
7.4 Detector and Sky Backgrounds	130
7.5 Extinction Correction	138
7.6 Examples	140
Chapter 8: Target Acquisitions	143
8.1 Introduction	144
8.2 Target Acquisition Overview	145
8.3 ACQ SEARCH Acquisition Mode	147
8.4 ACQ IMAGE Acquisition Mode	151
8.5 ACQ PEAKXD Acquisition Mode	153
8.6 ACQ PEAKD Acquisition Mode	156
8.7 Exposure Times	157

8.8 Centering Accuracy and Data Quality	160
8.9 Recommended Parameters for all COS TA Modes	162
8.10 Special Cases	164
Chapter 9: Scheduling Observations	166
9.1 Introduction	167
9.2 Generic Observatory Overheads	169
9.3 Spectral Element Movement Overheads	170
9.4 Acquisition Overheads	171
9.5 Science Exposure Overheads	172
9.6 First Exposure Overhead Adjustment	176
9.7 Examples of Orbit Estimates	177
9.8 Visit Length Considerations	189
Chapter 10: Bright-Object Protection	190
10.1 Introduction	191
10.2 Screening Limits	192
10.3 Source V Magnitude Limits	193
10.4 Tools for Bright-Object Screening	197
10.5 Policies and Procedures	199
10.6 On-Orbit Protection Procedures	201
10.7 Bright Object Protection for Solar System Observations	203
10.8 SNAP, TOO, and Unpredictable Sources Observations with COS	205
Chapter 11: Data Products and Data Reduction	206
11.1 Overview	207
11.2 COS Data Files	208
11.3 Additional COS Files	210
Chapter 12: The COS Calibration Program	211
12.1 Introduction	212
12.2 Ground Testing and Calibration	213
12.3 SMOV4 Testing and Calibration	214
12.4 COS Monitoring Programs	216
12.5 Cycle 17 Calibration Program	225
12.6 Cycle 18 Calibration Program	226
12.7 Cycle 19 Calibration Program	228
12.8 Cycle 20 Calibration Program	229
12.9 Cycle 21 Calibration Program	230
12.10 Cycle 22 Calibration Program	231
12.11 Cycle 23 Calibration Program	232
12.12 Cycle 24 Calibration Program	233
12.13 Cycle 25 Calibration Program	235
12.14 Cycle 26 Calibration Program	237
12.15 Cycle 27 Calibration Program	238
12.16 Cycle 28 Calibration Program	239
12.17 Cycle 29 Calibration Program	241
12.18 Cycle 30 Calibration Program	243
12.19 Cycle 31 Calibration Program	244
Chapter 13: COS Reference Material	245
13.1 Introduction	246
13.2 Using the Information in this Chapter	247
13.3 Gratings	252
FUV Grating G130M	253
FUV Grating G130M with CENWAVE=1222	258
FUV Grating G130M with CENWAVE=1055 or 1096	263
FUV Grating G160M	268

FUV Grating G140L	273
NUV Grating G185M	278
NUV Grating G225M	283
NUV Grating G285M	288
NUV Grating G230L	293
13.4 Spectrograph Design Parameters	298
13.5 The Location of COS in the HST Focal Plane	300
13.6 The COS User Coordinate System	302
Glossary	304

COS Instrument Handbook

Version 16 – December 2023

[PDF version](#)

Cosmic Origins Spectrograph Instrument Handbook for Cycle 32

User Support

Please contact the HST Help Desk for assistance. We encourage users to access the new web portal where you can submit your questions directly to the appropriate team of experts.

- Web portal: <http://hsthhelp.stsci.edu>
- E-mail: help@stsci.edu

Additional Resources

Information and other resources are available from the COS website:

- <http://www.stsci.edu/hst/instrumentation/cos>

Revision History

Version	Date	Editors
16.0	December 2023	Hirschauer, A. S.
15.0	February 2023	Soderblom, D. R.
14.0	January 2022	James, B. L.
13.0	January 2021	Hirschauer, A. S.
12.1	April 2020	Dashtamirova, D., and Fischer, W. J.
12.0	December 2019	Dashtamirova, D., and Fischer, W. J.
11.0	January 2019	Fischer, W. J.
10.0	May 2018	Fischer, W. J.
9.0	January 2017	Fox, A. J.
8.0	January 2016	Debes, J.
7.0	January 2015	Debes, J.
6.0	January 2014	Holland, S. T.

5.0	December 2012	Holland, S. T.
4.0	December 2011	Dixon, W. V.
3.0	December 2010	Dixon, W. V.
2.0	January 2010	Dixon, W. V., and Niemi, S.-M.
1.0	December 2007	Soderblom, D. R.

Citation

In publications, please refer to this document as:

- Hirschauer, A. S. et al. 2023, *Cosmic Origins Spectrograph Instrument Handbook, Version 16.0* (Baltimore: STScI)

Acknowledgments

The technical and operational information contained in this handbook is the summary of the experience gained by members of the STScl COS Team and by the COS IDT at the University of Colorado in Boulder.

Current and former members of the STScl COS Team include Alessandra Aloisi, Tom Ake, Michael Asfaw, John Bacinski, George Becker, Azalee Bostroem, Dzhuliya Dashtamirova, John Debes, Gisella de Rosa, Rossy Diaz, Serge Dieterich, Van Dixon, Tom Donaldson, Leonardo Dos Santos, Linda Dressel, Justin Ely, Travis Fischer, Will Fischer, Mees Fix, Andrew Fox, Elaine Frazer, David French, Scott Friedman, Parviz Ghavamian, Sierra Gomez, Paul Goudfroofij, George Hartig, Sten Hasselquist, Jaq Hernandez, Svea Hernandez, Alec Hirschauer, Phil Hodge, Stephen Holland, Nick Indriolo, Bethan James, Robert Jedrzejewski, Christian Johnson, Mary Beth Kaiser, Darshan Kakkad, Nat Kerman, Tony Keyes, Jerry Kriss, Nimisha Kumari, Claus Leitherer, Kevin Lindsay, Sean Lockwood, Chris Long, Melissa McGrath, Matt McMaster, Camellia Magness, Derck Massa, Lauren Miller, Sami Niemi, Cristina Oliveira, Rachel Osten, Anna Payne, Steven Penton, Rachel Plesha, Charles Proffitt, Marc Rafelski (lead), Julia Roman-Duval, Kate Rowlands, David Sahnou, Hugues Sana, Ravi Sankrit, Ken Sembach, Brittany Shaw, Ed Smith, David Soderblom, Paule Sonnentrucker, Joanna Taylor, Katya Verner, Nolan Walborn, Alan Welty, Thomas Wevers, Tom Wheeler, James White, Mike Wolfe, Brian York, and Wei Zheng. All of these individuals contributed to this volume, as did Russ Makidon.

The COS Investigation Definition Team (IDT) included James Green (Principal Investigator), Cynthia Froning (Project Scientist), Steven Penton, Steven Osterman (Instrument Scientist), Stéphane Béland, Eric Burgh, Charles Danforth, Kevin France, and Brian Keeney, all of whom provided information and assistance. COS co-investigators are Dennis Ebbets (Ball Aerospace), Sara R. Heap (GSFC), Claus Leitherer (STScl), Jeffrey Linsky (University of Colorado), Blair D. Savage (University of Wisconsin-Madison), Ken Sembach (STScl), J. Michael Shull (University of Colorado), Oswald Siegmund (University of California, Berkeley), Theodore P. Snow (University of Colorado), John Spencer and Alan Stern (Southwest Research Institute), and John T. Stocke (University of Colorado). K. Brownsberger, J. Morse, and E. Wilkinson have also been part of the COS IDT and have made significant contributions.

The prime contractor for COS was Ball Aerospace, Boulder, Colorado. The XDL detector was built at the University of California Berkeley by O. Siegmund, J. McPhate, J. Vallergera, and B. Welsh.

References and Additional Information

This document relies heavily on information provided by the COS team at the University of Colorado in Boulder. The primary documents used are:

Soderblom, D. R.. 2022, *COS Data Handbook* (v5.1);

Morse, J. 2004, *Cosmic Origins Spectrograph Science Operations Requirements* Document (referred to as OP-01);

Wilkinson, E. 2002, *COS Calibration Requirements and Procedures, rev. B.* (referred to as AV-03); and

Wilkinson, E. 2008, *COS Prelaunch Calibration Data* (referred to as AV-04).

We also used the *STIS Instrument Handbook* (J. Biretta et al. 2016, v15.0).

Chapter 1: An Introduction to COS

Chapter Contents

- [1.1 Overview](#)
- [1.2 Observing with COS](#)
- [1.3 COS Quick Reference Guide](#)
- [1.4 COS FAQ](#)
- [1.5 Purpose of this Handbook](#)

1.1 Overview

The Cosmic Origins Spectrograph (COS) was installed on the *Hubble Space Telescope* (HST) in May 2009. Working at far-ultraviolet wavelengths, COS was designed to study the origins of large-scale structure in the Universe, the formation and evolution of galaxies, the origin of stellar and planetary systems, and the cold interstellar medium. COS significantly enhances the spectroscopic capabilities of HST at ultraviolet wavelengths, and provides observers with unparalleled opportunities for observing faint sources of ultraviolet light.

COS offers two independent observing channels, a far-ultraviolet (FUV) detector, which is sensitive to wavelengths between 900 and 2150 Å, and a near-ultraviolet (NUV) detector for wavelengths from 1650 to 3200 Å. Both channels are equipped with medium-resolution ($R \sim 20,000$) and low-resolution ($R \sim 3000$) gratings. The NUV channel can also be used in imaging mode for both target acquisitions and scientific observations. There are two circular COS science apertures, each 2.5 arcsec in diameter: The clear primary science aperture (PSA) and attenuated bright object aperture (BOA).

In this chapter, we provide a brief overview of COS operations, tables of instrument and detector parameters, a list of frequently-asked questions, and a guide to using this handbook.

1.2 Observing with COS

- [1.2.1 Target Acquisitions](#)
- [1.2.2 Observing Modes: Spectroscopic and Imaging](#)
- [1.2.3 Observing Modes: TIME-TAG and ACCUM](#)
- [1.2.4 Typical Observing Sequences](#)

1.2.1 Target Acquisitions

The two COS entrance apertures are 2.5 arcsec in diameter. To ensure that the target is centered in the aperture, a target-acquisition procedure must be performed at the beginning of each visit (but not at the beginning of subsequent orbits within the visit).

The COS flight software provides two methods for acquiring and centering a target in the aperture. The first method obtains a direct image of the aperture with the NUV channel and moves the telescope to the center of light. The second method centers the target using its dispersed spectrum and can be performed with either the NUV or FUV channel. For both methods, the target's center of light can be computed from either a single exposure or from a series of exposures that map out a grid on the sky. Target acquisitions are described in [Chapter 8](#).

1.2.2 Observing Modes: Spectroscopic and Imaging

While COS was designed as a spectrograph, the NUV channel can also be used for imaging observations. The COS/NUV plate scale of 23.5 mas per pixel provides the highest spatial sampling of any instrument aboard HST. The image is corrected for the telescope's spherical aberration, but is degraded by zonal (polishing) errors on HST's primary and secondary mirrors (see [Chapter 3](#)). Because COS' detectors are photon-counting, there are limits to the brightness of sources for a given configuration. For the PSA, the NUV imaging count-rate screening limit of 50 counts per second per pixel ([Table 10.1](#)) corresponds to a *GALEX* NUV magnitude of 17.6.

1.2.3 Observing Modes: TIME-TAG and ACCUM

COS provides two observing modes, `TIME-TAG` and `ACCUM`. In `TIME-TAG` mode the position, arrival time, and (for the FUV channel) pulse height of each detected photon are recorded in the memory buffer. With regard to the accuracy of the arrival time, the HST spacecraft computer (HST486) clock has a precision of 125 milliseconds (1/8th second per tick). Our goal is to maintain the clock's accuracy compared to UTC to within 10 milliseconds. In `ACCUM` mode, only the locations of arriving photons are recorded.

`TIME-TAG` mode is preferred because it allows for more sophisticated data reduction. For example, an observer may compare data from the night and day sides of the orbit or compute the count rate of an object whose intensity varies on short time scales. `TIME-TAG` observations through the primary science aperture (PSA) allow the taking of occasional wavelength-calibration spectra during an exposure. These spectra are used by the COS data-reduction pipeline, [CalCOS](#), to correct drifts in the spectrum due to small motions of COS' Optics Select Mechanism (OSM). `ACCUM` mode is designed for observations of targets that are too bright for `TIME-TAG` mode. Because the lower information content of `ACCUM` data reduces their utility for archival researchers, its use must be justified for each target.

Both `TIME-TAG` and `ACCUM` modes may be used with either the FUV or NUV channel. For more information comparing `TIME-TAG` and `ACCUM` see [Section 5.2](#).

1.2.4 Typical Observing Sequences

In the majority of cases the following sequence of events will produce high-quality data:

- Acquire the object using `COS/NUV ACQ/IMAGE`. This typically takes about three minutes total time. See examples in [Chapter 9](#).
- Obtain spectra in `TIME-TAG` mode using the `FP-POS=ALL` setting and `FLASH=YES` so the spectra can be corrected for flat-field anomalies and OSM drifts. (For dual-segment spectroscopy at LP5 with cenwave 1291, `FP-POS=ALL` is not available) The [COS Exposure Time Calculator webpage](#) (ETC) provides a means of calculating essential parameters, such as the `BUFFER-TIME`.
- Obtain additional spectra during subsequent orbits to achieve the desired signal-to-noise ratio or wavelength coverage.

1.3 COS Quick Reference Guide

Table 1.1: COS Detector and Spectrograph Characteristics

Property	FUV XDL (A/B)	NUV MAMA
Photocathode	CsI (opaque)	Cs ₂ Te (semi-transparent)
Window	None	MgF ₂ (re-entrant)
Wavelength range	< 900-2150 Å	1650-3200 Å
Active area	85 × 10 mm (each for two segments)	25.6 × 25.6 mm
Pixel format (full detector)	16,384 × 1,024 (each for two segments)	1,024 × 1,024
Image size recorded per spectrum	16,384 × 128 (each for two segments, ACCUM) 16,384 × 1,024 (each for two segments, TIME-TAG)	1,024 × 1,024
Pixel size	6 × 24 μm	25 × 25 μm
Spectral resolution element size (= resel)	6 × 10 pix	3 × 3 pix
Detector quantum efficiency	~26% at 1335 Å ~12% at 1560 Å	~10% at 2200 Å ~8% at 2800 Å
Typical dark-count rate (away from South Atlantic Anomaly) ¹	1.38 counts s ⁻¹ cm ⁻² 1.99 × 10 ⁻⁶ counts s ⁻¹ pix ⁻¹ 1.19 × 10 ⁻⁴ counts s ⁻¹ resel ⁻¹	180.80 counts s ⁻¹ cm ⁻² 1.13 × 10 ⁻³ counts s ⁻¹ pix ⁻¹ 1.02 × 10 ⁻² counts s ⁻¹ resel ⁻¹
Detector Global Count rate limit ²	60,000 counts s ⁻¹	770,000 counts s ⁻¹
Local count-rate limit ^{2,3}	~1.67 counts s ⁻¹ pix ⁻¹ ~100 counts s ⁻¹ resel ⁻¹	~200 counts s ⁻¹ pix ⁻¹ ~1800 counts s ⁻¹ resel ⁻¹
Screening limits for bright objects	see Table 10.1	
Dead-time constant	7.4 μs	280 ns

Approximate detector plate scale ⁴ (dispersion axis)	G130M: 22.9 milliarcsec pixel ⁻¹ G160M: 24.3 milliarcsec pixel ⁻¹ G140L: 23.0 milliarcsec pixel ⁻¹	G185M: 24.3 milliarcsec pixel ⁻¹ G225M: 24.3 milliarcsec pixel ⁻¹ G285M: 24.3 milliarcsec pixel ⁻¹ G230L: 24.3 milliarcsec pixel ⁻¹
Approximate detector plate scale ⁴ (cross-dispersion axis)	G130M: 100 milliarcsec pixel ⁻¹ G160M: 90 milliarcsec pixel ⁻¹ G140L: 90 milliarcsec pixel ⁻¹	G185M: 23.8 milliarcsec pixel ⁻¹ G225M: 23.1 milliarcsec pixel ⁻¹ G285M: 24.4 milliarcsec pixel ⁻¹ G230L: 24.0 milliarcsec pixel ⁻¹

¹ The dark rate varies with time. The reported values are measured as of September 2020. FUVa and FUVb values differ slightly (see [Table 7.1](#)). See also [COS Dark Rate Monitoring](#) for updated values.

² Count rates higher than these limits will trigger a detector shut-down. Bright-object screening limits are lower. See [Chapter 10](#).

³ The FUV values are not applicable to the COS FUV G130M blue cenwaves, 1055 and 1096. The local count rate limit for these two modes is 0.2 counts s⁻¹ pix⁻¹.

⁴ Exact value of plate scale depends on grating and Lifetime Position.

Table 1.2: COS Calibration Accuracies

Property	FUV channel	NUV channel
Wavelength zero point: M gratings	15 km s ⁻¹	15 km s ⁻¹
Wavelength zero point: L gratings	150 km s ⁻¹	175 km s ⁻¹
Wavelength scale ¹	15 km s ⁻¹	15 km s ⁻¹
Absolute photometry ²	5%	5%
Relative photometry (same object at different times) ²	2%	2%

Flat field quality (spectral S/N) per resel, using standard techniques	35:1	100:1
Flat field quality (spectral S/N) per resel, using special techniques	100:1 ³	100:1

¹ With updated dispersion solutions, the wavelength scales for the FUV M gratings are now accurate to 7 km s⁻¹. See the [COS ISR 2018-22](#) for more details.

² Value for the NUV channel applies to spectroscopy, not imaging.

³ See [Section 5.8.1](#).

Table 1.3: Useful Figures and Tables

Topic	Source	Content
Usage planning	Table 5.1	Grating parameters
	Table 5.3	FUV grating wavelength ranges
	Table 5.4	NUV grating wavelength ranges
	Table 10.1	Count-rate screening limits
Aperture parameters and PSFs	Figure 3.2	BOA transmission
	Figure 3.6	Model LSFs for the COS FUV channel
	Figure 4.10	Model LSFs for the COS NUV channel
	Figure 3.7	Resolving Power of FUV gratings
	Figure 6.4	Cross section of the COS imaging PSF
	Figure 8.5	Relative transmission of the COS PSA in the NUV
	Figure 13.29	HST focal plane and COS aperture
Effective Area	Figure 5.1	FUV spectroscopy
	Figure 5.2	NUV spectroscopy
	Figure 6.3	NUV imaging
Acquisitions	Figure 8.1	Examples of spiral search patterns
	Figure 8.2	Point-source images with all apertures and mirrors
	Figure 8.3	ACQ/IMAGE exposure times
	Figure 8.4	Dispersed-light exposure times

Detector characteristics	Figure 4.1	FUV XDL detector schematic layout
	Figure 4.9	NUV MAMA detector layout
	Table 7.1	Detector background count rates
Overheads and observing parameters	Table 5.2	TAGFLASH exposure durations
	Table 9.1	Overhead estimates for Phase I proposals
	Table 9.2	Generic observatory overhead times
	Table 9.3	Overhead times for OSM1 movements
	Table 9.4	Overhead times for OSM2 movements
	Table 9.5	Science exposure overhead times
Celestial backgrounds	Figure 7.1	Sky background versus wavelength
	Figure 7.2	Moon, Earth and zodiacal-light background levels
	Figure 7.3	Galactic extinction model
	Table 7.3	Earthshine and zodiacal light fluxes
	Table 7.4	Strengths of airglow lines
Data quality	Figure 5.13	FUV flat-field example
	Figure 5.17	NUV flat-field example

1.4 COS FAQ

Table 1.5: COS Frequently Asked Questions

Question	Answer
Should I use COS or STIS? Does COS have an imaging mode?	Section 2.1 Chapter 6
What detectors are available? What apertures? What gratings? What are their properties?	Chapter 4 Section 3.1.2 Tables 5.1, 5.3, 5.4
What do COS images look like? What do COS spectra look like? Do the spectra have gaps?	Figure 6.1 Figures 4.3, 4.9 Section 5.5
What is the difference between ACCUM and TIME-TAG mode? How do I estimate the BUFFER-TIME for TIME-TAG exposures? How do I obtain wavelength-calibration exposures?	Section 5.2 Section 5.4 Section 5.7
What are the science impacts of the COS line-spread function? What is the COS sensitivity and resolution below 1150 Å? Which COS gratings suffer from second-order contamination?	Section 3.3 Figs. 5.3, 5.5; Sec. 5.1.4 Section 5.1.3
How accurate is COS absolute/relative photometry? How accurate are the COS wavelength scale and zero point?	Section 5.1.10 Section 5.1.11
How do I plan a successful target acquisition?	Chapter 8
What are the bright-object limits? How do I confirm that my target/field is safe to observe?	Table 10.1 Section 10.5
How much time should I request for my observations?	Chapter 9
What are the current COS FUV detector lifetime positions?	Section 5.12

1.5 Purpose of this Handbook

1.5.1 Document Conventions

This *COS Instrument Handbook* describes the design, performance, operation, and calibration of the Cosmic Origins Spectrograph. It is meant to be the principal reference manual for users of COS. This handbook is written and maintained at STScI. While it presents the best available information about COS at the time of the most recent update, tabulated parameters, such as dark rates or sensitivities, can evolve with time during a cycle.

The handbook is designed for readers who are:

- preparing a Phase I proposal to observe with HST,
- writing a Phase II program once a proposal has been accepted, or
- analyzing data from observations that have already been made.

This handbook is not meant to be the primary reference for COS data reduction or analysis. That information is provided in the *COS Data Handbook*. For quick reference, information on COS data products is provided in [Chapter 11](#).

1.5.1 Document Conventions

This document follows the usual STScI conventions:

- Terms, words, or phrases that are to be entered by the user in a literal way in an HST proposal are shown in a typewriter or Courier font, such as "COS/FUV" or "TIME-TAG."
- Names of software packages or commands (such as **CalCOS**) are shown in boldface.

Wavelengths in this handbook, and in COS data products, are always measured in vacuum and are quoted in Angstroms (Å).

Chapter 2: Proposal and Program Considerations

Chapter Contents

- [2.1 Choosing between COS and STIS](#)
- [2.2 Essential questions for preparing COS observations](#)

2.1 Choosing between COS and STIS

With the installation of COS and the repair of the Space Telescope Imaging Spectrograph (STIS), HST has two spectrographs with significant overlap in spectral range and resolving power. Each has unique capabilities, and the decision of which to use will be driven by the science goals of the program and the nature of the target to be observed.

In the far-UV (from about 1100 to 1800 Å), the throughput of the COS FUV channel exceeds that of the STIS FUV MAMA by factors of 10 to 30, and the combination of the spectroscopic resolving power (~17,000) and wavelength coverage (300 to 370 Å per setting) of the medium-resolution COS FUV modes, as well as the extremely low detector dark rate of the XDL detector, results in a discovery space (throughput times wavelength coverage) for observations of faint FUV point sources that is at least 10 times greater for most targets than that of STIS modes with comparable resolution, and as much as 70 times greater for faint, background-limited point sources.

Because of its MgF₂ windows, the STIS FUV MAMA is insensitive to wavelengths below about 1150 Å. The COS FUV XDL detector is windowless and provides useful throughput to at least 900 Å. See [Section 5.1.2](#) for details.

In the near-UV (~1700 to 3200 Å), COS and STIS have complementary capabilities. To accommodate the NUV detector format the COS NUV spectrum is split into three non-contiguous stripes, each of which covers a relatively small range in wavelength. Obtaining a full NUV spectrum of an object requires several set-ups and exposures (six or more for the medium-resolution gratings and three for G230L grating). When broad NUV wavelength coverage is needed obtaining a single STIS spectrum will often be more efficient than taking separate COS spectra. Users should note that for the shorter NUV wavelengths COS modes often have a substantial throughput advantage over the comparable STIS modes, while at the longer NUV wavelengths it can be STIS that has the advantage. They should also consider that the STIS NUV modes have produced a large set of existing observations, while the COS NUV modes have so far seen limited use. As a result, the calibration of the STIS NUV modes is likely to be superior to that of comparable COS modes for the foreseeable future.

After installation into HST in 2009, the dark rate of the COS NUV detector had initially been substantially lower than that of STIS NUV detector. However, the dark rates for the two detectors have converged over the years. Observers are advised to perform detailed calculations using both the COS and STIS ETCs and to consider carefully the relative instrument overheads to determine which combination of instruments and modes is best for their science.

For observations of extended sources, the spatial resolution offered by STIS must be weighed against the superior sensitivity of COS. One of the primary design goals of STIS was to provide spatially resolved spectra in the UV, optical, and near-IR. The STIS long slits, when used with the first-order gratings, allow spatially resolved observations that exploit the intrinsically high resolution of HST over the full width of the detectors (approximately 0.05 arcsec per 2-pixel spatial resolution element over a length of 25 arcsec with the NUV and FUV MAMAs, and approximately 0.1 arcsec per 2-pixel spatial-resolution element over a length of 52 arcsec with the CCD).

COS was optimized for point-source observations. While COS has relatively large entrance apertures (2.5 arcsec diameter), flux from regions more than 0.4 arcsec from the aperture center is significantly vignetted. These large apertures also mean that objects extended in the dispersion direction will yield spectra with lower spectral resolution. In addition, the optical design of the FUV channel limits the achievable spatial resolution; measured values of the FWHM in the spatial dimension vary between about 0.25 and 1.5 arcsec, depending on grating and wavelength ([Section 5.1.9](#)). The COS NUV channel uses a different optical design and has a spatial resolution comparable to that of the STIS first-order NUV modes (~ 0.05 arcsec), with somewhat better sampling. However, for sources extending more than 1 arcsec in the spatial direction, the various NUV spectral segments will begin to overlap.

The line-spread functions (LSFs) of both instruments exhibit non-Gaussian wings due to mid-frequency zonal (polishing) errors in the Optical Telescope Assembly (OTA). Using STIS, one can minimize their effects through the use of narrow apertures. Narrow apertures are not available on COS. The broad wings of the LSF, especially in the short wavelengths of the FUV band, can limit the ability of COS to resolve faint, narrow features, and blend closely-spaced lines. Studies that require accurate knowledge of the line profile will require full consideration of the COS LSF ([Section 3.3](#)). The non-Gaussian wings of the COS LSF should have only modest impact on science programs targeting broad lines and continuum sources.

Both COS detectors and the STIS MAMA detectors are prohibited from observing objects that exceed specific brightness levels (see [Chapter 10](#) in this handbook and [Sections 13.8](#) and [14.8](#) of the *STIS Instrument Handbook*). Some brightness limits have been established for the health and safety of the instrument, while others are practical limits that are set to ensure good data quality. Because STIS is less sensitive than COS, the brightness limits for STIS tend to be significantly less stringent. In the NUV range, the STIS G230LB and G230MB gratings can also be used with the STIS CCD, which has no bright-object limitations. STIS also has a number of small and neutral-density apertures that can be used with the MAMA detectors to attenuate the light of a too-bright object. COS has only a single neutral-density filter that attenuates by a factor of about 200, but also degrades the spectral resolution by a factor of 3 to 5. In most cases some combination of STIS gratings and apertures will be a better choice for observing a UV-bright object than COS with its neutral-density filter. Users are advised to compare results from the COS and STIS ETCs when deciding on an appropriate strategy for their target.

The STIS high-dispersion echelle modes E140H and E230H have resolving powers of $\sim 114,000$ (or even $R \sim 200,000$ with the 0.1×0.03 aperture and specialized data reduction; see [Section 12.6](#), "Improving the Sampling of the Line Spread Function," of the *STIS Instrument Handbook*), significantly higher than the best COS resolution. Also, STIS can obtain spectra in the optical and near-IR at wavelengths up to $10,200 \text{ \AA}$, while the maximum wavelength observable by COS is about 3200 \AA .

Both STIS and COS can perform observations in *TIME-TAG* mode, whereby the time of each photon's arrival is recorded. STIS is capable of a much finer time resolution ($125 \mu\text{s}$ vs. 32 ms for COS), although few programs require such a high sampling rate. Due to its lower sensitivity, STIS may be able to observe a target in *TIME-TAG* mode that is too bright for *TIME-TAG* observations with COS. On the other hand, *TIME-TAG* data acquired with the COS FUV detector includes information on the pulse-height distribution, while *TIME-TAG* data acquired with the STIS and COS MAMAs do not. Pulse-height information can be valuable in identifying and rejecting background counts in the spectra of faint sources.

Lifetime Impact Considerations

The COS bright-object safety screening limits ([Section 10.2](#)) for the FUV were chosen to protect the detector over short time periods. However, very UV bright sources or emission lines can still deplete a significant percentage of lifetime for a given detector Lifetime Position (LP) without violating the screening limits. Approximately 27,000 counts can fall on a pixel before the reduced gain at that location results in significant flux loss. Historically, the brightest COS observations of continuum sources placed as much as $0.1 \text{ counts sec}^{-1} \text{ pixel}^{-1}$ across FUVA or FUVB for $>10,000 \text{ sec}$. In such rare cases, the integrated counts on the detector consumed as much as 5% of the total available lifetime at these regions. Exhausting the gain at a particular lifetime position in an accelerated fashion is inconsistent with the goal of retaining the functionality of the COS FUV detector for as long as the lifetime of Hubble, and we therefore provide guidance on observations that may be better suited for observations with STIS than COS.

Of primary concern are sources that have a significant continuum over one or both segments with a high enough count rate to negatively impact the lifetime at a particular position when observed for a long duration. This is most likely to be the case for observations of nearby hot stars that last for one orbit or more. Additionally, some emission lines that are as bright or brighter than geocoronal Lyman alpha could potentially cause localized gain holes. More quantitatively, FUV observations where the estimated total counts in the brightest pixel exceed 1% of a pixel's lifetime, or 270 counts in a given pixel, may be more suitable for STIS if the science can be accomplished in that way within a reasonable observing time. For a source where the continuum is responsible for the brightest flux on a pixel, this threshold refers to the total exposure time on a target per grating, irrespective of the number of FP-POS used. For a source dominated by an emission line, the threshold refers to the total exposure time per FP-POS, since the emission line will fall on different parts of the detector with each FP-POS.

The procedure for determining whether an observation could exceed the above threshold is to perform an ETC calculation for the science target and make note of the brightest pixel for each segment. That count rate should be multiplied by the total exposure time per visit if the brightest pixel is on the continuum, or the exposure time per FP-POS per visit if the brightest pixel is an emission line. Finally, multiply the count rate by the number of visits used for the science target to get the total counts for that pixel. For Segment B of G130M/1291 and Segment A of G140L/800 or G140L/1105, the brightest pixel could be geocoronal Lyman alpha. In these cases, users can estimate the brightest pixel due to the target by selecting the "No airglow" option in Question 5c of the ETC. If the resulting calculations shows the possibility of exceeding 270 counts in a given pixel and the science can be accomplished with STIS, it is highly recommended that PI's consider moving to an equivalent mode of STIS (i.e., E140M in place of G130M). COS contact scientists (CSs) will perform similar checks while reviewing Phase II proposals, and reach out to PIs if lifetime impact concerns are identified.

2.2 Essential questions for preparing COS observations

Each of HST's science instruments has its own unique qualities, and COS particularly does for reasons closely related to its design. Here are the key factors that the COS team looks at when reviewing accepted programs to ensure science goals are achieved, enhancing the archival value of the observations, and extending the useful lifetime of COS.

Is COS well-suited to the stated science goals?

Considerations include:

- Signal-to-noise: COS is limited to a maximum S/N of 40-50 ([Section 5.8](#)) due to fixed-pattern noise, so STIS would be better in some cases.
- Target brightness: STIS is better suited to very bright targets, but COS does include some features such as the Bright Object Aperture ([Section 3.1](#)).
- Wavelength coverage and resolution needed: see [Section 5.1.2](#). COS is unique in being able to record spectra below 1150 Å.
- Preferring STIS when it is adequate: this is done to conserve COS' unique capabilities as long as possible.
- Extended sources: COS' small 2.5-arcsec apertures can limit total flux, and STIS includes long slit apertures.

How good are the relevant available target data?

Accurately estimating source brightness and variability are critical for assessing the safety of observations and for calculating the BUFFER-TIME for TIME-TAG observations. For example, many sources have existing ultraviolet data in the Hubble Legacy Archive.

Good-quality astrometry also helps to ensure a good acquisition and to determine ORIENT ranges if a bright, nearby source must be kept out of COS' apertures.

Is the acquisition strategy optimal?

A specific acquisition exposure is almost always required. To get reliable flux and wavelength calibrations an ACQ exposure is needed to center the source in COS' small (2.5 arcsec) apertures. There are several ways to acquire a target (see [Chapter 8: Target Acquisitions](#)).

Is the exposure safe for COS? (Ch. 10)

Most acquisitions are done in the NUV in imaging mode, for efficiency reasons. This concentration of the source's light can risk the very sensitive photon-counting detectors on COS. Spectroscopy can also raise brightness concerns. In either case, the COS Exposure Time Calculator (see [Chapter 7](#)) will warn of potential over-bright conditions, and these need to be addressed. As noted, observers should provide information on the quality of the data used to estimate count rates, including sources of information, and estimates of (potential) variability.

COS can be used to observe objects with brightnesses that are not easily predicted, but only under carefully controlled circumstances (see [Chapter 10](#)).

Do the observations use TIME-TAG when possible, and not ACCUM?

Nearly all COS exposures are taken in TIME-TAG mode, as that leads to better data quality and flexibility. ACCUM mode may be used for objects too bright for TIME-TAG, but in those cases STIS may be a better choice (see [5.2 TIME-TAG vs. ACCUM Mode](#)).

Is the BUFFER-TIME calculated properly?

In TIME-TAG mode, individual photon detections are recorded in a buffer of finite capacity. Calculating the time in which the buffer will fill is important to avoid losing data while minimizing buffer read times. Reliable estimates of count rates help ensure BUFFER-TIME is calculated accurately (see [5.4 Estimating the BUFFER-TIME in TIME-TAG Mode](#)).

Are the chosen FP-POS positions correct and reasonable?

In the FUV, the inherent nature of the COS detectors limits the top S/N to ~40-50. A key factor is fixed pattern noise (see [section 5.8 Fixed-Pattern Noise](#)), and so to improve data quality observers are ordinarily required to use all the FP-POS positions available for a given grating+wavelength setting. Deviations must be justified.

Are scheduling factors taken into account?

Some visits are more easily scheduled than others. Use of the ORIENT Special Requirement constrains when visits can occur, even if sometimes ORIENT must be used to avoid having a nearby bright star fall in a COS aperture (See [Target Orientation Visit-Level Special Requirements in the Phase II Proposal Instructions](#)).

The length of a visit matters, with short 1- and 2- orbit visits especially easy to schedule, and 4-orbit visits particularly difficult (see [Section 5.2 TIME-TAG vs. ACCUM Mode](#)).

Is it advantageous to use a non-default Lifetime Position?

Other factors may need to be considered in constructing a program. The overall useful life of COS is being extended by commissioning new Lifetime Positions (LPs; see [5.12 FUV Detector Lifetime Positions](#)) as older ones get depleted. Each grating+wavelength setting has a default LP, but in some circumstances it may be advantageous to use a different LP.

All of these topics are discussed in depth in the referenced sections of this Handbook.

Chapter 3: Description and Performance of the COS Optics

Chapter Contents

- [3.1 The Optical Design of COS](#)
- [3.2 Size of a Resolution Element](#)
- [3.3 The COS Line-Spread Function](#)

3.1 The Optical Design of COS

[3.1.1 External Shutter](#)

[3.1.2 The Apertures and Aperture Mechanism](#)

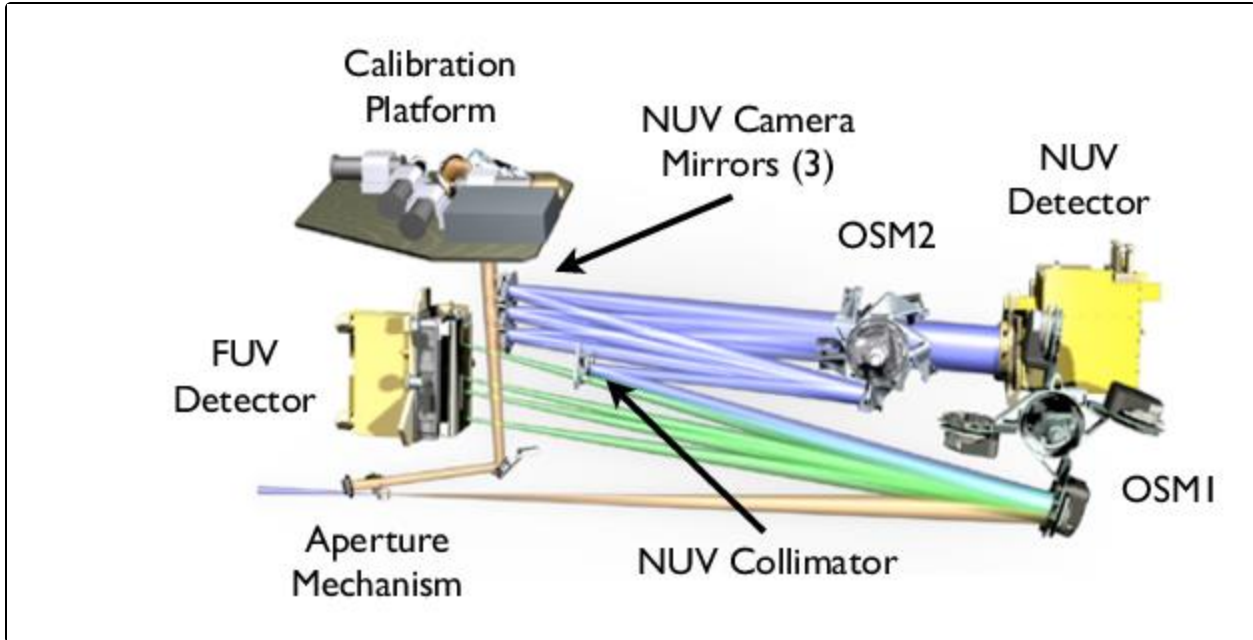
[3.1.3 Gratings and Mirrors: The Optics Select Mechanisms](#)

In most spectrographs the light from the telescope is focused onto a slit, which is then re-imaged onto the detector. In such a design the slit width and the way that the slit is illuminated determine the resolving power and Line Spread Function (LSF). COS is different. It is essentially a slitless spectrograph with an extremely small field of view. In this section we follow the light from the HST Optical Telescope Assembly (OTA) as it progresses through COS to each optical element and mechanism. The optical path and mechanism locations are shown in [Figure 3.1](#).

3.1.1 External Shutter

The external shutter is located at the front of the COS enclosure. When closed the shutter blocks all external light from entering the COS instrument and prevents light from the COS internal lamps from exiting the instrument. The opening and closing of the external shutter does not define the duration of an exposure, as the shutter may be opened before an exposure begins to allow for target acquisition and bright-object checking.

Figure 3.1: The COS Optical Path and the Locations of the Mechanisms.



The optical path is drawn to scale, with all elements in proportion and in their correct relative locations.

3.1.2 The Apertures and Aperture Mechanism

After passing through the external shutter, the light from the OTA first encounters one of the COS entrance apertures (Table 3.1), which are mounted on the Aperture Mechanism (ApM). Selecting an aperture can involve movement of the Aperture Mechanism.

Primary Science Aperture

The Primary Science Aperture (PSA) is a circular field stop 2.5 arcsec (700 μm) in diameter. It is located, not at the HST focal surface, but near the point of the circle of least confusion. The aperture transmits $\geq 95\%$ of the light from a well-centered, aberrated point-source image delivered by the HST optics. The PSA is used for almost all COS science observations. It is in place, ready to use, at the start of a new visit. Note that, when the PSA is in place, the Wavelength Calibration Aperture (WCA; see below) is also in place and available to acquire simultaneous wavelength-calibration spectra. External light entering the PSA and internal light entering the WCA are dispersed by the same grating. Thus, for a given grating and central-wavelength setting, no additional motion of the Aperture Mechanism is required to obtain a wavelength-calibration exposure.

Table 3.1: COS Entrance Apertures.

Aperture	Full Name	Purpose	Size (mm)
PSA	Primary Science Aperture	science aperture	0.700 diameter
BOA	Bright Object Aperture	science aperture with ND2 filter	0.700 diameter
WCA	Wavelength Calibration Aperture	wavecals with Pt-Ne lamp	0.020 \times 0.100

FCA	Flat-Field Calibration Aperture	Flat field with deuterium lamp	0.750 × 1.750
-----	---------------------------------	--------------------------------	---------------

Wavelength Calibration Aperture

The Wavelength Calibration Aperture (WCA) is offset from the PSA by 2.5 mm (about 9 arcsec) in the cross-dispersion direction. The WCA is illuminated by one of two Pt-Ne wavelength-calibration (wavecal) lamps. It does not receive light from external sources. The wavecal spectrum is used by the COS pipeline to assign wavelengths to the science spectra obtained through either the PSA or BOA. During target acquisitions light from the Pt-Ne lamps provides a reference from which the location of the target aperture is determined.

Bright Object Aperture

Like the PSA, the Bright Object Aperture (BOA) is 2.5 arcsec (700 μm) in diameter, but it incorporates a neutral-density (ND2) filter. The transmission of the ND2 filter varies with wavelength (Figure 3.2), but is roughly 0.6%. The BOA is offset from the PSA by 3.7 mm (about 13 arcsec) in the cross-dispersion direction opposite the WCA. For scientific observations the aperture block is shifted, via movement of the Aperture Mechanism, to place the BOA in the position normally occupied by the PSA. Thus, spectra obtained through either the PSA or BOA use the same optical path and detector region (for a given channel), and so may employ the same fixed pattern calibrations. *Moving the BOA into place for scientific use shifts the WCA as well, precluding simultaneous use of the WCA for a wavecal exposure.* Before or after an observation through the BOA the Aperture Mechanism must be moved to properly position the WCA, so that a wavecal exposure may be obtained. Currently, the BOA has not been calibrated to the same accuracy as other modes and is an available-but-unsupported option.

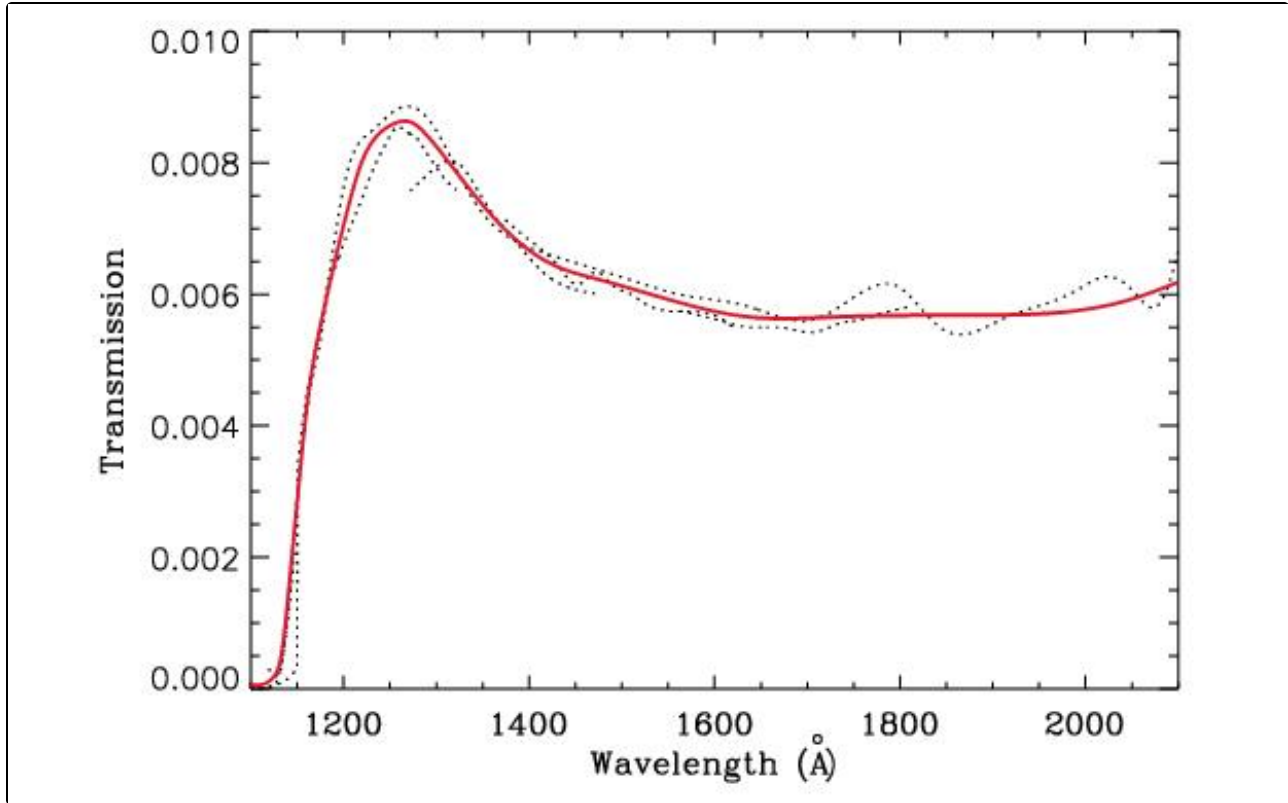
Flat-Field Calibration Aperture

The Flat-Field Calibration Aperture (FCA) is used to obtain flat-field exposures using one of the two deuterium hollow-cathode flat-field calibration lamps. The FCA is used only for calibration and is not available to general observers.

3.1.3 Gratings and Mirrors: The Optics Select Mechanisms

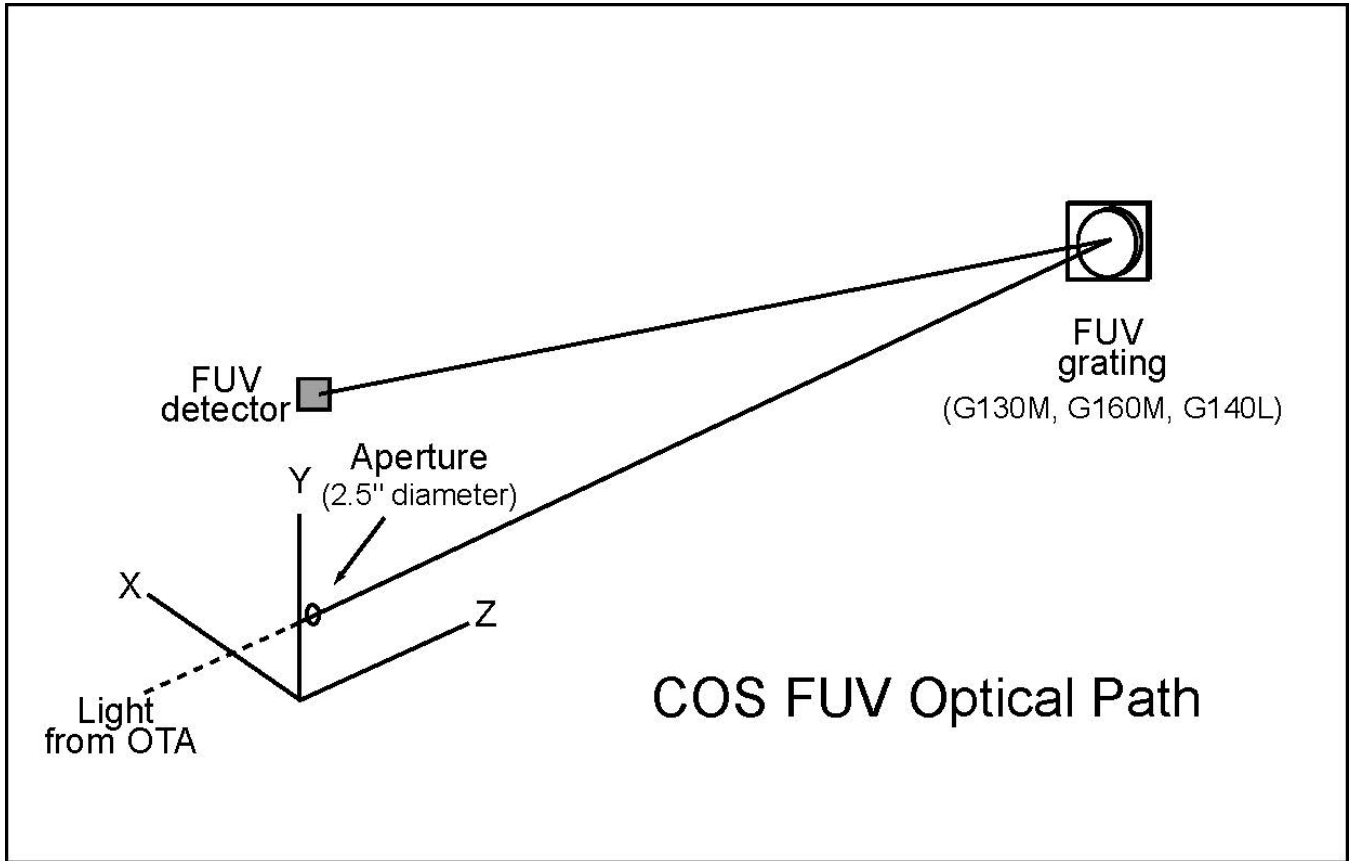
After passing through one of the COS apertures light next encounters the Optics Select Mechanism 1 (OSM1), a rotating mechanism that can bring one of four optical elements into the beam. One of these, NUV Collimating Mirror 1 (NCM1), is a flat mirror that directs the beam to the NUV channel. The other three elements are the G130M, G160M, and G140L gratings for the FUV channel. As a consequence of this design the FUV and NUV channels cannot be used simultaneously.

Figure 3.2: Transmission of the COS BOA as a Function of Wavelength.



Ratio of BOA sensitivity curves derived from observations of GD71 to PSA sensitivity curves derived from observations of LDS749b (dashed curves). The thick red curve is a spline fit to the dashed curves, giving a uniform BOA transmission curve as a function of wavelength.

Figure 3.3: The COS FUV Optical Path.



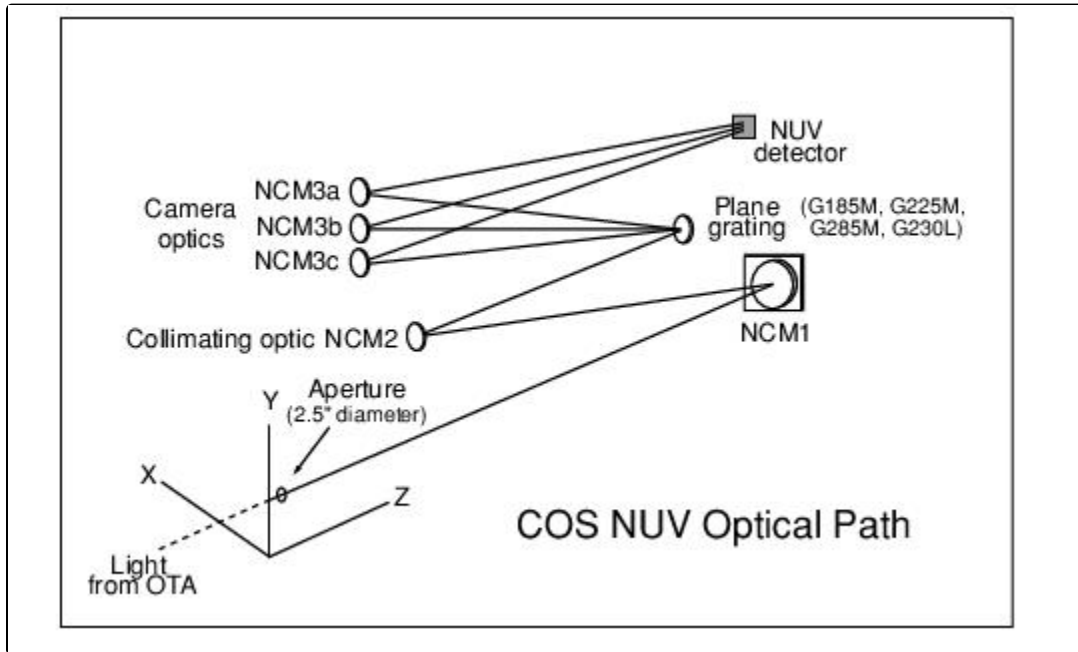
The optical path is drawn to scale, with all elements in proportion and in their correct relative locations.

FUV Channel Optical Design

The COS FUV optical path is illustrated schematically in [Figure 3.3](#). To maximize throughput a single FUV grating is used to disperse the light, remove the spherical aberration introduced by the HST primary mirror, and focus the beam onto the detector. Because the FUV gratings introduce astigmatism in the direction perpendicular to dispersion, the height of the spectrum varies with wavelength ([Section 5.1.9](#)). Given the location of OSM1 in the HST optical path it is possible for the FUV gratings to disperse, focus, and correct the beam optimally only for a point source that is centered in the aperture. Performance is degraded when the source is moved away from the aperture center. Fortunately, this degradation is low for displacements up to about 0.4 arcsec ([Section 8.8](#)).

The COS FUV channel provides spectra from 900 to 2150 Å at low and moderate spectral resolution ([Section 5.1](#)). The FUV detector is described fully in [Chapter 4](#), but it is important to note that it consists of two independent detector segments with a small physical gap between them. Light falling into the gap is not recorded. Though the gap prevents a continuous spectrum from being obtained at a single central-wavelength setting, the missing wavelengths can be recovered by obtaining additional exposures at other central-wavelength settings (corresponding to small rotations of the OSM1 mechanism; see [Section 5.5](#)).

Figure 3.4: The COS NUV Optical Path for Spectroscopic Observations.



OSM2 and the NUV Channel

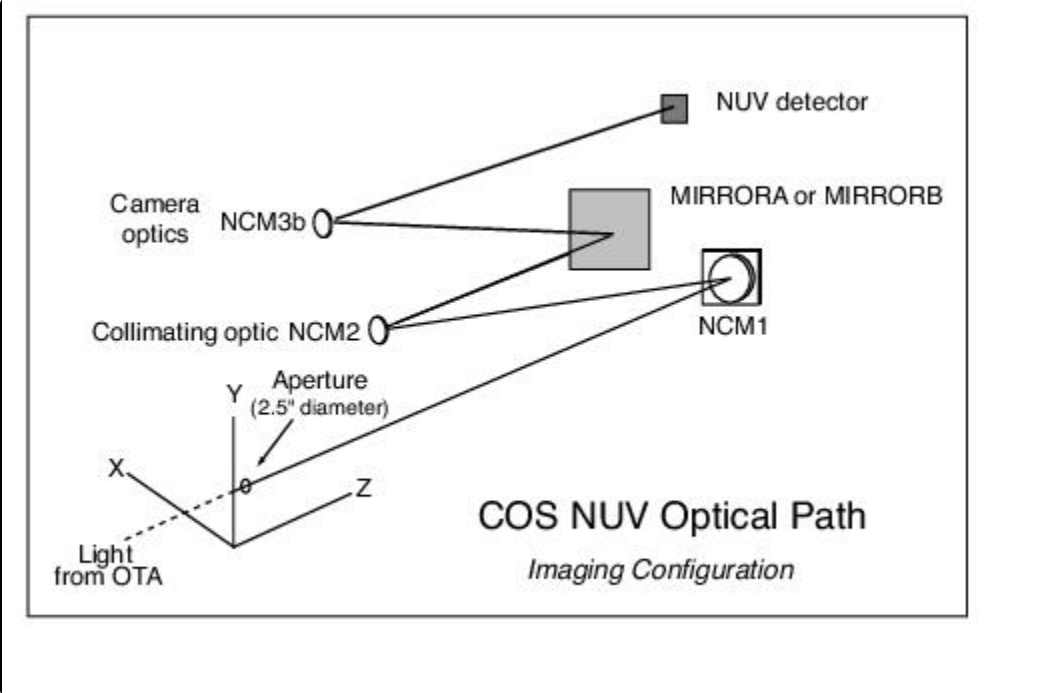
The COS NUV channel, illustrated schematically in [Figure 3.4](#), provides coverage from about 1650 to 3200 Å at low and moderate spectral resolution. If the NUV channel is to be used OSM1 is turned to place mirror NCM1 in the beam. NCM1 corrects the beam for the spherical aberration of HST, magnifies it by a factor of four, and directs it to the NUV Collimating Mirror 2 (NCM2). The NCM2 collimates the light and directs it to Optics Select Mechanism 2 (OSM2). OSM2 holds five optical elements: the four NUV diffraction gratings (G185M, G225M, G285M, and G230L), and a mirror for target acquisitions or imaging.

To accommodate the NUV detector format, dispersed light from the NUV gratings is imaged onto the detector by three parallel mirrors (NCM3a, 3b, 3c). For the medium-dispersion gratings the spectra appear as three non-contiguous 35–40 Å stripes on the MAMA detector, providing 105–120 Å wavelength coverage per exposure. The low-dispersion grating provides ~400 Å per stripe. The layout of the stripes is shown in [Figure 4.9](#). The gratings can be shifted via slight rotations of OSM2 to cover the entire NUV wavelength band. The NCM3 mirrors are spaced such that several correctly-chosen exposures will produce a complete spectrum, from the low end of the short-wavelength stripe to the high end of the long-wavelength stripe.

Imaging with the NUV Mirror

For imaging observations OSM2 is turned to place a mirror (TA1) in the light path instead of a grating ([Figure 3.5](#)). When used in direct specular reflection this mirror is designated as MIRRORA. For bright targets, the flux can be attenuated by adjusting OSM2 so that the order-sorting filter in front of the mirror reflects the light onto the detector. This configuration is referred to as MIRRORB. COS imaging is described in [Chapter 6](#).

Figure 3.5: COS NUV Optical Path for Imaging Observations.



3.2 Size of a Resolution Element

Throughout this document, we assume that a resolution element (resel) spans 6×10 pixels on the FUV detector (in the dispersion and cross-dispersion directions, respectively) and 3×3 pixels on the NUV detector ([Table 1.1](#)). These values were determined before launch. Even then, it was known that the true size of a resel would vary with wavelength. In-flight data suggests that the FUV resel is somewhat larger than previously assumed (see the discussion of the line-spread function in [Section 3.3](#)), while the NUV resel is smaller. For the G130M 1055 Å and 1096 Å settings the resel is between 8 and 32 pixels. For the 1222 Å setting it is 7–13 pixels. We will continue to refine our analysis of the instrument parameters. In the mean time, keep in mind that, for the FUV, the [COS Exposure Time Calculator](#) (ETC) uses a 6-pixel resel size (dispersion) in most of its calculations in the FUV. It uses resel sizes of 8, 9, and 6 for the G130M/1055 and G130M/1096 blue modes, and G130M/1222 respectively. Users who adopt a larger or smaller resel should adjust the [ETC](#) results accordingly.

3.3 The COS Line-Spread Function

- [3.3.1 Non-Gaussianity of the COS LSF](#)
- [3.3.2 Quantifying the Resolution](#)
- [3.3.3 Impact on Equivalent Width Measurements](#)
- [3.3.4 Extended Wings of the COS LSF](#)
- [3.3.5 Enclosed Energy of COS LSF](#)

The COS optics correct for the spherical aberration of the HST primary mirror, but not for the mid-frequency wavefront errors (MFWFEs) due to zonal (polishing) irregularities in the HST primary and secondary mirrors. As a result, the COS spectroscopic line-spread function (LSF) has extended wings and a core that is slightly broader and shallower than a Gaussian. The extended wings of its LSF limit the ability of COS to detect faint, narrow spectral features. The effect is greater at short wavelengths, and it may have consequences for some COS FUV science. The most severely impacted programs are likely to be those that:

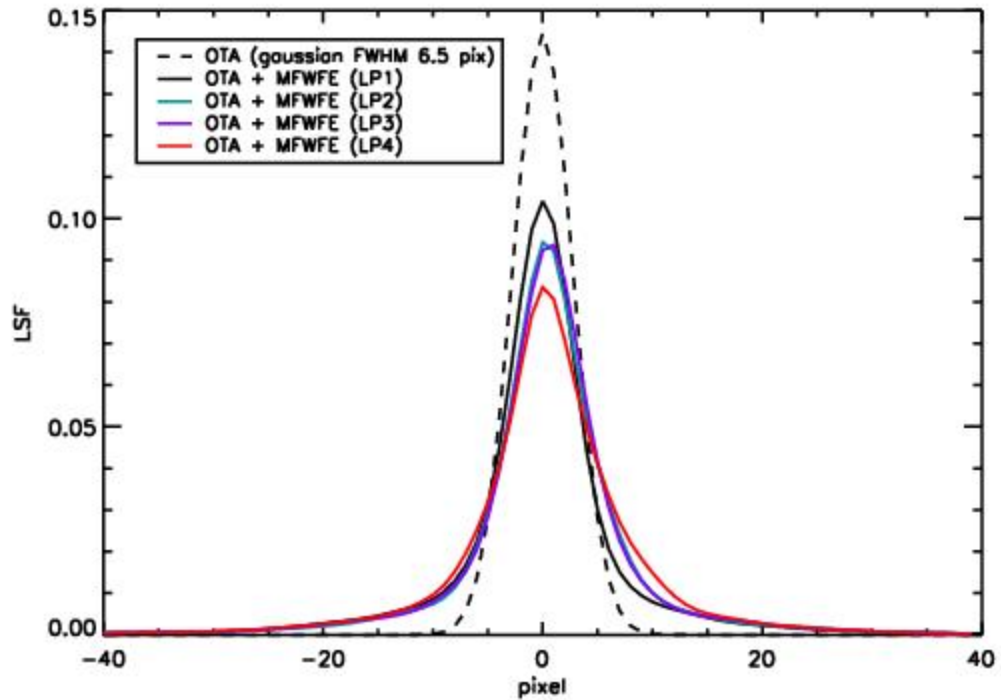
- rely on models of the shapes of narrow lines,
- search for very weak lines,
- aim to measure line strengths in complex spectra with overlapping, or nearly overlapping, lines, or
- require precise estimates of residual intensity in very strong or saturated lines.

Modeled line spread functions and cross-dispersion spread functions are available for all cenwaves and LPs at <https://www.stsci.edu/hst/instrumentation/cos/performance/spectral-resolution>.

3.3.1 Non-Gaussianity of the COS LSF

Initial results from an analysis of the on-orbit COS LSF at the original lifetime position are reported by Ghavamian et al. (2009) in [COS ISR 2009-01](#). They find that model LSFs incorporating HST MFWFEs are required to reproduce the absorption features observed in stellar spectra obtained with COS. [Figure 3.6](#) shows model LSFs computed for grating G130M at 1309 Å. The dashed line represents a model incorporating the spherical aberration of the HST OTA. It is well-fit by a Gaussian with FWHM = 6.5 pixels. The solid black line represents a model that includes the MFWFEs at the original lifetime position, while the solid colored lines represent models that include the MFWFEs at subsequent lifetime positions. The model at the original lifetime position has a FWHM of 7.9 pixels, slightly larger than that of the dashed curve, and broad non-Gaussian wings. The models at subsequent lifetime positions have similar FWHM. The non-Gaussian wings can hinder the detection of closely-spaced narrow spectral features. Model LSFs for all of the COS gratings at the original and subsequent lifetime positions are available on the [COS website](#).

Figure 3.6: Model Line-Spread Functions for the COS FUV Channel.



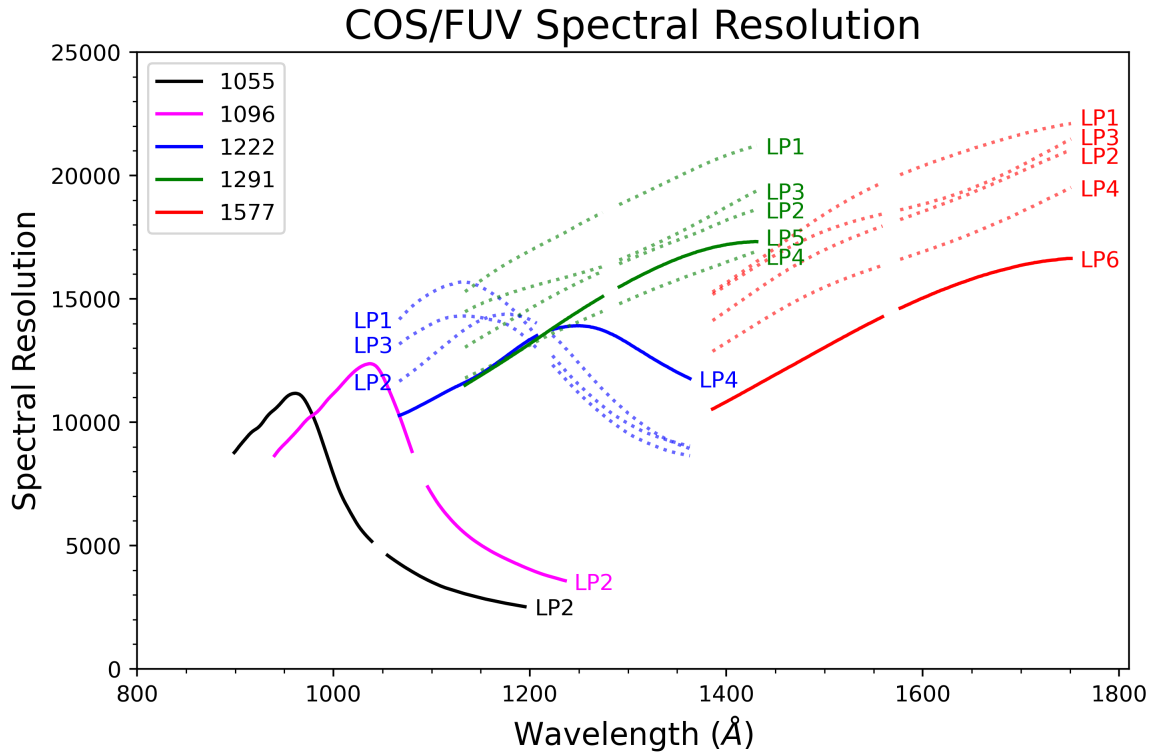
Model LSFs for G130M at 1309 Å normalized to a sum of unity. The dashed line represents a model LSF that incorporates the spherical aberration of the OTA. It is well fit by a Gaussian with FWHM = 6.5 pixels. The solid black line represents a model that also includes the HST mid-frequency wavefront errors at the original lifetime position. The solid colored lines represent models that include the HST mid-frequency wavefront errors at subsequent lifetime positions. These LSFs show a larger FWHM and broad non-Gaussian wings.

3.3.2 Quantifying the Resolution

When a substantial fraction of the power in an LSF is transferred to its extended wings traditional measures of resolution, such as the FWHM of the line core, can be misleading. For example, an observer assuming that the resolving power $R = 16,000$ at 1200 Å quoted for the G130M grating represents the FWHM of a Gaussian would mistakenly conclude that COS can resolve two closely-spaced narrow absorption features, when in fact it may not be able to. Nevertheless, the FWHM is a convenient measure, and we use it to describe the COS gratings in tables throughout this handbook. When using these tables keep in mind that the quoted resolving power R is computed from the empirically determined FWHM of the line core, and careful modeling may be needed to determine the feasibility of a particular observation or to analyze its result.

Figure 3.7 shows the resolving power of selected cenwaves.

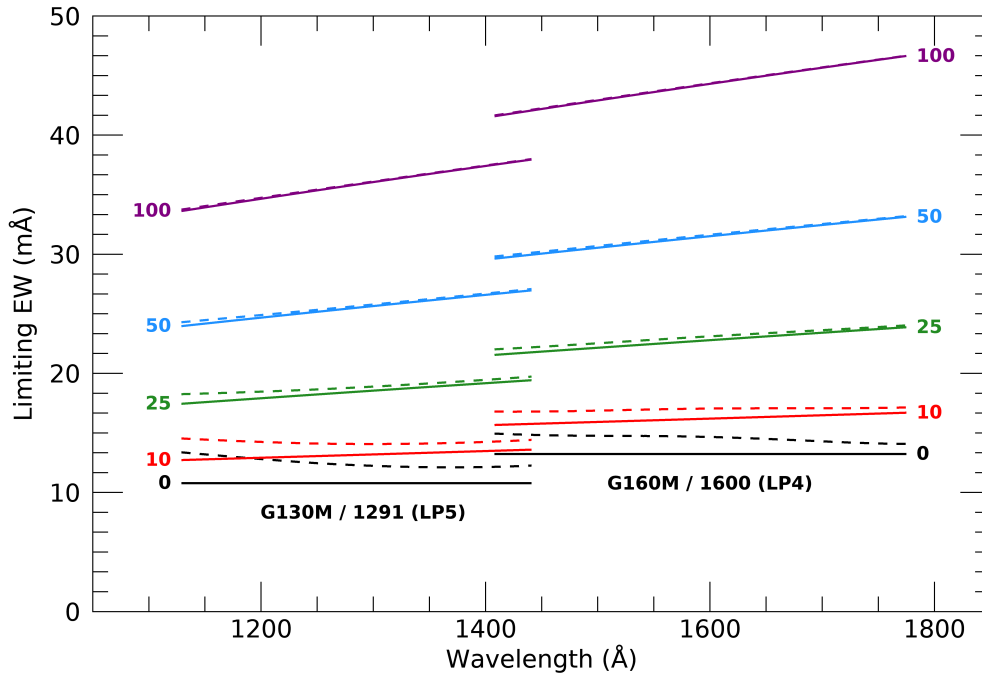
Figure 3.7: Resolving Power of FUV Gratings at select cenwaves, and for all Lifetime Positions (LPs). Solid lines show the current default LP for each cenwave.



3.3.3 Impact on Equivalent Width Measurements

The broad core and extended wings of the COS LSF increase the limiting equivalent width for absorption features in COS spectra. Figure 3.8 shows the limiting equivalent widths as a function of wavelength for a 3σ FUV detection of absorption features at $S/N = 10$ per pixel at lifetime position 4. A series of Gaussian spectral features with nominal Doppler parameters of $b = 0, 10, 25, 50,$ and 100 km/s have been convolved with both a Gaussian instrumental LSF and the modeled on-orbit COS LSF for the G130M and G160M gratings. The results are similar for the NUV gratings, although the effect of the MFWFEs is more moderate for the long-wavelength G285M grating.

Figure 3.8: Limiting Equivalent Width of FUV Medium-Resolution Gratings.

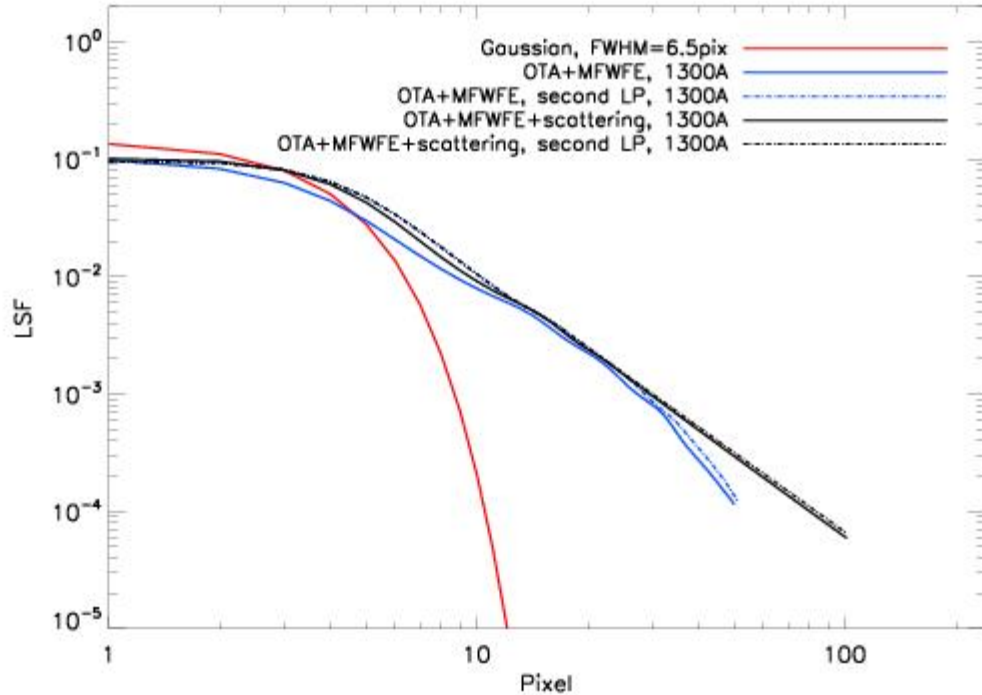


Limiting equivalent width as a function of wavelength for 3σ detections of absorption features at a S/N of 10 per pixel at lifetime position 5 (G130M/1291) and lifetime position 4 (G160M/1600). Dashed lines represent the full on-orbit LSFs including MFWFEs. Solid lines represent Gaussian LSFs without MFWFEs. The colors correspond to features with intrinsic Doppler parameters $b = 0 \text{ km s}^{-1}$ (black), 10 km s^{-1} (red), 25 km s^{-1} (green), 50 km s^{-1} (blue) and 100 km s^{-1} (purple).

3.3.4 Extended Wings of the COS LSF

The LSF models of Ghavamian et al. (2009) successfully characterize the basic profile and integrated properties of narrow spectral features in COS spectra. However, scientific investigations that depend on characterizing the depth of saturated or nearly-saturated absorption features may require a more careful treatment of the light scattered into the wings of the LSF. To address this concern, Kriss (2011) in [COS ISR 2011-01](#) has developed empirical LSF models for the G130M and G160M gratings. These models differ in two ways from the preliminary models discussed above. First, while the preliminary models extend only ± 50 pixels from the line center, the new models extend ± 100 pixels, which is the full width of the geocoronal Lyman- α line. Second, the new models include scattering due to the micro-roughness of the surface of the primary mirror, an effect that transfers an additional 3% of the light from the center of the line into its extended wings (Figure 3.9). For details, see [COS ISR 2011-01](#). The LSF models computed by Ghavamian et al. (2009) and predicted LSFs for the lifetime positions are available on the [COS website](#).

Figure 3.9: Comparison of LSF Models for Medium-Resolution FUV Gratings.

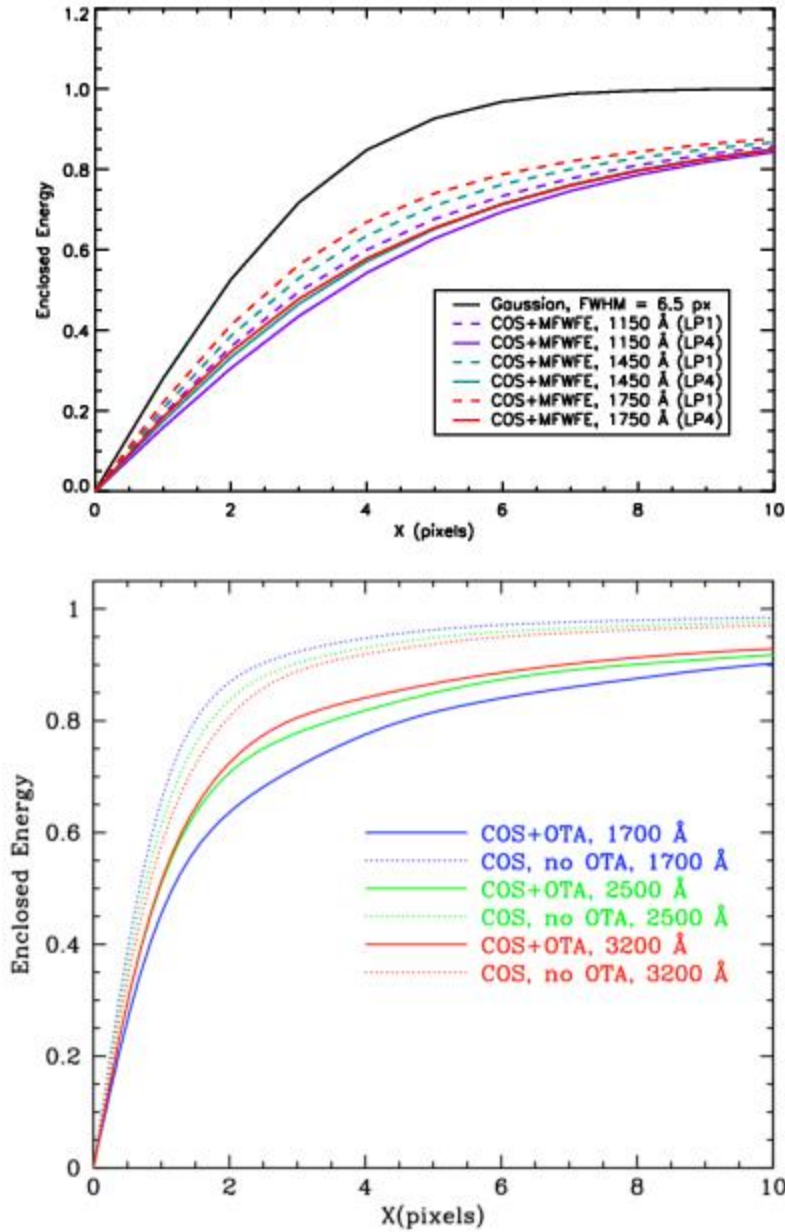


Comparison between a simple Gaussian LSF model (red line, FWHM = 6.5 pixels), the LSF profile from Ghavamian et al. (2009) that includes MFWFEs from the HST OTA (blue line, calculated at 1200 Å), and the LSF that includes power-law scattering wings of index -2.25 extending ± 100 pixels from line center (Kriss et al. 2011; black line). In the latter two cases solid lines represent the original lifetime position and the dot-dash lines represent the second lifetime position. Figure based on Figure 2 from Kriss (2011).

3.3.5 Enclosed Energy of COS LSF

Figure 3.10 shows the fraction of enclosed energy within the LSF, measured from the center of the profile, for both the FUV and NUV channels. The differences between the modeled on-orbit LSFs (MFWFEs included) and the Gaussian LSFs without MFWFEs are apparent in both spectroscopic channels. Though inclusion of the MFWFEs at longer NUV wavelengths widens the FWHM of the on-orbit LSF models only slightly, the wider wings decrease noticeably the spectral purity and the contrast level of the observed spectra.

Figure 3.10: Enclosed Energy Fraction of the COS Line-Spread Function.



The enclosed energy fraction of the COS LSF for an unresolved spectral feature as measured from the center of the profile (collapsed along the cross-dispersion direction). The top panel shows a Gaussian with FWHM = 6.5 px and FUV model profiles. The 1150 Å data (purple) use the G130M grating, while the 1450 Å (teal) and 1750 Å (red) data use the G160M grating. The dashed lines indicate results for the original lifetime position, while the solid lines indicate data for the fourth lifetime position. In the bottom panel, NUV model profiles with and without the effects of the OTA MFWFEs are shown (Ghavamian et al. 2009). The 1700 Å data (blue) use the G185M grating, the 2500 Å data (green) use the G225M grating, and the 3200 Å data (red) use the G285M grating.

Table 3.2: Distance from Line Center (in Pixels) versus Enclosed Energy Fraction and Wavelength for the G130M Grating.¹

Enclosed Energy Fraction	Wavelength (Å)

	1150	1200	1250	1300	1350	1400	1450
0.90	14.9/15.2	15.0/15.1	15.0/14.9	14.9/15.2	14.8/14.5	14.7/14.2	14.4/14.7
0.95	24.3/24.7	24.4/24.6	24.4/24.3	24.5/24.8	24.4/23.9	24.3/23.3	23.8/24.3
0.99	58.1/58.6	58.3/58.4	58.3/58.0	58.4/58.7	58.3/57.5	58.2/57.1	57.5/58.1

Table 3.3: Distance from Line Center (in Pixels) versus Enclosed Energy Fraction and Wavelength for the G160M Grating.²

Enclosed Energy Fraction	Wavelength (Å)						
	1450	1500	1550	1600	1650	1700	1750
0.90	14.7/14.4	14.6/14.9	14.4/14.2	14.2/14.0	14.0/13.8	13.6/13.7	13.2/13.2
0.95	24.5/24.0	24.3/24.7	24.0/23.8	23.8/23.7	23.5/23.4	23.1/23.1	22.6/22.8
0.99	58.3/57.6	58.1/58.7	57.8/57.4	57.4/57.1	57.0/56.8	56.3/56.4	55.6/55.9

Table 3.4: Distance from Line Center (in Pixels) versus Enclosed Energy Fraction and Wavelength for the G140L Grating.³

Enclosed Energy Fraction	Wavelength (Å)										
	1250	1300	1350	1400	1450	1500	1550	1600	1650	1700	1750
0.90	12.1	12.1	12.1	12.1	12.1	12.1	12.0	11.9	11.8	11.7	11.6
0.95	17.9	18.1	18.2	18.4	18.5	18.6	18.7	18.7	18.7	18.7	18.7
0.99	30.5	30.7	31.0	31.3	31.6	31.9	32.1	32.4	32.6	32.9	33.2

Table 3.2, Table 3.3, and Table 3.4 present the enclosed-energy fractions for gratings G130M, G160M, and G140L respectively. The distances reported in the tables are half-widths. The G130M and G160M data include the effects of scattering and are for both the original and the second lifetime position. Values for subsequent lifetime positions are not expected to differ appreciably. The G140L data are taken from Ghavamian et al. (2009) and are for the original lifetime position. The G140L data do not include the effects of micro-roughness. Please see the [COS website](#) for updated cenwave-dependent tabulations of the LSFs at all lifetime positions.

¹The values in each cell are from the original lifetime position/second lifetime position.

²The values in each cell are from the original lifetime position/second lifetime position.

³The values in each cell are from the original lifetime position.

Chapter 4: Description and Performance of the COS Detectors

Chapter Contents

- [4.1 The FUV XDL Detector](#)
- [4.2 The NUV MAMA Detector](#)

4.1 The FUV XDL Detector

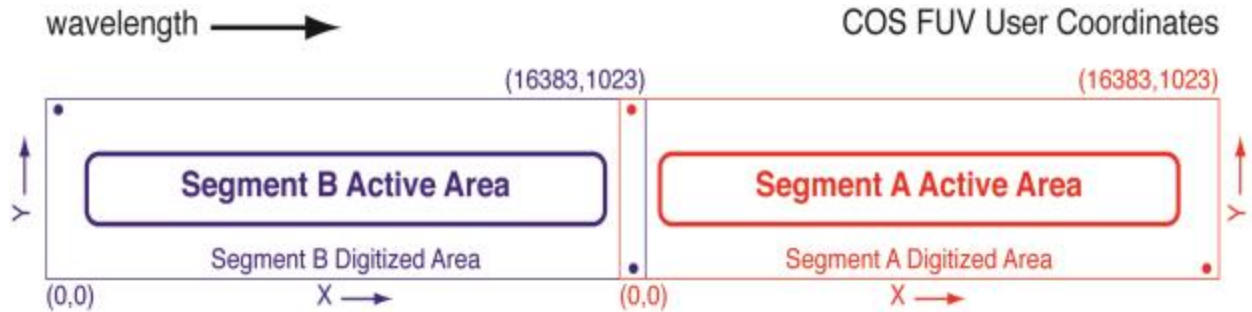
- [4.1.1 XDL Properties](#)
- [4.1.2 XDL Spectrum Response](#)
- [4.1.3 XDL Dark Rate](#)
- [4.1.4 XDL Read-out Format](#)
- [4.1.5 Non-linear Photon Counting Effects \(Dead Time\)](#)
- [4.1.6 Stim Pulses](#)
- [4.1.7 Pulse-height Distributions](#)
- [4.1.8 Spatial Variation of the Dark Rate](#)

4.1.1 XDL Properties

The COS FUV detector is a windowless cross delay line (XDL) device that is similar to the detectors used on the *Far Ultraviolet Spectroscopic Explorer (FUSE)*. The XDL is a photon-counting micro-channel plate (MCP) detector with two independently operable segments (FUVA and FUVB). Each segment has an active area of 85×10 mm; they are placed end-to-end and separated by a 9-mm gap. When the locations of detected photons are digitized they are placed into a pair of arrays (one per detector), each $16,384 \times 1,024$ pixels, though the active area of the detector is considerably smaller. Individual pixels span 6×24 μm . The long dimension of the array is in the direction of dispersion; increasing pixel number (the detector's x axis in user coordinates) corresponds to increasing wavelength. The XDL format is shown schematically in [Figure 4.1](#). Detector parameters are listed in [Table 1.2](#).

The FUV XDL is optimized for the 1150 to 1775 \AA bandpass, with a cesium iodide photocathode on the front MCP. The front surfaces of the MCPs are curved with a radius of 826 mm to match the curvature of the focal plane. When photons strike the photocathode they produce photoelectrons that are multiplied by a stack of MCPs. The charge cloud that comes out of the MCP stack, several millimeters in diameter, lands on the delay-line anode. There is one anode for each detector segment, and each anode has separate traces for the dispersion (x) and cross-dispersion (y) axes. The location of an event on each axis is determined by measuring the relative arrival times of the collected charge pulse at each end of the delay-line anode for that axis. The results of this analog measurement are digitized to 14 bits in x and 10 bits in y . In `TIME-TAG` mode the total charge collected from the event, called the pulse height, is saved as a 5-bit number.

Figure 4.1: The FUV XDL Detector.



This diagram is drawn to scale, and the slight curvature at the corners is also present on the masks of the flight detectors. Wavelength increases in the direction of the increasing x coordinate. The red and blue dots show the approximate locations of the stim pulses (see 4.1.6 below) on each segment. The numbers in parentheses show the pixel coordinates at the corner of the segment's digitized area; the two digitized areas overlap in the region of the inter-segment gap.

The detector electronics generate pulses that emulate counts located near the corners of the anode, outside the active area of the MCPs. These "stim pulses" (see Section 4.1.6) provide a means of tracking and correcting thermal distortions.

The XDL's quantum efficiency is improved by the presence of a series of wires, called the quantum-efficiency (QE) grid, placed above the detector (i.e., in the light path). These wires create shadows in the spectrum that are flagged and corrected by **CalCOS** during data reduction. The XDL also includes an ion-repeller grid that reduces the background rate by preventing low-energy thermal ions from entering the open-faced detector. It acts as a 95% transmission neutral-density filter.

4.1.2 XDL Spectrum Response

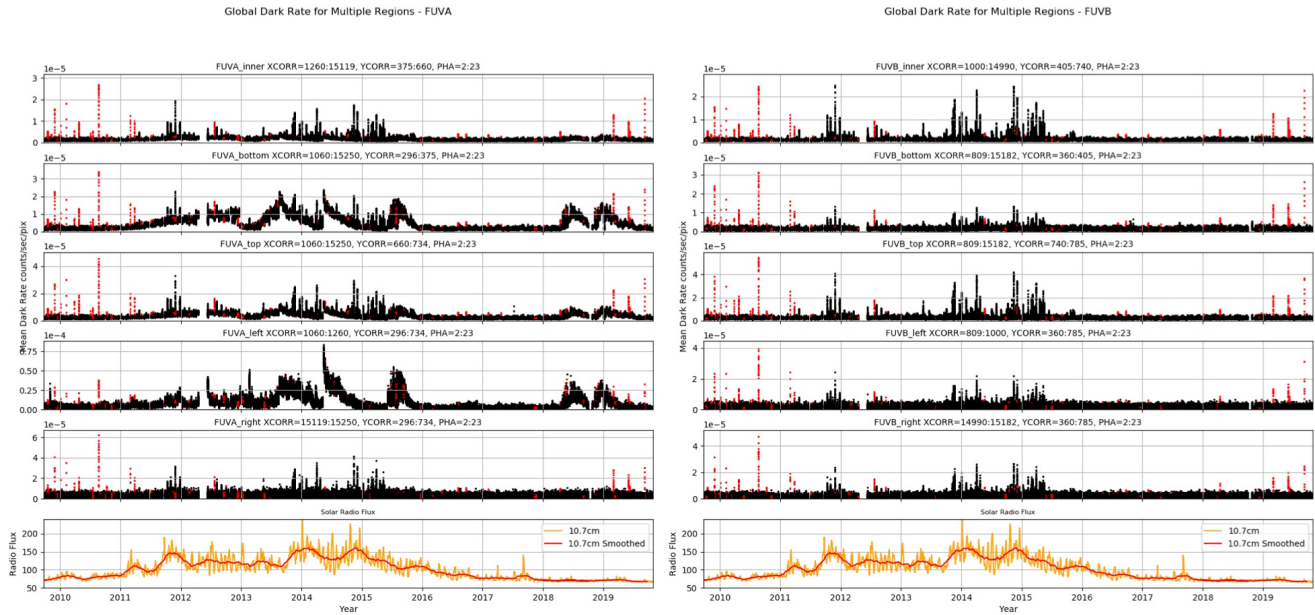
COS is considerably more sensitive than STIS and earlier-generation HST instruments at comparable spectral resolutions in the FUV. Effective areas for the COS FUV gratings are shown in Figure 5.1. The maximum count rates for the FUV detector are listed in Table 10.1. The time-dependent changes in the sensitivity of the COS FUV channel are discussed in Section 5.1.5.

4.1.3 XDL Dark Rate

The standard dark rate monitoring program is undertaken largely for the benefit of the exposure time calculator (ETC; see Section 7). Observations to ascertain dark rates are carried out through implementation of a variety of high voltages, and are taken on a best effort basis if requested in Phase I files under Special Requirements. Users should note that darks are not guaranteed to have been taken on a concurrent timescale with science observations.

The XDL detector segments have extremely low intrinsic dark rates, on the order of 10^{-6} counts s^{-1} pixel $^{-1}$; see [Section 7.4.1](#). Background counts can also be caused by external events, such as proximity to the South Atlantic Anomaly (SAA). **CalCOS** estimates the dark rate by measuring the counts in an un-illuminated region on the detector and subtracting this from the spectrum during processing. Each segment has a distinct dark current that varies with time and may be correlated with the Solar Cycle (see [Figure 4.2](#)). The dark rates vary with time, so observers, particularly those with faint, background-limited targets, should consider how the changing dark rates may affect their orbital estimates. In particular, some exposures experience sharp increases in the dark rate over short periods of time. The COS spectroscopic ETC estimates the dark rate for a typical exposure and segment based on the value that encompasses 95% of all observations. For the ETC version 31.2, the dark rate assumed in science exposures is 3.83×10^{-6} counts s^{-1} pixel $^{-1}$ for FUVB and 4.93×10^{-6} counts s^{-1} pixel $^{-1}$ for FUVB. A webpage which monitors dark rates can be found at <https://www.stsci.edu/hst/instrumentation/cos/performance/monitoring>.

Figure 4.2: COS FUV Dark Rates and the Solar Cycle.



Left panel: COS/FUV dark rates on FUVB as a function of time for each of the different areas on the detector monitored. The top five panels show the measured dark rate in 25 s increments throughout every exposure. The red dots represent dark rates that were observed close to when HST was passing over the South Atlantic Anomaly. The bottom panel display the 10.7 cm solar radio emission, tracking the solar cycle. The orange curve shows the corresponding Solar Radio Emission, which is a proxy for stellar activity, a smoothed version of which is shown in red. The gap in data corresponds to the shutdown of COS due to a detector anomaly on April 30, 2012. Right panel: This is the same as the left panel, but for the COS FUVB detector. See [COS ISR 2019-11](#) for further details on updates to COS FUV dark monitoring.

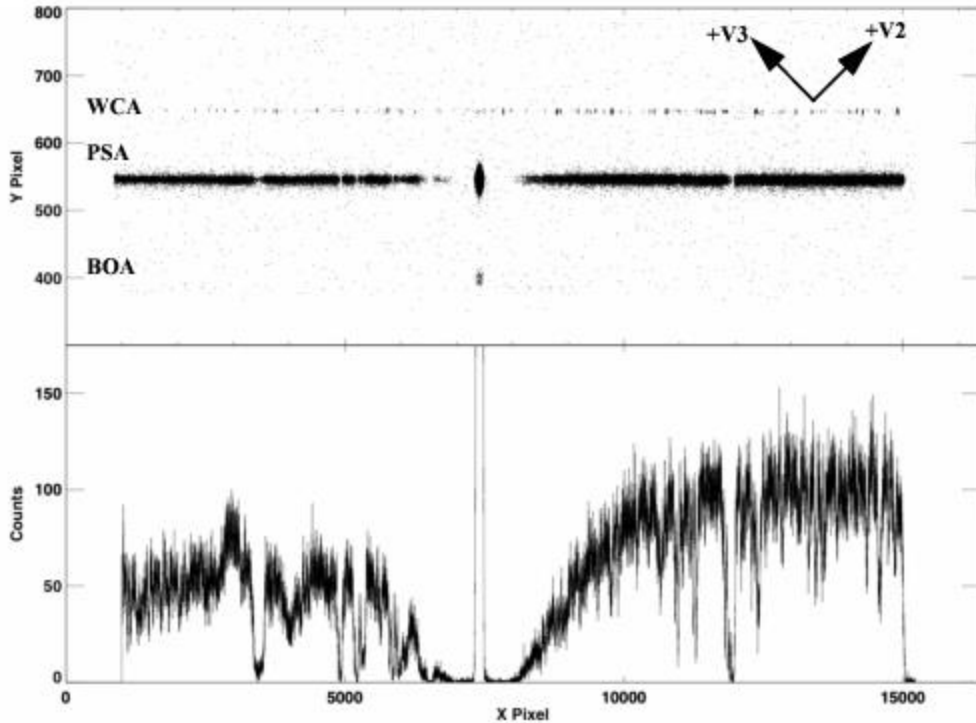
4.1.4 XDL Read-out Format

The FUV channel creates one spectral stripe on each detector segment for the science spectrum and another for the wavelength-calibration spectrum. The aperture not being used for science may also create a spectrum. If so, it will appear below the science spectrum if the PSA is being used, and above it if the target is in the BOA. Since the non-target aperture is usually observing blank sky, it will normally be visible only if airglow lines fall in the spectral range. [Figure 4.3](#) shows an example of an FUV spectrum obtained on orbit with Segment B. The upper panel shows the two-dimensional image; the lower panel shows the extracted PSA spectrum. Note the difference in the x- and y-axis scales in the upper figure.

Although the gap between the two FUV detector segments prevents the recording of an uninterrupted spectrum, it can be made useful. For example, when the G140L grating is used with a central wavelength of 1280 Å, the bright Lyman- α airglow feature falls in the gap. For suggestions on spanning the gap, see [Section 5.5](#).

Should a high count rate on one of the segments be a safety concern, the detector can be operated in single-segment mode, whereby the high voltage on one segment is lowered to a value that prevents it from detecting light. This adjustment is required for central wavelengths 800 Å and 1105 Å on G140L, since the zero-order light falling on Segment B in those modes is too bright.

Figure 4.3: Example of a COS FUV Spectrum.



Upper panel: A stellar spectrum obtained with Segment B of the COS FUV detector using the G130M grating at a central wavelength of 1309 Å. (This configuration is not allowed by the COS 2025 policy.) The wavelength calibration (WCA) spectrum is on top, and the stellar spectrum (PSA) is below. Both the PSA and BOA are open to the sky when the COS shutter is open, so Lyman- α airglow through the BOA is also visible below the PSA. The HST +V2 and +V3 axes are over plotted. Note that the size of the active area of the MCP is smaller than the overall digitized area (16,384 \times 1,024). Lower panel: the extracted stellar spectrum from the PSA.

4.1.5 Non-linear Photon Counting Effects (Dead Time)

The electronics that control the COS detectors have a finite response time t , called the dead time, that limits the rate at which photon events can be processed. If two photons arrive within time t , the second photon will not be processed. For the FUV channel three factors limit the detected count rate. The first is the Fast Event Counter (FEC) for each segment, which has a dead time of 300 ns. The FEC dead time matters only at count rates well above what is usable, introducing a 1% error at a count rate of 33,500 per segment per second.

The second factor is the time required to digitize a detected event. For a given true count rate C , the detected count rate D is:

$$D = \frac{C}{1 + C \times t},$$

where t is the dead-time constant. For the COS FUV detector $t = 7.4 \mu\text{s}$, so the apparent count rate deviates from the true count rate by 1% when $C = 1350$ counts/s and by 10% when $C = 15,000$ counts/s. Note that, when the effect is near the 10% level, then the FUV detector is near its global count-rate screening limit (see [Table 10.1](#)), so non-linear effects are relatively small.

Finally, the Detector Interface Board (DIB) combines the count streams from the two FUV segments and writes them to a single data buffer. The DIB is limited to processing about 250,000 count/s in `ACCUM` mode and only 30,000 count/s in `TIME-TAG` mode (the highest rate allowed for `TIME-TAG` mode). The DIB interrogates the A and B segments alternately; because of this a count rate that is high in one segment, but not the other, could cause a loss of data from both segments. Tests have shown that the DIB is lossless up to a combined count rate for both segments of 20,000 count/s; the loss is 100 count/s at a rate of 40,000 count/s. Thus, this effect is less than 0.3% at the highest allowable rates. Furthermore, information in the engineering data characterizes this effect.

Corrections for dead-time effects are made in the **CaICOS** pipeline, but they are not included in the [ETC](#), which will over-predict count rates for bright targets.

4.1.6 Stim Pulses

The signals from the XDL anodes are processed by Time-to-Digital Converters (TDCs). Each TDC contains a circuit that produces two alternating, periodic, negative-polarity pulses that are capacitively coupled to both ends of the delay-line anode. These stim pulses emulate counts located near the corners of the anode, beyond the active area of the detector. Stim pulses provide a means for **CaICOS** to correct the temperature-dependent shift and stretch of the image during an exposure, and they provide a first-order check on the dead-time correction. They are recorded in both `TIME-TAG` and `ACCUM` modes, and appear in the data files.

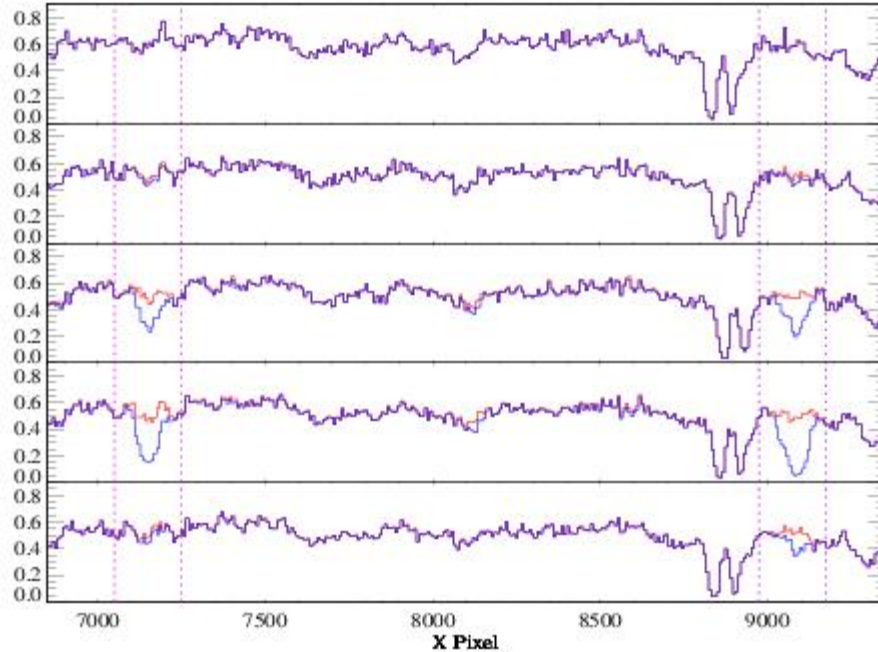
six stim-pulse rates are used: 0 (i.e., off), 2, 30, and 2000 Hz per segment. These rates, which are only approximate, are *not* user selectable. Exposures longer than 100 s will use the 2 Hz rate, those between 10 and 100 s use 30 Hz, and those shorter than 10 s use 2000 Hz.

4.1.7 Pulse-height Distributions

An ultraviolet photon incident on the front MCP of the XDL detector creates a shower of electrons, from which the detector electronics calculate the x and y coordinates and the total charge, or pulse height. The number of electrons created by each input photon, or "gain" of the MCPs, depends on the high voltage across the MCPs, the local properties of the MCPs at that location, and the high voltage across the plates. *It is not a measure of the energy of the incident photon.* A histogram of pulse heights for multiple events is called a pulse-height distribution (PHD).

The PHD from photon events on a particular region of the detector typically shows a peaked distribution, which can be characterized by the modal gain (the location of the peak) and its width. Background events, both internal to the detector and induced by cosmic rays, tend to have a falling exponential PHD, with most events having the lowest and highest pulse heights. On-board charge-threshold discriminators filter out very large and small pulses to reduce the background and improve the signal-to-noise ratio. In `TIME-TAG` mode the pulse height is recorded for each detected photon event. By rejecting outlier pulse-height events, **CaICOS** further reduces the background rate. In `ACCUM` mode only the integrated pulse-height distribution is recorded ([Section 5.2.2](#)), so pulse-height filtering is not possible.

Figure 4.4: Spectra Showing the Effects of Gain Sag on FUV Detector Segment B.



Spectra (G160M/1623/FP-POS=4) of a target observed five times over 19 months: from top to bottom, September 2009, June 2010, September 2010, January 2011, and May 2011. The blue curve includes only photon events with pulse heights in the range 4–30; the red curve includes pulse heights 2–30. The spectral features near pixels 7200 and 9011 are not astrophysical, but represent the effect of gain sag on regions of the detector illuminated by Lyman α in other observing modes. These features become more pronounced with time until March 2011, when the Segment B high voltage was raised.

Gain Sag

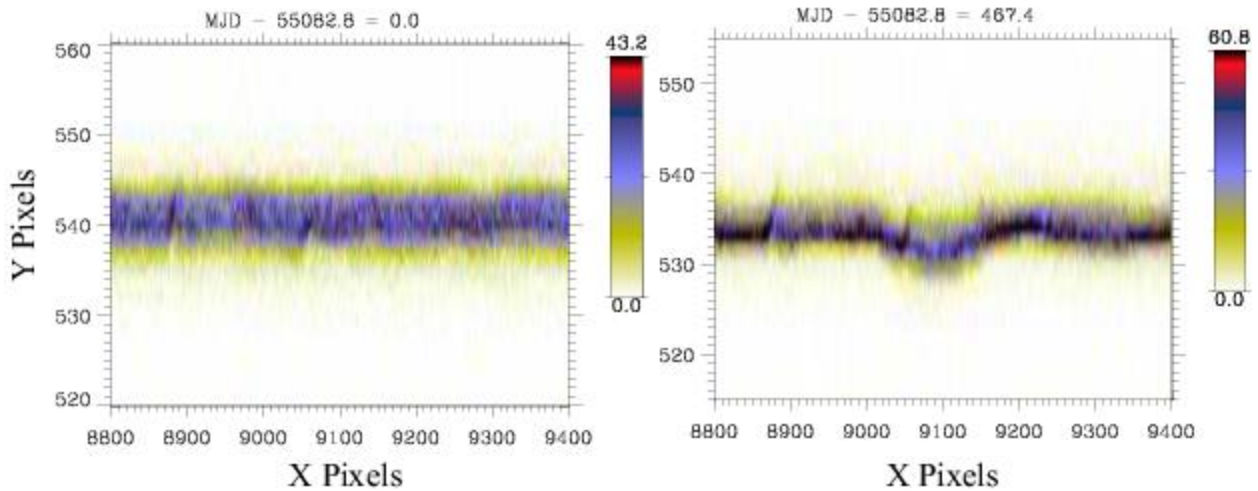
Prolonged exposure to light causes the number of electrons per incident photon to decrease, a phenomenon known as "gain sag." As a result, the peak of the PHD in each region of the detector shifts to lower values as the total (time-integrated) illumination of that region increases. As long as all pulse heights are above the minimum threshold imposed by the onboard electronics and **CalCOS**, there is no loss in sensitivity. However, if the gain drops low enough that the pulse heights of the photon events from the target fall below the threshold, these events are discarded and the apparent throughput decreases. The amount of gain sag increases with the total amount of previous illumination at that position on the detector, so gain sag appears first in regions of the detector that are illuminated by bright airglow lines, but eventually affects the entire spectrum. [Figure 4.4](#) shows the effect of gain sag on Segment B of the COS FUV detector. These data were obtained using the grating setting G160M/1623/FP-POS=4 at LP1. A portion of the extracted spectrum from the same object taken at five different times is shown. The blue curve was constructed using only photon events with pulse heights in the range 4–30, while the red curve includes pulse heights of 2–30. The current pulse height limits used by the COS pipeline are 2–23. Two regions that suffer the most serious gain sag are marked: the region near pixel 7200 is illuminated by Lyman α when grating setting G130M/1309/FP-POS=3 is used, and the region near pixel 9100 is illuminated by Lyman α when the setting is G130M/1291/FP-POS=3. Initially, the pulse heights were well above either threshold, so the blue and red curves are indistinguishable. As time progressed, all of the pulse heights decreased. However, the two Lyman- α regions decreased faster, causing the blue spectra to exhibit spurious absorption features. This trend continued until the Segment B high voltage was raised in March 2011. The bottom plot shows that increasing the voltage has recovered most of the lost gain.

More details on the gain sag can be found in the [COS Data Handbook](#) and [COS ISR 2011-05](#).

Detector Walk

As the pulse height of a photon event decreases, the detector electronics begin to systematically miscalculate its position. On the COS FUV detector this effect, called detector walk, occurs in both x and y , but is much larger in the y (cross-dispersion) direction. The shift is approximately 0.5 pixel per pulse-height bin, which means that the entire spectrum may be shifted by several pixels, and the regions with the lowest gain may be noticeably shifted relative to the rest of the spectrum ([Figure 4.5](#)). **CalCOS** applies a y -walk correction to `TIME-TAG` data, but the current algorithm does not completely correct the data; future versions of **CalCOS** will improve the correction. In addition, the walk is uncorrected in `ACCUM` mode, where no pulse-height information is available. The spectral extraction should remain unaffected, because the extraction regions are large enough to include the misplaced counts.

Figure 4.5: Y-Walk on the FUV Detector.



Two-dimensional spectra, uncorrected for walk, taken in September 2009 (left) and December 2010 (right). The entire spectrum has shifted down by several pixels due to gain sag and detector walk. A larger shift is seen in the region near $X = 9100$, where the gain sag is greater due to the geocoronal Lyman- α feature that falls there when the G130M/1291 when the $FP-POS=3$ setting is used.

Mitigation Strategies

A range of strategies have been used to minimize the effects of gain sag and detector walk on the science data. Several of these are modifications to **CalCOS**, which means that previously collected data can be improved by reprocessing. Others involve changes to the on-orbit settings, and thus only affect exposures taken after the changes are made.

CalCOS Changes

Pulse-Height Thresholding: At present, the lower pulse-height threshold used by **CalCOS** when processing **TIME-TAG** data has been decreased to near its minimum value (2). This ensures that as few events as possible are lost due to low gain, but it will have the effect of slightly increasing the detector background. We hope to eventually implement time- and position-dependent pulse-height thresholds in **CalCOS**.

Walk Correction: **CalCOS** applies a walk correction to **TIME-TAG** events. The pulse height and measured position of an event are used to apply a correction factor to its position. Although the walk correction is not time-dependent, it may be modified as we learn more about the walk properties of the detector.

Gain Sag Table: Low-gain pixels are flagged by **CalCOS** and excluded when combining spectra taken at multiple **FP-POS** positions.

Onboard Changes

Voltage Adjustments: In an effort to keep the MCP gain in the spectral regions within the range that gives acceptable position determination, while simultaneously minimizing gain sag, the high voltage on each segment has been adjusted numerous times since launch. The voltages used for a particular exposure can be found in the file headers, but the effects should be transparent to the user, since any effects on the data will be handled by **CalCOS**. More details on the high voltage changes are given in the [COS Data Handbook](#).

Change in Lifetime Position: After years of collecting exposures—and tens of thousands of counts per pixel in the most exposed areas—the gain at certain areas on the MCPs drops so much that none of the techniques described above can return the detector to an acceptable level of performance. Once that occurs, the only way to obtain satisfactory data is to move the spectra to a new location on the detector, which can be accomplished by adjusting the position of the aperture and the pointing of HST. This moves the spectra to a pristine region on the detector, which defines a new lifetime position. COS has been operated at a total of six lifetime positions. Because the optical path is slightly different for each lifetime position, the properties of the spectrograph are also slightly different. Thus, the resolving power, throughput, flat field, etc., may differ at different lifetime positions. A keyword in the header of the data files tells **CalCOS** which lifetime position was used, and reference files appropriate to that position are applied when processing the data.

Multiple LPs are in use simultaneously (see [Section 5.12](#)), with both the LP and high voltage chosen to optimize performance on the grating and central wavelength of each exposure. The position and voltage values are determined by STScI based on the performance of the detector, so they cannot be specified by general observers.

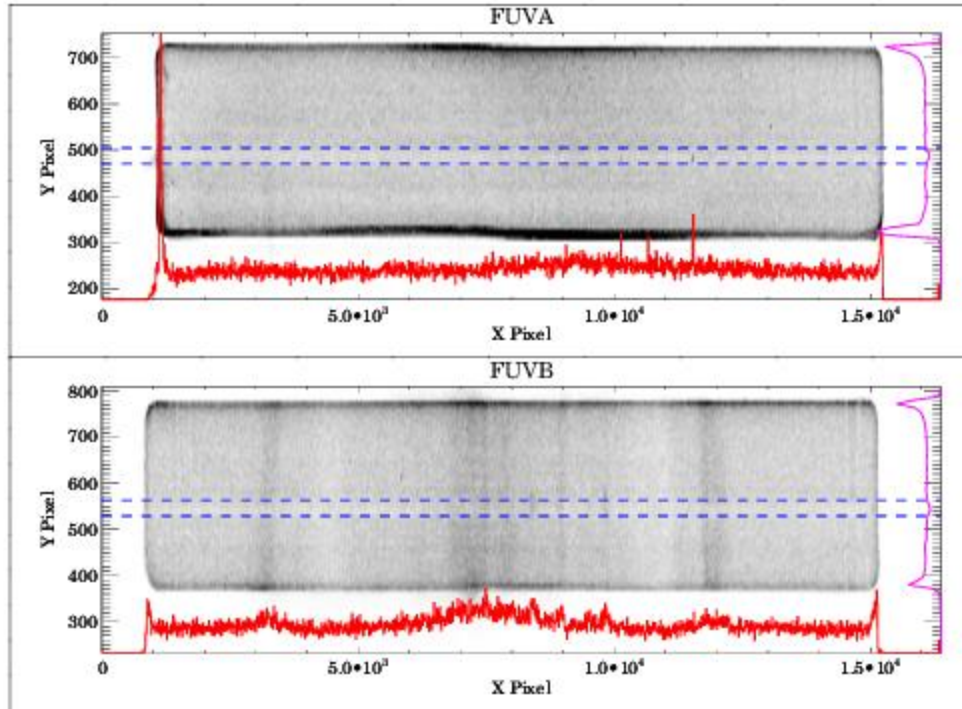
Details on associated new calibrations are reported in [ISRs](#) that are available in the [COS Data Handbook](#) and periodic [STANs](#) will also document these changes.

4.1.8 Spatial Variation of the Dark Rate

The dark rate varies spatially over the FUV detector. [Figure 4.6](#) shows the sum of approximately 80,000 s of dark exposures taken over a five-month period in 2011. With the standard lower pulse-height threshold of 2, Segment A is relatively featureless away from the edges of the active area, except for a few small spots with a higher rate. Segment B shows several large regions with a slightly elevated rate; they are enhanced by less than a factor of two over the quieter regions.

For most `TIME-TAG` observations these features will have a negligible effect on the extracted spectra, because the variation is small and the overall rate is low (see [Table 7.1](#)). In `ACCUM` mode, where no lower pulse-height threshold is used, additional features appear. `ACCUM` mode is used only for bright targets, so these features should constitute a negligible fraction of the total counts.

Figure 4.6: FUV Detector Dark Features.



Summed dark exposures showing spatial variations on the detector. The approximate position of the G130M extraction window for the original lifetime position is marked in blue, and a sum of the dark counts in this extraction window as a function of x pixel is shown in red below the image. A sum as a function of y pixel is shown on the right side of the figure. Segment A is nearly featureless aside from a few small hot spots, while Segment B shows larger variations. Both segments show a slightly lower dark rate in the region where the most counts have fallen. This is due to gain sag. The data are binned by 8 pixels in each dimension for display purposes.

4.2 The NUV MAMA Detector

- [4.2.1 MAMA Properties](#)
- [4.2.2 MAMA Spectrum Response](#)
- [4.2.3 MAMA Dark Rate](#)
- [4.2.4 MAMA Read-Out Format](#)
- [4.2.5 MAMA Dead Time](#)
- [4.2.6 Non-Gaussian Wings in the MAMA PSF](#)

4.2.1 MAMA Properties

The COS NUV detector is a Multi-Anode Micro-channel Array (MAMA) identical to that used for the NUV in STIS. (In fact, it is the STIS NUV flight spare.) The COS MAMA has a semi-transparent cesium telluride photocathode on a magnesium fluoride window and is sensitive to photons with wavelengths from 1150 to 3200 Å. The NUV optics focus light through the MgF₂ window onto the Cs₂Te photocathode. A photoelectron generated by the photocathode then falls onto a curved-channel micro-channel plate (MCP), which generates a cloud of electrons. The active area of the anode array is 25.6 mm square and is divided into 1,024 × 1,024 pixels on 25 μm centers. The spatial resolution at 2500 Å is 35 μm FWHM. Detector parameters are listed in [Table 1.2](#).

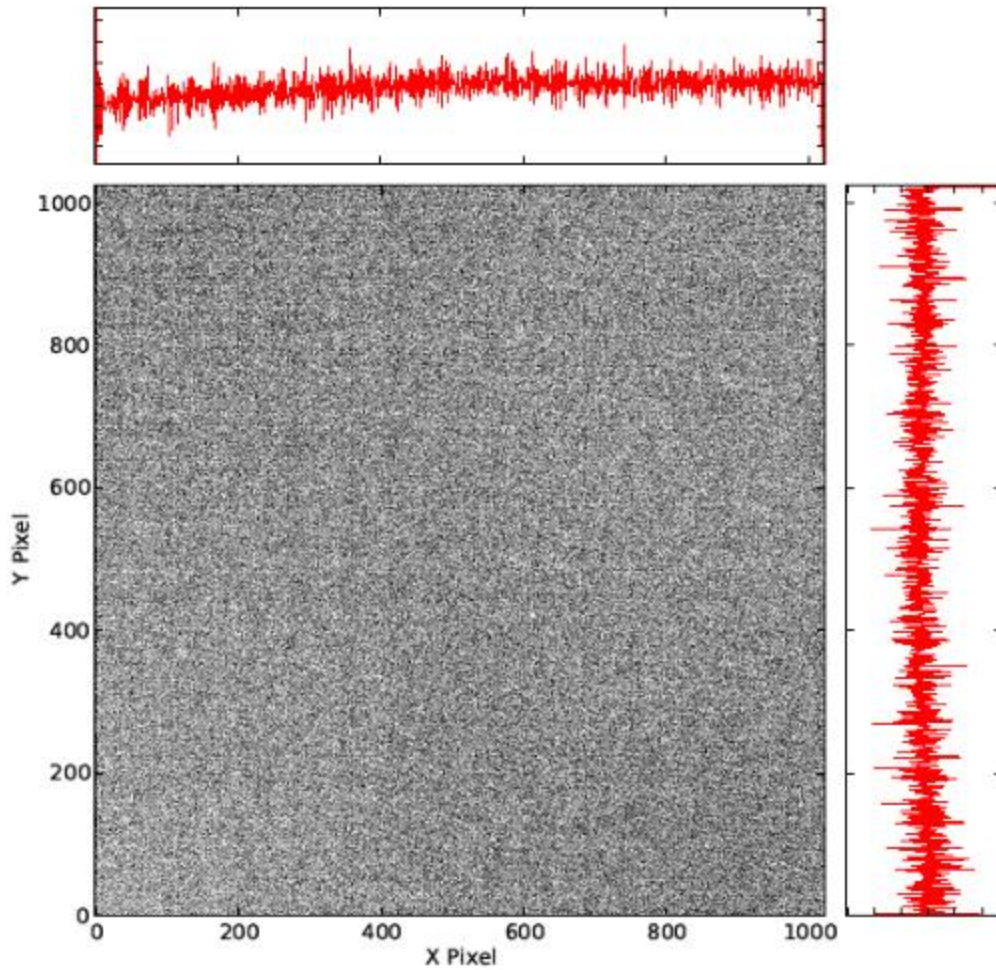
4.2.2 MAMA Spectrum Response

The inherent spectral response of the COS NUV MAMA is essentially identical to that of the STIS NUV MAMA. However, the overall optical train of COS differs from that of STIS, so the throughputs are different ([Figure 5.2](#)). The maximum count rates for the NUV detector are listed in [Table 10.1](#).

4.2.3 MAMA Dark Rate

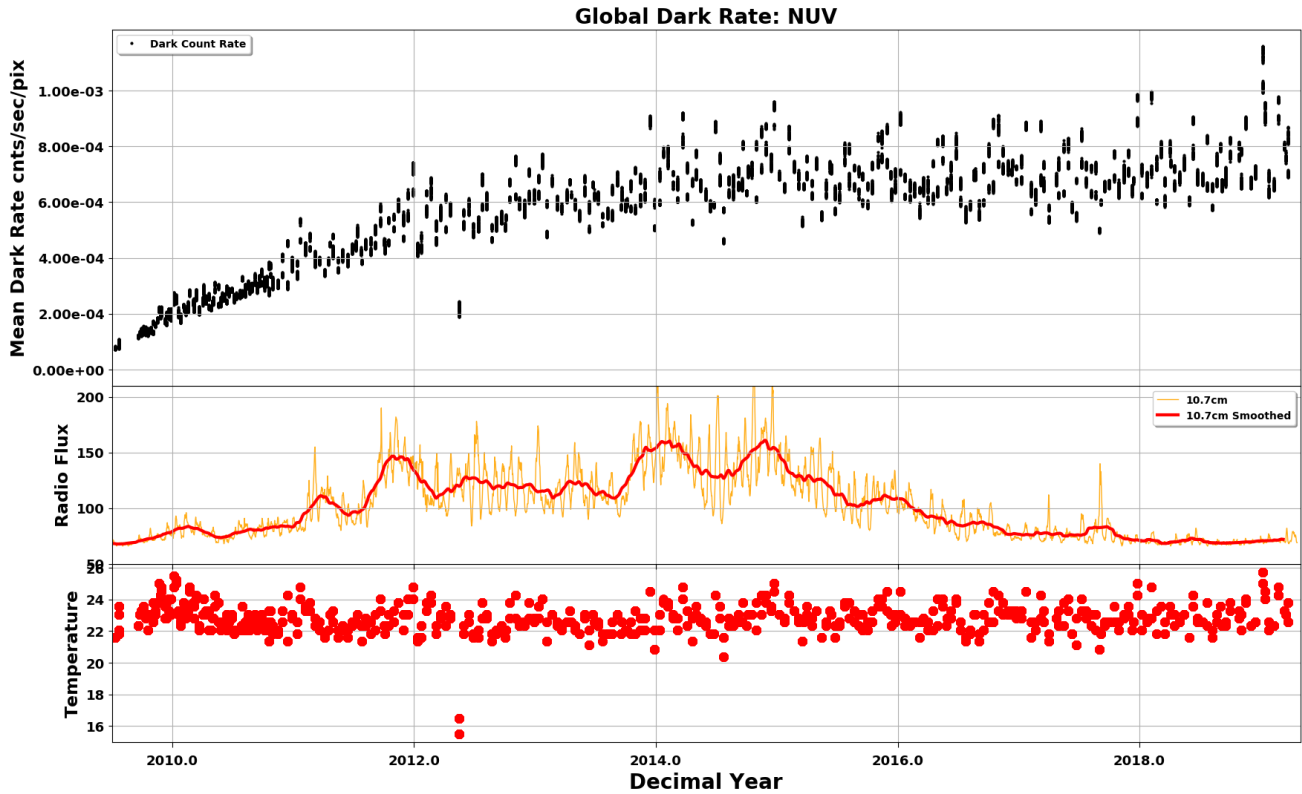
A sum of dark exposures taken away from the SAA shows a relatively featureless background, with slight enhancements at two of the corners ([Figure 4.7](#)). Although the early dark rate was lower than had been measured on the ground, the rate has steadily increased since launch, as shown in [Figure 4.8](#). For version 31.2 of the COS ETC, the dark rate adopted for NUV is 1.25×10^{-3} counts s⁻¹ pixel⁻¹, encompassing 95% of observations through 2023. A webpage which monitors dark rates can be found at <https://www.stsci.edu/hst/instrumentation/cos/performance/monitoring>.

Figure 4.7: Spatial Variation in the NUV Dark Rate.



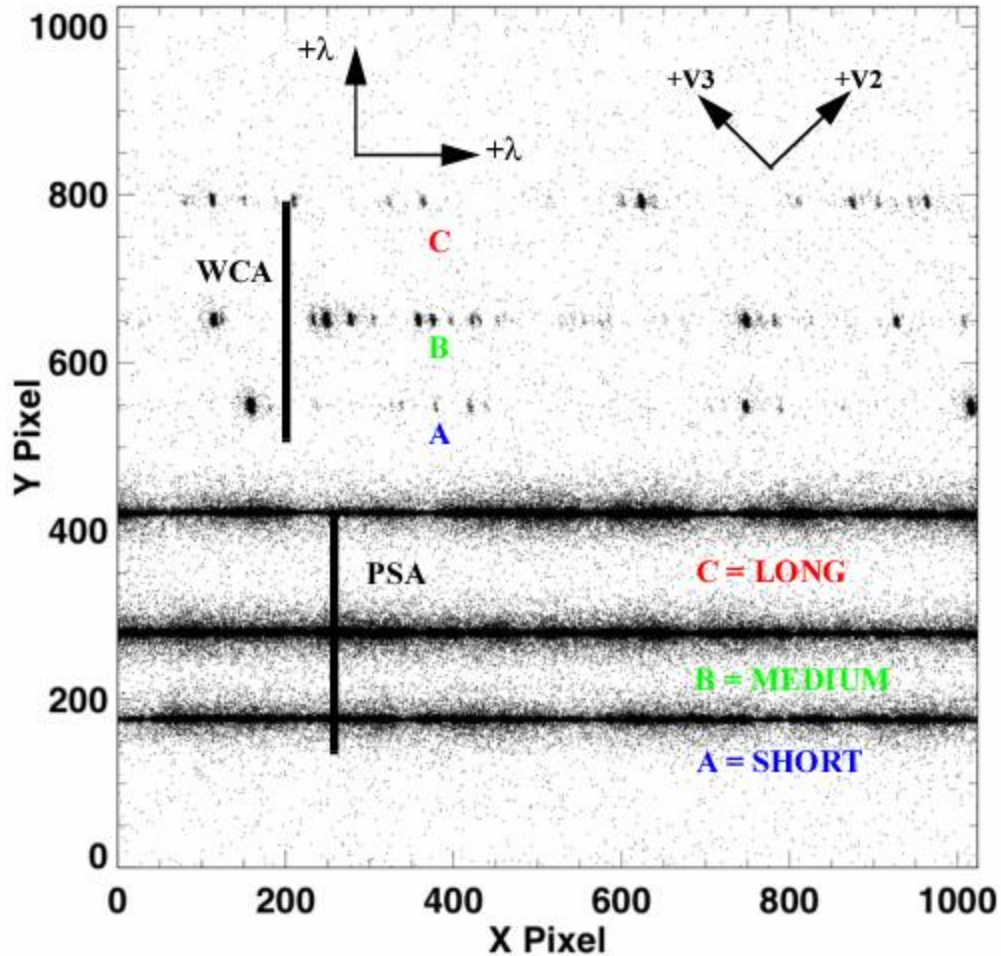
Summed dark exposures show the uniformity of the NUV dark rate across the detector. There is very little variation across the detector, with only a small depression in the dark rate in the lower left corner. The cumulative histograms show the collapsed rows (above) and columns (right).

Figure 4.8: NUV Detector Dark Rate versus Time.



Measured dark rate as a function of time. When the periods affected by the SAA are excluded, the dark rate increased by roughly 200 count s^{-1} per year until 2013, when the trend flattened. Neither the increase in the dark rate, nor the increase in the scatter that is seen in the later observations, are understood. The middle panel shows the radio flux of the sun for comparison. The lower panel shows the detector temperature (LNTUBET). This demonstrates the temperature dependence of the dark rate. The two observations of exceptionally low dark rate at 2012.35 are due to a much lower than normal temperature caused by the shut-off of the FUV detector.

Figure 4.9: Example of a COS NUV Spectrum.

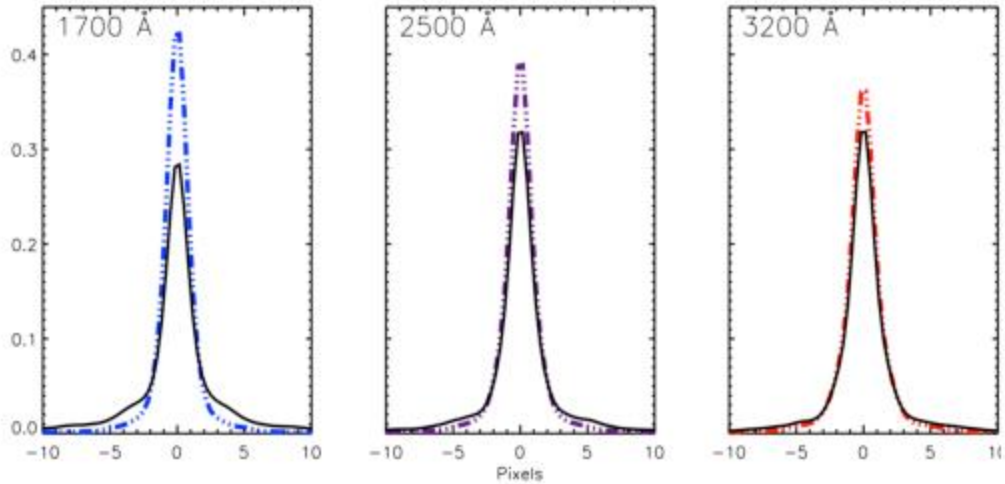


A COS NUV spectrum obtained in `TIME-TAG` mode with `FLASH=YES`. The stellar spectrum (labeled PSA) is on the bottom, and the wavelength-calibration spectrum (labeled WCA) on the top; each has three stripes. From bottom to top, these stripes are designated A, B, and C, as illustrated. Wavelength increases to the right and toward the top of the detector. The HST +V2 and +V3 axes are also shown. The SHORT, MEDIUM, and LONG designations are used in Phase II with the `ACQ/PEAKXD` command and the `STRIPE` optional parameter.

4.2.4 MAMA Read-Out Format

The NUV channel creates six spectral stripes on the MAMA detector, three for the science data and three for the wavelength-calibration data. Stripes are separated by 94 to 143 pixels (2.1 to 3.3 arcsec), center to center, in the cross-dispersion direction. The NUV detector is read out as a $1,024 \times 1,024$ array, but in all other respects the data are handled in the same way as for the FUV detector. No pulse-height information is provided for MAMA data. An NUV spectrum obtained in `TAGFLASH` mode is shown in [Figure 4.9](#).

Figure 4.10: Model LSFs for the COS NUV Channel.



LSFs including the MFWFEs are plotted as solid lines, those without as dotted lines.

4.2.5 MAMA Dead Time

The dead time for the COS NUV MAMA is 280 ns, the same as for the STIS NUV MAMA. The 1% level of non-linearity is reached for $C = 36,000$ count/s. Corrections for dead-time effects are made in the **CalCOS** pipeline, but they are not included in the **ETC**, which will over-predict count rates for bright targets.

4.2.6 Non-Gaussian Wings in the MAMA PSF

While most NUV observations should be minimally affected by the mid-frequency wavefront errors (MFWFEs) discussed in [Section 3.3](#), they will reflect the point-spread function of the COS MAMA detector, which exhibits faint, extended wings that are unrelated to the telescope optics. While the telescope-induced wings weaken as wavelength increases, the detector wings become stronger with increasing wavelength. [Figure 4.10](#) shows model NUV detector LSFs with and without the MFWFEs at various wavelengths. Beyond 2500 Å, the detector wings dominate.

Chapter 5: Spectroscopy with COS

Chapter Contents

- 5.1 The Capabilities of COS
 - 5.1.13 COS Observations below 1150 Angstroms
- 5.2 TIME-TAG vs. ACCUM Mode
- 5.3 Valid Exposure Times
- 5.4 Estimating the BUFFER-TIME in TIME-TAG Mode
- 5.5 Spanning the Gap with Multiple CENWAVE Settings
- 5.6 FUV Single-Segment Observations
- 5.7 Internal Wavelength Calibration Exposures
- 5.8 Fixed-Pattern Noise
- 5.9 COS Spectroscopy of Extended Sources
- 5.10 Wavelength Settings and Ranges
- 5.11 Spectroscopy with Available-but-Unsupported Settings
- 5.12 FUV Detector Lifetime Positions
- 5.13 Spectroscopic Use of the Bright Object Aperture

5.1 The Capabilities of COS

- [5.1.1 First-Order Sensitivity](#)
- [5.1.2 Sensitivity below 1150 Å](#)
- [5.1.3 Second-Order Sensitivity](#)
- [5.1.4 Spectroscopic Resolving Power](#)
- [5.1.5 Time-Dependent Sensitivity Changes](#)
- [5.1.6 Dip in Sensitivity around 1180 Å](#)
- [5.1.7 Zero-Order Image](#)
- [5.1.8 Internal Scattered Light](#)
- [5.1.9 Spatial Resolution and Field of View](#)
- [5.1.10 Photometric \(Flux\) Precision](#)
- [5.1.11 Wavelength Accuracy](#)
- [5.1.12 Vignetting of the NUV Channel](#)

COS has two detectors and seven diffraction gratings (three for FUV, four for NUV), which enable high-sensitivity spectroscopy at low and moderate resolution across the FUV and NUV bands. The bandpass and resolution of each grating are presented in [Table 5.1](#). Links to pages with additional information for each grating ([Section 13.3](#)) are provided in [Table 5.1](#), noting that, in addition to the standard G130M central wavelengths, the first two rows of [Table 5.1](#) give the bandpass and resolution for the 1055/1096 and 1222 central wavelengths, respectively.

For each exposure the observer selects a detector (FUV or NUV), a grating, a central wavelength, an FP-POS setting, one of the two apertures (PSA or BOA), and a data-taking mode (TIME-TAG or ACCUM). [Chapter 13](#) provides detailed specifications for each grating and aperture. Note that the two channels cannot be used simultaneously as the NUV channel is fed by the NCM1 mirror on the FUV optics select mechanism (OSM1). Spectroscopic observations with the BOA aperture are considered "Available-but-Unsupported" (See [Section 5.11](#) and [5.13](#)).

Table 5.1: COS Grating Parameters.

Grating	Approximate Wavelength Range (Å)	Bandpass per Exposure and FUV Gap ¹ (Å)	Inferred PSA Resolving Power $R = \lambda/\text{FWHM}^2$	Approximate BOA Resolving Power	Dispersion (mÅ pixel ⁻¹)
FUV Channel					
G130M	900-1236	295/16	up to ~13,000 ³	—	9.97
	1065-1365	296/15.7	12,000-17,000 ³	—	9.97
	1150-1450	292/14.3	12,000-17,000	7600 ⁴	9.97
G160M	1360-1775	360/18.1	13,000-20,000	4400 ⁴	12.23
G140L	<900-2150	>1150/112	1500-4000	1100 ⁴	80.3

NUV Channel					
G185M	1700–2100	3 × 35	16,000–20,000	3500	37
G225M	2100–2500	3 × 35	20,000–24,000	4600	33
G285M ⁵	2500–3200	3 × 41	20,000–24,000	5000	40
G230L	1650–3200 ⁶	(1 or 2) × 398	2100–3900	500	390

¹ Width of gap between FUV detector segments; see [Section 5.5](#).

² Empirically determined FWHM of the LSF, which is not Gaussian. *R* increases approximately linearly with wavelength.

³ For these settings, *R* reaches a maximum in the middle of the wavelength range. See [Figure 5.5](#).

⁴ At LP1. For subsequent LP, the resolution may be slightly reduced.

⁵ The G285M grating is Available-but-Unsupported. See [Section 5.11](#) for details.

⁶ Some shorter wavelengths are recorded in second-order light. They are listed in [Table 5.4](#).

5.1.1 First-Order Sensitivity

COS is considerably more sensitive than STIS and earlier-generation HST instruments at comparable spectral resolutions, particularly in the far ultraviolet. Effective areas for targets observed through the PSA are shown in [Figure 5.1](#), [Figure 5.2](#), and [Figure 5.3](#). Note that the COS sensitivity changes with time ([Section 5.1.5](#)). Please consult the [COS website](#) for updated information.

i *While the figures and tables in this handbook can be used to estimate count rates and exposure times, we recommend the use of the COS ETC in all cases, because it properly computes instrument throughput, accounts for detector and astronomical backgrounds, and checks for violations of local and global count-rate screening limits.*

Figure 5.1: Effective Areas for the FUV Channel through the PSA as of April 2016.

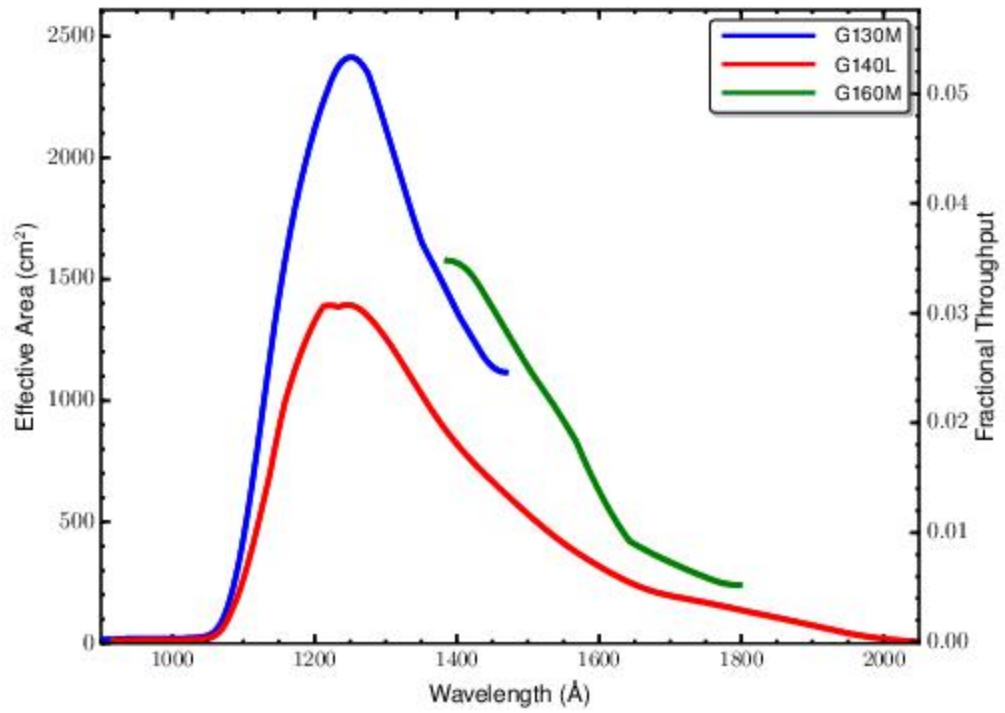


Figure 5.2: Effective Areas for the NUV Channel through the PSA as of April 2016.

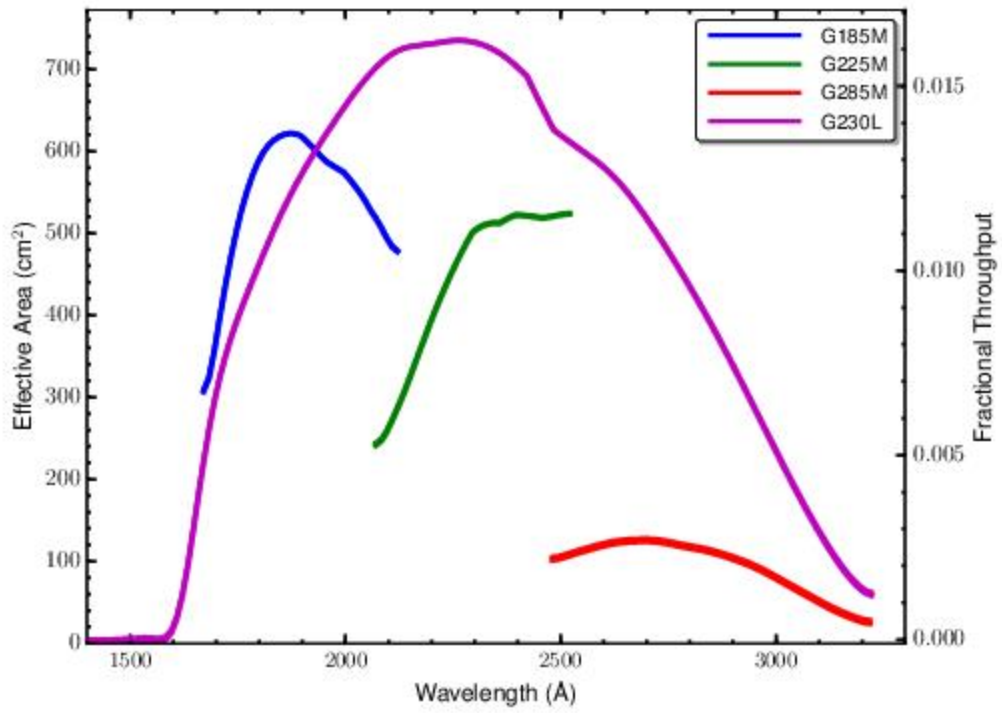
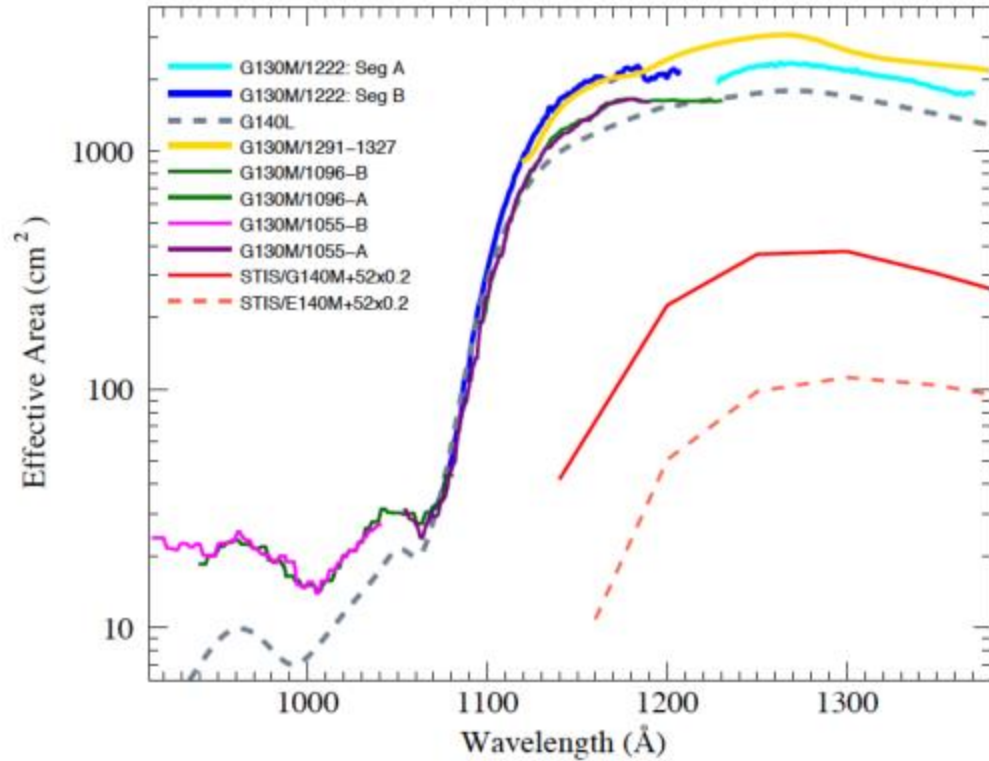


Figure 5.3: Effective Area at Wavelengths below 1400 Å.



The effective areas of the various G130M central-wavelength settings are compared with those of G140L and STIS. Effective areas are not well characterized below 920 Å.

5.1.2 Sensitivity below 1150 Å

Figure 5.3 compares the effective areas of the G130M and G140L gratings at the short-wavelength end of the COS bandpass. (The G140L curve at short wavelengths presented here was tentative pending calibration of cenwave 800; see [COS ISR 2019-04](#) for this calibration.) From this figure we can draw two fundamental conclusions. First, COS can obtain useful spectra at wavelengths between 900 and 1150 Å. Second, the contrast between the throughputs at 1070 and 1150 Å is roughly a factor of 100.

For G140L observations at short wavelengths, use `CENWAVE=800` for targets where there is no count-rate violation at long wavelengths. For some targets, however, the count rate at 1150 Å will exceed the local bright screening limit, while the count rate at shorter wavelengths is perfectly safe. In this case, using `CENWAVE=1280` with Segment A turned off is the recommended approach. Using only `FP-POS=4` to avoid the longest wavelengths in the Segment B range is an additional strategy that may protect against count-rate violations.

When grating G130M is used with `CENWAVE=1055`, Segment B records wavelengths shortward of ~1050 Å, depending on the `FP-POS` setting employed ([Section 13.3](#)). Using this grating mode with Segment A turned off further reduces the danger of high count rates at longer wavelengths. Special configurations to allow proper wavelength calibration must be used (see [Section 5.7.4](#)). Note that both the sensitivity and resolving power ([Section 5.1.4](#)) of G130M are greater than those of G140L in this wavelength range.

The sensitivity for the G140L/800 and 1280 setting changes by a factor of 100 between the wavelengths of 1070 Å and 1150 Å, so the flux vs. wavelength calibration is extremely sensitive to small misalignments in the wavelength scale. For cenwave 1280, this is complicated by the absence of usable calibration lamp lines on Segment B (see [Section 5.7.4](#)). Therefore, even small wavelength misalignments will lead to sizable artifacts in the extracted flux for the calibrated spectra. The flux and wavelength calibrations should be used with caution when interpreting the default pipeline products. For these settings, the sensitivity has not been measured shortward of 912 Å. Photons at these wavelengths are preserved in the "net counts" column of the `*x1d*.fits` files, but they are set to unrealistically small fluxes.

5.1.2.1 Resolution and Wavelength Calibration below 1150 Angstroms

Starting in Cycle 21 the spectral resolutions of the FUV G130M 1055 and 1096 central wavelength settings were substantially increased above the values offered during earlier cycles and, when combined with the 1222 setting first offered in Cycle 20, this now allows resolutions of 7300 to 11,000 to be obtained at any wavelength between 900 and 1150 Å (see [Figure 5.5](#)). Users should note, however, that for each of these modes the focus values have been set to optimize the resolution over a limited part of their wavelength range, and it will be necessary to use multiple settings to get the maximum resolution over this full range. At longer wavelengths the resolutions offered by any of these settings will be inferior to those available with the original complement of G130M central wavelength settings (1291, 1300, 1309, 1318, and 1327).

Users should also note that targets that are too bright to observe at longer wavelengths with the COS G130M grating may be observable on Segment B with the 1055 and 1096 settings by turning off Segment A, which covers longer wavelengths. However, in this case there is no usable TAGFLASH wavelength calibration lamp spectrum recorded because there are no visible wavelength calibration lines that fall on Segment B. As a result, the spectrum observed on Segment B cannot be corrected for mechanism drift or zero-point offsets. *In such cases, for each CENWAVE and FP-POS position, a separate GO-wavecal exposure should be taken with Segment A "on" immediately adjacent to the Segment B science observations. This Segment A wavecal will allow the zero-point offset of the wavelength scale of Segment B to be corrected to within 10 pixels.* Several minutes are required to reconfigure the COS FUV detector each time the segments are powered on or off. However, with careful planning much of this overhead can often be hidden in the occultations or other overheads. Additional details and examples of observing scenarios can be found in [Chapter 5](#) and in [Section 9.7](#) "Examples of Orbit Estimates."

The 1280 setting of G140L also covers from below 900–1185 Å on Segment B of the FUV detector with resolution of 900–1800 over this range. In principle, the spectral format of this setting may allow observations at even shorter wavelengths; however, the throughput and resolution between 500 and 900 Å are poorly characterized. The 800 setting of G140L places the entire wavelength range from 800 to 1950 Å on Segment A of the FUV detector, and it is optimized to reduce the astigmatic height of the spectrum below about 1100 Å. This allows for decreased detector noise and correspondingly better S/N at these wavelengths compared to that attainable on segment B with the 1280 setting.

Limited amounts of data were taken using the G130M 1055 and 1096 central wavelength settings at the first lifetime position (before July 23, 2012). Calibrated data from these observations can be obtained by contacting the [HST Help Desk](#).

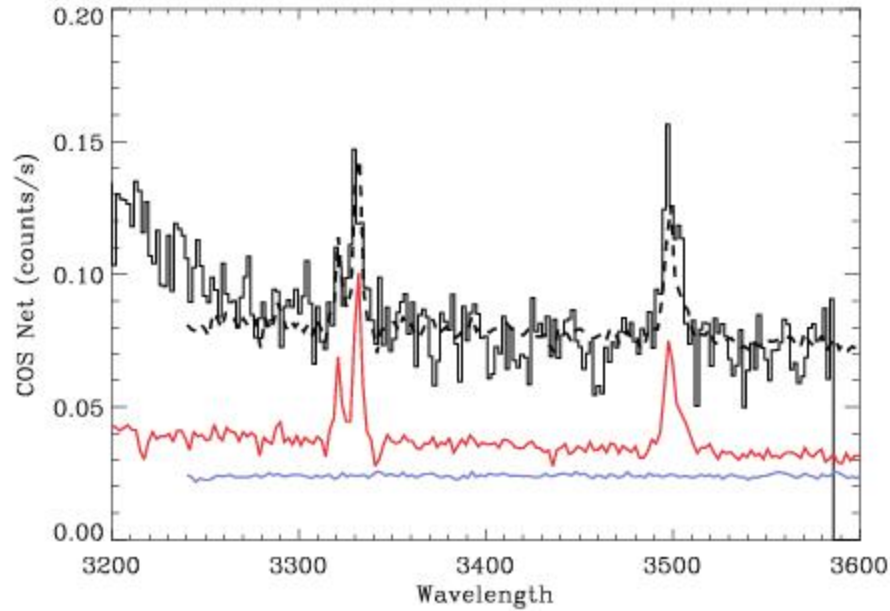
5.1.3 Second-Order Sensitivity

Because the MAMA detector is sensitive to wavelengths as short as 1150 Å, NUV spectra longward of 2300 Å are vulnerable to contamination from second-order light. To mitigate this problem the COS NUV optics were designed to provide peak reflectivities between 1600 and 2000 Å. Gratings G225M and G285M are coated with bare aluminum, which, when oxidized, has poor reflectivity below 1800 Å. After six reflections (two MgF₂ mirrors in the HST OTA and four bare-Al optics in COS) light from below 1250 Å is attenuated by 99%. Mounted directly on gratings G230L and G285M are order-sorting filters that block most light from below 1700 Å.

For the G230L grating, stripes B and C are still affected by second-order flux. When `CENWAVE=3360`, stripe B is contaminated by second-order light beyond 3200 Å. In a spectrum of the planetary nebula NGC 6833 obtained with `CENWAVE=3360`, second-order light accounts for roughly 40% of the flux at 3320 Å, and more than 50% at 3500 Å (Figure 5.4). Above 1700 Å stripe C is more sensitive to second-order light than first-order by design (Table 5.4), but on-orbit observations reveal that first-order light is detectable at a level of 5% from wavelengths greater than 3700 Å at all central-wavelength settings (COS ISR 2010-01).

In the FUV channel second-order light is present at long wavelengths ($\lambda > 2150$ Å) in spectra taken with G140L `CENWAVE=1280` FUV. These photons are rejected by the COS pipeline during processing, but they are available in the "net counts" column of the `*x1d*.fits` files.

Figure 5.4: Second-Order Light in G230L Spectrum.



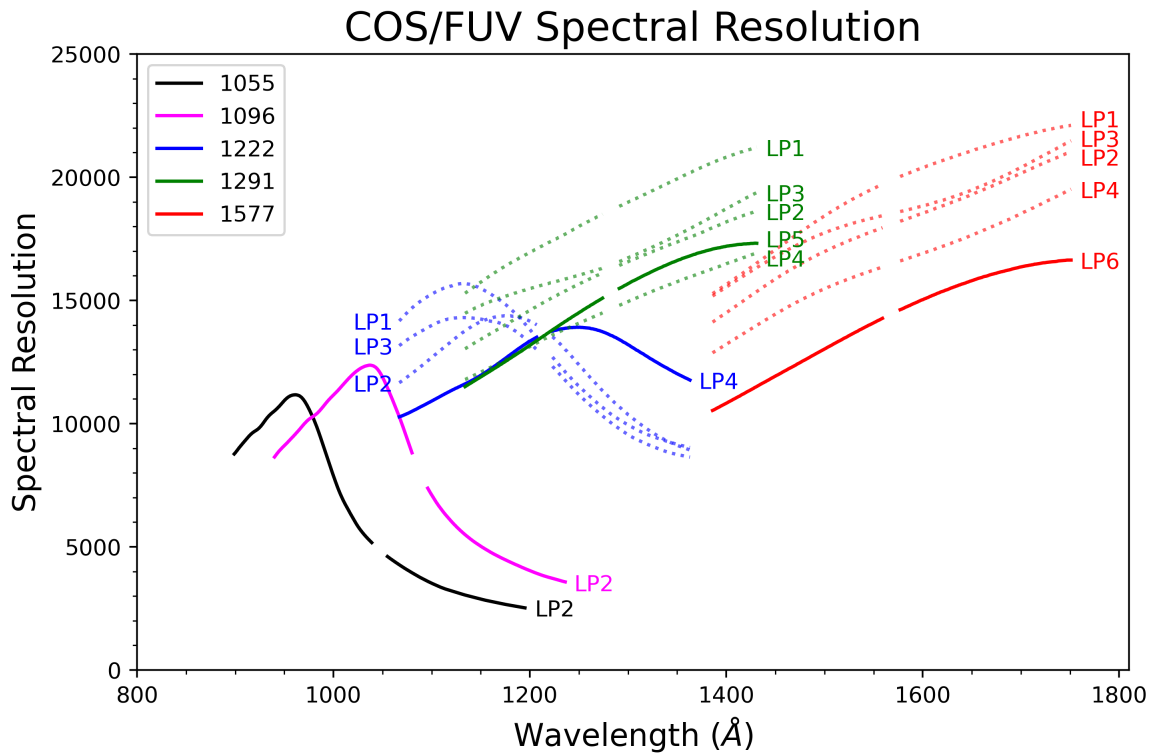
The black curve is stripe B of the G230L $CENWAVE=3360$ spectrum of NGC 6833, a planetary nebula. The blue curve is an FOS spectrum over the same wavelength range (units are Å). The red curve is an FOS spectrum of the 1600–1800 Å region, plotted as $f(2\lambda)$. The FOS spectra have been rescaled by arbitrary amounts for display purposes. The dashed black curve, a combination of the two FOS spectra, reasonably reproduces the COS spectrum.

5.1.4 Spectroscopic Resolving Power

The spectroscopic resolving power ($R = \lambda/FWHM$) of each COS grating is listed in [Table 5.1](#), and plotted as a function of wavelength for the FUV gratings in [Figure 3.7](#) and [Figure 5.5](#). These values correspond to the FWHM of the model line-spread functions (LSFs) that are described in [Section 3.3](#), which have been validated with on-orbit measurements ([COS ISR 2013-07](#), [COS ISR 2017-06](#), [COS ISR 2018-07](#)). Measurements and model predictions of the resolving power for the 1055, 1096, and 1222 Å central wavelength settings of the G130M grating are shown in [Figure 5.5](#). Adjustments made during Cycle 20 to the focus for the 1055 and 1096 central wavelength settings of the G130M grating have increased their short wavelength resolution by a factor of several over that available before Cycle 20. The quantitative values quoted in [Table 5.1](#) and shown in [Figure 5.5](#) are based on ray-trace models and actual resolution may be slightly different. However, comparison with on-orbit test data appears consistent with the predictions of these models. Users who would benefit from a more rigorous treatment of spectral resolution are referred to the ISRs listed above. An ISR describing the validation of the G130M cenwaves at LP5 is in preparation. The resolution of the G160M cenwaves at LP6 is presented in [COS ISR 2023-02](#). In all cases, users are cautioned that the uncertainties obtained from the validation tests do not support using different cenwaves in the same grating as a means of obtaining different resolutions. A comparison of data obtained with cenwaves 1055 and 1096 with archival *FUSE* data for the same target is shown in [Figure 5.6](#). Users should note, however, that for each of these modes the focus values have been set to optimize the resolution over a limited part of their wavelength range, and it will be necessary to use multiple settings to get the maximum resolution over the full FUV wavelength range ([Figure 5.5](#)).

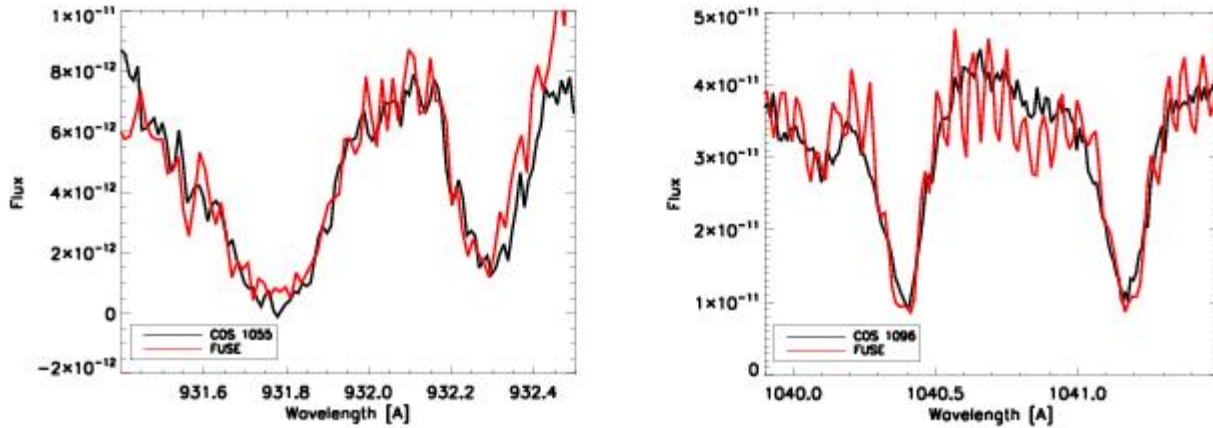
The COS LSF is not a Gaussian, so simple rules relating R to the observability of narrow spectral features may not apply. Careful modeling of the LSF may be required to determine the feasibility of an observation.

Figure 5.5: Resolving Power of Representative Cenwaves.



Spectral resolving power ($R = \lambda/\text{FWHM}$) as a function of wavelength for representative cenwaves of the medium-resolution FUV gratings. The cenwaves are shown at the Lifetime Position (LP) in which they are offered in Cycle 31. These values correspond to the FWHM of the model line-spread functions (LSFs) that are described in [Section 3.3](#). The observed spectral resolution may deviate slightly from these values, as discussed in the text. The gap in the center of each curve corresponds to the gap between the FUVB and FUYA segments.

Figure 5.6: Comparison of COS and *FUSE* Spectra.



The profiles of selected interstellar H_2 lines in the spectrum of the O3.5V binary HD 93205 as seen in COS exposures (black lines) at the 1055 (left, association Ic3n02010q, 1320 s) and 1096 (right, association Ic3n03110q, 1000 s) central wavelength settings done using the optimized focus values are compared with the 4265 s *FUSE* observation E1590103 (red lines) of the same target.

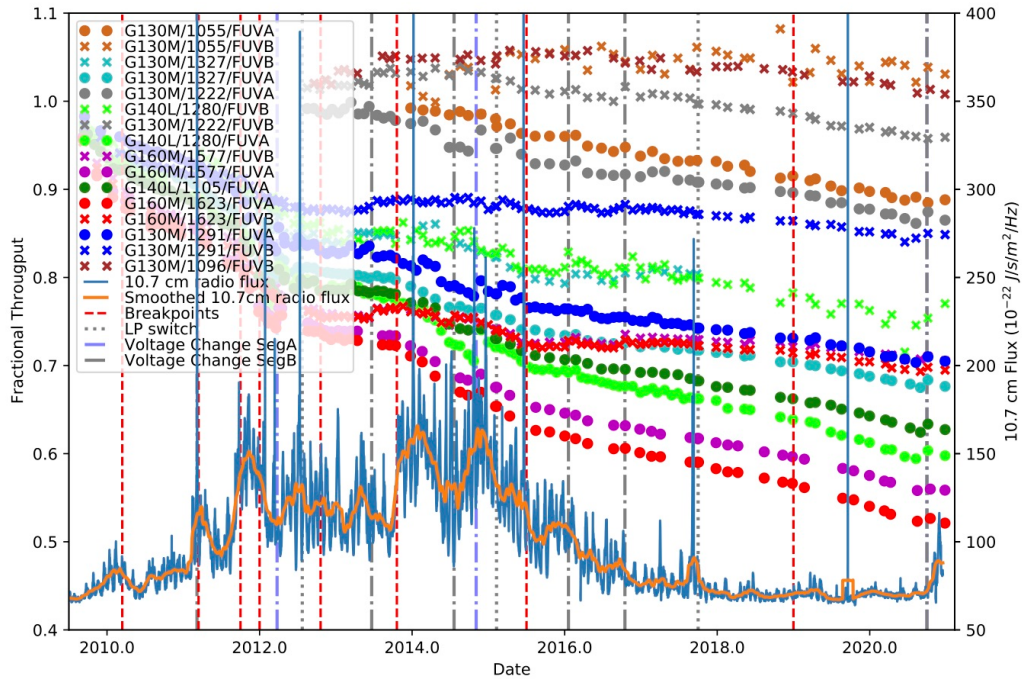
5.1.5 Time-Dependent Sensitivity Changes

Observations of HST primary spectrophotometric standard stars show that there is a significant time dependence of the COS sensitivity for some spectrographic modes. The reflectivity of the G225M and G285M NUV gratings, which are coated with bare aluminum (rather than MgF_2 over aluminum like the other gratings), showed a time-dependent degradation before launch that has continued on orbit, decreasing at a rate of $\sim 3\%$ and $\sim 10\%$ per year respectively, independent of wavelength.

The time variation of the COS FUV sensitivity is shown in [Figure 5.7](#) for different detector segments and central wavelengths. The variations appear to be correlated with Solar activity, and they are consistent with a degradation of the quantum efficiency of the CsI photocathode of the FUV detector caused by reactions with residual atmospheric atomic oxygen. As Solar activity increases, the higher UV flux from the Sun heats the Earth's upper atmosphere, inflating it and exposing the open-faced COS FUV XDL detector to increased levels of atomic oxygen. For details, see [COS ISR 2011-02](#) and the [COS website](#).

The COS data-reduction pipeline **CaICOS** includes a time-dependent sensitivity calibration, and regular monitoring of standard stars is used to update the sensitivity reference files. The [ETC](#) reflects the best estimate of current sensitivity.

Figure 5.7: Relative throughput of the COS FUV over time.

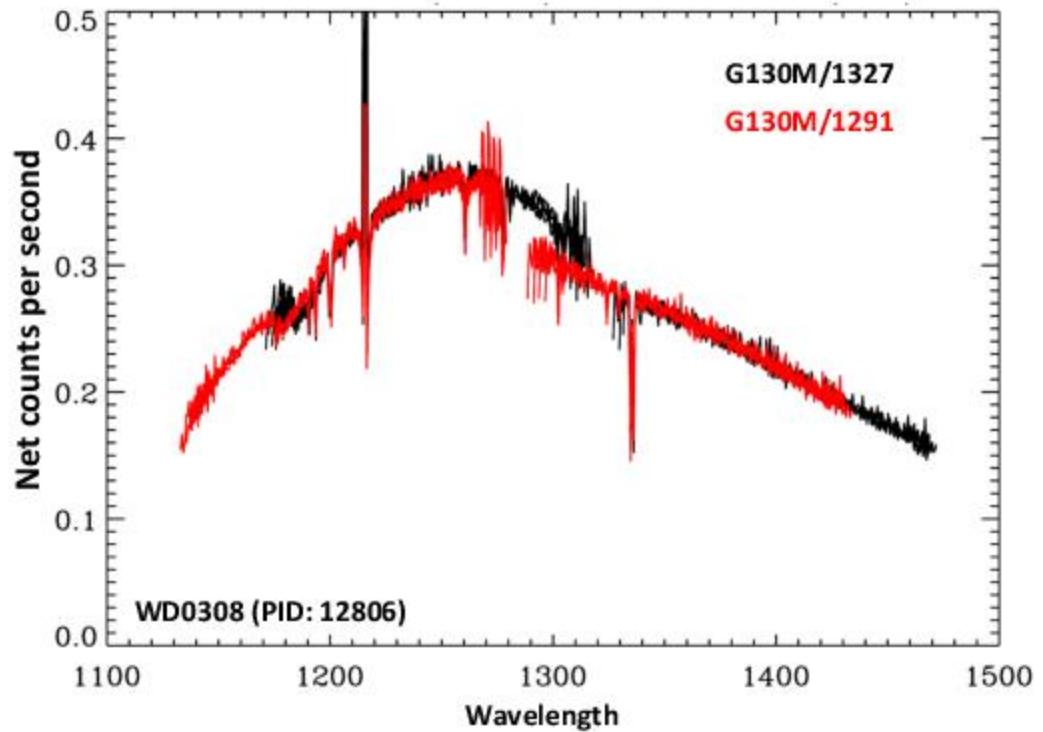


Relative throughput of the COS FUV settings as a function of time. The Solar activity, as measured by the 10.7 cm radio flux, is overplotted in blue (and a smoothed curve is shown in orange). Dashed vertical lines (red) mark the breakpoints in the time-dependent sensitivity curve. These are the times when the slope of the sensitivity decline changed. The breakpoints appear to be correlated with changes in the intensity of the 10.7 cm radio flux.

5.1.6 Dip in Sensitivity around 1180 Å

High S/N observations of standard stars have allowed us to uncover a dip in the sensitivity at about 1180 Å that is due to a Wood’s anomaly. Figure 5.8 shows the spectrum of WD0320-539 observed in Program 12086 with the G131M/1291 and G131M/1327 settings. The sensitivity dip, of ~10% of the continuum value, is seen near 1180 Å in the G130M/1291 data and near 1190 Å in the G130M/1327 data. The data shown in Figure 5.8 were taken at the original lifetime position, but this feature is also present in data taken at subsequent lifetime positions. Analysis indicates that this feature is not fixed in pixel or wavelength space, but that it moves to longer wavelengths with increasing CENWAVE settings. More details about this feature and the procedure for correcting it are available in COS ISR 2016-15.

Figure 5.8: The 1180 Å Dip.



The spectrum of WD0320-539 (from Program 12086) observed with the G130M/1291 (black) and G130M/1327 (red) settings. A dip of approximately 10% in sensitivity is seen between 1180 Å and 1190 Å.

5.1.7 Zero-Order Image

The 800 Å and 1105 Å central-wavelength settings of grating G140L place the zero-order image from the grating on Segment B of the FUV detector, violating detector count-rate screening limits, while a useful first-order spectrum falls onto Segment A. For these central wavelengths, observations can be made only in single-segment mode, with the high voltage for Segment B reduced ([Section 5.6](#)). After final alignment of COS on-orbit the zero-order image was also found to fall on Segment B for the 1230 Å setting with `FP-POS=4`. In Cycle 18, `CENWAVE=1230` was replaced with `CENWAVE=1280` to keep the zero-order image off the detector. Two-segment observations are allowed for all `FP-POS` settings with `CENWAVE=1280`.

5.1.8 Internal Scattered Light

The internal scattered-light level within COS is quite low. In ground-test measurements light scattered along the dispersion axis represents less than 1% of the nearby continuum. On orbit the COS LSF dominates the scattered light ([Chapter 3](#)). Scattering within the instrument is negligible ([COS ISR 2011-01](#)).

5.1.9 Spatial Resolution and Field of View

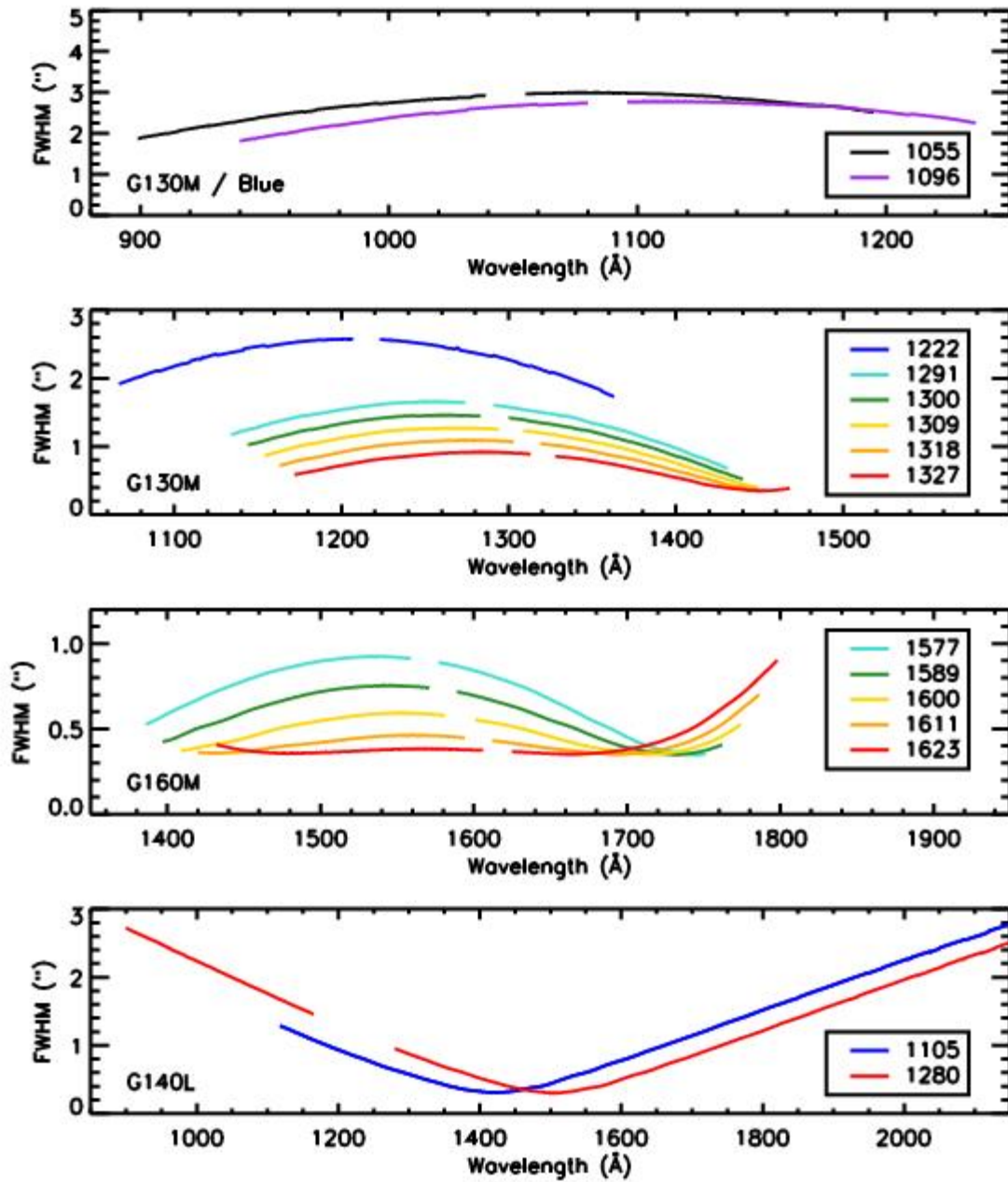
The spatial resolution of COS is affected by the mid-frequency wavefront errors (MFWFEs) via the non-Gaussian wings they introduce ([Section 3.3](#)). The NUV channel corrects for the telescope's spherical aberration, but not for the MFWFEs. For PSA observations the spatial resolution is ~ 0.07 arcsec for G185M and G230L, and 0.06 arcsec for G225M and G285M. For BOA observations, the spatial resolution is 0.29 arcsec for G185M, 0.22 arcsec for G225M, 0.24 arcsec for G285M, and 0.30 arcsec for G230L.

In the FUV the situation is more complex, because of the uncorrected astigmatism in the cross-dispersion direction. [Figure 5.9](#) and [Figure 5.10](#) show the strong dependence on wavelength of the FWHM of the cross-dispersion profiles for each of the FUV gratings at the first and the currently used lifetime positions, respectively. The spatial resolutions at different lifetime positions differ by not more than 3 pixels (0.3 arcsec). At wavelengths for which the profile width is large, the spectra of two objects separated by less than the profile width in the cross-dispersion (XD) direction would be combined.

The COS field of view is determined by the entrance apertures, which are 1.25 arcsec in radius, but the aberrated beam entering the aperture allows objects up to 2 arcsec from the center of the aperture to contribute to the recorded spectrum.

For additional information, please see "FUV Spectroscopic Performance" ([COS ISR 2010-09](#)), "NUV Spectroscopic Performance" ([COS ISR 2010-08](#)), and "The Spatial Resolution of the COS FUV Channel at Lifetime Position 4" ([COS ISR 2018-08](#)).

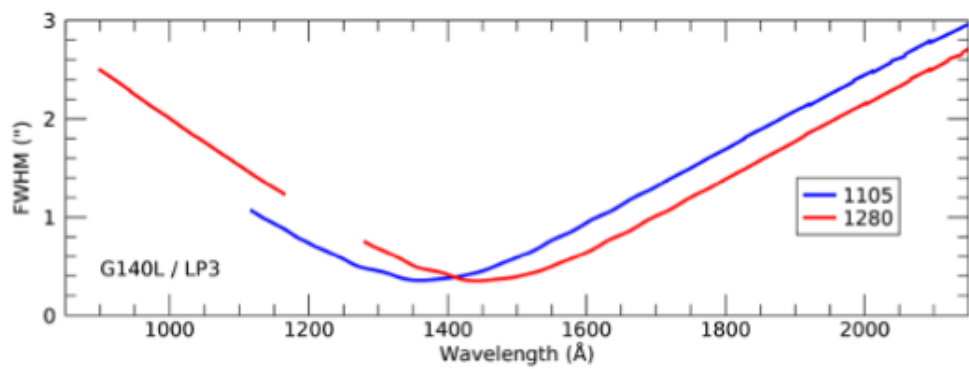
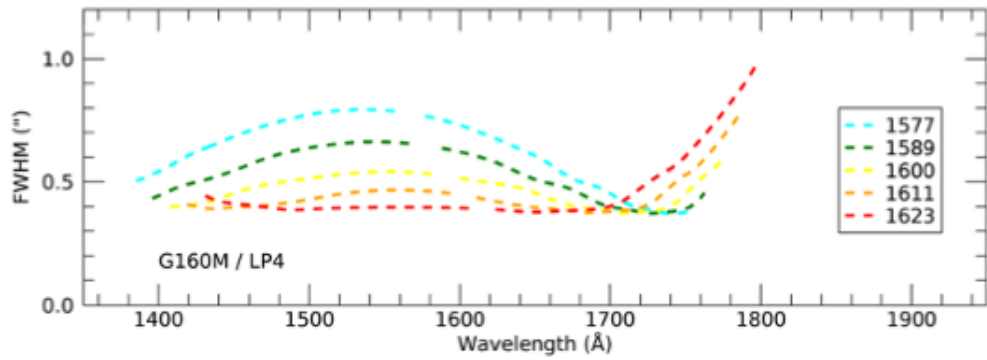
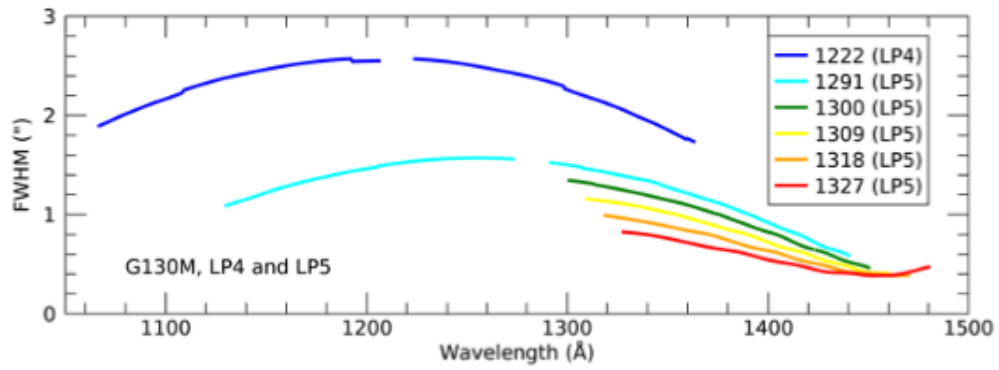
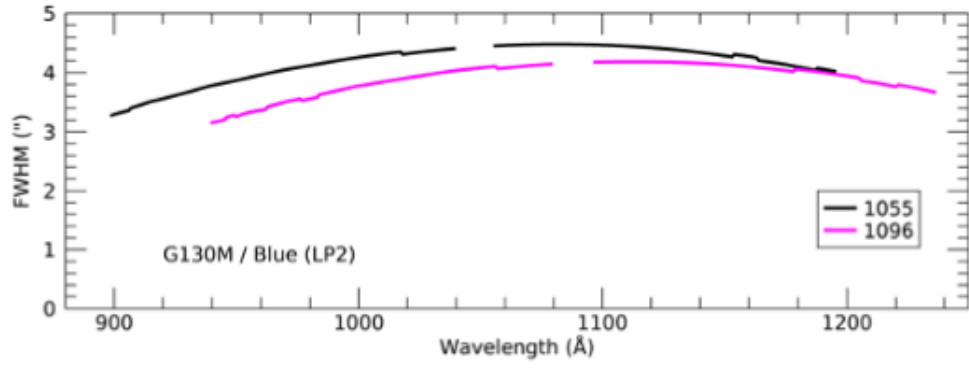
Figure 5.9: Cross-Dispersion Profile Widths for FUV Gratings at Lifetime Position One.



0

Variation in the width of the FUV spatial profile at the original lifetime position. The widths are obtained via Gaussian fits to the cross-dispersion profiles of a point source observed through the PSA. Widths are plotted as a function of wavelength for each of the central-wavelength settings.

Figure 5.10: Cross-Dispersion Profile Widths for FUV Gratings at the current lifetime positions.



Variation in the width of the FUV spatial profile at the at the current lifetime positions. The G160M cenwaves are plotted at the available LP4 configuration. The spatial profiles at LP6 have not yet been determined. The widths are obtained via Gaussian fits to the cross-dispersion profiles of a point source observed through the PSA. Widths are plotted as a function of wavelength for each of the central-wavelength settings.

5.1.10 Photometric (Flux) Precision

Based on measurements made during and since SMOV, we estimate that the absolute flux calibration of COS is accurate to about 5% in the FUV, though uncertainties may be larger at wavelengths less than 1150 Å. The relative flux calibration is good to about 2%. In the NUV the calibration is accurate up to 3% for the medium-resolution gratings, and is slightly less accurate in some parts of the G230L bandpass. Time-dependent sensitivity corrections should be accurate to about 2% ([Section 5.1.5](#)).

5.1.11 Wavelength Accuracy

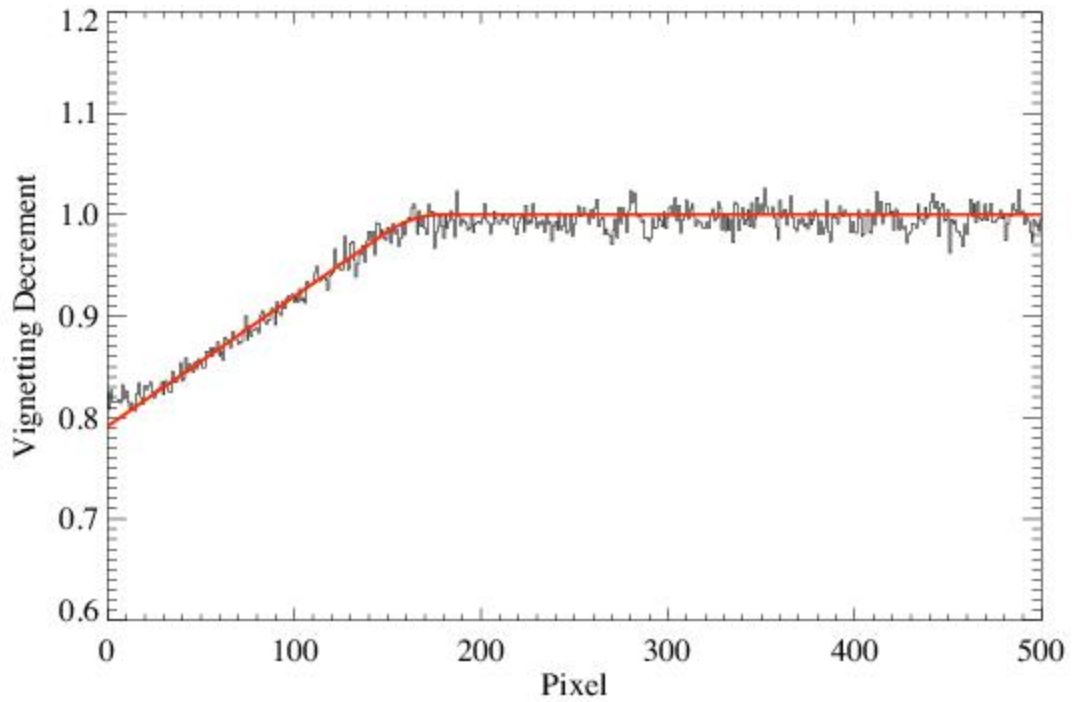
The COS medium-resolution channels are required to achieve a wavelength accuracy of 15 km s⁻¹ (resel 0.06 Å). With improvements to the FUV dispersion solutions for the M gratings, the wavelength calibration accuracy has been improved to ± 3 pixels, or half a resolution element. For G140L the requirement is 150 km s⁻¹. It is 175 km s⁻¹ for G230L. Analysis of COS data obtained on orbit suggest that these requirements are routinely met. To do so, targets must be properly centered in the desired aperture. Target acquisitions are discussed in [Chapter 8](#).

For modes where the wavelength shift determined from FUV Segment A is applied to Segment B (for example, if there are no wavelength calibration lamp lines present on FUVB) there is an additional uncertainty of up to 10 pixels that must be applied. For the G140L grating this corresponds to a wavelength accuracy of 250 km s⁻¹. Neither the wavelength solution for the BOA nor the throughput at blue wavelengths is well characterized, so we recommend that the BOA not be used for wavelengths bluer than 1200 Å.

5.1.12 Vignetting of the NUV Channel

After on-orbit alignment of COS in HST, fluxes of external targets in the PSA were found to be depressed at the short wavelength ends of the NUV stripes. For the medium-resolution gratings the reduction is about 20% at the first pixel and rises linearly to expected levels over approximately the next 160 pixels ([Figure 5.11](#)). For G230L the reduction is about 15% at the first pixel and extends about 110 pixels. (The slope is the same as in [Figure 5.11](#); it is as though the ramp were shifted by 50 pixels.) The depression is thought to be due to vignetting of the beam at the NUV camera mirrors that image the spectrum on the detector. Corrections for this vignetting are not included in either the [ETC](#) or the [CalCOS](#) data-reduction pipeline. Users are advised to consult the [COS webpages](#), where additional information will be posted as it becomes available.

Figure 5.11: Vignetting Profile for NUV M Gratings.



Vignetting profile of the medium-resolution gratings as a function of pixel location showing the linear decrease in throughput near the low-pixel edge of the NUV detector. The red line shows the best fit to the profile obtained from observations of the white dwarf G191-B2B.

5.1.13 COS Observations below 1150 Angstroms

Starting in Cycle 21 the spectral resolutions of the FUV G130M 1055 and 1096 central wavelengths settings were substantially increased above the values offered during earlier cycles and, when combined with the 1222 setting first offered in Cycle 20, this now allows resolutions of 7300 to 11,000 to be obtained at any wavelength between 900 and 1150 Å (see [Figure 5.5](#)). Users should note, however, that for each of these modes the focus values have been set to optimize the resolution over a limited part of their wavelength range, and it will be necessary to use multiple settings to get the maximum resolution over this full range. At longer wavelengths the resolutions offered by any of these settings will be inferior to those available with the original complement of G130M central wavelength settings (1291, 1300, 1309, 1318, and 1327).

Users should also note that targets that are too bright to observe at longer wavelengths with the COS G130M grating may be observable on Segment B with the 1055 and 1096 settings by turning off Segment A, which covers longer wavelengths. However, in this case there is no usable TAGFLASH wavelength calibration lamp spectrum recorded because there are no visible wavelength calibration lines that fall on Segment B. As a result, the spectrum observed on Segment B cannot be corrected for mechanism drift or zero-point offsets. *In such cases, for each CENWAVE and FP-POS position, a separate GO-wavecal exposure should be taken with Segment A "on" immediately adjacent to the Segment B science observations. This Segment A wavecal will allow the zero-point offset of the wavelength scale of Segment B to be corrected to within 10 pixels.* Several minutes are required to reconfigure the COS FUV detector each time the segments are powered on or off. However, with careful planning much of this overhead can often be hidden in the occultations or other overheads. Additional details and examples of observing scenarios can be found in [Chapter 5](#) and in [Section 9.7](#) "Examples of Orbit Estimates."

The 1280 setting of G140L also covers from below 900–1185 Å on Segment B of the FUV detector with resolution of 900–1800 over this range. In principle, the spectral format of this setting may allow observations at even shorter wavelengths; however, the throughput and resolution between 500 and 900 Å are poorly characterized. The 800 setting of G140L places the entire wavelength range from 800 to 1950 Å on Segment A of the FUV detector, and it is optimized to reduce the astigmatic height of the spectrum below about 1100 Å. This allows for decreased detector noise and correspondingly better S/N at these wavelengths compared to that attainable on segment B with the 1280 setting.

Limited amounts of data were taken using the G130M 1055 and 1096 central wavelength settings at the first lifetime position (before July 23, 2012). Calibrated data from these observations can be obtained by contacting the [HST Help Desk](#).

5.2 TIME-TAG vs. ACCUM Mode

[5.2.1 TIME-TAG Mode](#)

[5.2.2 ACCUM Mode](#)

COS exposures may be obtained in either a time-tagged photon-address mode (`TIME-TAG`), in which the position, arrival time, and pulse height (for FUV observations) of each detected photon are saved in an event stream, or in accumulation (`ACCUM`) mode, in which only the positions of the photon events are recorded.

To optimize the scientific return of COS, we recommend that all observations be performed in `TIME-TAG` mode, employ the default wavelength-calibration procedures (i.e., `TAGFLASH=YES`), and with all four FP-POS positions (See [Section 5.8](#)) of each `CENWAVE` setting for the FUV gratings. Observers who wish to employ non-optimal observing techniques must strongly justify their observing strategy in the "Description of Observations" section of their Phase I proposal. A modest reduction in observational overheads will not normally be a sufficient justification for adopting non-optimal observing techniques. Whenever possible, observers should use the recommended techniques, even if this requires requesting additional resources in their Phase I proposal.

5.2.1 TIME-TAG Mode

In `TIME-TAG` mode each photon is kept as a separate event in a list in COS memory. Each entry in that list contains the (x , y) coordinates of the photon together with the pulse height of the charge cloud generated by it (for FUV observations). Time markers are inserted in the list every 32 ms by the instrument electronics. When data are processed by the ground system arrival times are assigned to the events according to the time marker preceding the event.

COS observations should be obtained in `TIME-TAG` mode whenever possible because it provides significant opportunities for temporal sampling, exclusion of poor quality data, and, for the FUV, improved thermal correction (by tracking the stim-pulse positions as a function of time) and background removal (by using the pulse-height information). `TIME-TAG` mode should always be used for exposures that will generate count rates of 21,000 count/s or less from the entire detector (including both detector segments for the FUV). At count rates between 21,000 and 30,000 count/s, `TIME-TAG` may be used to obtain properly flux-calibrated data, but the loss of some continuous time periods within extended exposures will occur (see the discussion of the buffer time in [Section 5.4](#)). At present, `TIME-TAG` should not be used for count rates greater than 30,000 count/s. `ACCUM` mode should be used for such high count-rate targets.

We recommend that `TIME-TAG` mode always be used with `FLASH=YES` (the so-called `TAGFLASH` mode) unless circumstances prevent it (see [Section 5.7.1](#)).

Doppler Correction for `TIME-TAG` Mode

No on-board corrections are made for shifts in the spectrum due to the orbital motion of HST while in `TIME-TAG` mode. This is done later in pipeline processing.

Pulse-Height Data for `TIME-TAG`

In FUV `TIME-TAG` mode the pulse height of each photon event is recorded, along with its position and arrival time. Pulse heights are stored as 5-bit words, so their values range from 0 to 31. Post-observation pulse-height screening is useful for rejecting unwanted background events, and can often improve the S/N ratio in the extracted science spectrum. Pulse-height information is not provided by the NUV detector.

5.2.2 `ACCUM` Mode

In `ACCUM` mode an image of the detector is stored in a 16-bit memory buffer. As each photon arrives from the detector the location in the buffer at coordinates (x, y) is incremented by one. Each location can hold at most 65,535 counts; the next event will cause the value to roll over to zero. To conserve memory only a $16,384 \times 128$ region of each segment is stored, as well as the regions around each stim pulse. Timing and pulse-height information are not saved, preventing the application of the data-correction techniques available in `TIME-TAG` mode. For example, no walk correction is possible, so there could be distortions in the wavelength scale due to gain variations.

`ACCUM` mode is designed for bright targets whose high count rates would fill the on-board buffer memory too rapidly if the data were taken in `TIME-TAG` mode. In some instances one may observe a relatively bright object in `TIME-TAG` mode by using the BOA instead of the PSA, but the BOA degrades the spectroscopic resolution. The BOA is offered as an available-but-unsupported mode (see [Section 5.13](#) for further discussion of BOA usage for FUV science observations). Observers wishing to use `ACCUM` mode will be asked to justify doing so when submitting their Phase II program.

Observing Efficiencies with `ACCUM`

FUV `ACCUM` images do not include the entire detector. To conserve memory photons are collected only from the stim regions and that portion of the detector actually illuminated by the target (1/8 of the full detector area, or 128 pixels in y). Each FUV `ACCUM` image fills one-half of the total COS memory, so it is possible to acquire two FUV images before dumping the on-board buffer.

NUV `ACCUM` images cover the entire detector. Because they are smaller, up to nine of them can be stored in the memory buffer. Unlike `TIME-TAG` mode, no data may be acquired during an `ACCUM` readout. NUV `ACCUM` mode is thus most efficient when repeated identical observations are stored in memory, then read out all at once. (Within APT, the [Astronomer's Proposal Tool](#), one may easily schedule multiple iterations of an exposure using the `Number_of_Iterations` parameter.)

Doppler Correction for `ACCUM` Mode

In `ACCUM` mode, the COS flight software adjusts the pixel coordinates of detected events to correct for the orbital motion of HST. The correction (always by an integer number of pixels) is updated whenever HST's velocity with respect to the target changes enough to shift the spectrum by an additional pixel. This is done via a small table, computed on the ground, that lists the time of each pixel shift based on the orbital motion and the dispersion of the grating in use.

Note that `ACCUM` mode exposures longer than 900 s that use the G130M or G160M gratings may blur the FUV spectra by 1 to 2 pixels (about 1/6 to 1/3 of a resolution element) since shifts are performed in pixel, not wavelength, space.

Pulse-Height Distribution Data for ACCUM Mode Observations

Some pulse-height information is available for FUV ACCUM observations. A pulse-height histogram, consisting of 256 bins (128 bins for each detector segment) of 32 bits each, is dumped for every ACCUM mode image obtained with the FUV detector. (In ACCUM mode individual pulse heights are stored as 7-bit words, so their values range from 0 to 127, whereas in TIME-TAG mode pulse heights are 5-bit words.) Pulse-height data are not provided for NUV exposures.

Reducing ACCUM data in the COS Pipeline

The CalCOS pipeline does support ACCUM data, but the extraction uses the older "BOXCAR" method, while TIME-TAG uses "TWOZONE." The use of BOXCAR means that there will be more "bad" columns than might be expected when compared to a TWOZONE extraction of a TIME-TAG COS spectrum at the same location/cenwave.

5.3 Valid Exposure Times

The minimum COS exposure duration is 0.1 s (but `FLASH=YES TIME-TAG` exposures impose a longer minimum; see [Section 5.7.1](#)), and this is enforced by APT. The maximum is 6500 s. Between these extremes COS exposure times must be integer multiples of 0.1 s. If the observer specifies an exposure time that is not a multiple of 0.1 s, its value is rounded down to the next lower integer multiple of 0.1 s, (or set to 0.1 s if a smaller value is specified). Exposure times larger than about 3000 s are normally appropriate only for visits with the Continuous Viewing Zone (which is a special requirement that must be requested and justified in the Phase I proposal) because the visibility period of a typical orbit is ~50 minutes. See the [HST Primer](#) for information about HST's orbit and visibility periods.

For `TARGET=WAVE` exposures, `DEF` (default) must be entered as the exposure time. The value appropriate for the optical configuration will be chosen from a table established at STScI for best performance. At present `TARGET=WAVE` flash durations are identical to those given in [Table 5.2](#).

Table 5.2: TAGFLASH Exposure Durations.

Grating	Central Wavelength (Å)	Flash Duration (s)	Grating	Central Wavelength (Å)	Flash Duration (s)
G130M	1055	142	G225M (cont.)	2339	12
	1096	52		2357	12
	1222	52		2373	22
	all others	12		2390	7
G160M	all	12		2410	7
G140L	all	7	G285M	2617	12
G185M	1786	12		2637	12
	1817	12		2657	7
	1835	12		2676	22
	1850	22		2695	22
	1864	32		2709	12
	1882	17		2719	7
	1890	12		2739	7
	1900	22		2850	22
	1913	17		2952	7
	1921	12		2979	17
	1941	12		2996	17

	1953	17		3018	22
	1971	17		3035	27
	1986	12		3057	32
	2010	12		3074	32
G225M	2186	7		3094	32
	2217	12	G230L	2635	7
	2233	7		2950	7
	2250	22		3000	7
	2268	12		3360	12
	2283	12	MIRRORA	...	7
	2306	12	MIRRORB	...	12
	2325	12			

5.4 Estimating the BUFFER-TIME in TIME-TAG Mode

Introduction to the BUFFER-TIME

COS maintains two on-board data buffers, each with a capacity of 9 MBytes (2.35×10^6 counts). For every COS TIME-TAG calculation, the Exposure Time Calculator (ETC) reports the time it takes to fill the buffer based on the total expected counts, including those from the source, the sky, and the detector dark count. The calculation includes the STIM pulses for the FUV detector and accounts for the instrument quantum efficiency and dead time. The "Buffer Fill Time" reported is approximately 2.3×10^6 divided by the total count-rate.

The BUFFER-TIME is a keyword in APT that COS uses to establish the pattern and timing of memory dumps during a TIME-TAG exposure. The exposure counts are recorded on the first data buffer for a period corresponding to BUFFER-TIME, at the end of which the recording switches to the second data buffer while the first buffer is read out. This pattern is repeated after every BUFFER-TIME period to the end of the exposure. It takes 110 seconds to empty a COS data buffer.

If the BUFFER-TIME is set to too long a period and the buffer fills before the input switches to the other buffer, then the subsequently-arriving photons will be lost, leaving a gap in the data. The pipeline will correct the exposure times for any such gaps, and the flux calibrations will be correct, but the overall S/N will be lower than expected. If the BUFFER-TIME is set to too short a period, the input will switch to the second buffer before the first is full. No data will be lost, but there are impacts on spacecraft resources, which could preclude other activities such as parallel or internal calibration observations, since HST can process science data readouts from only one instrument at a time. For bright targets, using a shorter BUFFER-TIME may lower the overheads and therefore be advantageous by providing more on-source exposure time.

The BUFFER-TIME for each exposure should be chosen carefully based on all these factors. The recommended methods for determining the BUFFER-TIME, based on the exposure time (EXP-TIME) and the Buffer Fill Time reported by the COS ETC, are discussed below.

For targets with brightness levels which may vary on short timescales, including observations which require the Safe Target Offset Procedure (STOP; see [Section 10.5](#)), the BUFFER-TIME should be set to reflect the brightest expected state which is deemed still safe to observe, rather than the more-likely scenario of a quiescent observation.

COS TIME-TAG Handling

COS reads out only the fraction of the buffer that is expected to contain recorded events. This fraction is based on the specified BUFFER-TIME, and exposure time, EXP-TIME.

- If $\text{BUFFER-TIME} > \text{EXP-TIME}$, only a fraction $\text{EXP-TIME}/\text{BUFFER-TIME}$ of the buffer will be read out.
- If $\text{BUFFER-TIME} < \text{EXP-TIME}$, there will be multiple dumps. At the end of the exposure, for the last dump, time will be allocated for COS to read only the fraction of the buffer expected to contain data. The full buffer will be read out for all other dumps occurring during the exposure.

This approach increases observing efficiency by avoiding the allocation of more time than necessary for the buffer dump at the end of the exposure. It also implies that more caution is required in specifying the BUFFER-TIME in the Phase II proposal - if the actual count-rate is greater than expected, some events that were recorded in the buffer memory will never be read out.

Users familiar with the `TIME-TAG` mode of the STIS instrument will note that the COS buffer management described above differs from that of STIS. At the end of a STIS exposure, the entire buffer is read out, regardless of the buffer time set, or the number of counts expected.

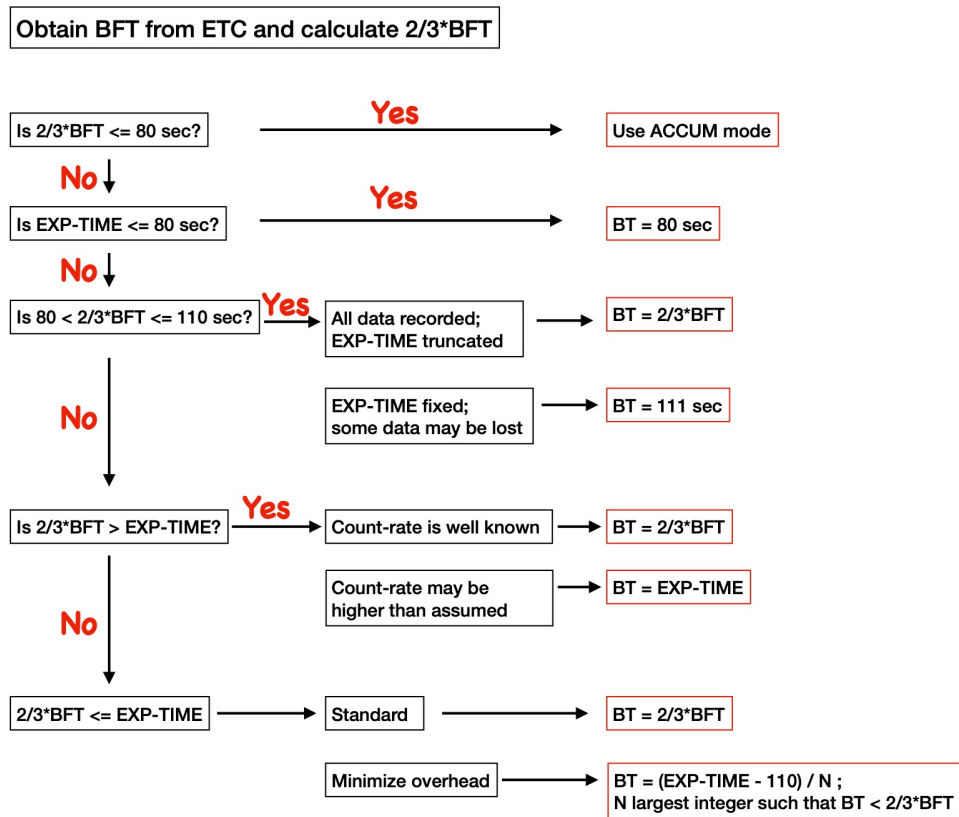
The guidelines in the following subsection are designed to help COS users maximize observing efficiency and avoid data loss.

Choosing the `BUFFER-TIME`

It is strongly recommended that the COS ETC be used with the most reliable input spectrum to complete an accurate Buffer Fill Time (BFT, henceforth).

If the count-rate is underestimated, the BFT will be correspondingly overestimated, and data will be lost. To prevent against this, the `BUFFER-TIME` (BT, henceforth), which is the value entered in APT, should be set equal to $2/3 \times \text{BFT}$. While this will be sufficient for many COS observations, there are several circumstances where a different value of BT may be required, or preferred. These circumstances are discussed below, and [Figure 5.12](#) is a flow chart that provides a guide to selecting the appropriate BT for different values of the BFT and `EXP-TIME`.

Figure 5.12: Flow chart for guiding the selection of `BUFFER-TIME` (BT) based on the values of the exposure time (`EXP-TIME`), and the Buffer Fill Time (BFT) returned by the ETC. For observations using the keyword `FP-POS=ALL`, `EXP-TIME` is the exposure time per `FP-POS` position. Do not set `BT > 20,000` seconds.



1. `BFT < 120` sec; $(2/3 \times \text{BFT} < 80)$ sec).

The minimum `BUFFER-TIME` is 80 seconds. The source is too bright for `TIME-TAG`, and should be observed in `ACCUM` mode.

2. `EXP-TIME < 80` sec.

If the ETC reported BFT is 120 seconds or longer, then set `BUFFER-TIME` = 80 seconds. This ensures the whole buffer will be read, so if the target is brighter than expected, all counts will be recorded. With a longer buffer time only a fraction of it would be read (see `COS TIME-TAG` handling section above).

3. BFT is between 120 sec and 165 sec; $(2/3 \times \text{BFT}$ is between 80 sec and 110 sec).

It takes 110 seconds to empty a COS data buffer. If the count-rate exceeds 21,000 counts sec⁻¹, and the BUFFER-TIME is set to 110 seconds, then the second data buffer will be filled before the first buffer has been completely read out. In this situation, the two options are to shorten the exposure, or accept gaps in the recorded data stream. In either case **CalCOS** will compute the actual exposure time correctly, but the S/N will be limited by 21,000 counts sec⁻¹.

Option A: Use the standard BUFFER-TIME = 2/3 × BFT. The APT will issue a warning and truncate EXP-TIME at 2 × BUFFER-TIME to ensure that all data are recorded.

Option B: Set BUFFER-TIME = 111 seconds. Some fraction of the data during each BUFFER-TIME interval will be lost, but the exposure time will not be truncated.

The remaining cases assume additionally that BFT is longer than 165 seconds, i.e., 2/3 × BFT is longer than 110 seconds.

4. 2/3 × BFT > EXP-TIME.

In this case, the time allocated to read the buffer dump is proportional to the number of events expected in the buffer. If there is a concern that the count-rate may be even higher than the 50% margin of error that the 2/3 factor accounts for, then set BUFFER-TIME = EXP-TIME. This will ensure that the entire buffer is read out at the end of the exposure time (see COS TIME-TAG Handling section above).

Note that the combined global dark rate for both segments has exceeded 90 counts sec⁻¹ and to ensure all detected events are dumped from the COS buffer, even for very faint sources, the BUFFER-TIME must not exceed 20,000 seconds.

5. Minimizing Overhead when 2/3 × BFT < EXP-TIME.

The value of BUFFER-TIME can be specified such that there are only between 100 and 110 seconds of exposure left for the last buffer dump.

$n = (\text{EXP-TIME} - 110) / (2/3 \times \text{BFT})$ rounded to the next highest integer
BUFFER-TIME = (EXP-TIME - 110) / n, rounded up to whole seconds.

Example: EXP-TIME = 2300 sec, BFT = 1050 sec.

$n = (2300 - 110) / (2/3 \times 1050) = 3.13$ rounded up = 4.


BUFFER-TIME = (2300 - 110)/4 = 547.5 sec rounded up = 548 sec.

After four buffer reads, there will be 108 seconds left in the exposure, and the last buffer read will have a lower overhead and allow the following exposure to start sooner.

Note, however, that the BUFFER-TIME specified should be 111 seconds or longer. Otherwise the exposure time will be truncated to 2 × BUFFER-TIME.

6. BUFFER-TIME and AUTO-ADJUST

APT allows individual exposures (or groups of exposures) to be adjusted automatically to fill the orbits. If this is used, then the BUFFER-TIME value should be set after obtaining the final exposure times.

 *The software and parameters that control dumps of the data buffer have been designed to avoid any loss of data from an observation. The duration and timing of data dumps depend on several factors, and observers are urged to experiment with [APT](#) to optimize the efficiency of their observations.*

5.5 Spanning the Gap with Multiple CENWAVE Settings

COS spectra exhibit wavelength gaps due to the physical layout of the detectors and the optics (see [4.1 The FUV XDL Detector](#)). The FUV detector consists of two segments whose active areas are separated by a gap approximately 9 mm wide. The optical image of the spectrum is continuous across the segments, but the wavelengths that fall in the gap (which depend on the CENWAVE selected) are not recorded. These wavelengths can be brought onto the active area of the detector by choosing one of the alternate central-wavelength settings listed in [Table 5.3](#). For the FUV M gratings, the gap (14–18 Å) is about twice the size of the difference in central wavelength shifts (9 Å). To span it we recommend obtaining exposures at two or more FP-POS positions at each of two non-consecutive CENWAVE settings. For the G140L grating, all CENWAVES offer broad spectral coverage, and users will likely find that they can meet their needs with just one setting. If necessary, the gap in CENWAVE 1280 can be filled with data obtained at one of the other two settings. If users would like to fill the gap in CENWAVE 1291, users will need to include CENWAVE 1222.

Table 5.3: Wavelength Ranges for FUV Gratings for FP-POS=3.

Grating	Central wavelength setting (Å) ¹	Recorded wavelengths ²	
		Segment B	Segment A
G130M	1055	899-1040	1055-1196
	1096	940-1080	1096-1236
	1222	1067-1207	1223-1363
	1291	1134-1274	1291-1431
	1300	(1144-1283) ³	1300-1441
	1309	(1154-1294) ³	1309-1450
	1318	(1163-1303) ³	1319-1460
	1327	(1172-1313) ³	1328-1469
G160M	1533	1342-1515	1533-1707
	1577	1386-1559	1577-1751
	1589	1397-1571	1589-1762
	1600	1409-1581	1601-1774
	1611	1420-1594	1612-1786
	1623	1432-1606	1625-1798
G140L	800	HV OFF	815-1948
	1105	HV OFF	1118-2251 ⁴

1280	<900-1165	1280-2391 ⁴
------	-----------	------------------------

¹ The central wavelength is (approximately) the shortest wavelength recorded on Segment A.

² All wavelength ranges quoted here are approximate, due to uncertainties in the position of the OSM1 mechanism.

³ Segment B of this cenwave is not allowed by the COS 2025 policy.

⁴ G140L spectra are flux calibrated up to 2150 Å. At longer wavelengths, second-order light may be present (see [Section 5.1.3](#)).

For the NUV channel dispersed light from the gratings is imaged onto the detector by three camera mirrors resulting in three non-contiguous spectral stripes being recorded at once. The gaps between the stripes are approximately 64 Å for the G185M and G225M gratings, 74 Å for G285M, and 700 Å for G230L ([Table 5.4](#)). To acquire a complete medium-resolution spectrum requires six settings with G185M, six with G225M, and eight with G285M ([Table 5.5](#)). A full spectrum with G230L requires three CENWAVE settings ([Table 5.4](#)). Such a complete spectrum can probably be acquired more efficiently with STIS, but COS may be a better choice when a limited number of specific wavelengths is desired.

Table 5.4: Wavelength Ranges for NUV Gratings for FP-POS=3.

Grating	Central wavelength setting (Å) ¹	Recorded wavelengths		
		Stripe A	Stripe B	Stripe C
G185M	1786	1670-1705	1769-1804	1868-1903
	1817	1701-1736	1800-1835	1899-1934
	1835	1719-1754	1818-1853	1916-1951
	1850	1734-1769	1833-1868	1931-1966
	1864	1748-1783	1847-1882	1945-1980
	1882	1766-1801	1865-1900	1964-1999
	1890	1774-1809	1872-1907	1971-2006
	1900	1783-1818	1882-1917	1981-2016
	1913	1796-1831	1895-1930	1993-2028
	1921	1804-1839	1903-1938	2002-2037
	1941	1825-1860	1924-1959	2023-2058
	1953	1837-1872	1936-1971	2034-2069
	1971	1854-1889	1953-1988	2052-2087
	1986	1870-1905	1969-2004	2068-2103
	2010	1894-1929	1993-2028	2092-2127

G225M	2186	2070-2105	2169-2204	2268-2303
	2217	2101-2136	2200-2235	2299-2334
	2233	2117-2152	2215-2250	2314-2349
	2250	2134-2169	2233-2268	2332-2367
	2268	2152-2187	2251-2286	2350-2385
	2283	2167-2202	2266-2301	2364-2399
	2306	2190-2225	2288-2323	2387-2422
	2325	2208-2243	2307-2342	2406-2441
	2339	2223-2258	2322-2357	2421-2456
	2357	2241-2276	2340-2375	2439-2474
	2373	2256-2291	2355-2390	2454-2489
	2390	2274-2309	2373-2408	2472-2507
	2410	2294-2329	2393-2428	2492-2527
G285M	2617	2480-2521	2596-2637	2711-2752
	2637	2500-2541	2616-2657	2731-2772
	2657	2520-2561	2636-2677	2751-2792
	2676	2539-2580	2655-2696	2770-2811
	2695	2558-2599	2674-2715	2789-2830
	2709	2572-2613	2688-2729	2803-2844
	2719	2582-2623	2698-2739	2813-2854
	2739	2602-2643	2718-2763	2837-2878
	2850	2714-2755	2829-2870	2945-2986
	2952	2815-2856	2931-2972	3046-3087
	2979	2842-2883	2958-2999	3073-3114
	2996	2859-2900	2975-3016	3090-3131
	3018	2881-2922	2997-3038	3112-3153
	3035	2898-2939	3014-3055	3129-3170
	3057	2920-2961	3036-3077	3151-3192
	3074	2937-2978	3053-3094	3168-3209
3094	2957-2998	3073-3114	3188-3229	

G230L	2635	1334-1733 ²	2435-2834	1768-1967 ³
	2950	1650-2050	2750-3150	1900-2100 ³
	3000	1700-2100	2800-3200	1950-2150 ³
	3360	2059-2458 ⁴	3161-3560 ⁵	2164-2361 ³

¹ The central wavelength setting corresponds to the approximate midpoint of stripe B.

² For central wavelength 2635 Å, the stripe A wavelengths are listed for completeness only (and in case a bright emission line falls onto the detector). The NUV detector's sensitivity at these wavelengths is extremely low. To obtain a low-resolution spectrum at wavelengths below ~1700 Å, we recommend the FUV grating G140L.

³ The values in shaded cells are wavelength ranges observed in second order light. Their dispersion is twice that of the first-order spectrum. First-order flux, from wavelengths twice those of the listed range, will be present at the ~5% level.

⁴ Lyman α may be present in second order light.

⁵ Longward of 3200 Å, second-order light may be present. At these wavelengths, the flux calibration applied by CalCOS is unreliable (Section 5.1.3).

Table 5.5: COS modes required to obtain a complete medium-resolution NUV spectrum.

Grating	Central Wavelength (Å)	Stripe Wavelength Ranges (Å)			Cumulative Wavebands (Å)		
G185M	1786	1670-1705	1769-1804	1868-1903	1670-1705	1769-1804	1868-1903
	1817	1701-1736	1800-1835	1899-1934	1670-1736	1769-1835	1868-1934
	1850	1734-1769	1833-1868	1931-1966	1670-1966		
	1953	1837-1872	1936-1971	2034-2069	1670-1971	2034-2069	
	1986	1870-1905	1969-2004	2068-2103	1670-2004	2034-2103	
	1921	1804-1839	1903-1938	2002-2037	1670-2103		

G225M	2217	2101- 2136	2200- 2235	2299- 2334	1670- 2136	2200- 2235	2299- 2334
	2250	2134- 2169	2233- 2268	2332- 2367	1670- 2169	2200- 2268	2299- 2367
	2283	2167- 2202	2266- 2301	2364- 2399	1670- 2399		
	2410	2294- 2329	2394- 2428	2492- 2527	1670- 2428	2492- 2527	
	2339	2223- 2258	2322- 2357	2421- 2456	1670- 2456	2492- 2527	
	2373	2256- 2291	2355- 2390	2454- 2489	1670- 2489	2492- 2527	
G285M	2617	2480- 2521	2596- 2637	2711- 2752	1670- 2527	2596- 2637	2711- 2752
	2657	2520- 2561	2636- 2677	2751- 2792	1670- 2561	2596- 2677	2711- 2792
	2695	2558- 2599	2674- 2715	2789- 2830	1670- 2830		
	2952	2815- 2856	2931- 2972	3046- 3087	1670- 2856	2931- 2972	3046- 3087
	2979	2842- 2883	2958- 2999	3073- 3114	1670- 2883	2931- 2999	3046- 3114
	3018	2881- 2922	2997- 3038	3112- 3153	1670- 2922	2931- 3038	3046- 3153
	3057	2920- 2961	3036- 3077	3151- 3192	1670- 3192		
	3094	2957- 2998	3073- 3114	3188- 3229	1670- 3229		

This table gives the NUV medium-resolution grating and central wavelength combinations that are needed to create a continuous COS NUV spectrum from 1670 Å to 3229 Å. The Stripe Wavelength Ranges columns give the wavelength ranges covered by each of the three NUV stripes, using the nominal $FP-POS=3$ setting, corresponding to each of the grating and central wavelength values on the left. The Cumulative Wavebands columns give the cumulative wavebands covered by the current setting, and all the grating and central wavelength settings above it.

5.6 FUV Single-Segment Observations

The FUV detector segments are operated and read out independently. For all FUV gratings, Segment A detects the longer-wavelength light and Segment B the shorter wavelengths. Normally both segments are used for a science exposure, but there are circumstances in which operating with one detector segment at the nominal high voltage and the other effectively turned off may be beneficial. The `SEGMENT` optional parameter allows this choice. STScI strongly recommends use of both segments (the default for all but the G140L 800 Å and 1105 Å settings as well as G130M cenwaves that are impacted by the COS 2025 policy; see [Section 5.12](#)) unless special circumstances exist. Such circumstances include:

- Sources with unusual spectral energy distributions at FUV wavelengths (bright emission lines or rapidly increasing/decreasing continuum slopes), for which the count rate on one detector segment exceeds the bright-object protection limit, while the other segment is safe for observing. In some cases, this problem may be mitigated by adjusting the central wavelength or `FP-POS` setting.
- Sources for which the count rate on one detector segment is high but safe, while the other segment has a relatively low count rate. If the science to be done were on the low count-rate segment, operating just that segment would reduce data losses due to dead-time effects and increase the S/N of the resulting spectrum.

The optional parameter `SEGMENT` specifies which segment of the FUV detector to use for an observation. A value of `BOTH` will activate both segments. This is the default setting. If `SEGMENT=A` is selected, only Segment A of the detector will be activated for photon detection, and the spectrum will contain data from only the long-wavelength half of the detector. If `SEGMENT=B` is selected, only the short-wavelength Segment B of the detector will be activated and used to generate data. Wavelength and flat-field calibration procedures remain the same for a particular segment whether or not the other segment is operating. Observers should take care to set `SEGMENT` appropriately for the G130M/1055, 1096, and 1222 `CENWAVE` settings.

If any of the modes are specified for which Segment B spectroscopy is not permitted, then the value defaults to `SEGMENT=A`. Switching from two-segment to single-segment operation (or back again) incurs a substantial overhead time; see [Table 9.5](#).

5.7 Internal Wavelength Calibration Exposures

- 5.7.1 Concurrent Wavelength Calibration with TAGFLASH
- 5.7.2 AUTO Wavecal (when TAGFLASH is not used)
- 5.7.3 GO Wavecal (User-Specified)
- 5.7.4 No-Cal Wavecal
- 5.7.5 Inserting Wavecal in Observations with G130M/1055 and G130M/1096, SEGMENT=B
- 5.7.6 SPLIT Wavecal (default non-concurrent wavelength calibration at LP6)

Four types of internal wavelength calibration exposures may be inserted in the observation sequence by the scheduling system or by the observer:

1. FLASH=YES (so-called TAGFLASH) lamp flashes (TIME-TAG observing with the PSA at LP1-LP5),
2. AUTO wavecal,
3. user-specified GO wavecal, and
4. SPLIT wavecal (TIME-TAG observing with the PSA at LP6).

Note that *all* wavelength-calibration exposures are taken in TIME-TAG mode. Wavelength calibration exposure overheads are higher when the BOA is used for science observations or when science observations are performed at LP6 because the aperture mechanism must be moved to place the wavecal spectrum at the appropriate location on the detector.

While it is possible to suppress the taking of any wavelength-calibration spectra, doing so significantly lessens the archival quality of COS data and must be justified on a case-by-case basis.

5.7.1 Concurrent Wavelength Calibration with TAGFLASH

The optional parameter FLASH indicates whether or not to "flash" the wavelength calibration lamp during TIME-TAG exposures utilizing the PSA. These flashes provide data used by the CalCOS pipeline to compensate for drifts of the Optics Select Mechanisms. In this mode, when the external shutter is open to observe an external target, the wavecal lamp is turned on briefly at the beginning of, and at intervals throughout, the exposure. Light from the science target and the internal wavelength calibration source is recorded simultaneously on different portions of the detector. Other than the flash at the start, the timing of flashes is determined by the elapsed time since the last OSM motion. As a result flashes may occur at different times in different exposures. The grating-dependent flash durations (Table 5.2) and the flash intervals are defined and updated as necessary by STScI. Observers may not specify either flash duration or interval. (Details of TAGFLASH execution are presented in COS ISR 2011-04.) When flashing is enabled the exposure time must be at least as long as a single flash. Science exposures shorter than the flash durations listed in Table 5.2 may be obtained by setting FLASH=NO, in which case a wavecal exposure will automatically be inserted after the science exposure.

TIME-TAG sequences with FLASH=YES provide the highest on-target exposure time, as no on-target time is lost to wavelength-calibration exposures. Therefore, we strongly recommend use of the optional parameter FLASH=YES with all TIME-TAG observations through the PSA when possible. (Since FLASH=YES is the default for TIME-TAG spectroscopic exposures, the observer need not specify it.) FLASH=YES may not be specified for ACCUM mode or when the BOA is selected. Users should be aware that the BOA is not well-calibrated at wavelengths below 1200 Å. FLASH=YES observations are not permitted for spectral elements supported at LP6 (Section 5.12). SPLIT wavecals are automatically inserted for spectrographic science exposures at LP6 (Section 5.7.6).

5.7.2 AUTO Wavecals (when TAGFLASH is not used)

For ACCUM, BOA, or FLASH=NO, TIME-TAG exposures, a separate wavelength calibration exposure will be automatically scheduled by the APT for each set of external spectrographic science exposures using the same spectral element, central wavelength, and FP-POS value. These AUTO wavecals are always obtained in TIME-TAG mode with the external shutter closed. This automatic wavelength calibration exposure will be added before the first associated science exposure, and after each subsequent science exposure if more than 40 minutes of visibility time has elapsed since the previous wavelength calibration exposure and if the same spectrograph set-up has been in use over that time. The calibration exposure will often use some science target orbital visibility. The calibration lamp configuration and exposure time will be based on the grating and central wavelength of the science exposure. Utilization of a GO wavecal (see below) resets the 40 minute interval timer. Insertion of a FLASH=YES exposure in the timeline does not affect the 40-minute clock.

AUTO wavecals may not ordinarily be turned off by the observer. If there is a science requirement to turn off AUTO wavecals, specific permission must be sought from the STScI Contact Scientist.

FLASH=NO observations will be less efficient than FLASH=YES observations in terms of on-target utilization of orbital visibility, and in the quality of their wavelength calibration, due to possible OSM residual motions.

AUTO wavecals are not permitted for spectral elements supported at LP6 (Section 5.12). SPLIT wavecals are automatically inserted for spectrographic science exposures at LP6 (Section 5.7.6).

5.7.3 GO Wavecals (User-Specified)

Observers may request additional wavelength-calibration exposures, called GO wavecals, by selecting TARGET=WAVE, EXPTIME=DEF, and FLASH=NO. The exposure must be made in TIME-TAG mode. GO wavecals use the same calibration lamp configuration and exposure times as the automatic wavelength calibrations discussed above. The default modes of operation automatically secure needed wavelength-calibration information to go with your science data, so GO wavecals are rarely required.

5.7.4 No-Cal Wavecals

The COS Pt-Ne wavelength-calibration lamps produce no lines on FUV Segment B in the following observing modes:

- G130M, central wavelength 1055 Å, all FP-POS settings;
- G130M, central wavelength 1096 Å, all FP-POS settings; and
- G140L, central wavelength 1280 Å, all FP-POS settings.

To reduce these data, **CaICOS** assigns the wavelength shifts derived from the Segment A spectrum. If no Segment A data are present (i.e., if `SEGMENT=B`), then no shift is assigned, and the wavelength calibration is highly uncertain.

5.7.5 Inserting Wavecals in Observations with G130M/1055 and G130M/1096, `SEGMENT=B`

Due to the 100x difference in sensitivity between the COS FUVB and FUVB segments when observing with the G130M/1055 and 1096 `CENWAVES`, it is expected that many observers will need to turn off FUVB when observing bright targets. Only those observers using these two configurations are affected by this issue.

Under these conditions the zero point of the wavelength solution cannot be determined because the MgF_2 window on the Pt-Ne lamps (`WAVECAL`) blocks light below $\sim 1180 \text{ \AA}$ (all `WAVECAL` light falls on FUVB). This results in a degradation of the resolution when `FP-POS` are combined by **CaICOS** and decreases the archival value of the COS data. *In these cases, normal `TAGFLASHS` are not available and `WAVECAL` exposures with FUVB turned ON must be inserted into the observing sequence adjacent to each `CENWAVE/FP-POS` setting used. As a result, in these cases `FP-POS=ALL` should not be used.* Individual `FP-POS` science exposures should be used instead.

For non-Continuous Viewing Zone (CVZ) science exposures at the start of an orbit not containing a target acquisition (TA) sequence, the `WAVECAL` can be inserted into the prior occultation with no impact on the timeline. For non-CVZ science exposures at the end of an orbit, the `WAVECAL` can be inserted into the following occultation with no impact on the timeline. For science exposures that immediately follow TA, or do not start or end an orbit, a `WAVECAL` must be inserted. This can take anywhere from 500 to 900 s (8-15 minutes) depending on configuration and observing sequence. For more information, consult with your contact scientist.

5.7.6 `SPLIT` Wavecals (default non-concurrent wavelength calibration at LP6)

For science exposures using spectral elements supported at LP6 (Table 5.12.1) a non-concurrent wavelength calibration exposure will be automatically scheduled by the `APT` for each set of external spectrographic science exposures using the same spectral element, central wavelength, and `FP-POS` value. These `SPLIT` wavecals are always obtained in `TIME-TAG` mode with the external shutter closed. This wavelength calibration exposure will be added before and after each science exposure (depending on the length of the exposure and if the same spectrograph set-up has been in use over that time). `SPLIT` wavecal exposures are not taken concurrently with the science exposures and are instead executed by moving the aperture to a different position on the detector in order to use the wavecal lamp. The calibration exposure will often use some of the science target orbital visibility. The calibration lamp configuration and exposure time will be based on the grating and central wavelength of the science exposure.

`SPLIT` wavecals may not be turned off by the observer. If there is a science requirement to turn off `SPLIT` wavecals, specific permission must be sought from the STScI Contact Scientist.

FLASH=YES observations are not permitted for science exposures using spectral elements supported at LP6 (Table 5.12.1). FLASH=NO is the default for TIME-TAG spectroscopic exposures at LP6, the observer need not specify it.

5.8 Fixed-Pattern Noise

5.8.1 COS Flat Fielding

5.8.2 Use of Multiple FP-POS Settings

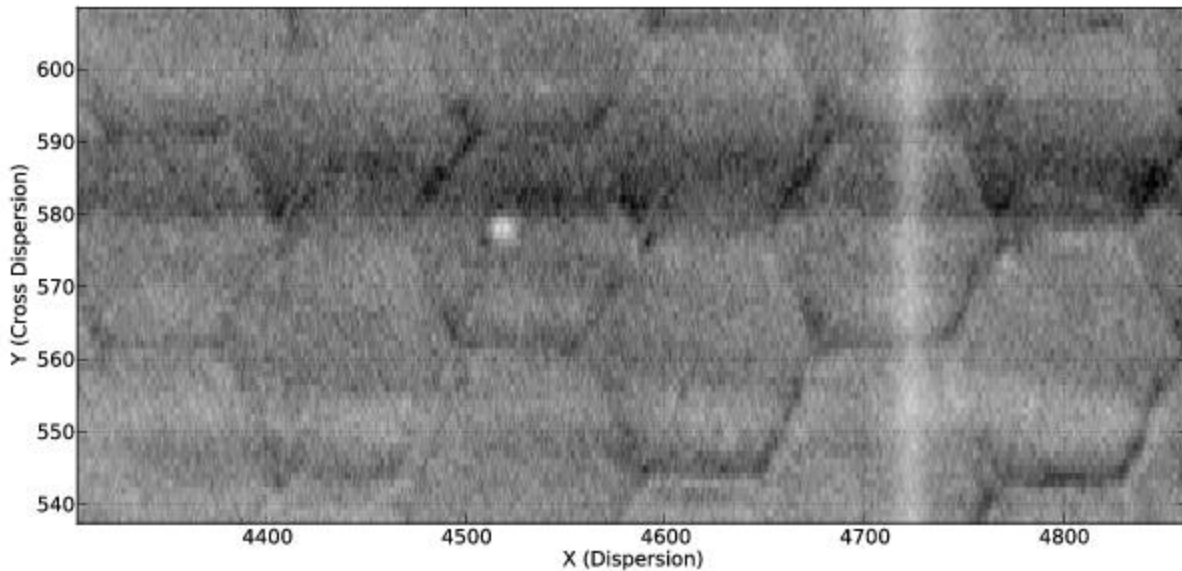
The S/N of COS observations in **CalCOS** is improved through two techniques, flat fielding and coadding spectra taken at different central wavelengths or **FP-POS** settings. Flat fielding removes low-frequency variations on the detector by dividing the data by a high S/N flat-field response image. **FP-POS** exposures smooth out pixel-to-pixel detector variations by combining in wavelength space data taken at different positions on the detector.

5.8.1 COS Flat Fielding

The internal flat-field calibration system consists of two deuterium lamps and the flat-field calibration aperture (FCA). The system was designed such that light from the lamps follows nearly the same optical path as that from an external target. The FCA is placed near the usual location of the PSA, and the lamp beam illuminates the gratings and mirrors from this slightly offset position.

The deuterium lamps are not bright enough to map out the flat field at FUV wavelengths, so the FUV flats are constructed from on-orbit observations of bright white dwarfs. An image of the FUV detector using the deuterium lamp is shown in [Figure 5.13](#). The light, vertical stripe is a shadow cast by a grid wire in front of the detector ([Section 4.1.1](#)). A detector dead spot and the hexagonal pattern of the fiber bundles in the micro-channel plate are also visible. Although significant structure is present in the FUV flats, it is reproducible and can be removed during data reduction.

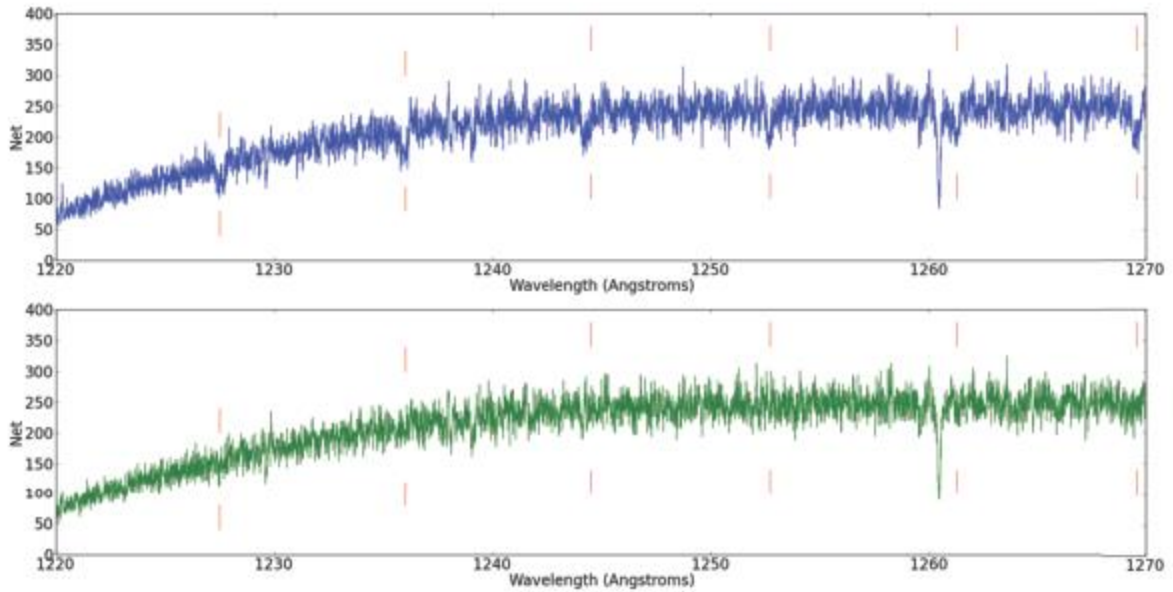
Figure 5.13: Section of a Flat-Field Image for the FUV XDL.



A section of the FUV flat field showing representative detector features and a grid wire (the light vertical stripe at a pixel position of 4720).

Grid-wire shadows are the greatest source of fixed-pattern noise. In the past **CalCOS** flagged these regions and eliminated their contributions to the final, summed spectra. During Cycle 18 a grid-wire flat-field calibration file was developed for the G130M and G160M gratings, and it was updated in Cycle 21 for all FUV gratings. Pixels affected by grid wires are still flagged by **CalCOS**, but their corrected values are included in the summed spectra. [Figure 5.14](#) shows the effect of correcting the grid-wire shadows on a single G130M FUVB exposure of the white dwarf WD0320-539 obtained at the original lifetime position. This star has a relatively smooth continuum, making the corrections obvious. The upper (blue) spectrum contains grid-wire shadows (indicated by the vertical lines), which are corrected in the lower (green) spectrum. The affected regions are clearly improved, but residual structure, much of it fixed-pattern noise in the FUV detector, remains. This structure can be reduced through the use of multiple `FP-POS` settings ([Section 5.8.2](#)).

Figure 5.14: Correcting Grid-Wire Shadows with Flat-Field Reference File.



G130M FUVB exposure of the white dwarf WD0320-539 obtained at the original lifetime position. The upper (blue) spectrum contains grid-wire shadows (indicated by the vertical lines), which are corrected in the lower (green) spectrum.

Table 5.6 gives the limiting S/N for the G130M and G160M gratings when the grid-wire flat field is used, both with and without multiple FP-POS settings. To attain higher S/N ratios special analysis procedures, such as those described in Bagnuolo & Gies (1991, ApJ, 376, 266), and Lambert et al. (1994, ApJ, 470, 756) are required. Consult with your contact scientist for details.

Table 5.6: Limiting S/N for FUV Spectroscopy.

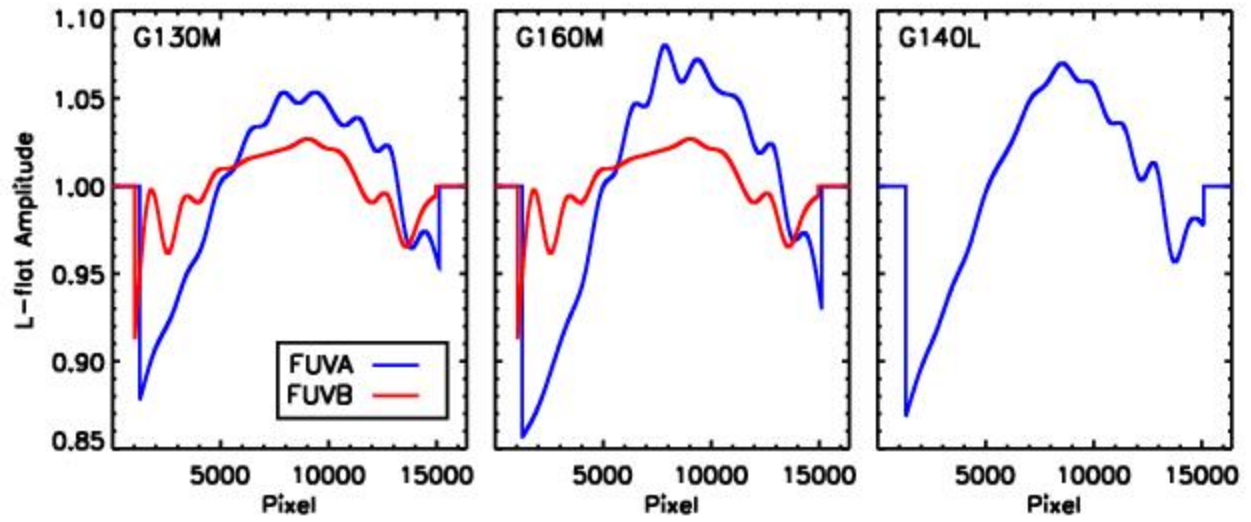
Grating	FUVA	FUVB
Single FP-POS Exposure		
G130M	17.9	23.8
G160M	14.9	20.4
Combining 4 FP-POS Exposures		
G130M	35.7	47.6
G160M	29.9	40.8

Because the grid wires are oriented perpendicular to the spectrum, their effect on the data is relatively insensitive to the location of the spectrum in the cross-dispersion direction. Much of the remaining fixed-pattern noise depends strongly on the spectrum location, and will require considerably more effort to characterize and correct. The grid-wire flats have been shown to be independent of the y position on the detector, so they can be applied at all lifetime positions.

In addition to grid-wire shadows, grid-wire "impostors" were discovered in COS FUV data. The morphology of the impostors in the extracted spectra is similar overall to that of the grid-wire shadows. However, unlike the grid-wire shadows, the impostor features depend strongly on the y position on the detector. From the appearance of these features in the dark exposures, it was determined that the impostors are artifacts introduced by the geometric distortion correction. However, due to the way that the geometric distortion corrections are integrated into nearly every other aspect of calibration, this reference file cannot be changed quickly. Therefore, a 2D correction for the "impostors" has been incorporated into the FLATFIELD reference file until a fix to the geometric distortion correction can be fully investigated and tested. As a result **CalCOS** now corrects these features through the flat-field correction.

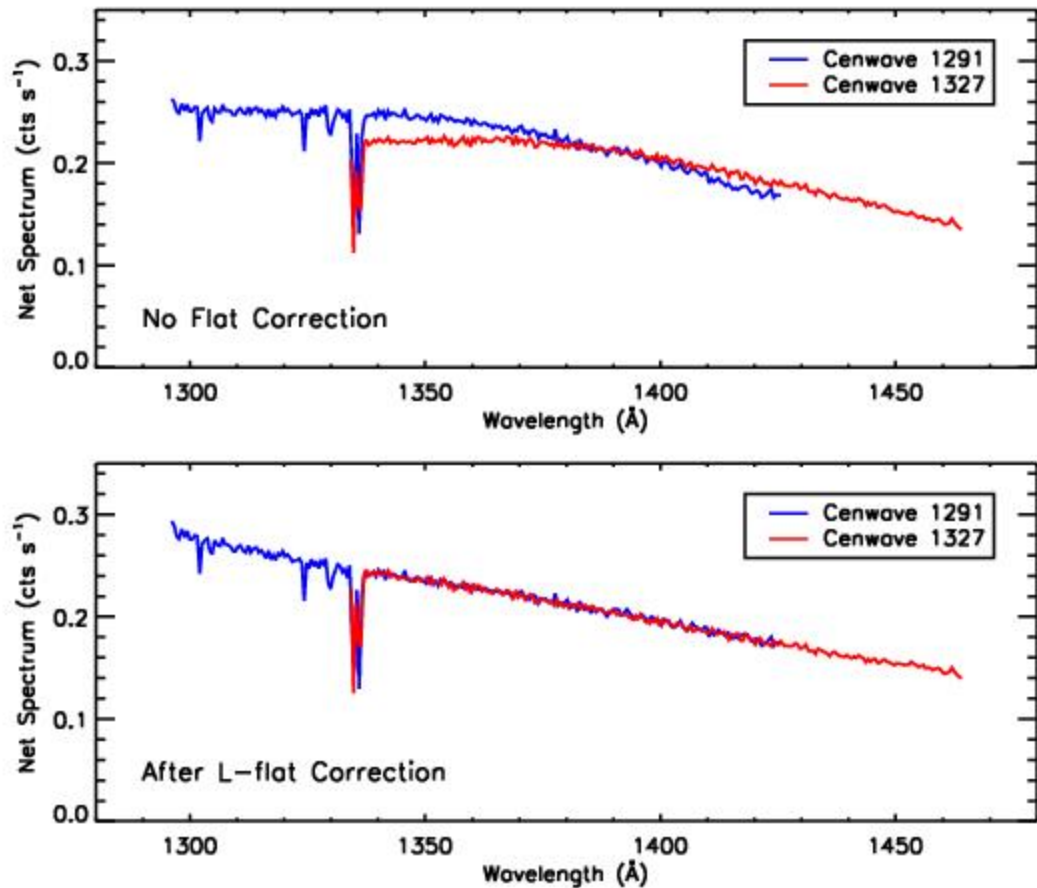
Comparison of extracted spectra at difference `FP-POS` and `CENWAVE` settings has revealed y -independent illumination variations on each detector segment. These variations are corrected in **CalCOS** by applying a low-order flat-field correction (L-flat) that has been incorporated into the FLATFIELD reference file. The L-flats applicable to the fourth lifetime position are shown in [Figure 5.15](#), and an example of the improvement obtained using the L-flat is shown in [Figure 5.16](#).

Figure 5.15: L-Flat Amplitudes for COS FUV.



The amplitudes of the L-flats for the COS FUV A and B segments.

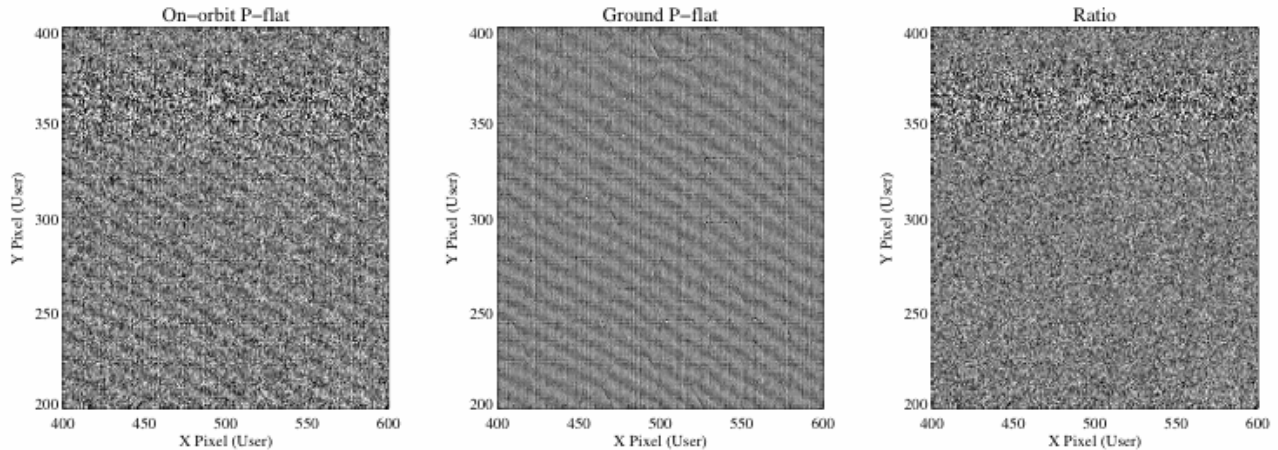
Figure 5.16: A Comparison of COS Spectra with and without the L-Flat Correction.



The top panel shows two COS spectra without the L-flat correction. The bottom panel shows the same two spectra with the L-flat correction.

The NUV flat field used by CalCOS was built from a combination of external PSA deuterium lamp exposures taken on the ground and internal FCA observations taken on the ground and on orbit. Figure 5.17 presents a comparison between two NUV flat-field frames, one obtained on orbit and one on the ground. Each image was divided by a low-order polynomial to isolate the high-order fringe pattern characteristic of the NUV detector. Their ratio is consistent with the noise in the on-orbit image, confirming that the two flat fields may be safely combined. Pre-flight ground tests with COS show that the NUV MAMA can deliver S/N up to about 50 without using a flat field. Using a flat field it should be possible to routinely achieve S/N of 100 or more per resolution element.

Figure 5.17: Flat-Field Exposures for the NUV MAMA.



5.8.2 Use of Multiple FP-POS Settings

Fixed-pattern noise in the COS detectors limits the S/N that can be achieved in a single exposure to 15-25 per resolution element for the FUV and 50 for the NUV. To achieve higher S/N ratios one can obtain a series of exposures, each slightly offset in the dispersion direction, causing spectral features to fall on a different part of the detector. For STIS these motions are known as `FP-SPLITS`. For COS these motions are specified by the `FP-POS` optional parameter.

Four `FP-POS` offset positions are available: a nominal position (0), two positions toward longer wavelengths (-2 and -1), and one position toward shorter wavelengths (+1). Positions -2, -1, 0, and +1 are designated respectively as `FP-POS=1, 2, 3, and 4`. The nominal position, `FP-POS=3`, is the setting used to define the wavelength range associated with the grating central wavelengths (Table 5.3 and Table 5.4). In pipeline processing `CalCOS` creates individual calibrated spectra for each `FP-POS` position, then aligns and combines them into a merged spectral product, using only good-quality data at each wavelength.

The optical mechanism on which the grating is mounted is rotated by one step for each adjacent `FP-POS` position. The amount that a particular spectral feature moves in the dispersion direction on the detector is approximately 250 pixels per step for the FUV channel and 52 pixels for the NUV. The corresponding wavelength shifts for each grating are given in Chapter 13. There is a preferred direction for moving the grating mechanism. Overheads are reduced if `FP-POS` exposures are obtained in increasing order (see Section 9.5). When moving to a new grating or central-wavelength setting you may select any `FP-POS` position without paying an additional overhead penalty. Thus, the most efficient order is `FP-POS=1, 2, 3, 4`, as it requires no backward motion of the grating mechanism.

A wavelength calibration exposure will be obtained each time the `FP-POS` changes. For `FLASH=YES` exposures the time-since-last-grating-motion clock is not reset by an `FP-POS` movement. However, there will always be at least one lamp flash during each individual `FP-POS` exposure. For `FLASH=NO` exposures a separate wavelength calibration exposure will be taken for each `FP-POS` position change. Using all four `FP-POS` for each `CENWAVE` can be achieved by using the `FP-POS=ALL` parameter in `APT` for each `CENWAVE` or by spreading out the four `FP-POS` positions over multiple orbits within a visit for each `CENWAVE` or over multiple visits to the same target.

Please consult the [COS 2025 website](#) for rules and restrictions pertaining to the use of the G130M grating to reduce the impact of Ly- α airglow. Note that certain COS observing settings are disallowed for certain scenarios.

Requirements for Use of Multiple FP-POS Settings in the FUV

The use of multiple FP-POS positions for each CENWAVE setting of the COS FUV detector is required unless a strong scientific justification to do otherwise is provided in the Phase I. (There is no such requirement for NUV observations.) Using multiple FP-POS positions improves the limiting S/N and minimizes the effects of flat-field artifacts. The use of multiple FP-POS positions is especially important for the FUV detector as the fixed pattern noise is larger and more poorly characterized than that of the NUV detector.

Since this simple shift-and-add technique significantly improves the signal-to-noise ratio of the resulting spectrum, and will extend the lifetime of the COS FUV detector, the use of multiple FP-POS for each CENWAVE setting is required for FUV science observations. *Proposers using the FUV channel of COS, but who do not intend to use **all four** FP-POS settings for each CENWAVE setting, must justify their observing strategy in their Phase I proposals. (Under the COS 2025 rules, the G130M/1291 setting has only two FP-POS for SEGMENT = B or BOTH; both FP-POS must be used in this case.) A modest reduction in observational overheads will not normally be considered sufficient justification for not using all four FP-POS settings, unless using G160M. Starting in Cycle 30, users of G160M are permitted to use fewer than 4 FP-POS based on the S/N limits described in [Section 9.5.1](#).* The exposure times per FP-POS should be as equal as practical, but if there are multiple orbits for a target, the four FP-POS may be distributed among the orbits in such a way that FP-POS changes during an orbit are minimized.

5.9 COS Spectroscopy of Extended Sources

5.9.1 ORIENT Constraints for Extended Sources

COS spectra of extended objects can have significantly lower resolution than those of point sources, depending on the spatial distribution of the source. For example, measurements of Lyman- α airglow lines, which uniformly fill the COS aperture, show $R = 1450$ for G130M and $R = 165$ for G140L. Filled-aperture observations of SNR N132D confirm $R \sim 1500$ for both FUV M gratings (France et al. 2009, *ApJL*, 707, L27). In the NUV the situation is much worse, because a source that fills the aperture will lead to cross-contamination among the three spectral stripes on the MAMA detector.

A similar situation arises when multiple point sources fall within the aperture. COS was designed to resolve two point sources separated by 1 arcsec in the cross-dispersion direction, but on-orbit measurements of the XD profile reveal that such observations are possible only for selected grating and central-wavelength settings (Section 5.1.9). Note that light from a point source falling more than 0.4 arcsec from the center of the PSA will be attenuated (Section 8.8.2).

While the performance of COS when observing extended targets was never optimal, the extended target flux calibration was reasonably accurate during operations at LP1 and LP2 (through February 2015). This is however not the case at the newer LPs due to their location near to previously sagged lifetime positions.

For extended targets larger than $\sim 0.6''$ (FWHM), the spatial distribution of incoming light on the COS /FUV detector is significantly wider than that of a point source. As a result, the light distribution of extended targets may overlap low-gain regions from earlier lifetime positions, and may incur significant flux loss.

In addition, the two-zone extraction algorithm implemented to support science observations extracts counts in 2D profiles that tightly follow the optical footprint of the light from a point source on the detector, thus reducing the number of dark counts and avoiding large portions of spectra from being discarded when bad or sagged pixels overlap with the wings of those profiles. This algorithm therefore provides accurate calibration for point sources, but the flux calibration of extended targets (i.e., with FWHM larger than $\sim 0.6''$) may be significantly off because the spatial distribution of their flux on the detector is wider than that of a point source.

Combined with the aperture vignetting, these effects may result in unreliable flux calibration for COS /FUV observations of extended targets (larger than $0.6''$ FWHM), including spatial distortion.

Starting with Cycle 23, COS observers are required to define their targets as EXTENDED = "YES" or "NO" at the target description level. This new field is required for COS observations only. This change is intended to provide an indication as to whether the source extent might be large enough to affect the reliability of the default pipeline extraction which is currently optimized for point source targets. In the future this keyword may also be used to allow the pipeline to use an alternate extraction procedure better suited to extended sources. Both COS FUV and NUV observations of targets with FWHM larger than about 0.6 arcsec or radius larger than 0.35 arcsec should be considered as extended. "YES" should be selected for such targets and "NO" for targets of smaller angular extent. The field should be left blank if the target is not being observed by COS. If this new target-level description keyword is not provided, APT will trigger a warning message asking the PI to define it, and any proposals submitted without a value specified for all COS targets will be sent back to the PI to be corrected. See [COS ISR 2015-03](#) for further details. Note that the old exposure-level EXTENDED keyword, set via the "optional parameters" prior to Cycle 23, is still present in APT but has been deprecated. As a result, the exposure-level EXTENDED keyword should no longer be selected for any exposure in Cycle 23 or later.

Imaging acquisitions of extended sources are subject to special bright-object screening procedures; see [Section 8.10.2](#).

5.9.1 ORIENT Constraints for Extended Sources

Detailed instructions on performing COS spectroscopy on extended sources (i.e., sources with FWHM > 0.6") are provided above. Here we remind users that observing extended sources at different position angles can result in changes in the cross-dispersion and dispersion profiles on the COS detector. Such changes can lead to differences in spectral resolution and flux that may prove problematic when combining spectra across visits or performing science on separate spectra taken at different position angles. This can be mitigated by the user by implementing an ORIENT constraint across visits during within the APT file. **ORIENT constraints are considered 'Special Requirements' and must be specified by the user within the Phase I proposal document.**

5.10 Wavelength Settings and Ranges

Table 5.3 and Table 5.4 show the wavelength ranges recorded on the detectors for each valid combination of grating and central-wavelength setting at the nominal $\text{FP-POS}=3$ position (Section 5.8.2). The wavelength ranges spanned at other FP-POS settings may be estimated using the FP-POS step values provided in Chapter 13. Note, however, that uncertainties in the positioning of the Optics Select Mechanisms (Section 3.1.3) correspond to about half of an FP-POS step. These wavelength ranges are subject to change as the instrumental calibration evolves. The most recent measurements are available from the [COS website](#).

To assist users in preparing their Phase II proposals for Cycle 25 and later COS observations, a [COS /FUV Wavelength Tool](#) has been developed which allows users to visualize how the wavelength ranges covered by the allowed COS FUV settings (i.e., settings in supported mode) overlap with those of settings that have been withdrawn (i.e., not in supported mode) to preserve the lifetimes of the COS FUV detectors. Unlike Table 5.3, the FUV wavelength tool shows estimated coverage for each FP-POS as well as the locations of narrow regions that lack coverage due to Ly α gain sag. These narrow regions are also listed in Tables 3a and 3b on the [COS2025 page](#).

5.11 Spectroscopy with Available-but-Unsupported Settings

This section details COS settings that are classed as 'Available but Unsupported' and provides details for proposers considering using such settings. COS settings that currently fall within this category are:

- **COS/NUV G285M:** The COS/NUV G285M grating lost sensitivity at a rate of about 10% per year after the 2009 installation of COS. By 2018, its sensitivity had fallen to less than 15% of its original value. Due to a lack of use and the loss of sensitivity, the COS team elected in 2018 to discontinue monitoring its sensitivity and the stability of its wavelength solution. Exposure time estimates, flux calibration, and wavelength calibration for this grating may not be reliable. COS /NUV observations with the G285M grating are therefore Available but Unsupported. Alternative COS gratings are described in [Section 13.3](#). Users interested in medium-resolution spectroscopic coverage of the wavelength region from 2500 to 3200 Å are encouraged to use STIS instead.

For a setting that is Available but Unsupported, proposers should only consider use if their science cannot be performed with supported instrument parameters, and only if the technical requirement and scientific justifications are particularly compelling. STScI adopts a policy of shared risk with the observer for the use of unsupported capabilities. Requests to repeat failed observations taken with unsupported capabilities will not be honored if the failure is related to the use of the unsupported capability. In addition, user support from STScI for observation planning, as well as data reduction and analysis, with unsupported capabilities will be limited and provided at a low priority. Users taking data with unsupported capabilities should be prepared to shoulder the increased burden of the planning, calibration, reduction and analysis. Available but Unsupported mode capabilities should only be implemented in the Phase II APT when observers have been specifically granted permission to do so, and some options accessible in the APT software may be prohibited for a variety of technical or policy reasons. Finally, calibrations for unsupported capabilities will not be provided by STScI. Either users must determine that they can create calibration files from data in the HST Archive or they must obtain calibrations as part of their observations. The STScI pipeline will not calibrate data taken in unsupported modes but will deliver uncalibrated FITS files (or in some cases partially calibrated FITS files) to the observer and the HST Archive.

During the Phase II proposal submission process, STScI must also formally approve your use of an available but unsupported mode. This allows STScI to evaluate your request and ensures that no problems associated with your request have come to light since the submission of your Phase I proposal.

The increased burden of calibrating data taken using Available but Unsupported modes also makes the use of such data for archival research significantly more difficult. As a result, requests for use of unsupported modes which do not adequately address the above four points, or which will result in only marginal improvements in the quality of the data obtained, may be denied by STScI, even if the request was properly included in your Phase I proposal.

5.12 FUV Detector Lifetime Positions

Prolonged exposure to light causes the COS FUV detectors to become less efficient at photon-to-electron conversion, a phenomenon called "gain sag." The more a particular region of the detector has been used, the smaller the "pulse height" of the charge cloud generated by an individual photon becomes. As long as all pulse heights are above the minimum threshold needed to distinguish real photons from detector background events there is no loss in sensitivity. However, as the average pulse height at a location on the detector approaches and drops below this threshold, real photon pulses are increasingly misidentified as background and the effective throughput decreases. Since the amount of gain sag increases with the total amount of previous illumination, these effects appear first on regions of the detector that are illuminated by the bright Lyman- α airglow line, but eventually the entire spectrum becomes affected.

STScI is undertaking a number of actions to mitigate the effects of gain sag and extend the lifetime of the COS FUV XDL detector. Primarily, the position of the science spectrum on the COS FUV detectors is periodically moved to an un-sagged region, to start afresh without the Lyman- α gain-sag holes and other gain-sag artifacts.

- On July 23, 2012 the spectrum was moved from its original lifetime position (LP1) to its second lifetime position (LP2). LP2 is offset by +3.5 arcsec from LP1 in the cross-dispersion direction.
- On February 9, 2015, the spectrum was moved to the third lifetime position (LP3), which is offset by -2.5 arcsec from LP1, for all modes except the G130M 1055 and 1096 central wavelengths. These settings have wide cross-dispersion profiles that would be severely impacted by the proximity of LP3 to LP1, and so they continue to be executed at LP2. The G130M 1222 central wavelength executed at LP3, but has been operated at a higher voltage setting to minimize the impact of gain-sagged regions.
- The commissioning of the fourth lifetime position (LP4) took place on October 2, 2017, at the beginning of Cycle 25 and at the same time as the introduction of the COS 2025 policy (see Section 5.12.1 below). LP4 is located at -5.0 arcsec from LP1.

Starting in Cycle 29, COS began to use multiple lifetime positions at the same time, with the aim of extending the COS FUV lifetime to 2030 and beyond

- G130M cenwaves 1291, 1300, 1309, 1318, and 1327 were moved to LP5 (located at +5.4 arcsec from LP1).
- The two blue-mode G130M cenwaves (1055 and 1096) remain at LP2.
- G130M/1222 remains at LP4.
- G140L cenwaves were moved to LP3, but with G140L acquisition modes remaining at LP4.
- G130M BOA observations also remain at LP4.

The spectral resolving power at LP5 is approximately 20% higher than it was at LP4 and approximately the same as it was at LP3, depending on wavelength. A summary of the supported and available FUV gratings at each lifetime positions for COS FUV is provided in Table 5.12.1.

Starting with Cycle 30, G160M cenwaves were moved to a new LP6, located at +6.5 arcsec from LP1.

- Wavelength calibration exposures at LP6 incur larger overheads than those taken at previous LPs (Section 5.7.6). To minimize the impact of these overheads at LP6, G160M users may under certain conditions use fewer than 4 FP-POS or may take data at LP4.
- Changes in LP yield minor changes in sensitivity, and resolution. The COS team will provide additional updates to users as they become available via STScI Analysis Newsletters (STANs), the COS website, and updates to the COS IHB.

Table 5.12.1 Supported and Available-but-Unsupported FUV Gratings versus Lifetime Position for COS FUV.

Lifetime Position (LP)	1	2	3	4	5	6
Supported Grating/cenwave	-	G130M/1055 /1096	G140L	G130M /1222	G130M	G160M
Available-but-Unsupported Grating /cenwave	-	-	G130M	G160M	-	-

Starting with the commissioning of LP3, and continuing at LPs 4-6, a new spectral extraction algorithm was implemented. This `TWOZONE` algorithm uses the shape of a point source profile to define the region over which counts are included in the extracted spectrum and to decide when bad pixels in the profile wings compromise the accuracy of the spectral extraction. Sources that have substantial spatial extent may have significant overlap with the gain-sagged regions and may require specialized extractions that are currently not performed with **CalCOS**. For these reasons, observations of extended sources will not be optimally calibrated. Users should set the optional APT parameter `EXTENDED=YES` to flag such sources (see [Section 5.9](#)), even if the **CalCOS** pipeline calibration will not treat extended sources differently from point sources.

Throughput and most other calibrations at LPs 4-6 are very similar to those at the original position. See the [COS website](#) and the [COS Instrument Science Reports](#) (ISRs) for additional information about the calibration of the different lifetime positions.

Gain sag is an inevitable result of using the detector. Gain sag holes will appear at LP5, with the timing of their appearance depending on the locally accumulated signal. The restricted use of FP-POS positions at LP5 to reduce the impact of Ly α airglow is described next.

5.12.1 COS 2025 Policy

A "COS 2025" policy was developed with the goal of retaining the full science capability of COS/FUV until 2025 (which has now been extended to 2030 and beyond). It was implemented at LP4 at the start of Cycle 25, on October 2, 2017. It places restrictions on the G130M cenwaves with the goal of reducing the impact of Ly α airglow. The [COS 2025 website](#) includes tables to illustrate the policy, which also appear below, a graphical tool to examine the effects of the policy at different wavelengths, and examples of how observations for different science cases might be modified to align with the policy.

The primary restriction is that spectroscopy with the FUVB detector segment is no longer permitted at cenwaves 1300, 1309, 1318, or 1327. At cenwave 1291, FUVB spectroscopy is allowed only at FP-POS 3 and 4. Furthermore, FUV target acquisition with segment B is no longer permitted at cenwaves 1300, 1309, 1318, or 1327. Tables 1 and 2 at the [COS 2025 website](#) as well as Tables 5.12.2 and 5.12.3 below illustrate these restrictions.

Even with this policy, FUVB spectroscopy with the 1291 cenwave and FP-POS 3 or 4 will continue to place Ly α on the detector. Over time, airglow will sag the region of the detector exposed to Ly α , which will become unusable. Therefore, at other settings, the 5–6 Å range of wavelengths located in this region on the detector will be affected. Tables 3a and 3b at the [COS 2025 website](#) as well as Tables 5.12.2 and 5.12.3 below list these ranges as a function of grating, cenwave, and FP-POS.

Table 5.12.2: Supported and Available-but-Unsupported Science Modes versus Lifetime Position (LP) for COS FUV.

LP	2	3	4	5	5	5	5	5	6
FP-POS	ANY	ANY	ANY	1	2	3	4	ALL	ANY
G130M/1055, 1096	◆	X	X	X	X	X	X	X	X
G130M/1222	X	X	◆	X	X	X	X	X	X
G130M/1291	X	AbU	X	FUVA	FUVA	◆	◆	FUVA	X
G130M/OTHERS	X	AbU	X	FUVA	FUVA	FUVA	FUVA	FUVA	X
G160M/ALL	X	X	AbU	X	X	X	X	X	◆
G140L/ALL	X	◆	X	X	X	X	X	X	X

AbU = Available-but-Unsupported mode use only (Phase I approval needed)

◆ = Supported mode (all General Observers may use; no approval needed)

FUVA = Supported mode, but only with Segment = FUVA (all General Observers may use)

X = Not supported or available to General Observers

ALL = FP-POS ALL (i.e., 1+2+3+4)

ANY = any FP-POS value, including FP-POS ALL.

Table 5.12.3: Supported and Available Target Acquisition Modes versus Lifetime Position for COS FUV.

LP	2	3	4	5	6
FP-POS	3	3	3	3	3
G130M/1055	X	X	X	X	X
G130M/1096	X	X	X	X	X
G130M/1222	X	X	X	X	X
G130M/1291	X	AbU	X	◆	X
G130M/OTHERS	X	AbU	X	FUVA	X
G160M/1533	X	X	X	X	X
G160M/OTHERS	X	X	AbU	X	◆
G140L/800	X	X	X	X	X

G140L/1105	X	X	FUVA	X	X
G140L/1280	X	X	FUVA, BOTH	X	X

◆ = Supported mode (all guest observers may use)

FUVA = Supported mode, but only with Segment = FUVA (all General Observers may use)

X = Not supported or available to guest observers

Note: FP-POS = 3 is the default FP-POS for dispersed-light target acquisition.

AbU = Available-but-Unsupported mode use only (approval needed in Phase I)

FUVA, BOTH = Supported mode, but only with Segment = FUVA or Segment = BOTH (all GOs may use)

Table 5.12.4: G130M Wavelength Ranges Affected by Segment B Gain Sag.

Cenwave	FP-POS	λ_{\min} (Å)	λ_{\max} (Å)
1222	1	1152.8	1157.8
1222	2	1150.3	1155.3
1222	3	1147.8	1152.8
1222	4	1145.4	1150.3
1291	3	1212.9	1217.9
1291	4	1210.4	1215.4

Table 5.12.5: G160M Wavelength Ranges Affected by Segment B Gain Sag.

Cenwave	FP-POS	λ_{\min} (Å)	λ_{\max} (Å)
1533	1	1444.9	1451.1
1533	2	1441.9	1448.0
1533	3	1438.8	1444.9
1533	4	1435.8	1441.9
1577	1	1489.5	1495.6
1577	2	1486.4	1492.6
1577	3	1483.4	1489.5
1577	4	1480.3	1486.4
1589	1	1501.2	1507.3
1589	2	1498.1	1504.2
1589	3	1495.0	1501.2

1589	4	1492.0	1498.1
1600	1	1512.5	1518.7
1600	2	1509.5	1515.6
1600	3	1506.4	1512.5
1600	4	1503.4	1509.5
1611	1	1524.4	1530.5
1611	2	1521.3	1527.5
1611	3	1518.3	1524.4
1611	4	1515.2	1521.3
1623	1	1536.5	1542.6
1623	2	1533.4	1539.5
1623	3	1530.3	1536.5
1623	4	1527.3	1533.4

5.13 Spectroscopic Use of the Bright Object Aperture

Spectroscopic observations with the BOA have had very little demand over the past cycles. For that reason, it has been decided that spectroscopic observations with the BOA will not be supported at the level that is used for the PSA. Spectroscopic observations with the BOA should be performed only if the technical requirement and scientific justification are particularly compelling. Proposers should be aware of the following caveats regarding use of the BOA:

- Further calibrations for the BOA will not be provided by STScI. Either users must determine that they can create calibration files from data in the HST Archive or they must obtain calibrations as part of their observations. Spectroscopic observations using the BOA will be calibrated by **CaICOS**, but will be based on reference files primarily derived for use with the PSA and will use a the new `TWOZONE` extraction algorithm described in Section 3.2.1 of the [COS Data Handbook](#).
- User support from STScI for observation planning, as well as data reduction and analysis, with the BOA will be limited. Users taking spectroscopic data with the BOA should be prepared to shoulder the increased burden of the planning, calibration, reduction, and analysis.
- BOA observations with G130M and G160M will take place at LP4, while those with G140L will take place at LP3.

Phase I proposals that include spectroscopic use of the BOA must include a justification of why the science cannot be done with the PSA.

Chapter 6: Imaging with COS

Chapter Contents

- [6.1 Introduction to COS Imaging](#)
- [6.2 Sensitivity](#)
- [6.3 Image Characteristics](#)

6.1 Introduction to COS Imaging

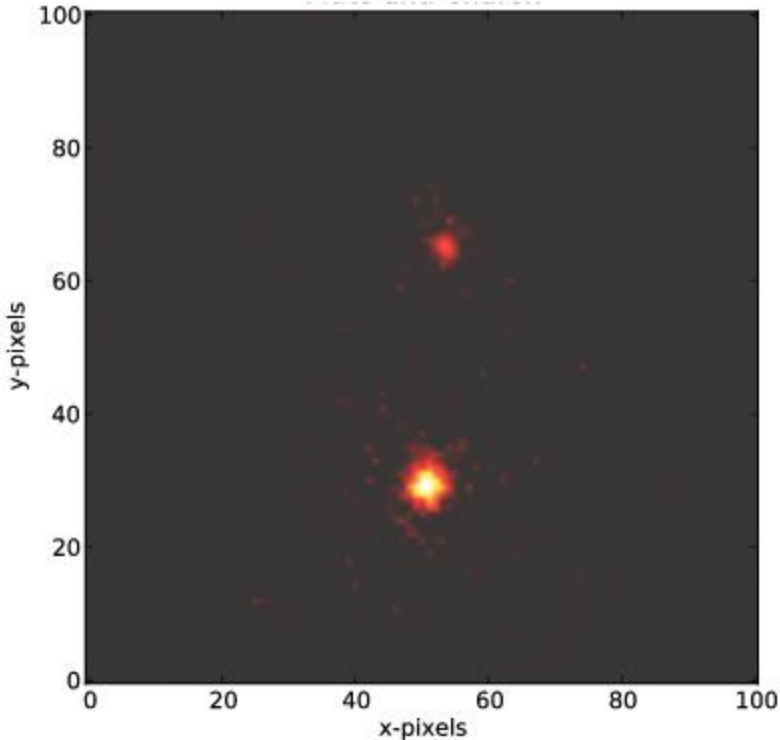
The COS NUV channel has a plate scale of 23.5 mas per pixel, which provides the highest spatial sampling of any instrument aboard HST. [Figure 6.1](#) shows an image of Pluto and its moon Charon obtained with COS. COS images are fully corrected for the telescope's spherical aberration, though not for the zonal (polishing) errors on its primary and secondary mirrors ([Section 3.3](#)). Because the optics image the sky onto the detector, rather than the aperture, COS images extend to a radius of 2 arcsec, but suffer considerable vignetting at radii greater than 0.4 arcsec, as shown in [Figure 6.2](#).

To request an imaging observation specify `CONFIG=COS/NUV` and `MODE=TIME-TAG` or `ACCUM`. In `TIME-TAG` mode the minimum `BUFFER-TIME` is 80 seconds, which may be longer than the expected exposure time. `ACCUM` mode is recommended for such short exposures. The minimum COS exposure duration is 0.1 s, as discussed in [Section 5.3](#). `MIRRORB` and/or the BOA can be used to obtain images of bright objects, but at some cost in spatial resolution; see [Section 8.4](#) for details.

For long exposures, drifting of the Optics Select Mechanisms (OSMs) can be significant, ~ 3.5 pixels in the x dimension with an e-folding time of ~ 50 minutes ([COS ISR 2010-10](#)). Observers taking images with exposure times longer than ~ 200 s are urged to use `MODE=TIME-TAG` and `FLASH=YES`. The resulting lamp flash will illuminate the WCA, allowing one to track the drift accurately. By default, `FLASH=NO` for all imaging modes.

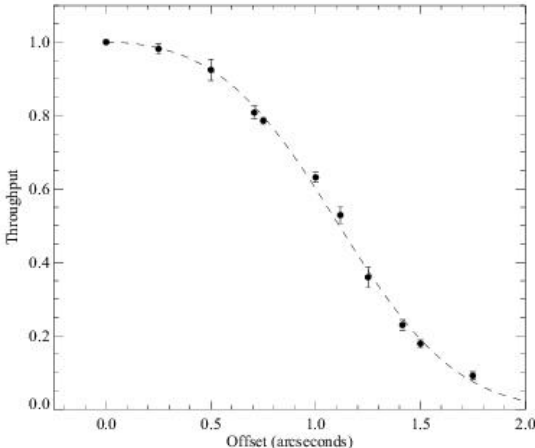
COS imaging in `TIME-TAG` mode allows for high-speed NUV photometry with a temporal resolution of 32 ms. STIS is capable of much finer time resolution (125 μ s), but at lower sensitivity.

Figure 6.1: Pluto and Charon Observed with COS.



NUV exposure of Pluto and Charon, separated by 0.8 arcsec. The exposure time is 25 s. Note that the pixel numbers refer only to this sub-section of the full image. Image courtesy of J. Green.

Figure 6.2: Relative Throughput of the COS PSA in NUV Imaging Mode.



Throughput variation as a function of the offset position. See "COS NUV Image Performance" ([COS ISR 2010-10](#)).

6.2 Sensitivity

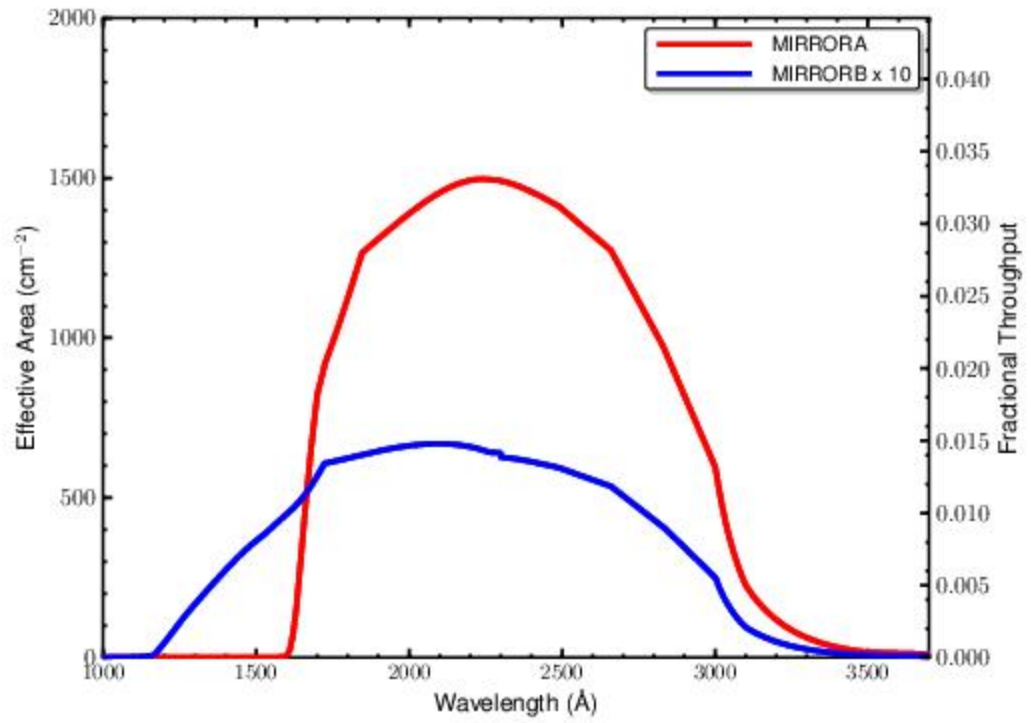
When used in imaging mode, COS concentrates the target's NUV flux into a diffraction-limited image rather than dispersing the light. The local count-rate screening limit for COS/NUV, 50 counts s⁻¹ pixel⁻¹ (Table 10.1), is easily reached, even for fairly faint objects. Observers should use the [COS Exposure Time Calculator](#) (ETC) to get an accurate estimate of expected count rates, but the following values will provide a guide. These have been calculated for a flat-spectrum source (flux independent of wavelength). The approximate flux levels where the limiting count rate is reached are listed in Table 6.1.

Table 6.1: Approximate Flux Limits for a Flat Spectrum.

Aperture and Mirror	Flux Limit (erg cm ⁻² s ⁻¹ Å ⁻¹)
PSA + MIRRORA	2×10^{-15}
BOA + MIRRORA	4×10^{-13}
PSA + MIRRORB	4×10^{-14}
BOA + MIRRORB	7×10^{-12}

When MIRRORA is used for imaging observations, sensitivity extends from about 1600 to 3300 Å, peaking at ~2300 Å (Figure 6.3). Both MIRRORA and MIRRORB have sensitivity tails that extend to about 8000 Å (see COS ISR 2010-10), so care must be taken when observing cool stars ($T_{\text{eff}} < 5000$ K) and other red objects, as high count rates at long wavelengths could damage the detector. When MIRRORB is employed, its use of a first-surface reflection allows short-wavelength light to reach the detector, therefore sensitivity extends to the NUV detector cut-off, about 1150 Å, for the primary image.

Figure 6.3: Effective Area for COS NUV Imaging with the PSA.



6.3 Image Characteristics

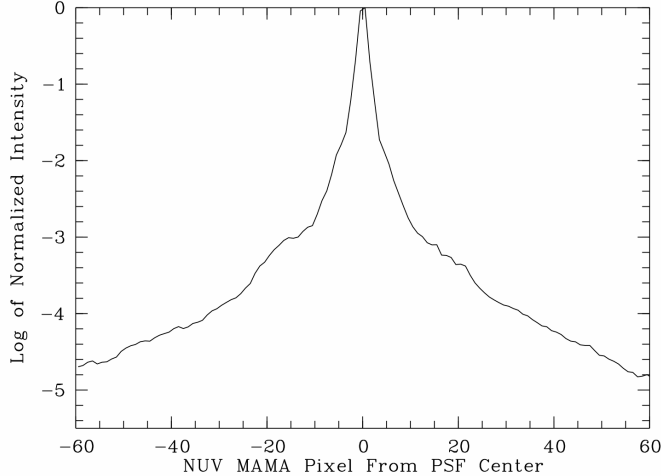
A two-dimensional Gaussian fit to a typical imaging point-spread function (PSF) has a FWHM of 1.97 pixels (47.1 mas), with 13.4% of the light in the brightest pixel. Because the HST focus varies with orbital phase, FWHM values can range from 1.8 to 2.4 pixels.

As discussed in [Section 3.3](#), mid-frequency wavefront errors (MFWFEs) contribute significantly to the PSF wings at wavelengths $< 2500 \text{ \AA}$, so the spatial resolution of a point source will depend somewhat on its spectral energy distribution. For an M star, which has little photospheric flux at the shortest wavelengths, the image would be close to diffraction limited. For a hot white dwarf, the MFWFEs would have the maximum impact on the spatial resolution.

Deep images reveal the detailed shape of the COS imaging PSF. [Figure 6.4](#) shows the PSF, averaged over 180 degrees of azimuth and plotted on a log scale to reveal its extended wings. [Figure 6.5](#) shows a 2-dimensional grayscale image of a deep imaging observation that reveals two low-level "ghosts" located approximately 20 pixels to the right and the upper left of the center of the PSF.

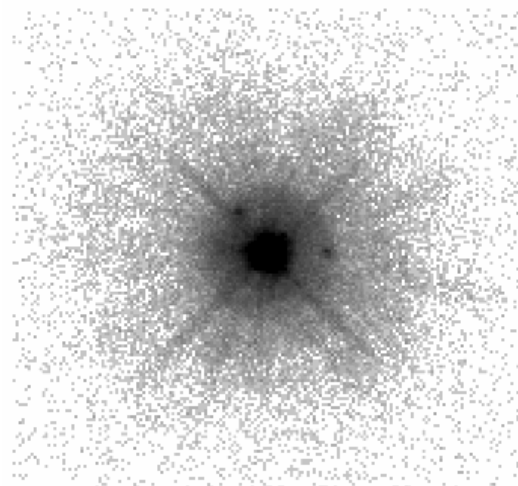
The peak intensity of the brightest of the two ghosts is roughly 0.1% of that of the main PSF. These features may complicate the analysis of faint objects located in the wings of a brighter object.

Figure 6.4: Extended Wings in the COS Imaging PSF.



Azimuth-averaged COS imaging PSF plotted with a logarithmic intensity scale.

Figure 6.5: Ghosts in COS NUV Images.



Negative grayscale rendering of a deep COS NUV image of a point source. This figure is plotted with a logarithmic intensity scale and covers about 6.5 arcsec along each axis. Note the two ghost images to the right and upper left of the center of the PSF.

Chapter 7: Exposure-Time Calculator - ETC

Chapter Contents

- [7.1 The COS Exposure Time Calculators](#)
- [7.2 Imaging Observations of Red Objects](#)
- [7.3 Sensitivity, Count Rate, and Signal-to-Noise](#)
- [7.4 Detector and Sky Backgrounds](#)
- [7.5 Extinction Correction](#)
- [7.6 Examples](#)

7.1 The COS Exposure Time Calculators

To help with proposal preparation, four [COS Exposure Time Calculators](#) (ETCs) are available on the STScI ETC webpage:

<http://etc.stsci.edu>

These calculators model spectroscopic and imaging exposures for both target acquisitions and scientific observations. They estimate count rates for given source and background parameters, and calculate either the signal-to-noise ratio for a given exposure time or the exposure time needed to achieve a desired signal-to-noise ratio. If you have a calibrated spectrum of your source you can upload it to the Exposure Time Calculators. The ETCs warn you if your observations exceed local or global brightness limits (see [Table 10.1](#)). The ETCs offer extensive on-line help that provides instructions and explains their calculations.

A unique exposure ID is assigned to each calculation performed by the ETCs, allowing results from previous calculations to be retrieved easily. *This number must be included in the appropriate box in your Phase II proposal to document your work and to facilitate Phase II review.* Proposers are urged to check the [COS ETC webpage](#) for any updates or issues related to the COS ETCs before performing ETC simulations.

The spectroscopic ETC can display the input spectrum, a simulated one-dimensional output spectrum, the S/N as a function of wavelength, and the number of counts per resolution element for the selected instrument configuration and source. These outputs can be downloaded in ASCII format. The ETC also computes the `BUFFER-TIME`, which is required for `TIME-TAG` observations. Scale this value by 2/3 and, following the discussion in [Section 5.4](#), enter it in the [Astronomer's Proposal Tool](#).

The imaging ETC allows for the selection of either the PSA or BOA and either MIRRORA or MIRRORB. It reports the count rate in the brightest pixel, total counts in the detector, and S/N per resolution element.

The target-acquisition ETCs return the acquisition exposure time to be entered in [APT](#) for both imaging and spectroscopic acquisitions. Target acquisition is described in [Chapter 8](#).

7.2 Imaging Observations of Red Objects

As shown in [Figure 6.3](#), the COS NUV channel is sensitive to wavelengths above 3200 Å, an important consideration when imaging red objects. For stars with effective temperatures above 6000 K, the effect is negligible, but it grows to about 20% at 5000 K, and below 5000 K it quickly becomes large.

If you upload a spectrum into the ETC to calculate exposure time of an imaging exposure, whether for a target acquisition or a scientific observation, be sure that the spectrum spans the full range of wavelengths to which the NUV channel is sensitive, from about 1600 Å to 12,000 Å. Failure to do so can produce a misleading result.

The COS ETC expects input spectra to extend out to 12,000 Å and will return a warning message ("Partial overlap between instrument throughput band and input spectrum") if they do not. This message indicates that the ETC may return incorrect results due to the incomplete source spectrum. Users should take care to be sure that the input source spectrum covers the entire wavelength range of the detector, accounting for any impact to the spectral coverage due to the redshift of the source.

7.3 Sensitivity, Count Rate, and Signal-to-Noise

A complete theoretical discussion of the exposure time as a function of instrument sensitivity and signal-to-noise ratio is given in [Chapter 6](#) of the *STIS Instrument Handbook* and will not be repeated here. However, COS has several characteristics that simplify signal-to-noise calculations.

Both COS detectors are photon counters, which means that they have no read noise and their gain is unity. COS is optimized for point sources, and in this case the signal-to-noise ratio is given by

$$\frac{S}{N} = \frac{C \times t}{\sqrt{C \times t + N_{\text{pix}} (B_{\text{sky}} + B_{\text{det}}) \times t}},$$

where:

C = the signal from the astronomical source, in count s^{-1} ,

t = the integration time, in seconds,

N_{pix} = the total number of detector pixels integrated to achieve C ,

B_{sky} = the sky background, in count $\text{s}^{-1} \text{ pixel}^{-1}$, and

B_{det} = the detector dark count rate, in count $\text{s}^{-1} \text{ pixel}^{-1}$.

With no detector read noise, the signal-to-noise ratio is proportional to the square root of the exposure time whether the target is bright or faint compared to the backgrounds and dark count.

Note that the detector dead-time effects discussed in [Section 4.1.5](#) and [Section 4.2.5](#) are not included in the ETC, which will over-predict the count rates and resulting S/N ratios for bright targets.

7.4 Detector and Sky Backgrounds

- [7.4.1 Detector Dark Count](#)
- [7.4.2 Earthshine](#)
- [7.4.3 Zodiacal Light](#)
- [7.4.4 Airglow Emission](#)
- [7.4.5 Tabular Sky Backgrounds](#)

The primary background sources that affect COS observations are detector dark count, earthshine, zodiacal light, and airglow emission; neither of the COS detectors suffers from read noise. The ETC allows the user to select among several levels of intensity for each of the sky backgrounds, corresponding to a variety of observing environments.

7.4.1 Detector Dark Count

[Table 7.1](#) lists the detector dark-count rates assumed by the ETC as of November 2023 (pyETC v32.1). We assume that a resolution element, or "resel," spans 6×10 pixels on the FUV detector and 3×3 pixels on the NUV MAMA. The dark rate on the FUV detectors can sometimes vary by a factor of a few on very short timescales, impacting less than 5% of observations. See [Sections 4.1.3](#) and [4.2.3](#) for more information.

Beginning with Cycle 21, the ETC uses separate dark rates for science observations and target acquisitions obtained with the FUV detector. **CalCOS** filters the data by pulse height, while the COS flight software does not, so the effective dark rate for science data is lower than that for target acquisitions. In either mode the dark rate on the FUV detector is truly small, due in part to its windowless design. The NUV detector has a window and thus a higher dark rate.

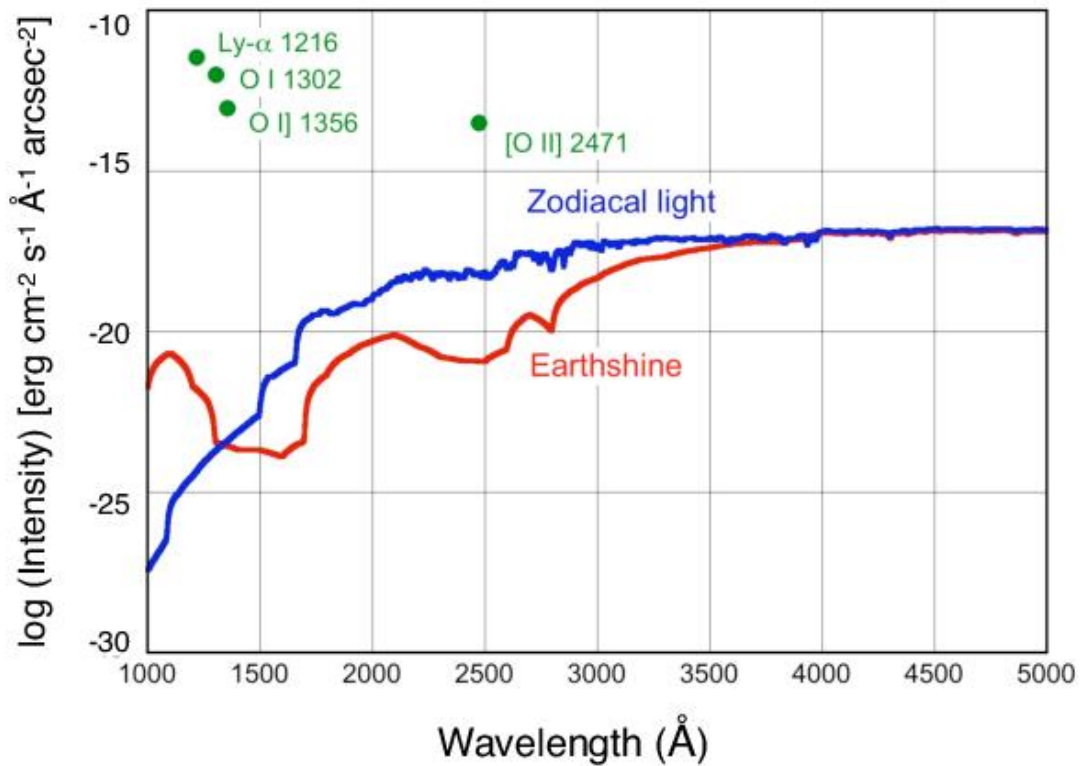
Table 7.1: Assumed Detector Dark Count Rates.

	FUV (A/B) in acq Mode	FUV (A/B) in Science Mode	NUV
Dark rate (counts s ⁻¹)	4.95/5.48 per cm ²	2.66/3.42 per cm ²	199 per cm ²
	$7.10 \times 10^{-6}/7.88 \times 10^{-6}$ per pixel	$3.83 \times 10^{-6}/4.93 \times 10^{-6}$ per pixel	1.25×10^{-3} per pixel
	$4.26 \times 10^{-4}/4.73 \times 10^{-4}$ per resel ¹	$2.30 \times 10^{-4}/2.96 \times 10^{-4}$ per resel ¹	1.13×10^{-2} per resel ¹

¹ Resel size can vary for the 1055 and 1096 central wavelengths. See [Appendix B of the ETC User's Guide](#) for more information.

A website which monitors dark rates can be found at <https://www.stsci.edu/hst/instrumentation/cos/performance/monitoring>.

Figure 7.1: Sky Background Intensity as a Function of Wavelength.

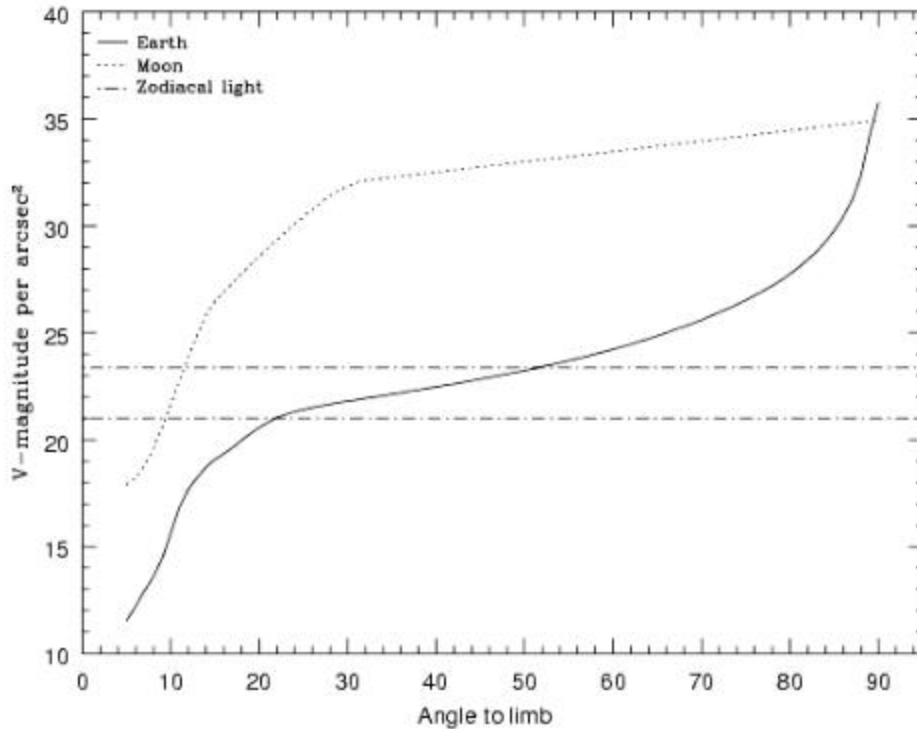


Earthshine (red curve) for a target 24° above the limb of the sunlit Earth, corresponding to the "high" level in the ETC. Use [Figure 7.2](#) to estimate background contributions at other angles. The zodiacal light level ($m_V = 22.7$ mag per arcsec², the "average" level in the ETC, blue curve) corresponds to a helio-ecliptic latitude and longitude of 30° and 180° , respectively. The airglow line intensities are integrated fluxes, corresponding to the "Day" level in [Table 7.4](#). The upper limit to the [O II] $\lambda 2471$ intensity is shown.

7.4.2 Earthshine

Four earthshine intensity levels, with scaling factors of (none, average, high, extremely high) = (0.0, 0.5, 1.0, 2.0), are available in the ETC. Earthshine intensity is a strong function of the angle between the target and the bright Earth limb. The earthshine surface brightness for a target 24° degrees above the limb, corresponding to the "high" level, is shown in [Figure 7.1](#). The limb angle is approximately 24° when *HST* is aligned toward its orbit pole (i.e., the center of the CVZ). The variation of earthshine with limb angle is shown in [Figure 7.2](#).

Figure 7.2: Background Contributions from the Moon, Earth, and Zodiacal Light.



The values are V magnitude per square arcsec due to the moon and the sunlit Earth as a function of angle between the target and the limb of the bright Earth or Moon. Zodiacal light levels range between $m_V = 22.1$ and 23.3 mag arcsec⁻².

7.4.3 Zodiacal Light

Away from the airglow lines, at wavelengths between about 1300 and 3000 Å the sky background is dominated by zodiacal light, which is generally fainter than the intrinsic detector background, especially for the NUV detector. Figure 7.1 shows the zodiacal light for the "average" level in the ETC. Table 7.2 gives the variation of the zodiacal background as a function of helio-ecliptic longitude and latitude. For a target near (50°,0°) or (-50°,0°), the zodiacal light is relatively bright at $m_V = 20.9$ mag arcsec⁻², about 9 times the polar value of $m_V = 23.3$ mag arcsec⁻². These limits are plotted in Figure 7.2. The intensity levels and the factors by which they are scaled in the ETC are (none, low, average, high) = (0.0, 0.576, 1.0, 1.738), corresponding to $m_V =$ (none, 23.3, 22.7, 22.1) mag arcsec⁻².

Observations of the faintest objects may need the special requirement LOW-SKY in the Phase II observing program. LOW-SKY observations are scheduled during the part of the year when the zodiacal background is no more than 30% greater than the minimum possible value for the given sky position. LOW-SKY also invokes the restriction that exposures will be obtained at angles greater than 40° from the bright Earth limb to minimize earthshine and the UV airglow lines. The LOW-SKY requirement limits the times at which targets within 60° of the ecliptic plane will be scheduled and limits visibility to about 48 minutes per orbit.

Table 7.2: Approximate Zodiacal Sky Background (V mag arcsec⁻²) as a Function of Helio-ecliptic Coordinates.

Helio-ecliptic Longitude (deg)	Helio-ecliptic Latitude (deg)						
	0°	15°	30°	45°	60°	75°	90°
180°	22.1	22.4	22.7	23.0	23.2	23.4	23.3
165°	22.3	22.5	22.8	23.0	23.2	23.4	23.3
150°	22.4	22.6	22.9	23.1	23.3	23.4	23.3
135°	22.4	22.6	22.9	23.2	23.3	23.4	23.3
120°	22.4	22.6	22.9	23.2	23.3	23.3	23.3
105°	22.2	22.5	22.9	23.1	23.3	23.3	23.3
90°	22.0	22.3	22.7	23.0	23.2	23.3	23.3
75°	21.7	22.2	22.6	22.9	23.1	23.2	23.3
60°	21.3	21.9	22.4	22.7	23.0	23.2	23.3
45°	SA	SA	22.1	22.5	22.9	23.1	23.3
30°	SA	SA	SA	22.3	22.7	23.1	23.3
15°	SA	SA	SA	SA	22.6	23.0	23.3
0°	SA	SA	SA	SA	22.6	23.0	23.3

Note: A value of "SA" denotes positions in the solar avoidance zone. See [Leinert et al. \(1998\)](#) for more on diffuse sky brightness.

The ETC provides the user with the flexibility to adjust both the zodiacal (none, low, average, high) and earthshine (none, average, high, extremely high) sky background components to determine if the use of LOW-SKY is advisable for a given program. However, the absolute sky levels that can be specified in the ETC may not be achievable for a given target. As shown in [Table 7.2](#), the minimum zodiacal background level for an ecliptic target is $m_V = 22.4$ mag, which is brighter than both the low and average options with the ETC. By contrast, a target near the ecliptic pole would always have a zodiacal = low background in the ETC. The user is cautioned to consider sky levels carefully, as the backgrounds obtained in *HST* observations can span a significant range.

7.4.4 Airglow Emission

In the ultraviolet, the sky background contains important contributions from airglow emission lines, which vary from day to night and as a function of *HST*'s orbital position. These features originate mainly from hydrogen and oxygen atoms in the exosphere of the Earth. Airglow lines may be an important consideration for spectroscopic observations at wavelengths near the lines.

The brightest airglow line by far is Lyman α at 1216 Å. The strength of the Lyman- α line varies between about 2 and 20 kilo-Rayleighs (i.e., between 6.3×10^{-14} and 6.3×10^{-13} erg cm⁻² s⁻¹ arcsec⁻², where 1 Rayleigh = 10^6 photons cm⁻² s⁻¹ per 4π steradians, which equals 3.15×10^{-17} erg cm⁻² s⁻¹ arcsec⁻² at Lyman α) depending on the time of the observation and the position of the target relative to the Sun. The next-strongest feature is the O I line at 1302 Å, which rarely exceeds 10% of Lyman α . The typical strength of the O I λ 1302 line is about 2 kilo-Rayleighs (about 7×10^{-14} erg cm⁻² s⁻¹ arcsec⁻²) on the daylight side and about 150 times fainter on the night side of the *HST* orbit. The O I λ 1356 and [O I] λ 2471 lines may appear in observations on the daylight side of the orbit, but these lines are at least 10 times weaker than the O I λ 1302 line. The widths of the lines also vary, but a representative value for a temperature of 2000 K is about 3 km s⁻¹. Airglow emission from N I λ 1200 is also seen, particularly on the day side of the orbit, with fluxes up to 1.6×10^{-16} erg cm⁻² s⁻¹ arcsec⁻². The N I line is not included in the ETC. Airglow emission lines are essentially unresolved at the resolution of COS, but the emission fills the aperture in the spectral and spatial directions. For the FUV modes, the aperture width is approximately 114 pixels, or 1.12, 1.36, and 9.46 Å for G130M, G160M, and G140L, respectively. For the NUV modes, the aperture width is approximately 105 pixels, or 3.87, 3.46, 4.18, and 41.21 Å for G185M, G225M, G285M, and G230L, respectively.

The COS ETC provides four airglow intensity levels (none, low, average, high), whose scaling factors depend on the airglow line considered: (0.0, 0.1, 0.5, 1.0) for Lyman α , (0.0, 0.0667, 0.5, 1.0) for O I λ 1302, (0.0, 0.006, 0.5, 1.0) for O I λ 1356, and (0.0, 0.005, 0.5, 1.0) for [O I] λ 2471.

It is possible to request that exposures be taken when *HST* is in the earth's shadow to minimize airglow emission (e.g., if you are observing weak lines at 1216 Å or 1302 Å) using the special requirement *SHADOW*. Exposures using this special requirement are limited to roughly 25 minutes per orbit, exclusive of the guide-star acquisition (or reacquisition) and can be scheduled only during a small percentage of the year. *SHADOW* reduces the contribution from the airglow emission lines by roughly a factor of ten, while the continuum earthshine is essentially nil. If you require *SHADOW*, you should request and justify it in your Phase I proposal (see the [Call for Proposals](#)).

An alternate strategy for reducing the effects of airglow emissions is to use time-resolved observations, so that any data badly affected by airglow emission can simply be excluded from the final co-addition. This can be done either by using *TIME-TAG* mode, the default for all COS observations if the target is not too bright, or by taking a series of short (~5 min) *ACCUM* mode exposures over the course of each orbit.

As noted, geocoronal Lyman α is by far the strongest airglow feature. On the day side of the *HST* orbit, when Lyman α is at its strongest, it will produce a net count rate of 20 counts/s/resel, too faint to be a safety concern, but bright enough to make a significant contribution to gain sag on the FUV detector ([Section 4.1.7](#)).

7.4.5 Tabular Sky Backgrounds

Table 7.3 lists the high sky background numbers as plotted in [Figure 7.1](#). The high sky values are defined as the earthshine at 24° from the limb and by the average zodiacal light of $m_V = 22.7$ mag.

The quoted values represent the zodiacal and earthshine backgrounds (excluding the contributions from airglow emission lines) averaged over each wavelength interval. The line intensities of some important airglow lines in the COS bandpass are listed in [Table 7.4](#).

Table 7.3: Earthshine and Zodiacal Light in the COS PSA.

Wavelength (Å)	Earthshine	Zodiacal Light	Total
1000	6.48 E-7	1.26 E-12	6.48 E-7
1100	1.66 E-6	6.72 E-11	1.66 E-6
1200	4.05 E-7	6.23 E-10	4.06 E-7
1300	2.66 E-8	3.38 E-9	2.99 E-8
1400	2.28 E-9	1.32 E-8	1.54 E-8
1500	1.95 E-9	2.26 E-7	2.28 E-7
1600	1.68 E-9	1.14 E-6	1.14 E-6
1700	6.09 E-8	3.19 E-5	3.19 E-5
1800	6.19 E-7	6.63 E-5	6.69 E-5
1900	2.30 E-6	1.05 E-4	1.07 E-4
2000	5.01 E-6	2.07 E-4	2.12 E-4
2100	6.97 E-6	5.95 E-4	6.02 E-4
2200	3.94 E-6	9.82 E-4	9.86 E-4
2300	1.83 E-6	9.67 E-4	9.69 E-4
2400	1.27 E-6	1.05 E-3	1.05 E-3
2500	1.37 E-6	1.01 E-3	1.01 E-3
2600	6.33 E-6	2.32 E-3	2.32 E-3
2700	2.66 E-5	4.05 E-3	4.08 E-3
2800	3.79 E-5	3.67 E-3	3.71 E-3
2900	2.17 E-4	7.46 E-3	7.68 E-3
3000	4.96 E-4	8.44 E-3	8.94 E-3

3100	1.04 E-3	9.42 E-3	1.05 E-2
3200	1.72 E-3	1.10 E-2	1.27 E-2
3300	2.18 E-3	1.34 E-2	1.56 E-2
3400	3.12 E-3	1.30 E-2	1.62 E-2
3500	4.06 E-3	1.31 E-2	1.72 E-2
3600	5.15 E-3	1.24 E-2	1.77 E-2
3700	5.89 E-3	1.49 E-2	2.18 E-2
3800	6.19 E-3	1.41 E-2	2.03 E-2
3900	7.80 E-3	1.39 E-2	2.17 E-2
4000	1.14 E-2	2.07 E-2	3.21 E-2
4250	1.13 E-2	2.17 E-2	3.40 E-2
4500	1.33 E-2	2.53 E-1	3.86 E-2
4750	1.35 E-2	2.57 E-2	3.92 E-2
5000	1.30 E-2	2.50 E-2	3.80 E-2

These rates correspond to the high level in the ETC and are listed in units of 10^{-15} erg cm⁻² s⁻¹ Å⁻¹ for the total COS PSA, which is 4.91 arcsec² in area.

Table 7.4: Typical Strengths of Important Ultraviolet Airglow Lines.

Airglow features	Intensity					
	Day			Night		
	Rayleighs	10^{-15} erg cm ⁻² s ⁻¹ arcsec ⁻²	10^{-15} erg cm ⁻² s ⁻¹ per PSA	Rayleighs	10^{-15} erg cm ⁻² s ⁻¹ arcsec ⁻²	10^{-15} erg cm ⁻² s ⁻¹ per PSA
O I λ911	17	0.7	3.5	8.3	0.35	1.7
O I λ989	161	6.2	30	0.6	-	-
H I λ 1026	571	21	105	2.7	-	-
O I λ 1027	64	2.4	12	0	-	-
O I λ 1152	28	0.93	4.6	0	-	-

N λ1200 1	5.2	0.16	0.8	0.26	0.008	0.04
H I λ 1216	20,000	630	3100	2,000	63	310
O I λ 1302	2,000	59	290	13	0.38	1.9
O I] λ 1356	204	5.8	28	1.3	0.035	0.17
[O II λ 2471	45	0.70	3.4	1	-	-

¹ This feature is not included in the ETC.

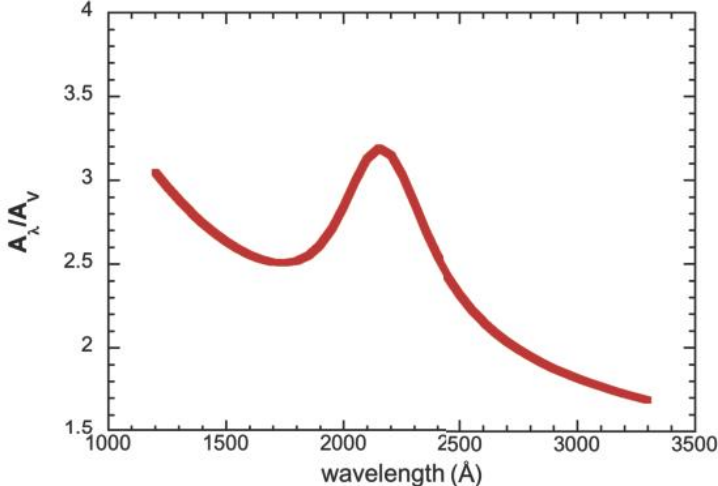
7.5 Extinction Correction

Extinction can dramatically reduce the observed intensity of your source, particularly in the ultraviolet. [Figure 7.3](#) shows $A\lambda/A_V$ values applicable to our Galaxy, taken from Cardelli, Clayton, & Mathis (1989, *ApJ*, 345, 245) assuming $R_V = 3.1$. This corresponds to the *Milky Way Diffuse* ($R_V = 3.1$) selection of the ETC.

Extinction curves have a strong metallicity dependence, particularly at ultraviolet wavelengths. Sample extinction curves are presented in Gordon et al. [2003, *ApJ*, 594, 279 (LMC Average, LMC 30 Dor Shell, and SMC Bar)], Calzetti et al. [2000, *ApJ*, 533, 682 (starburst galaxies)], and references therein. At lower metallicities, the 2200 Å bump that is so prominent in the Galactic extinction curve disappears, and $A_\lambda/E(B - V)$ increases at shorter UV wavelengths.

The ETC allows the user to select among a variety of extinction curves and to apply the extinction correction either before or after the input spectrum is normalized. Be aware that not all extinction laws in the ETC extend below 1200 Å, which may cause incorrect calculations for the 1222, 1055, and 1096 Å central wavelengths.

Figure 7.3: Extinction in Magnitude as a Function of Wavelength.



The Galactic extinction model of Cardelli et al. (1989), computed for $R_V = 3.1$.

7.6 Examples

- [7.6.1 A Flat-Spectrum Source](#)
- [7.6.2 An Early-Type Star](#)
- [7.6.3 A Solar-Type Star with an Emission Line](#)
- [7.6.4 A Faint QSO](#)

We present a few examples of how the COS ETCs may be used. They illustrate the information that is returned by the ETCs and how they can be used to plan your observations. The examples were computed using version 25.2 of the ETC; later versions may return slightly different results.

7.6.1 A Flat-Spectrum Source

One often does not know the exact spectrum shape of the object to be observed, so the answer to a simple question is desired: how long will it take to achieve a given signal-to-noise ratio at a given wavelength if the flux at that wavelength is specified? The easiest way to determine this is to use a flat spectrum as input. How long will it take to achieve $S/N = 10$ per resolution element at 1320 \AA for a point source with a flux of $10^{-15} \text{ erg cm}^{-2} \text{ s}^{-1} \text{ \AA}^{-1}$ using a medium resolution grating?

Only the G130M grating covers the desired wavelength at medium resolution, but several choices of central wavelength are available. We illustrate two approaches: one that uses a cenwave for which only Segment A is available under the [COS 2025 policy](#), and one that uses a dual-segment cenwave. In practice, the choice will depend on the user's science goal.

Single-Segment Operation

Here we select the 1309 \AA setting. We enter the grating and cenwave into the spectroscopic ETC, select the Primary Science Aperture (PSA), select "Exposure time needed to obtain an S/N ratio of 10.0," enter the specified wavelength of 1320 \AA , and select "Point Source" as the source type. For the spectrum distribution, choose a flat continuum in F_λ . Make sure the reddening, $E(B - V)$, is set to 0.

Normalize the target to $10^{-15} \text{ erg cm}^{-2} \text{ s}^{-1} \text{ \AA}^{-1}$ at 1320 \AA . The zodiacal light, earthshine, and airglow were not specified, so we choose average values.

When this case is computed with the ETC, we find the required time is 15,884 s; the total count rate is 43 counts s^{-1} in detector Segment A, well below the safety limit; the count rate in the brightest pixel has 1.5×10^{-4} counts s^{-1} , also well within the safe range (but see below); and the buffer time indicated by the ETC is 8,307 seconds (COS.sp.1033055). The results for Segment B can be ignored, since it will be off.

The buffer time of 8,307 seconds assumes that both segments are in use. The correct value for single-segment operation is not reported in version 25.2 of the ETC, but it can be determined by recalling that the buffer time is inversely proportional to the count rate ([Section 5.4](#)). We multiply the buffer time returned for both segments by the ratio of the count rate for the entire detector to the count rate in Segment A: $8,307 \text{ s} \times (283.976/43.290) = 54,493 \text{ s}$.

What if somewhat higher S/N were desired and one were willing to devote 10 HST orbits to the observation? Assuming that each orbit allows 50 minutes of observing time (ignoring the acquisition time here), we find that in 30,000 seconds we will get $S/N = 13.7$ per resel. Note that $(30,000/15,884)^{1/2} = (13.7/10.0)$. That is, the S/N ratio scales as $t^{1/2}$, as stated in [Section 7.3](#).

If a low-resolution observation is acceptable, then one could switch to the G140L grating. With a grating setting of 1105 Å and $S/N = 10$ per resel, we find the required exposure time is 2732 s, considerably less than the medium-resolution case required. Since this cenwave has always been offered in single-segment mode, the ETC returns the correct buffer time for Segment A only.

Note that the sensitivity of G130M is higher than that of G140L once resolving power is taken into account. In other words, a G130M spectrum that is rebinned to the same resolution as a G140L spectrum can be obtained in less time for a given S/N , although, of course, with diminished wavelength coverage. If only a limited portion of the source's spectrum is of interest, using G130M is more efficient than using G140L.

Dual-Segment Operation

For other science goals, the user may wish to retain the use of both segments by switching to a different cenwave, such as 1222. For this example, we use the same inputs as before, except the cenwave is set to 1222. When this case is computed with the ETC, we find the required time is 16,014 s; the total count rates are 63 and 38 counts s^{-1} in detector Segments A and B, respectively, well below the safety limit; the count rate in the brightest pixel has 0.008 counts s^{-1} , also well within the safe range; and the buffer time indicated by the ETC is 23,434 seconds (COS.sp.1033327).

These cases also illustrate that the earthshine and zodiacal light are completely negligible in the FUV, unless the target flux is much lower than that considered here. This is also true of the airglow if the wavelength of interest is far from the airglow lines. Of course, the airglow cannot be ignored in terms of the total count rate on the detector, or the local count rate if the source contributes at the same wavelengths as the airglow lines.

This is a toy example. For most targets, a more realistic model spectrum would be used to estimate exposure times and test for bright-object violations.

i *If only a limited portion of the source's spectrum is of interest, using G130M and binning over wavelength is more efficient than using G140L.*

7.6.2 An Early-Type Star

We wish to observe an O5V star at medium spectral resolution at a wavelength of 1650 Å. We know that the star has a magnitude of $V = 16$. How long will it take to obtain $S/N = 15$?

We select the G160M grating with a central wavelength of 1623 Å. We select a Kurucz O5V stellar model and set the normalization to be Johnson $V = 16$ mag. We find that the required exposure time is 1,163 s.

Suppose this star is reddened, with $E(B - V) = 0.2$. We select the *Milky Way Diffuse* ($R_V = 3.1$) extinction law, which is shown in [Figure 7.3](#). We must now decide if this extinction is to be applied before or after the normalization. Since the star has a measured magnitude, we want to apply the reddening before normalization. Otherwise, the extinction would change the V magnitude of the stellar model. Making this selection, we find that $S/N = 15$ can be obtained in 2762 s (COS.sp.1033334). The ETC returns a `BUFFER-TIME` of 3043 s. To be conservative, we scale it by 2/3 to get 2028 s.

7.6.3 A Solar-Type Star with an Emission Line

We want to observe a solar-type star with a narrow emission line. Consider the Si II $\lambda 1810$ feature with the following parameters: FWHM = 30 km s^{-1} or 0.18 \AA at 1810 \AA , and integrated emission line flux of $1 \times 10^{-14} \text{ erg cm}^{-2} \text{ s}^{-1}$. The measured magnitude of the star is $V = 12 \text{ mag}$. The desired exposure time is 1000 s.

In the ETC we select a Kurucz G2V star and an NUV grating, G185M, set to a central wavelength of 1817 \AA . We request an exposure time of 1000 s and specify that the S/N be evaluated at 1810 \AA . We add an emission line with the line center at 1810 \AA , FWHM = 0.18 \AA , and an integrated flux of $10^{-14} \text{ erg cm}^{-2} \text{ s}^{-1}$. We specify the normalization as Johnson $V = 12 \text{ mag}$. We set the zodiacal light, air glow, and earthshine to be average.

The ETC returns $S/N = 16.3$ per resel (COS.sp.1033356). The local and global count rates are within safe limits. The recommended buffer time is 2730 s. This `BUFFER-TIME` exceeds the exposure time of 1000 s, so, following the procedure outlined in [Section 5.4](#) we set the `BUFFER-TIME` to 2/3 of the `BUFFER-TIME` value returned by the ETC, which is 1820 s.

For this example, the ETC returns a warning that the S/N it calculates for NUV observations may overestimate the S/N in the standard reduction of the data provided by the archive. This is because the ETC uses a narrower extraction box. See [COS ISR 2017-03](#) for details.

7.6.4 A Faint QSO

An important science goal for the design of COS was to obtain moderate S/N spectra of faint QSOs in the FUV. In the ETC, use the FOS-based QSO spectrum (in the Non-Stellar Objects menu) and choose G130M at 1291 \AA , $S/N = 20$, and a continuum flux of $10^{-15} \text{ erg cm}^{-2} \text{ s}^{-1} \text{ \AA}^{-1}$ at 1320 \AA . (Note that only `FP-POS 3` and `4` are available at this cenwave, but these are sufficient to attain the S/N goal; see [Table 5.6](#).) The indicated exposure time is 63,154 s, or about 21.1 orbits (COS.sp.1033359). The source count rate is $0.001 \text{ count s}^{-1}$, with a background rate of $6.230 \times 10^{-5} \text{ count s}^{-1}$, 16 times less than that of the source. The background is completely dominated by the dark current of the detector. The count rate over the entire detector is 316 count/s, well below any safety limits, and the maximum `BUFFER-TIME` is 7459 s. Scaling by 2/3 yields 4972 s for the `BUFFER-TIME`.

Chapter 8: Target Acquisitions

Chapter Contents

- 8.1 Introduction
- 8.2 Target Acquisition Overview
- 8.3 ACQ SEARCH Acquisition Mode
- 8.4 ACQ IMAGE Acquisition Mode
- 8.5 ACQ PEAKXD Acquisition Mode
- 8.6 ACQ PEAKD Acquisition Mode
- 8.7 Exposure Times
- 8.8 Centering Accuracy and Data Quality
- 8.9 Recommended Parameters for all COS TA Modes
- 8.10 Special Cases

8.1 Introduction

The COS science apertures are 2.5 arcsec in diameter. An observation will yield high-quality data only if the target is properly centered in the science aperture. This chapter discusses the available target-acquisition (TA) methods, demonstrates the dependence of data quality on centering accuracy, and recommends acquisition scenarios for various combinations of target coordinate accuracy and brightness. Recommended parameters for all COS TA modes are presented in [Section 8.9](#).

Based on improvements in the COS-to-FGS alignment, together with an analysis of the distribution of positional errors in the GSC2, we estimate that an HST guide-star acquisition will place a target with good coordinates in the COS aperture 98.5% of the time. As a result, we do not require that all COS observations begin with an `ACQ/SEARCH` sequence if the uncertainty of the target coordinates is ≤ 0.4 arcsec. We do, however, recommend in almost all cases that some sort of target acquisition be performed to center the target in the aperture. The APT (the [Astronomer's Proposal Tool](#)) will issue a warning if an acquisition is omitted. Target acquisition is required only once for a series of observations in contiguous orbits (i.e., once per visit). Moving targets require an acquisition at the beginning of each orbit.

Bright-Object Protection

The COS detectors are vulnerable to damage or performance degradation if exposed to too much light. Imaging acquisitions present a special risk because they concentrate the light of an object on a small area of the detector. Users of COS must demonstrate that their targets are safe. Information on bright-object protection and screening is provided in [Chapter 10](#).

8.2 Target Acquisition Overview

COS has four target acquisition (TA) modes:

- **ACQ/SEARCH** performs a spiral search by executing individual exposures at each point in a square grid pattern on the sky (details are in [Section 8.3](#)). This mode can use either dispersed-light or imaging exposures.
- **ACQ/IMAGE** obtains an NUV image of the target field, moves the telescope to center the object, and obtains a second NUV image as confirmation (details are in [Section 8.4](#)). This is generally the fastest and most accurate method of target acquisition, but covers a limited area on the sky.
- **ACQ/PEAKXD** determines the location of the target in the cross-dispersion (XD) direction and moves the telescope to center the object in the XD direction (details are in [Section 8.5](#)).
- **ACQ/PEAKD** centers the target in the along-dispersion (AD) direction by executing individual exposures at each point in a linear pattern along the dispersion axis (details are in [Section 8.6](#)). **ACQ/PEAKXD** should always precede **ACQ/PEAKD**, and the two should always be performed together.

Coordinate accuracy and target brightness will inform your choice of target-acquisition strategy and optional parameters. Imaging acquisitions are more precise and often faster, but restrictions on the local count rate ([Chapter 10](#)) can prevent their use. While the TA modes can be used in any order or even repeated, the recommended strategies are given in [Table 8.1](#). We suggest evaluating these strategies in the following order:

1. NUV Imaging with the fastest allowable combination of aperture and mirror that does not violate NUV count rate limits, uses the least time overall, and achieves the desired S/N, even if the science to follow is performed with the FUV channel.
2. Dispersed-light acquisition using the same configuration as the first science exposure if this configuration will use the least time overall and is an allowed configuration for acquisition, or if option 1 violates NUV count rate limits even when the BOA and MIRRORB are used (see [Section 5.2](#)).
3. Dispersed-light acquisition with a different configuration if options 1 and 2 are not chosen for any of the reasons listed above.

The scenarios outlined here are for isolated point sources. See [Section 8.10](#) for additional information regarding crowded or complex fields and offset-target TAs.

Table 8.1: Basic COS Target Acquisition Strategies.

Type	Step 1	Step 2	Step 3
Imaging (if coordinates are good to 0.4")	ACQ/IMAGE	none	none
Imaging (if coordinates are less accurate)	ACQ/SEARCH	ACQ/IMAGE	none
Dispersed-Light (coordinates good to 0.4")	ACQ/PEAKXD	ACQ/PEAKD	none
Dispersed-Light (coordinates less accurate)	ACQ/SEARCH	ACQ/PEAKXD	ACQ/PEAKD

Either Imaging or Dispersed-Light (e.g., small, extended sources)	ACQ/SEARCH	2 × 2 × 1.767" ACQ/SEARCH	none
--	------------	---------------------------	------

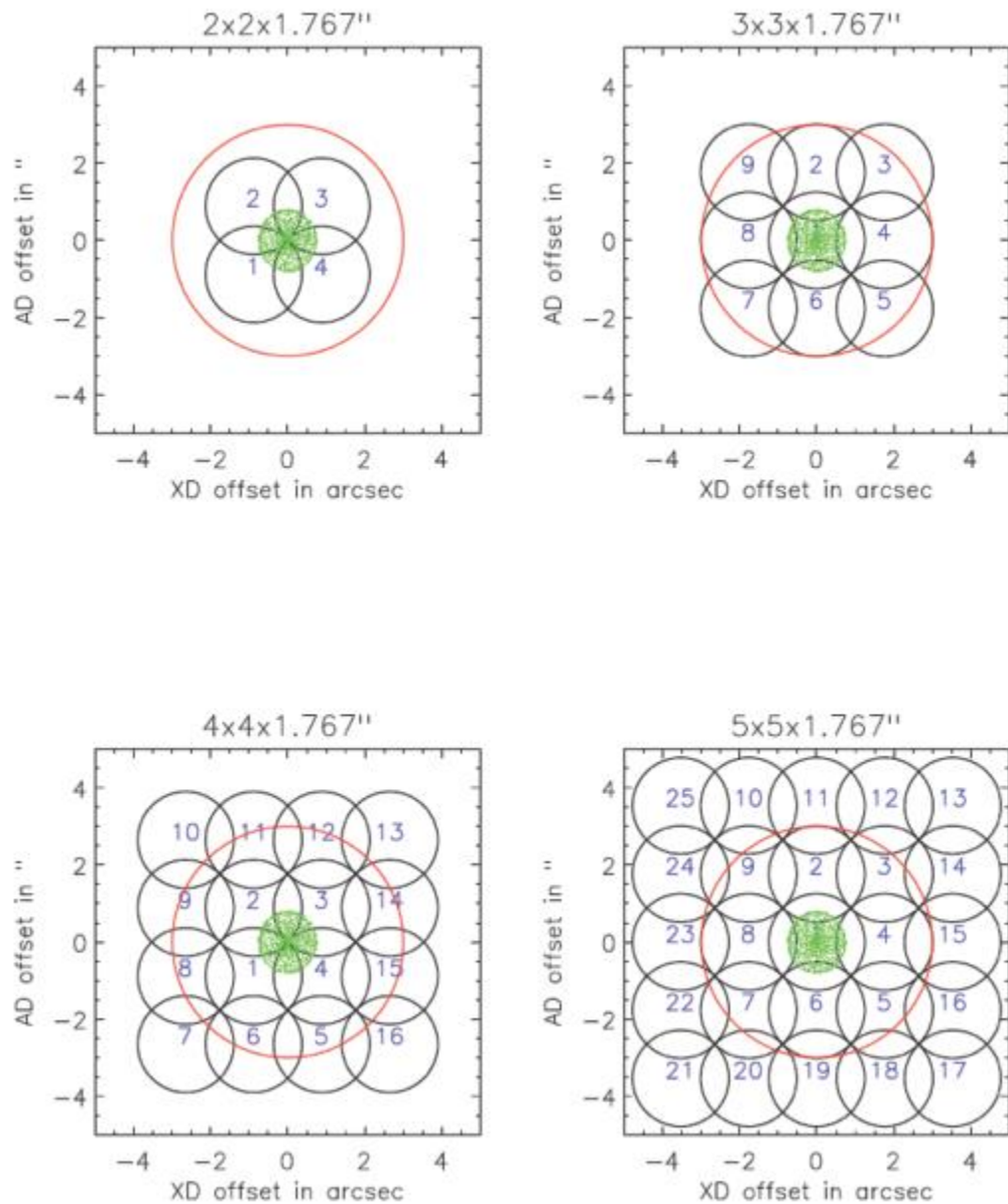
Please Note...

- It is the responsibility of the observer to provide coordinates and proper motions with the required accuracy. Be especially mindful of nearby stars, which generally have high proper motions, and binary stars, whose motions on the sky are highly non-linear. Observations that fail because of an inaccurate target position will not be repeated. STScI cannot be responsible for target-coordinate or proper-motion errors in published or on-line catalogs, or in the literature. If there is any doubt that the available coordinates meet the required accuracy, then an ACQ/SEARCH should be performed.
- If a target falls near the edge of the aperture at the initial pointing, the TA algorithms may slightly miscalculate its position. Users who require the best possible photometric or absolute wavelength accuracy may wish either to begin with an ACQ/SEARCH to ensure that the target is reasonably well centered before the final stages of the acquisition are performed, or to perform additional acquisition exposures in case the observation at the initial pointing was partially vignetted.
- The blue central-wavelength settings for G130M (1055, 1096, and 1222 Å) and new settings introduced in Cycle 26 (G160M/1533 and G140L/800) cannot be used for target acquisitions.
- For ACQ/IMAGE exposures, both the preliminary and confirmation images are downlinked and delivered to the observer. For the other three TA modes, no images or spectra are recorded.
- Many quantities useful for evaluating the success of COS TAs are recorded in the COS TA data products, for which the keywords and their meanings are listed in Table 5 of [COS ISR 2010-14](#).

8.3 ACQ SEARCH Acquisition Mode

In ACQ/SEARCH mode, the telescope is moved in a spiral pattern on the sky to cover a square grid up to 5×5 steps in size. At each scan point, the telescope stops and data are collected. A two-dimensional array containing the total counts measured at each dwell point is constructed. After completion of the full $n \times n$ pattern, the target position is calculated as described below, and the telescope is moved to center the target. [Figure 8.1](#) illustrates the spiral search patterns that are used for ACQ/SEARCH.

Figure 8.1: The Spiral Search Patterns Used for ACQ/SEARCH.



This Figure shows the 2×2 , 3×3 , 4×4 , and 5×5 spiral search patterns executed with the default `STEP-SIZE` of 1.767 arcsec. The black circles represent the positions of the 2.5 arcsec-diameter science aperture, and the numbers show the sequence of steps on the sky. The outer circle in red has a radius of 3 arcsec. The green pattern represents the approximate COS science aperture PSF.

For an ACQ/SEARCH, the user must specify:

- The aperture to use, either PSA or BOA.
- The spectral element (grating or mirror) and the central-wavelength setting (if applicable). For a spectroscopic ACQ/SEARCH these will generally be the grating and central wavelength of the initial science observation. However, an observer may specify ACQ/SEARCH with a different grating and central-wavelength setting if there are advantages to doing so.
- The `SCAN-SIZE`, which is 2, 3, 4, or 5, corresponding to spiral patterns of 2×2 , 3×3 , etc.

- The `STEP-SIZE`, or spacing between grid points. It may be any value from 0.2 to 2.0 arcsec, but we strongly recommend using the default value of 1.767 arcsec in most cases. This value has been chosen so that no part of the sky is missed, given the aperture diameter of 2.5 arcsec

$$(2.5/\sqrt{2} = 1.767).$$

- The exposure time per dwell point.
- For FUV searches, users may choose to use just one of the segments, A or B, but the use of both is recommended. The use of both segments is the default for all but G140L and the G130M cenwaves restricted by the COS 2025 rules; in these cases, only Segment A data are used. However, there is a substantial overhead associated with switching from two-segment to single-segment operation (and back again); see [Table 9.5](#).

Once the scan is complete, the flight software computes the centroid of the array and thus the position of the target. There are three centroiding options:

1. The first option is `CENTER=FLUX-WT`, which uses a flux-weighted centroiding algorithm to determine the center of light. It is the default for `SCANSIZE=2`.
2. A variation on `CENTER=FLUX-WT` is `CENTER=FLUX-WT-FLR`. In this case, a floor is subtracted from the counts at each dwell point before the centroid is computed. The floor is taken as the minimum number of counts seen at any one dwell point. `FLUX-WT-FLR` has the advantage of removing background counts, but leaves one or more points in the array with zero counts. As it can cause computational problems, `FLUX-WT-FLR` should not be used with `SCAN-SIZE=2`. `CENTER=FLUX-WT-FLR` should be used for `SCAN-SIZE > 2 × ACQ/SEARCHS`.
3. The last option for centering is `CENTER=BRIGHTEST`, which simply centers the dwell point with the most counts. This is straightforward, but not as accurate as the other centroiding methods. `CENTER=BRIGHTEST` is appropriate if coordinates are uncertain and the `ACQ/SEARCH` is followed by either a second `ACQ/SEARCH` using flux-weighted centering or an `ACQ/IMAGE`, or if the source is extended and it is only desired that the brightest point be in the aperture.

[Table 8.2](#) presents the recommended `ACQ/SEARCH` parameters as a function of coordinate uncertainty. For all values of `SCAN-SIZE > 2` we recommend `CENTER=FLUX-WT-FLR` as it is more accurate due to better sky and detector background suppression. The `CENTER` values in [Table 8.2](#) are the current default values for each `SCAN-SIZE`. Note that even `SCAN-SIZE` values (2 or 4) trigger additional overhead because of the telescope motion required to displace the aperture by half of a `STEP-SIZE` in both the dispersion and cross-dispersion directions, so that the overall pattern remains centered on the initial pointing.

Analysis of COS acquisitions indicate that a single `ACQ/SEARCH` acquisition, whether spectroscopic or imaging, provides a centering accuracy of 0.3 arcsec only 75% of the time. Additional TA stages are thus necessary to achieve the centering accuracy necessary to meet wavelength and photometric requirements.

Table 8.2: Recommended `ACQ/SEARCH` Parameters versus Coordinate Uncertainty.

Coordinate uncertainty (arsec)	SCAN-SIZE	STEP-SIZE	CENTER
$\sigma \leq 0.4$	ACQ/SEARCH not required.		
$0.4 < \sigma < 0.7$	2	1.767 ¹	FLUX-WT

$0.7 < \sigma < 1.0$	3	1.767 ²	FLUX-WT-FLR
$1.0 < \sigma < 1.3$	4	1.767 ²	FLUX-WT-FLR
$1.3 < \sigma \leq 1.6$	5	1.767 ²	FLUX-WT-FLR

¹ This is the default `STEP-SIZE` value and the largest to cover the search area without holes or gaps.

² If target coordinate uncertainty is on the lower edge of the given range, the `STEP-SIZE` may be reduced slightly (e.g., 1.5 arcsec) to improve centering accuracy at the expense of total area covered by the search.

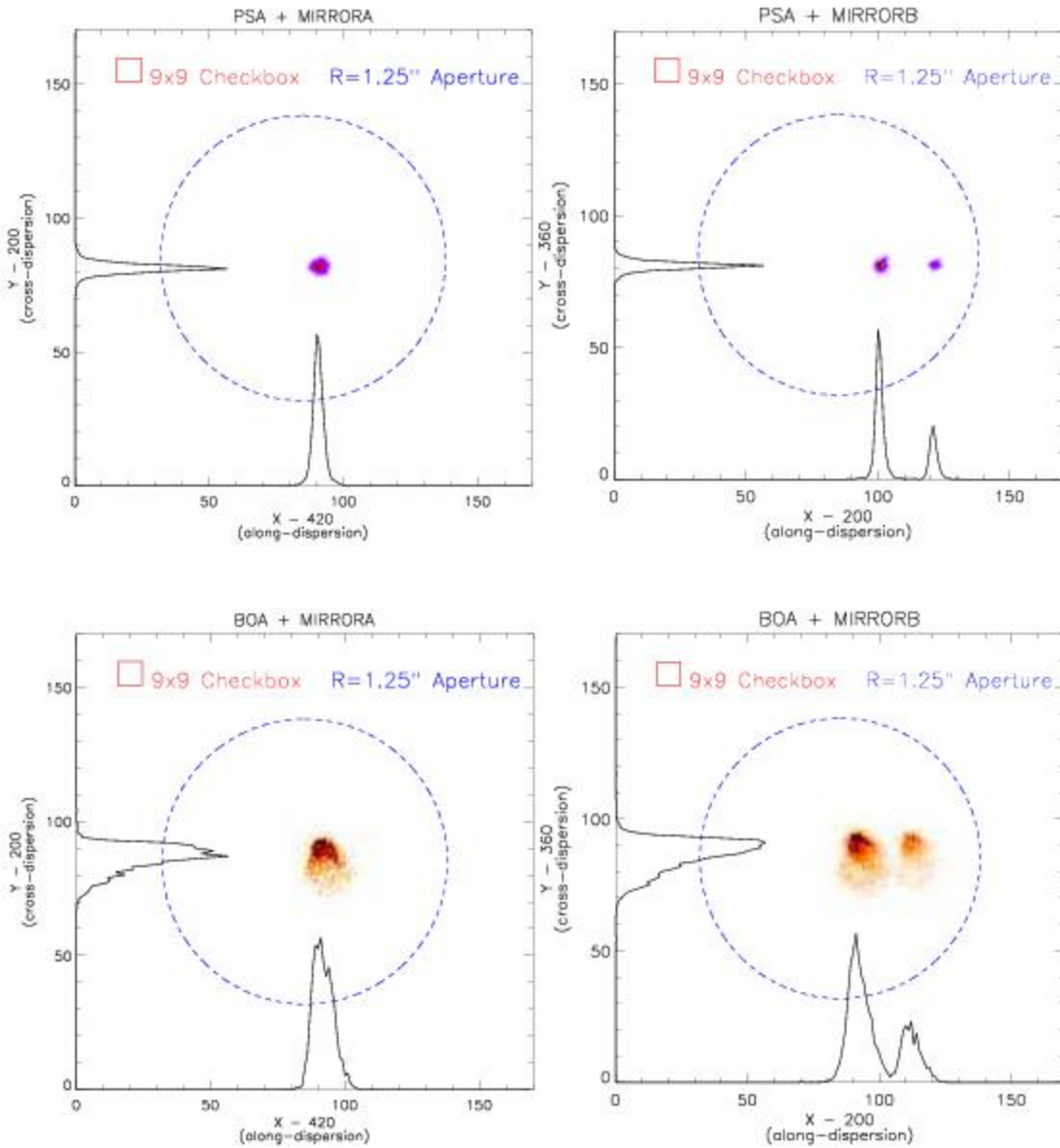
8.4 ACQ IMAGE Acquisition Mode

In `ACQ/IMAGE` mode COS obtains an NUV image of the target field, moves the telescope to center the object, and obtains a second NUV image as confirmation. `ACQ/IMAGE` may use either the primary science aperture (PSA) or the bright object aperture (BOA) and either `MIRRORA` or `MIRRORB`. All four combinations are illustrated in [Figure 8.2](#). Acquisition images obtained through the PSA should strive for a minimum S/N of 20. Due to the complex shape of images obtained through the BOA, $S/N > 30$ is recommended. (These thresholds were reduced beginning in Cycle 25.) Note the additional structures present in images obtained with `MIRRORB` or the BOA: The secondary image produced by `MIRRORB` is half the intensity of the primary image and is displaced by 20 pixels (about 0.5 arcsec) in the along-dispersion direction. The BOA produces a chevron-like image whose peak is displaced in both the along-dispersion (AD) and cross-dispersion (XD) directions. When the BOA is used with `MIRRORB`, two distorted peaks result. In this configuration, there is some overlap between the wings of the primary and secondary peaks, but they are well enough separated to allow for reliable acquisitions. The lamp and target images of `MIRRORA` and `MIRRORB` images are offset, and vary from exposure to exposure. Users should expect `MIRRORB` images to be offset from `MIRRORA` images by ~ 214 pixels in AD, and ~ 160 pixels in XD.

An `ACQ/IMAGE` exposure consists of the following steps:

1. An exposure of the internal Pt-Ne lamp is obtained through the WCA aperture. The onboard COS Flight Software (FSW) sets the exposure time for the lamp exposure automatically. The centroid of the WCA image is calculated by the FSW. Using the known offset between the center of the WCA and the science aperture (PSA or BOA), the location of the center of the science aperture on the detector is computed.
2. The shutter is opened and a TA image of the field is obtained. The telescope is not moved, meaning that an acquisition using `ACQ/IMAGE` will be successful only if the target lies within (or just outside of) the aperture. An area of 170×170 pixels, which corresponds to approximately 4×4 arcsec², centered on the aperture, is read out. This image is recorded and downlinked and becomes part of the archived data package. (It is stored in the first extension of the `_rawacq` file).
3. A 9×9 pixel checkbox array is then passed over the 170×170 pixel image. First, the checkbox with the most counts is identified. In the unlikely instance that two checkboxes have equal counts, the first one encountered is used. The brightest 9×9 array is then analyzed using a flux-weighted centroiding algorithm to calculate the target position.
4. Finally, HST is moved to place the calculated centroid at the center of the selected aperture. A second exposure, identical to the first, is taken and recorded for later downlink as a verification of the centering. (It is stored in the fourth extension of the `_rawacq` file). It is important to consider the throughput of the NUV `MIRRORA` or `MIRRORB` combinations when selecting a TA strategy ([Section 6.2](#) and [Figure 6.3](#)).

Figure 8.2: Point Sources Observed with all Four Aperture/Mirror Combinations.



NUV images of point sources observed through the PSA (top) and BOA (bottom) using MIRRORA (left) and MIRRORB (right). The limits of each plot represent the 170×170 pixel image used by ACQ/IMAGE. Also shown are the COS aperture (blue circle of radius 1.25") and the 9×9 checkbox used by ACQ/IMAGE. Histograms show the AD and XD profiles. The pointing is typical of that expected after an ACQ/SEARCH, but before additional peak-ups.

8.5 ACQ PEAKXD Acquisition Mode

[8.5.1 NUV PEAKXD Acquisitions](#)

[8.5.2 FUV PEAKXD Acquisitions](#)

An ACQ/PEAKXD sequence is used to improve centering in the cross-dispersion (XD) direction. We recommend a minimum S/N of 40 for all dispersed-light target acquisition exposures.

8.5.1 NUV PEAKXD Acquisitions

The steps executed for NUV ACQ/PEAKXD sequences are:

1. A short exposure of the Pt-Ne wavelength calibration lamp through the WCA aperture is obtained. The spectrum is collapsed along the dispersion direction, its centroid is calculated, and the center of the target aperture is computed.
2. A target spectrum is recorded for the user-specified time using a sub-array tailored to each grating and central wavelength (excluding edge effects and airglow lines). The spectrum is collapsed along the dispersion direction.
3. The target XD location is assumed to be the median position of the collapsed spectrum.
4. The slew required to move the target spectrum in the XD direction to the center of the aperture is computed.
5. The telescope is slewed by the calculated offset to center the target in the XD direction.

The user must specify the aperture (PSA or BOA, typically the same as for the science exposure), the grating and central wavelength, and the exposure time. The use of MIRRORA or MIRRORB is not allowed. The stripe (SHORT, MEDIUM, or LONG, corresponding to stripes A, B, or C) to be used in the computation may be specified; however, the default stripe B (MEDIUM) is recommended for most settings, as it achieves the best centering.¹

Note: For extended sources observed with the NUV detector, light from the three spectral stripes may overlap. In this case acquisitions will likely fail and should be avoided.

Due to increased NUV detector background and mechanism position uncertainties, certain NUV central wavelength (cenwave) settings have proven to be unreliable in the NUV ACQ/PEAKXD target acquisition phase. The cenwave settings listed below have been proven reliable. NUV ACQ/PEAKXD target acquisitions should use one of these settings. Users who wish to use other cenwaves should contact the COS team via the [Help Desk](#).

G185M: 1786, 1913, 1921, 1941
G225M: 2250, 2283, 2306
G285M: no settings recommended
G230L: 2635, 2950, 3000, 3360

8.5.2 FUV `PEAKXD` Acquisitions

As described in [Section 4.1.7](#), the COS FUV detector exhibits gain sag. Gain sag effects are alleviated by periodic lifetime moves, which place the FUV spectrum on unsagged regions of the detector (see [Section 5.12](#)).

One consequence of the gain sag effect is the mis-registration of photon events in the cross-dispersion (XD) or Y direction, commonly referred to as Y walk. While Y walk does not adversely affect science data, it can reduce the accuracy of target acquisitions obtained in dispersed light. If the target is centered in the aperture, but the Y walk shifts its spectrum in the XD direction, then the FUV `ACQ/PEAKXD` algorithm at previous lifetime positions (LP1-LP3) would miscalculate its centroid and move the target away from the aperture center.

The FUV Segment B is more affected by Y walk and gain sag than Segment A, mainly due to the intense geocoronal Lyman- α emission that hits the detector during G130M observations. To combat the effects of Y walk, the LP1-LP3 FUV `ACQ/PEAKXD` algorithm was modified to use only Segment A data.

From Cycle 25 onward (October 2, 2017), the FUV `ACQ/PEAKXD` sequence differs from the algorithm used in previous cycles. It uses only the total number of counts and is not affected by Y walk. For FUV `ACQ/PEAKXD` acquisitions, either segment A or B may be used when available, but use of `SEGMENT=DEFAULT` is recommended. All G140L `ACQ/PEAKXD` acquisitions and those with G130M cenwaves restricted by the COS 2025 rules use only segment A. In the case of cenwave G140L/1280, detector segment B is left on by default but counts from segment B are not used for acquisition calculations. The ETC correctly calculates the needed exposure time for cenwave 1280 acquisitions, and also lists the count rate for segment B. Any count rate violation warnings for segment B are real and should not be ignored.

The new `ACQ/PEAKXD` algorithm works much like `ACQ/SEARCH` except that, instead of a spiral, the spacecraft is moved linearly along the XD axis between exposures. An array containing the total counts at each dwell point is constructed. Its centroid is computed, and the telescope is moved to center the target in the aperture in the XD direction. The user must specify the aperture, grating, central wavelength, and the exposure time at each dwell point. The use of `MIRRORA` or `MIRRORB` is not allowed. The number of steps, called `NUM-POS`, may be 3, 5, 7, or 9. The `STEP-SIZE` is given in arcseconds. There are three options for the centering algorithm, `CENTER=FLUX-WT`, `FLUX-WT-FLR`, and `BRIGHTEST`, and they work just as described in [Section 8.3](#). For most applications, we recommend the use of `NUM-POS=3`, `STEP-SIZE=1.3`, and `CENTER=FLUX-WT`, as this combination (which is the default) is the fastest pattern that centers targets to within the requirements. Observers who wish to use `NUM-POS=5` are advised to use `STEP-SIZE=0.9` and `CENTER=FLUX-WT-FLR`. The special parameter `CENTER=DEFAULT` sets `CENTER=FLUX-WT` if `NUM-POS=3` and `CENTER=FLUX-WT-FLR` if `NUM-POS=5, 7, or 9`. If `NUM-POS` is 5, 7, or 9, then the value of `STEP-SIZE` should be manually entered in APT. While any combination of `NUM-POS` and `STEP-SIZE` is allowed, it should be noted that for `PEAKXD` `NUM-POS=3` with `STEP-SIZE=1.3` and `NUM-POS=5` with `STEP-SIZE=0.9` are the only two combinations that are routinely tested.

Note: FUV `ACQ/PEAKXDS` on extended sources are possible, but they require a `NUM-POS` and `STEP-SIZE` combination tuned to the extent of the source.

¹ There are special restrictions with the G230L grating, which positions first-order light on the detector only for certain stripes. The MEDIUM stripe is required for the 2635 central wavelength, the SHORT stripe is required for the 3360 wavelength, and either SHORT or MEDIUM may be used for the 2950 and 3000 wavelengths. The LONG stripe may not be used with G230L at all.

8.6 ACQ PEAKD Acquisition Mode

ACQ/PEAKD exposures are used to improve centering in the along-dispersion (AD) direction after an ACQ/PEAKXD. ACQ/PEAKD works much like ACQ/SEARCH except that, instead of a spiral, the spacecraft is moved linearly along the AD axis between exposures. An array containing the total counts at each dwell point is constructed. Its centroid is computed, and the telescope is moved to center the target in the aperture in the AD direction.

The user must specify the aperture, grating, central wavelength, and the exposure time at each dwell point. The use of MIRRORA or MIRRORB is not allowed. The number of steps, here called NUM-POS, may be 3, 5, 7, or 9. The STEP-SIZE is given in arcseconds. There are three options for the centering algorithm, CENTER=FLUX-WT, FLUX-WT-FLR, and BRIGHTEST, and they work just as described in [Section 8.3](#).

For most applications, we recommend the use of NUM-POS=5, STEP-SIZE=0.9, and CENTER=FLUX-WT-FLR, as this combination is the least sensitive to high or variable background rates and covers a large area on the sky. This combination is the only PEAKD configuration that is routinely tested. Observers who wish to use NUM-POS=3 are advised to use STEP-SIZE=1.3 and CENTER=FLUX-WT. The special parameter CENTER=DEFAULT sets CENTER=FLUX-WT if NUM-POS=3 and CENTER=FLUX-WT-FLR if NUM-POS=5, 7, or 9. For FUV ACQ/PEAKD acquisitions, either Segment A or B may be used when available, but use of SEGMENT=DEFAULT is recommended. All G140L ACQ/PEAKD acquisitions and those with G130M cenwaves restricted by the COS 2025 rules use only Segment A data.

8.7 Exposure Times

[8.7.1 Imaging Acquisitions](#)

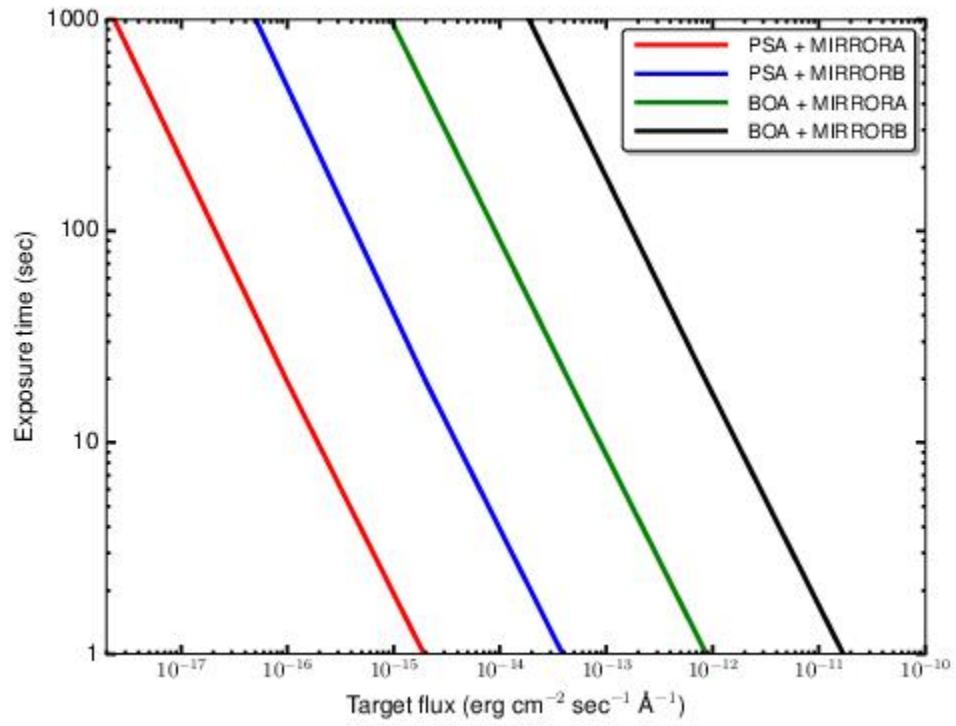
[8.7.2 Dispersed-Light Acquisitions](#)

While the figures in this section will help you to estimate exposure times for various acquisition scenarios, the [COS Exposure Time Calculator](#) (ETC) should be used for all proposal preparation.

8.7.1 Imaging Acquisitions

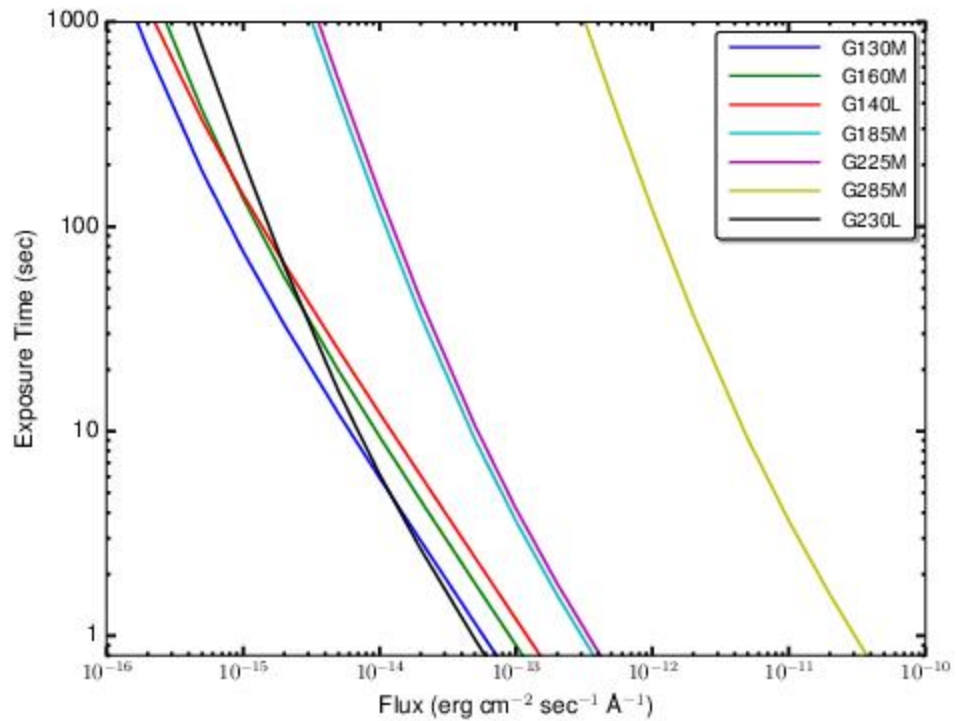
Acquisition images obtained through the PSA should strive for a minimum S/N of 20. Due to the complex shape of images obtained through the BOA, a $S/N > 30$ is recommended. For MIRRORB acquisitions, the recommended S/N refers only to the primary image; the ETC performs this calculation appropriately. [Figure 8.3](#) shows approximate exposure times needed to reach these S/N levels for various target fluxes. A flat source spectrum ($F_\lambda = \text{constant}$) is assumed.

Figure 8.3: Exposure Time Needed for an ACQ/IMAGE Acquisition.



Approximate exposure time needed to achieve $S/N = 20$ (PSA) or 30 (BOA) as a function of target flux. This calculation assumes a flat source spectrum.

Figure 8.4: Exposure Time Needed for a Dispersed-Light Acquisition with the PSA.



Approximate exposure time needed to achieve S/N of 40, assuming a flat source spectrum.

8.7.2 Dispersed-Light Acquisitions

We recommend a minimum S/N of 40 for all dispersed-light acquisition exposures. STScI calibration programs routinely use up to $S/N = 100$ to minimize the influence of Poisson noise and background when very precise pointing is required. Figure 8.4 is a guide to the exposure time needed for a dispersed-light acquisition with the PSA, assuming a flat source spectrum ($F_{\lambda} = \text{constant}$). Note that these exposure times apply to each separate dwell point of a pattern, which is the quantity entered into [APT](#) in Phase II.

8.8 Centering Accuracy and Data Quality

- [8.8.1 Centering Accuracy and Wavelength Accuracy](#)
- [8.8.2 Centering Accuracy and Photometric Precision](#)
- [8.8.3 Centering Accuracy and Spectroscopic Resolution](#)

A centering accuracy of 0.3 arcsec in the cross-dispersion (XD) direction is required to achieve optimum photometric accuracy and spectral resolution. In the along-dispersion (AD) direction, the minimum accuracy is set by velocity requirements: ± 15 km/s for the medium-resolution modes, ± 150 km/s for G140L, and ± 175 km/s for G230L. Since the AD requirements are in units of km/s, they are grating and wavelength dependent. Assuming that the wavelength error budget is split evenly between the COS TA and wavelength scale accuracy, the strictest pointing requirements are ± 0.041 arcsec for the NUV channel and ± 0.106 arcsec for the FUV channel.

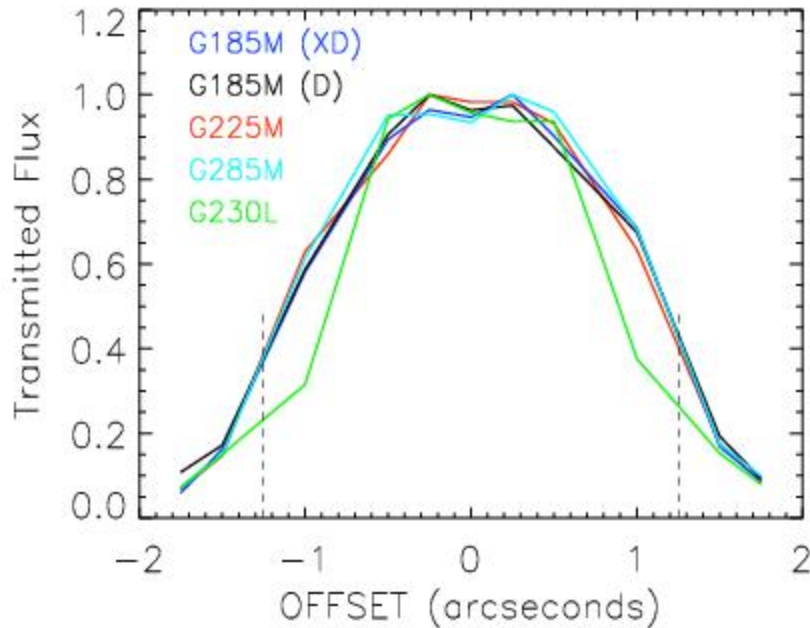
8.8.1 Centering Accuracy and Wavelength Accuracy

To achieve a wavelength accuracy of ± 15 km/s, the target should be centered to within about 0.04–0.07 arcsec for NUV observations and 0.1–0.2 arcsec for FUV observations. The throughput of COS is not affected by centering errors of less than 0.4 arcsec, so high centering precision is not strictly necessary if science goals do not require that the wavelength zero point be well constrained. For example, the spectra of some objects may include foreground interstellar or inter-galactic absorption lines that can be used to establish the zero point of the wavelength scale.

8.8.2 Centering Accuracy and Photometric Precision

[Figure 8.5](#) shows the relative transmission of the PSA as a function of the displacement of a point source from the aperture center, as measured using each of the four NUV gratings. These and the corresponding FUV curves are nearly identical and show that the transmission of the COS apertures is essentially flat within the central ± 0.4 arcsec, then tails off in a non-linear but approximately symmetrical profile ([COS ISR 2010-09](#)).

Figure 8.5: Relative Transmission of the COS PSA at NUV Wavelengths.



Transmitted flux as a function of displacement from aperture center for all four NUV gratings. The dotted lines mark the edge of the aperture (1.25"). The two curves labeled D and XD refer to offsets along the dispersion and cross-dispersion axes, respectively. The other curves trace offsets in the cross-dispersion direction. For all gratings, the absolute transmission through the PSA for a centered point source is at least 95%.

8.8.3 Centering Accuracy and Spectroscopic Resolution

Targets placed within 0.3 arcsec of the aperture center will achieve maximum spectral resolution. Centering errors larger than 0.3 arcsec will lead to progressively poorer resolution. Targets at the edge of the aperture have approximately half the spectral resolution of well-centered targets.

8.9 Recommended Parameters for all COS TA Modes

As the result of our analysis of the target acquisition (TA) performance of COS, we have adjusted many COS TA parameters and have refined our recommendations and guidelines for routine COS TAs. We present these recommendations and guidelines in the previous sections and summarize the most significant instructions below. [Table 8.3](#) provides our recommended values for optional parameters for each COS TA type.

- All TA modes provide good centering. For optimal wavelength accuracy, use NUV imaging mode; otherwise, use the mode that is fastest, as determined by the Orbit Planner in APT.
- Signal-to-noise (S/N) is important. Use $S/N > 40$, except for ACQ/IMAGE, which requires $S/N > 20$ through the PSA and $S/N > 30$ through the BOA.
- By default, FUV acquisitions for gratings G130M and G160M take place in the same Lifetime Position used for the grating/cenwave combination. FUV acquisitions for grating G140L take place at LP4 even though science exposures are taken at LP3. In standard cases users do not need to specify a choice of LIFETIME-POS in APT. Users observing with grating G160M at LP4 ([Section 9.5.1](#)) should select LIFETIME-POS=LP4 under optional parameters on APT.
- A single ACQ/SEARCH is not sufficient to CENTER a COS point-source target in the aperture. Always follow the first ACQ/SEARCH with an ACQ/IMAGE or with ACQ/PEAKXD+ACQ/PEAKD.
- ACQ/SEARCH exposures are not required for targets with coordinate accuracies of ± 0.4 arcsec or better in the ICRS/GSC2 frame. Spending extra time to validate target coordinates is the best way to save TA time. On-line catalogs often have coordinate errors that exceed 0.4 arcsec. *It is the user's responsibility to verify that target coordinates are correct.*
- For NUV spectroscopic ACQ/PEAKXDS, only a few cenwaves have been proven to be reliable. Users should choose one of these cenwaves, which are listed in [Section 8.4](#). The G185M, G225M, and G230L gratings each have three or four recommended cenwaves, while the G285M grating has none. For a full discussion of this issue, see [COS ISR 2017-05](#).
- If at all possible, use STRIPE=MEDIUM (stripe B) for NUV spectroscopic ACQ/PEAKXDs, which is the default. Primarily, this is because the WCA-to-PSA offsets in the flight software are optimized for stripe B in most modes. Choosing a different stripe will result in systematic offsets of the initial spectrum of order of a few pixels, which generally are still within typical target coordinate uncertainties.
- FUV ACQ/PEAKXD uses NUM-POS=3, STEP-SIZE=1.3, and CENTER=FLUX-WT as defaults. In most cases there is no need to change, or enumerate, these parameters.
- There are no defaults for FUV ACQ/PEAKD. Use NUM-POS=5, STEP-SIZE=0.9, and CENTER=FLUX-WT-FLR for most ACQ/PEAKD centerings. For the most accurate AD (ACQ/PEAKD) centering possible, use NUM-POS=9, STEP-SIZE=0.6, and CENTER=FLUX-WT-FLR. When a fast TA is required and lower centering accuracy can be tolerated, use NUM-POS=3, STEP-SIZE=1.3, and CENTER=FLUX-WT.

Table 8.3: COS Acquisition Modes, Options, and Recommended Values.

Acquisition Type	Description	SCAN-SIZE or NUM-POS	STEP-SIZE (arcsec)	Optional Parameters	Recommended Values	Recommended S/N
ACQ/SEARCH	Spiral pattern; multiple	2	1.767	CENTER=DEFAULT, FLUX-WT, FLUX-	FLUX-WT	40 (PSA a BOA)

	exposures. Can be used with either imaging or spectroscopic ACQs.	3 ¹		WT-FLR, BRIGHTEST ³	FLUX-WT-FLR	
		4		For FUV: SEGMENT= A, B, BOTH	FLUX-WT-FLR	
		5			FLUX-WT-FLR	
ACQ/ IMAGE	Initial and confirmation images (NUV only)					20 (PSA) 30 (BOA)
ACQ/ PEAKXD (NUV)	One exposure			STRIPE=SHORT, MEDIUM, LONG	STRIPE=MEDIUM ²	40
					(This is the default value.)	
ACQ/ PEAKXD (FUV)	Linear pattern; multiple exposures	3 ¹	1.3 ¹	CENTER=DEFAULT, FLUX-WT, FLUX- WT-FLR, BRIGHTEST ³	FLUX-WT	40
		5	1.0		FLUX-WT-FLR	
		7	0.8		FLUX-WT-FLR	
		9	0.65		SEGMENT= A, B, BOTH	
ACQ/ PEAKD	Linear pattern; multiple exposures	3	1.3	CENTER=DEFAULT, FLUX-WT, FLUX- WT-FLR, BRIGHTEST ³	FLUX-WT	40
		5 ¹	0.9 ¹		FLUX-WT-FLR	
		7	0.6		FLUX-WT-FLR	
		9	0.6		For FUV: SEGMENT= A, B, BOTH	

¹ Recommended value. For ACQ/PEAKD, FUV ACQ/PEAKXD, and ACQ/SEARCH, use of special parameter CENTER=DEFAULT is recommended.

² The G230L grating has special recommendations, see [Section 8.5.1](#).

³ For ACQ/PEAKD, FUV ACQ/PEAKXD, and ACQ/SEARCH, use of special parameter CENTER=DEFAULT is recommended. In the case of ACQ/PEAKD and FUV ACQ/PEAKXD this parameter sets CENTER=FLUX-WT if NUM-POS=3, and CENTER=FLUX-WT-FLR if NUM-POS=5, 7, or 9. For ACQ/IMAGE this parameter sets CENTER=FLUX-WT if NUM-POS=2 and CENTER=FLUX-WT-FLR if NUM-POS > 2.

8.10 Special Cases

- [8.10.1 Early Acquisitions and Preliminary Images](#)
- [8.10.2 Extended or Multiple Targets](#)
- [8.10.3 Offset Target Acquisitions](#)
- [8.10.4 Acquisition Failure Actions and Diagnostics](#)

8.10.1 Early Acquisitions and Preliminary Images

In some situations an observer may need to obtain an independent ultraviolet image of a region in order to ensure that no objects violate safety limits and that the target to be observed can be acquired by COS successfully. Such an early acquisition should be included in the Phase I proposal, and the observation should not use a photon-counting detector. The UVIS channel on WFC3 is recommended, but observers are encouraged to consult with an STScI instrument scientist.

8.10.2 Extended or Multiple Targets

Because most COS target-acquisition schemes were developed with the implicit assumption that the target is a point source, acquisitions of extended or multiple sources may require more careful planning.

If the target is sufficiently uniform and its coordinates are well known, then a target acquisition may not be required. To ensure that the brightest region of an extended source falls into the aperture, an ACQ/SEARCH with CENTER=BRIGHTEST may be sufficient ([Section 8.3](#)). ACQ/PEAKXD acquisitions with the NUV detector should be avoided for extended sources, because light from the three spectral stripes will overlap on the detector ([Section 8.5](#)). The pattern of dwell points for ACQ/PEAKD and FUV ACQ/PEAKXD should be tuned to the extent of the target.

Imaging acquisitions of extended sources are subject to special bright-object screening procedures. If an ETC calculation shows that the source is below the NUV local count-rate screening limit (50 cts/s/pixel) under the assumption that it is a point source (the worst-case scenario), then it passes. If it does not pass as a point source, but the maximum local count rate as an extended source is <5.9 cts/s/pixel, then the visit is safe. Above 25 cts/s/pixel, the visit is unsafe. Between 5.9 and 25 cts/s/pixel, the visit will be checked for safety by multiple reviewers. For more information, consult with your contact scientist.

Complex targets—such as two stars with very small angular separation, multiple bright knots, etc.—may confuse the acquisition algorithms. In such cases, consider an offset target acquisition, discussed in [Section 8.10.3](#). Take care when doing target acquisition for a target in a binary system since it is possible for the pointing to end up between the two stars. The coordinates of the target must be corrected for the orbital phase of the target in the binary system.

8.10.3 Offset Target Acquisitions

When targets are faint or lie in crowded fields, direct acquisition of the primary science target may be difficult or uncertain. In such cases, an offset acquisition, in which acquisition of a nearby field target is followed by a short slew to the science target, may be appropriate.

The size of the offset is limited by the requirement that the guide stars remain within the fields of view of their respective FGSs. Offset acquisition slews routinely involve displacements up to 1 arcmin and can be larger. Offset slews have a typical accuracy of ± 0.003 arcsec. The centering of the initial offset target should be refined (via either `ACQ/IMAGE` or `ACQ/PEAKXD+ACQ/PEAKD`) before the offset maneuver. For offset acquisitions, bright-object considerations apply to the acquisition target, the science target, and their fields. The region between the two targets does not need to be checked, because the shutter is closed during the slew. Refer to [Chapter 9](#) for a discussion of the modest overheads associated with the offset-acquisition spacecraft movement.

In unusual cases, including highly uncertain target coordinates or knotty, extended sources for which high wavelength accuracy is required, an offset target acquisition, followed by an additional `ACQ/IMAGE` or `ACQ/PEAKXD+ACQ/PEAKD` on the primary target, may be employed.

8.10.4 Acquisition Failure Actions and Diagnostics

Should any stage of the TA fail or a Local Rate Check (LRC) violation occur during a TA exposure, then the subsequent acquisition procedures in that visit (such as `ACQ/PEAKXD` or `ACQ/PEAKD`) will not be executed, but the science exposures will still occur. Note that HST will be left pointing at the last commanded position, which may differ substantially from the initial pointing.

Many quantities useful for evaluating the success of COS TAs are recorded in the COS TA data products (the `_rawacq` and `_spt` files). Table 5 of [COS ISR 2010-14](#) lists these keywords and their meanings.

Chapter 9: Scheduling Observations

Chapter Contents

- [9.1 Introduction](#)
- [9.2 Generic Observatory Overheads](#)
- [9.3 Spectral Element Movement Overheads](#)
- [9.4 Acquisition Overheads](#)
- [9.5 Science Exposure Overheads](#)
- [9.6 First Exposure Overhead Adjustment](#)
- [9.7 Examples of Orbit Estimates](#)
- [9.8 Visit Length Considerations](#)

9.1 Introduction

- 9.1.1 Phase I Proposal
- 9.1.2 Phase II Program

Once you have established the series of target-acquisition, scientific, and (if necessary) calibration exposures required for your program, you are ready to determine the total number of orbits to request. Generally, this is a straightforward exercise: compile the overheads on the individual exposures, assign the exposures to orbits, and tally the results to determine your orbit request. In some cases, it may be an iterative process, as you refine your observing plan to use each orbit most efficiently. This chapter provides simple tools to help you perform these calculations.

While exposures will execute in the order specified by the user, they are not guaranteed to be contiguous. A sequence of exposures may be split across multiple orbits even if APT's Orbit Planner appears to place them in a single orbit. If a program requires that the exposures must occur without gaps in time coverage, the exposures must be placed in a [SEQUENCE NON-INT container](#), and this Special Requirement must be justified in the Phase I proposal.

Once your proposal has been accepted you will return to this chapter to construct your Phase II proposal, which is the detailed observing plan that will eventually be transmitted to the telescope. Our goal is to help you schedule your observations as efficiently as possible.

Table 9.1: Phase I Estimates of Observatory and Instrument Overheads.

Acquisition or Exposure	Overhead Time (minutes)	Notes
Guide-star acquisition	6.5	First orbit of each visit
Guide-star re-acquisition	4	Each subsequent orbit
ACQ/IMAGE	3	Typical imaging acquisition
ACQ/SEARCH	7	Imaging or dispersed light, NUV or FUV
ACQ/PEAKXD + ACQ/PEAKD	7	Typical dispersed light acquisition, NUV or FUV
Science (Imaging or Dispersed Light)	5	First exposure in series
	2	Each subsequent exposure in series
	1	Add 1 minute for each instrument change (except to increment FP-POS)
	4	Wavelength calibration per exposure if using G160M at LP6 (Section 9.5)

9.1.1 Phase I Proposal

The *HST Primer* provides simple guidelines for estimating the overheads associated with a COS observation. These guidelines are summarized in [Table 9.1](#). These numbers are estimates only, and will usually overestimate the amount of time needed for overheads. However, additional observing time will not be granted in Phase II if the Phase I overheads were underestimated, so it is important that overhead times not be underestimated.

Each orbit must begin with a guide-star acquisition, which takes 6.5 minutes on the first orbit of a visit and 4 minutes on subsequent orbits. Next, the target must be acquired via an ACQ/SEARCH (7 min) and/or centered in the aperture via an ACQ/IMAGE (3 min) or a pair of ACQ/PEAKXD and ACQ/PEAKD exposures (7 min for both). The first science exposure requires 5 minutes of overhead. Subsequent identical exposures incur 2 minutes of overhead each. Add 1 minute for each instrument change (e.g., new grating or central wavelength; incrementing the FP-POS takes only 3 s, if ordering is efficient—see [Table 9.5](#)). If the same target is observed on contiguous orbits, a target acquisition is not required on the second and subsequent orbits.

These simple rules are remarkably successful at reproducing the total time required for a COS observation. To demonstrate, we list in [Section 9.7](#) both the Phase I times and the final times predicted by APT for a series of observing scenarios. These rules assume that acquisition exposure times are on the order of 20 s. If your targets are extremely faint, you must increase the length of the acquisition exposures accordingly ([Section 9.4](#)). Finally, note that some instrument changes, such as turning a detector segment on or off, take considerably longer than 1 minute ([Section 9.5](#)).

Allowing sufficient time for overheads in your Phase I proposal is important; additional time to cover unplanned or overlooked overheads will not be granted later. *Do not underestimate the amount of time that will be needed for overheads.*

9.1.2 Phase II Program

Once your proposal is approved, you will be responsible for building the observing sequences that will be executed by the telescope. The APT ([Astronomer's Proposal Tool](#)) scheduling software is used to prepare the Phase II; it automatically incorporates the appropriate overheads into your observing plan. While all COS overheads are automatically scheduled by APT, it is useful to understand where they come from. To that end, this chapter discusses the various observatory and instrument overheads in some detail, and [Section 9.7](#) provides observing scenarios as examples. Note that, when this chapter and the APT disagree, the APT overheads are the definitive values.

i *Accounting properly for all the overheads involved in an observation can be complicated. The information provided here is meant only to be illustrative. Proposers are urged to use APT to derive a complete and accurate determination of overhead times.*

9.2 Generic Observatory Overheads

The first time that you acquire an object, you must include a 6.5-minute overhead for the HST guide-star acquisition. In all subsequent orbits of the same visit, you must include the 6.5-minute overhead for the guide-star re-acquisition. If you are observing an object in the Continuous Viewing Zone (CVZ), then no guide-star re-acquisitions are required.

You must allocate additional time for each deliberate movement of the telescope; e.g., if you are performing a target-acquisition exposure on a nearby object and then offsetting to your target, or if you are taking a series of exposures in which you move the target on the detector (`POS-TARG`), then you must allow time for telescope motion. The time varies depending on size of the slew; see [Table 9.2](#).

Table 9.2: Generic Observatory Overhead Times.

Action	Overhead type	Time needed
Guide-star acquisition	Initial acquisition	6.5 min
	Re-acquisition	6.5 min per orbit
Spacecraft movements	$10 \text{ arcsec} < \text{Offset} < 1.5 \text{ arcmin}$ ¹	60 s
	$1.25 \text{ arcsec} \leq \text{Offset} \leq 10 \text{ arcsec}$	30 s
	$\text{Offset} < 1.25 \text{ arcsec}$	20 s

¹ Spacecraft motions larger than $\sim 1.5 \text{ arcmin}$ are likely to result in the loss of guide stars.

9.3 Spectral Element Movement Overheads

For any COS exposure, including target-acquisition exposures, any change of spectral elements incurs an overhead. A transition from FUV to NUV requires movement of OSM1 to the NCM1 position, followed by a possible OSM2 movement. On the other hand, a transition from NUV to FUV requires only the movement of OSM1 from NCM1 to the desired FUV grating and cenwave. [Table 9.3](#) gives the times required for movement between OSM1 spectral elements. These depend mildly on cenwave, so typical values are shown. [Table 9.4](#) gives the times for movement between OSM2 spectral elements. These do not depend on cenwave.

All COS visits start with OSM1 at the G130M position (with central wavelength 1291 Å) and OSM2 at the MIRRORA position. These gratings are highlighted in [Table 9.3](#) and [Table 9.4](#). OSM1 and OSM2 move sequentially, so the total overhead is the sum of the two separate overheads. The time required to move from one optical element to another is independent of the FP-POS settings.

Table 9.3: Overhead Times for Motions Between OSM1 Spectral Elements (seconds)

Movement time(s) from	to G140L	to G130M ¹	to G130M	to G160M	to NCM1
G140L	—	194	165	205	114
G130M ¹	198	—	—	156	158
G130M	172	—	—	117	119
G160M	212	162	122	—	165
NCM1	120	154	121	159	—

¹ Use these entries if the G130M cenwave is 1055 or 1096.

Table 9.4: Overhead Times for Motions Between OSM2 Spectral Elements (seconds).

Movement time(s) from	to G230L	to G185M	to G225M	to G285M	to MIRRORA	to MIRRORB
G230L	—	210	141	176	105	99
G185M	204	—	136	102	170	176
G225M	136	141	—	107	101	107
G285M	170	108	102	—	136	142
MIRRORA	100	175	106	141	—	71
MIRRORB	94	181	112	147	77	—

9.4 Acquisition Overheads

The various target-acquisition procedures are described in detail in [Chapter 8](#). The approximate total exposure plus associated overheads are given for each procedure below:

ACQ/SEARCH: Multiply the exposure time by the number of dwell points ($SCAN-SIZE^2$); add times to move OSM1, OSM2, and the aperture, if necessary; add the overhead below for the correct $SCAN-SIZE$; and add 37 s for readout to estimate the total ACQ/SEARCH time.

SCAN-SIZE	Overhead Time(s)
2	170
3	306
4	535
5	790

Note that these overheads assume the standard (default) $STEP-SIZE$ of 1.767". Overheads are slightly shorter for smaller $STEP-SIZES$.

ACQ/IMAGE: Multiply the exposure time by 2 (since images are obtained before and after centering); add times to move OSM1, OSM2, and the aperture, if necessary; add 120 s for setup; and add 56 s for readout to estimate the total ACQ/IMAGE time.

ACQ/PEAKXD: For NUV, start with the exposure time; add times to move OSM1, OSM2, and the aperture, if necessary; add 86 s for setup; and add 37 s for readout to estimate the total ACQ/PEAKXD time. For FUV, use the timing outlined below for ACQ/PEAKD. The default FUV ACQ/PEAKXD configuration uses $NUM-POS=3$ and $STEP-SIZE=1.3$.

ACQ/PEAKD: Multiply the exposure time by the number of dwell points ($NUM-POS$); add times to move OSM1, OSM2, and the aperture, if necessary; add the overhead below for the correct $NUM-POS$; and add 37 s for readout to estimate the total ACQ/PEAKD time. The numbers below assume the default $STEP-SIZE$ for each $NUM-POS$ as given in [Table 8.3](#).

NUM-POS	Overhead Time(s)
3	115
5	168
7	219
9	274

Note that the above estimates assume that all TA steps were taken with the same grating and cenwave or mirror configuration. If a change of configuration is used, add the appropriate overheads from [Table 9.3](#) and [Table 9.4](#).

9.5 Science Exposure Overheads

- [9.5.1 Policies when observing with G160M](#)

Science-exposure overheads are dominated by the time required to move OSM1 and OSM2 and to read out the on-board memory buffer at the end of each exposure. While the Phase II overheads computed by APT may be less than the values presented below, it is important to plan Phase I proposals using the conservative overheads given below to ensure adequate time for each exposure.

The full overhead calculation for science exposures depends upon a number of factors including generic exposure set-ups (which depend on the detector and observing mode), whether an aperture change is required, whether a grating change is required, whether the central wavelength setting for the grating is changed, and the directional sense of any required motion to implement an FP-POS change. Table 9.5 lists these additional overheads.

i *When moving to a new grating, you may specify any combination of central wavelength and FP-POS setting with no additional overhead penalty. The FP-POS sequence 1,2,3,4 is more efficient than 3,4,1,2, because no backward motion is required.*

New policies in effect for G160M observations are detailed in Section 9.5.1. In particular, G160M observations involve increased WAVECAL overheads, unless the G160M observations require the use of LP4. Figure 9.1 can be used to determine if G160M observations satisfy the requirements for an LP4 request.

Table 9.5: Science Exposure Overhead Times.

Overhead time(s)	FUV		NUV	
	TIME-TAG	ACCUM	TIME-TAG	ACCUM
Exposure set-up	66	70	35	33
Grating change	see Table 9.3		see Table 9.4	
Central wavelength change	80 ¹		75	
FP-POS forward ²	3		3	
FP-POS backward ²	70		70	
PSA – BOA Change	8		8	
WCA – BOA Change	10		10	
SEGMENT reconfiguration	300 (off); 315 (on)		N/A	
Memory readout ³	114	113 ³	114	56 ³

G160M Wavecal Exposures ⁴	$82 + 242 \times N_{\text{FP-POS}}$	N/A
--------------------------------------	-------------------------------------	-----

¹ This depends on the cenwaves involved and may vary by up to ± 6 s. For G130M, allow up to 105 s if one of the cenwaves is 1222 and up to 132 s if one of the cenwaves is 1055 or 1096 and the other is 1291 or greater.

² "Forward" refers to the preferred direction of motion of OSM1 or OSM2 (toward larger FP-POS values) and "backward" to the opposite direction.

³ ACCUM mode readout overheads can be hidden within subsequent exposures under certain circumstances, but the rules are complex. Use these values as safe upper limits for proposals.

⁴ $N_{\text{FP-POS}}$ = number of FP-POS exposures. 242 s of overhead time is required for each FP-POS exposure, with an additional 82 s of overhead time for the first FP-POS exposure. This overhead is not applicable to G160M observations that may be observed at LP4. To determine if G160M observations satisfy the requirements for an LP4 request, consult [Section 9.5.1](#).

To estimate the overhead for an exposure, round the desired exposure time up to the next whole second and add the generic exposure setup overhead from [Table 9.5](#). If a grating change has occurred from the previous exposure, add the appropriate values from [Table 9.3](#) and/or [Table 9.4](#). If a central wavelength change is made, add the appropriate value from [Table 9.5](#). If an FP-POS movement is made, add the appropriate value for motion in the preferred direction (toward larger FP-POS) or non-preferred direction. Note that all dispersed-light target-acquisition exposures are obtained with $\text{FP-POS}=3$. For all FUV observations except the G140L 800 Å and 1105 Å settings and those impacted by [the COS 2025 policy](#), both detector segments are powered on by default. To turn one of them off, set SEGMENT to A or B and add the associated overhead. For G160M observations add on the associated overhead for WAVECAL exposures per FP-POS used. Lastly, add the appropriate detector memory readout overhead.

Due to the 100x difference in sensitivity between the COS FUV A and FUV B segments when observing with the G130M/1055 and 1096 CENWAVES, it is expected that many observers will need to turn off FUV A when observing bright targets. (We refer to these SEGMENT=B observations here as either C1055B or C1096B). Only those observers using these two configurations are affected by this issue.

Under these conditions the zero point of the wavelength solution cannot be determined because the MgF_2 window on the PtNe lamps (WAVECAL) blocks light below $\sim 1180\text{\AA}$ (all WAVECAL light falls on FUV A). This results in a degradation of the resolution when FP-POS are combined by CalCOS and decreases the archival value of the COS data. In these cases, normal TAGFLASHes are not available and WAVECAL exposures with FUV A turned ON must be inserted into the observing sequence adjacent to each CENWAVE/ FP-POS setting used. As a result, in these cases $\text{FP-POS}=\text{ALL}$ should not be used. Individual FP-POS science exposures, and their associated WAVECALs, should be used instead. For more information, consult with your contact scientist.

Overheads associated with new settings introduced in Cycle 26 have not been tabulated, but they are expected to be similar to those of the other cenwaves in their respective gratings.

9.5.1 Policies when observing with G160M

The default lifetime position for G160M observations is now LP6. Wavelength calibration exposures at LP6 incur higher overheads than at other LPs due to the use of `SPLIT` wavecal (Section 5.7.6). In order to help minimize the impact of these overheads, a number of policies are in effect for G160M observations:

- The use of multiple `FP-POS` positions for each `CENWAVE` setting of the COS FUV detector is required in order to improve the limiting S/N and minimize the effects of flat-field artifacts (Section 5.8.2). While the use of all four `FP-POS` is required for FUV gratings (unless justified in the Phase I proposal), G160M users at LP6 are permitted to use less than 4 `FP-POS` based on the following S/N limits:
 - Users whose spectra require $S/N > 25$ are required to use 4 `FP-POS`
 - Users whose spectra require $S/N 20-25$ are required to use at least 3 `FP-POS`
 - Users whose spectra require $S/N < 20$ are permitted to use 2 `FP-POS`

The savings in overhead from using fewer than four `FP-POS` must be balanced against the potential reduction in wavelength coverage. Continuous coverage of the broadest possible wavelength range may be obtained by using either all four `FP-POS` or by using three `FP-POS`: 1, 4, and either 2 or 3. If there is a well-justified reason to use only two `FP-POS`, 1 and 4 are recommended. At LP6, this maximizes the wavelength coverage when two `FP-POS` are in use, leaving a gap of only 0.3 Å on Segment B. The 0.3 Å gap is expected to lie within the 1 Å ranges tabulated below, but its precise location cannot be predicted in advance due to mechanical uncertainty. If fewer than four `FP-POS` are desired, a justification must be included in the Phase I proposal.

G160M cenwave	Gap range (Å)
1533	1439.0 - 1440.0
1577	1483.0 - 1484.0
1589	1494.9 - 1495.9
1600	1506.6 - 1507.6
1611	1518.3 - 1519.3
1623	1531.0 - 1532.0

- If the total exposure time per target is less than one orbit, and there is a well-justified need for more than two `FP-POS`, users may request to use LP4 for their G160M observations. This is to mitigate the increase in overheads associated with wavelength calibration exposures at LP6, which are required for each `FP-POS` exposure. LP4 will be in 'available mode' for G160M to accommodate observations of this type and as such needs to be requested by the user during the Phase I process. Figure 9.1 provides a flow-chart to guide users in determining when the use of LP4 for G160M observations can be requested.

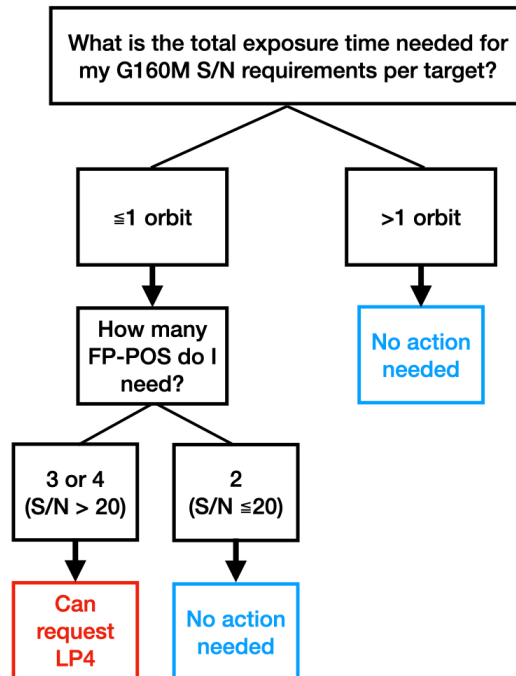


Figure 9.1: Users can request the use of LP4 for G160M observations by assessing the exposure time and S/N requirements per target.

- When calculating science exposure overheads for G160M observations, additional overheads should be included to account for *SPLIT* wavecal exposures (Section 5.7.6). G160M observations that satisfy the criteria for an LP4 request do not require the additional overheads. Science exposure overheads for all FUV gratings should be calculated using Table 9.5, or *APT* to derive a complete and accurate determination of overhead times.

9.6 First Exposure Overhead Adjustment

To increase observing efficiency, a special feature of the COS instrument commanding allows a portion of the instrumental overheads for the first exposure of a visit to be performed during the initial guide-star acquisition. These will usually be target-acquisition exposures. As a result, up to 340 s of instrumental overheads ([Table 9.3](#), [Table 9.4](#), and [Table 9.5](#)), but *not* observatory or acquisition overheads ([Table 9.2](#) and [Section 9.4](#)), may be hidden in this fashion. See [Section 9.7](#) for examples.

9.7 Examples of Orbit Estimates

- 9.7.1 NUV ACQ/IMAGE | Single FUV G130M cenwave TIME-TAG observation | 4 FP-POS in 1 Orbit
- 9.7.2 NUV ACQ/IMAGE | Single FUV G130M cenwave TIME-TAG observation | 4 FP-POS in 2 Orbits
- 9.7.3 NUV ACQ/IMAGE | Single FUV G160M cenwave TIME-TAG observation | 2 FP-POS in 1 Orbit
- 9.7.4 NUV ACQ/IMAGE | Single FUV G160M cenwave TIME-TAG observation | 4 FP-POS in 1 Orbit
- 9.7.5 FUV ACQ/PEAKXD + ACQ/PEAKD | Single FUV G140L cenwave TIME-TAG observation | 4 FP-POS in 1 Orbit
- 9.7.6 NUV ACQ/IMAGE | Single FUV G130M cenwave TIME-TAG observation with modified BUFFER-TIME | 4 FP-POS in 2 Orbits
- 9.7.7 NUV ACQ/SEARCH + ACQ/IMAGE | NUV G225M and FUV G160M TIME-TAG observations | 1 and 2 FP-POS in 1 Orbit
- 9.7.8 NUV ACQ/IMAGE | Single FUV G160M cenwave TIME-TAG observation with BOA aperture | 4 FP-POS in 2 Orbits

In this section we present eight example COS observations using both detectors and all of the target-acquisition modes. Besides the topics discussed in the previous sections we include examples of:

- **Multiple FP-POS settings** (Section 5.8.2): To improve the limiting S/N of an observation, proposers using the FUV channel of COS, but who do not intend to use all four FP-POS settings for each central wavelength setting, must justify this choice in the observing strategy section of their Phase I proposal. A modest reduction in observational overheads will not normally be considered sufficient justification for not using all four FP-POS settings. An exception to this policy are FP-POSs restricted by COS 2025 rules and users of G160M at LP6 (Section 9.5.1).
- **Adjusting the BUFFER-TIME** (Section 5.4): If BUFFER-TIME is greater than the exposure time, one would normally set $BUFFER-TIME = EXPTIME$. In orbits with a series of long FUV exposures, one can minimize overheads by setting $BUFFER-TIME = EXPTIME-100$. The full buffer takes 114 s to empty, so most of the data will be read out before the exposure is completed. The post-exposure data dump then requires only 38 s. For the final exposure of an orbit, the buffer dump can occur during the occultation, so adjusting the BUFFER-TIME will not save time. See the example in Section 9.7.6. (This is the same strategy outlined in Section 5.4.)

While the overhead rules presented in this chapter may appear complex, the actual rules used by the HST scheduling software are even more so. It is thus imperative that you use APT to construct your Phase II proposal. In the examples that follow, we present three sets of overhead estimates: one using the Phase I rules (Section 9.1), one using the rules in this chapter (Sections 9.2 to 9.6), and one computed using APT version 25.4.0.1. The version of APT available for constructing future Phase II proposals may return values that differ slightly from those given below. An up-to-date version of APT must be used for the Phase II planning of each visit.

9.7.1 NUV ACQ/IMAGE | Single FUV G130M cenwave TIME-TAG observation | 4 FP-POS in 1 Orbit

This example is a single orbit TIME-TAG observation using the G130M grating and the 1055 CENWAVE with FP-POS=ALL. It uses a 30 s ACQ/IMAGE target acquisition with MIRRORB and the BOA. The PSA is used for the science exposures.

Table 9.6: Overhead Values for NUV FUV TIME-TAG: 4 FP-POS in 1 Orbit.

Action	Phase I (s)	Chapter 9 (s)	APT Time (s) ¹	Comment
Initial guide star acquisition	390	390	393	Required at start of a new visit.
NUV ACQ/IMAGE with 30 s exposure	180	119 + 71 + 8 + 120 + 2 × 30 + 56 = 434	394 + 56 = 450	COS starts at G130M on OSM1, so move to NCM1 requires 119 s. OSM2 home position is MIRRORA, so move to MIRRORB takes 71 s. PSA to BOA change takes 8 s. Add 120 s ACQ/IMAGE setup, twice the exposure time, and memory readout.
First exposure overhead adjustment	N/A	-(119 + 71) = -190	-262	OSM1 and OSM2 movements may be hidden in guide-star acquisition.
FUV G130M at 1055 Å, TIME-TAG, FP-POS=ALL, BUFFER-TIME=500, 500 s exposure	500 + 300 = 800	66 + 154 + 500 + 114 = 842	228 + 500 + 114 = 842	Generic FUV TIME-TAG setup; change from MIRRORB to G130M (154 s); aperture change from BOA to PSA (8 s); exposure time; TIME-TAG memory readout.
	500 + 120 = 620	66 + 3 + 500 + 114 = 683	67 + 500 + 114 = 681	Generic FUV TIME-TAG setup; move to FP-POS=2 (3 s); exposure time; TIME-TAG memory readout.
	500 + 120 = 620	66 + 3 + 500 + 114 = 683	67 + 500 + 114 = 681	Generic FUV TIME-TAG setup; move to FP-POS=3 (3 s); exposure time; TIME-TAG memory readout.
	500 + 120 = 620	66 + 3 + 500 + 114 = 683	67 + 500 + 114 = 681	Generic FUV TIME-TAG setup; move to FP-POS=4 (3 s); exposure time; TIME-TAG memory readout.
Total science time	2000	2000	2000	
	3200	3495	3406	

Total time used in orbit				
--------------------------	--	--	--	--

¹ Periodic updates to APT may result in small discrepancies from the overheads shown here.

9.7.2 NUV ACQ/IMAGE | Single FUV G130M cenwave TIME-TAG observation | 4 FP-POS in 2 Orbits

This example is a two-orbit TIME-TAG observation using the G130M grating and the 1055 CENWAVE with FP-POS=ALL. It uses a 30 s ACQ/IMAGE target acquisition with MIRRORB and the BOA. The PSA is used for the science exposures.

Table 9.7: Overhead Values for FUV TIME-TAG: 4 FP-POS in 2 Orbits.

Action	Phase I (s)	Chapter 9 (s)	APT Time (s) ¹	Comment
Initial guide star acquisition	390	390	393	Required at start of a new visit.
NUV ACQ/IMAGE with 30 s exposure	180	119 + 71 + 8 + 120 + 2 × 30 + 56 = 434	394 + 56 = 450	COS starts at G130M on OSM1, so move to NCM1 requires 119 s. OSM2 home position is MIRRORA, so move to MIRRORB takes 71 s. PSA to BOA change takes 8 s. Add 120 s ACQ/IMAGE setup, twice the exposure time, and memory readout.
First exposure overhead adjustment	N/A	-(119 + 71) = -190	-262	OSM1 and OSM2 movements may be hidden in guide-star acquisition.
FUV G130M at 1055 Å, TIME-TAG, FP-POS=1, BUFFER-TIME=1075, 1175 s exposure	1175 + 300 = 1475	66 + 154 + 8 + 1175 + 38 = 1441	228 + 1175 + 38 = 1441	Generic FUV TIME-TAG setup; change from MIRRORB to G130M (154 s); aperture change from BOA to PSA (8 s); exposure time; short TIME-TAG memory readout (38 s).
FUV G130M at 1055 Å, TIME-TAG, FP-POS=2, BUFFER-TIME=1075, 1175 s exposure	1175 + 120 = 1295	66 + 3 + 1175 + 38 = 1282	67 + 1175 + 38 = 1280	Same as above but with FP-POS=2.

Total Science Time in Orbit 1	2350	2350	2350	
Total Time Used in Orbit 1	3310	3327	3242	
Guide star re-acquisition	240	240	222	
First exposure overhead adjustment	N/A	-3	-3	FP-POS movement may be hidden in guide star re-acquisition.
FUV G130M at 1055 Å, TIME-TAG, FP-POS=3, BUFFER-TIME=1275, 1375 s exposure	1375 + 120 = 1495	66 + 3 + 1375 + 38 = 1482	67 + 1375 + 38 = 1480	Generic FUV TIME-TAG setup; move to FP-POS=3 (3 s); exposure time; short TIME-TAG memory readout.
FUV G130M at 1055 Å, TIME-TAG, FP-POS=4, BUFFER-TIME=1275, 1375 s exposure	1375 + 120 = 1495	66 + 3 + 1375 + 38 = 1482	67 + 1375 + 38 = 1480	Same as above but with FP-POS=4.
Total science time	2750	2750	2750	
Total time used in orbit	3230	3201	3179	

¹ Periodic updates to APT may result in small discrepancies from the overheads shown here.

9.7.3 NUV ACQ/IMAGE | Single FUV G160M cenwave TIME-TAG observation | 2 FP-POS in 1 Orbit

This example is a single orbit TIME-TAG observation using the G160M grating and the 1533 CENWAVE with 2 FP-POS. It uses a 30 s ACQ/IMAGE target acquisition with MIRRORB and the BOA. The PSA is used for science exposures. With 2 FP-POS in a single orbit, it will execute at the current LP for G160M (see [Figure 9.5.1](#)) which includes additional WAVECAL overheads ([Section 5.7.6](#) and [Table 9.5](#)).

Table 9.8: Overhead Values for FUV TIME-TAG: 2 FP-POS in 1 Orbit.

Action	Phase I (s)	Chapter 9 (s)	APT Time (s) ¹	Comment
--------	-------------	---------------	---------------------------	---------

Initial guide star acquisition	390	390	393	Required at start of a new visit.
NUV ACQ/IMAGE with 30 s exposure	180	119 + 71 + 8 + 120 + 2 × 30 + 56 = 434	411 + 56 = 467	COS starts at G130M on OSM1, so move to NCM1 requires 119 s. OSM2 home position is MIRRORA, so move to MIRRORB takes 71 s. PSA to BOA change takes 8 s. Add 120 s ACQ/IMAGE setup, twice the exposure time, and memory readout.
First exposure overhead adjustment	N/A	-(119 + 71) = -190	-262	OSM1 and OSM2 movements may be hidden in guide-star acquisition.
FUV G160M ² at 1533 Å, TIME-TAG, FP-POS=1, BUFFER-TIME=500, 500 s exposure	500 + 300 + 240 = 1040	66 + 159 + 8 + 500 + 114 + 236 + 76 = 1159	418 + 62 + 500 + 114 = 1094	Generic FUV TIME-TAG setup; change from MIRRORB to G160M (159 s); aperture change from BOA to PSA (8 s); exposure time; TIME-TAG memory readout; G160M WAVECAL overheads 1st exposure (236 + 76 s).
FUV G160M ² at 1533 Å, TIME-TAG, FP-POS=4, BUFFER-TIME=500, 500 s exposure	500 + 120 + 240 = 860	66 + 3 + 500 + 114 + 236 = 919	236 + 62 + 500 + 114 = 912	Generic FUV TIME-TAG setup; move to FP-POS=4 (3 s); exposure time; G160M WAVECAL overheads (236 s); TIME-TAG memory readout.
Total science time	1000	1000	1000	
Total time used in orbit	2470	2712	2604	

¹ Periodic updates to APT may result in small discrepancies from the overheads shown here.

² Starting in Cycle 30 G160M observations have additional WAVECAL overheads (see [Section 9.5.1](#)).

9.7.4 NUV ACQ/IMAGE | Single FUV G160M cenwave TIME-TAG observation | 4 FP-POS in 1 Orbit

This example is a single orbit `TIME-TAG` observation using the G160M grating and the 1533 CENWAVE with 4 `FP-POS`. It uses a 30 s `ACQ/IMAGE` target acquisition with `MIRRORB` and the BOA. The PSA is used for the science exposures. With more than 2 `FP-POS` in a single orbit, it is eligible to execute at LP4 (see [Figure 9.5.1](#)), and this example assumes this to be the case.

Table 9.9: Overhead Values for FUV `TIME-TAG`: 4 `FP-POS` in 1 Orbit.

Action	Phase I (s)	Chapter 9 (s)	APT Time (s) ¹	Comment
Initial guide star acquisition	390	390	393	Required at start of a new visit.
NUV <code>ACQ/IMAGE</code> with 30 s exposure	180	119 + 71 + 8 + 120 + 2 × 30 + 56 = 434	388 + 56 = 444	COS starts at G130M on OSM1, so move to NCM1 requires 119 s. OSM2 home position is <code>MIRRORA</code> , so move to <code>MIRRORB</code> takes 71 s. PSA to BOA change takes 8 s. Add 120 s <code>ACQ/IMAGE</code> setup, twice the exposure time, and memory readout.
First exposure overhead adjustment	N/A	-(119 + 71) = -190	-255	OSM1 and OSM2 movements may be hidden in guide-star acquisition.
FUV G160M at 1533 Å, <code>TIME-TAG</code> , <code>FP-POS</code> =1, <code>BUFFER-TIME</code> =380, 490 s exposure	490 + 300 = 790	66 + 159 + 8 + 490 + 57 = 780	242 + 490 + 57 = 789	Generic FUV <code>TIME-TAG</code> setup; change from <code>MIRRORB</code> to G160M (159 s); aperture change from BOA to PSA (8 s); exposure time; short <code>TIME-TAG</code> memory readout (57 s).
FUV G160M at 1533 Å, <code>TIME-TAG</code> , <code>FP-POS</code> =2, <code>BUFFER-TIME</code> =380, 490 s exposure	490 + 120 = 610	66 + 3 + 490 + 57 = 616	67 + 490 + 57 = 614	Same as above but with <code>FP-POS</code> =2.
FUV G160M at 1533 Å, <code>TIME-TAG</code> , <code>FP-POS</code> =3, <code>BUFFER-TIME</code> =380, 490 s exposure	490 + 120 = 610	66 + 3 + 490 + 57 = 616	67 + 490 + 57 = 614	Same as above but with <code>FP-POS</code> =3.
FUV G160M at 1533 Å, <code>TIME-TAG</code> , <code>FP-POS</code> =4	490 + 120 = 610	66 + 3 + 490 + 57 = 616	67 + 490 + 57 =	Same as above but with <code>FP-POS</code> =4.

, BUFFER-TIME=380, 490 s exposure			614	
Total Science Time	1960	1960	1960	
Total Time Used in Orbit	3190	3262	3213	

¹ Periodic updates to APT may result in small discrepancies from the overheads shown here.

9.7.5 FUV ACQ/PEAKXD + ACQ/PEAKD | Single FUV G140L cenwave TIME-TAG observation | 4 FP-POS in 1 Orbit

In this example, we begin with an FUV ACQ/SEARCH followed by ACQ/PEAKXD and ACQ/PEAKD, all with G130M, then change to G140L for a set of FUV TIME-TAG exposures using FP-POS=ALL and SEGMENT=A. Since the COS 2025 policy requires SEGMENT=A for acquisition with CENWAVE=1309, there is no reconfiguration penalty for the G140L spectroscopy.

Table 9.10: Overhead Values for FUV Acquisition and FP-POS=ALL.

Action	Phase I (s)	Chapter 9 (s)	APT Time (s) ¹	Comment
Initial guide-star acquisition	390	390	393	Required at start of a new visit.
FUV ACQ/SEARCH, G160M at 1577 Å, 3 × 3 pattern, 15 s exposure	420	117 + 306 + 9 × 15 + 37 = 595	516	OSM1 home position is G130M, so move to G160M requires 117 s. OSM2 home position is MIRRORA, so no move is needed. Add 306 s SCAN-SIZE=3 setup, 9 times the exposure time, and memory readout.
First exposure overhead adjustment	N/A	-117	-85	OSM1 movement may be hidden in guide-star acquisition.
FUV ACQ/PEAKXD, G160M at 1577 Å, 25 s exposure	420	115 + 3 × 25 + 37 = 227	184	Setup (115 s); 3 times the exposure time; memory readout.
FUV ACQ/PEAKD, G160M at 1577 Å,			300 + 37	Setup (168 s); 5 times the exposure time; memory readout.

5 steps, 25 s exposure		$168 + 5 \times 25 + 37 = 330$		
FUV G140L at 1280 Å, TIME-TAG, FP-POS=ALL, SEGMENT=A, 268 s exposure	$300 + 268 = 568$	$66 + 172 + 268 = 620$	$233 + 268 + 114 = 620$	Generic FUV TIME-TAG setup; OSM1 change from G130M to G140L (172 s); exposure time; memory readout (note: FP-POS=1).
	$120 + 268 = 388$	$66 + 3 + 268 + 114 = 451$	$67 + 268 + 114 = 451$	Generic FUV TIME-TAG setup; change to FP-POS=2 (3 s); exposure time; memory readout.
	$120 + 268 = 388$	$66 + 3 + 268 + 114 = 451$	$67 + 268 + 114 = 451$	Same as above, but with FP-POS=3.
	$120 + 268 = 388$	$66 + 3 + 268 + 114 = 451$	$67 + 268 + 114 = 451$	Same as above, but with FP-POS=4.
Total science time	1072	1072	1072	
Total time used in orbit	2932	3288	3247	

¹ Periodic updates to APT may result in small discrepancies from the overheads shown here.

9.7.6 NUV ACQ/IMAGE | Single FUV G130M cenwave TIME-TAG observation with modified BUFFER-TIME | 4 FP-POS in 2 Orbits

In this example, we begin with an NUV ACQ/IMAGE exposure, then switch to the FUV channel for four long G130M exposures, one at each FP-POS position. We use a couple of tricks to maximize the exposure time. First, we shorten the BUFFER-TIME for the first exposure of each orbit as described in [Section 5.4.2](#), which reduces the length of the memory read-out following the exposure from 114 to 38 seconds. Second, we extend the exposure times, pushing the final memory read-out of each orbit into the occultation period. Note that we do not use FP-POS=ALL, because that would generate four identical exposures; instead, we increment the FP-POS by hand.

Table 9.11: Overhead Values for FUV TIME-TAG with Modified BUFFER-TIME.

Action	Phase I (s)	Chapter 9 (s)	APT Time (s) ¹	Comment

Initial guide star acquisition	390	390	393	Required at start of a new visit.
NUV ACQ / IMAGE with 10 s exposure	180	119 + 120 + 2 × 10 + 56 = 315	272 + 56 = 308	COS starts at G130M on OSM1, so move to NCM1 requires 119 s. OSM2 home position is MIRRORA, so no move is needed. Add 120 s ACQ/IMAGE setup, twice the exposure time, and memory readout.
First exposure overhead adjustment	N/A	-119	-179	OSM1 movement may be hidden in guide star acquisition.
FUV G130M at 1291 Å TIME-TAG, FP-POS=1, BUFFER-TIME=1210, 1310 s exposure ²	300 + 1310 = 1610	66 + 121 + 1310 + 38 = 1535	204 + 1310 + 38 = 1552	Generic FUV TIME-TAG set-up; OSM1 change from NCM1 to G130M (121 s); exposure time; short TIME-TAG memory readout (38 s).
TIME-TAG, FP-POS=2, BUFFER-TIME=1310, 1310 s exposure ²	120 + 1310 = 1430	66 + 3 + 1310 + 114 = 1493	67 + 1310 + 114 = 1491	Generic FUV TIME-TAG set-up; move to FP-POS=2 (3 s); exposure time; TIME-TAG memory readout.
Total science time in orbit 1	2620	2620	2620	
Total time used in orbit 1	3580	3584	3585	
Guide star re-acquisition	240	240	392	Required at start of next orbit.
First exposure overhead adjustment	N/A	-3	-3	FP-POS movement may be hidden in guide star re-acquisition.
TIME-TAG, FP-POS=3, 1498 = 1618	120 + 1498 = 1618		67 + 1498 + 38	As for FP-POS=2, but with short TIME-TAG memory readout.

BUFFER-TIME=1398 , 1498 s exposure		$66 + 3 + 1498 + 38 = 1603$ 1605		
TIME-TAG, FP-POS=4, BUFFER-TIME=1498 , 1498 s exposure	$120 + 1498 = 1618$	$66 + 3 + 1498 + 114 = 1681$	$67 + 1498 + 114 = 1679$	As for FP-POS=2.
Total science time in orbit ²	2996	2996	2996	
Total time used in orbit ²	3476	3523	3671	

¹ Periodic updates to APT may result in small discrepancies from the overheads shown here.

9.7.7 NUV ACQ/SEARCH + ACQ/IMAGE | NUV G225M and FUV G160M TIME-TAG observations | 1 and 2 FP-POS in 1 Orbit

In this example, we begin with an NUV ACQ/SEARCH target acquisition followed by an ACQ/IMAGE target acquisition. We obtain an NUV TIME-TAG exposure, then switch to the FUV channel for a pair of FUV TIME-TAG exposures. To minimize damage to the detector, we employ two FP-POS settings.

Table 9.12: Overhead Values for ACQ/SEARCH plus ACQ/IMAGE.

Action	Phase I (s)	Chapter 9 (s)	APT Time (s) ¹	Comment
Initial guide star acquisition	390	390	393	Required at start of a new visit.
NUV ACQ/SEARCH, MIRRORA, 3 × 3 pattern, 10 s exposure	420	$119 + 306 + 9 \times 10 + 37 = 552$	515	COS starts at G130M on OSM1, so move to NCM1 requires 119 s. OSM2 home position is MIRRORA, so no move is needed. Add 306 s SCAN-SIZE=3 setup, 9 times the exposure time, and memory readout.
First exposure overhead adjustment	N/A	-119	-129	OSM1 movement may be hidden in guide-star acquisition.

NUV ACQ/IMAGE with 10 s exposure	180	120 + 2 × 10 + 56 = 196	123 + 56 = 179	No OSM movement, ACQ/IMAGE setup, twice the exposure time, and memory readout.
NUV G225M at 2250 Å, TIME-TAG, FP-POS=3, 1200 s exposure	300 + 1200 = 1500	35 + 106 + 1200 + 114 = 1455	135 + 1200 + 114 = 1449	Generic NUV TIME-TAG setup; OSM2 change from MIRRORA to G225M (106 s); exposure time; TIME-TAG memory readout.
FUV G130M at 1309 Å, TIME-TAG, FP-POS=2, 300 s exposure ²	120 + 60 + 300 = 480	66 + 121 + 300 + 114 = 601	190 + 300 + 114 = 604	Generic FUV TIME-TAG setup; OSM1 change from NCM1 to G130M (121 s); exposure time; TIME-TAG memory readout.
FUV G130M at 1309 Å, TIME-TAG, FP-POS=4, 300 s exposure ²	120 + 300 = 420	66 + 3 + 300 + 114 = 483	67 + 300 + 114 = 481	Generic FUV TIME-TAG setup; increment FP-POS (3 s); exposure time; TIME-TAG memory readout.
Total science time	1800	1800	1800	
Total time used in orbit	3360	3528	3432	

¹ Periodic updates to APT may result in small discrepancies from the overheads shown here.

² Starting in Cycle 25, only Segment A spectroscopy is permitted at cenwave 1309.

9.7.8 NUV ACQ/IMAGE | Single FUV G160M cenwave TIME-TAG observation with BOA aperture | 4 FP-POS in 2 Orbits

In this example, we start with an NUV ACQ/IMAGE, followed by a switch to the FUV channel and a TIME-TAG science exposure using G160M, FP-POS=ALL, the BOA, and, as required with the BOA, FLASH=NO. The science exposure will be followed automatically by a 12 s wavecal (see Table 5.2). As required, we obtain two exposures with FP-POS=1 and 2. In the second orbit (not shown), we obtain exposures with FP-POS=3 and 4.

Table 9.13: Overhead Values for FUV TIME-TAG Using the BOA.

Action	Phase I (s)	Chapter 9 (s)	APT Time (s) ¹	Comment
	390	390	393	Required at start of a new visit.

Initial guide-star acquisition				
NUV ACQ/IMAGE with 2 s exposure	180	119 + 120 + 2 × 2 + 56 = 299	236 + 56 = 292	COS starts at G130M on OSM1, so move to NCM1 requires 119 s. OSM2 home position is MIRRORA, so no move is needed. Add 120 s ACQ/IMAGE setup, twice the exposure time, and memory readout.
First exposure overhead adjustment	N/A	-119	-160	OSM1 movement may be hidden in guide star acquisition.
FUV G160M at 1600 Å, TIME-TAG, BOA, FLASH=NO, FP-POS=1, 1100 s exposure	300 + 1100 = 1400	66 + 159 + 8 + 1100 + 114 = 1447	229 + 1100 + 114 = 1443	Generic FUV TIME-TAG setup; OSM1 change from NCM1 to G160M (159 s); aperture change from PSA to BOA (8 s); exposure time; TIME-TAG memory readout.
FUV G160M at 1600 Å, TIME-TAG, AUTO WAVECAL, WCA, FP-POS=1, 12 s exposure	120 + 12 = 132	66 + 10 + 12 + 114 = 202	75 + 12 + 38 = 125	AUTO WAVECAL inserted, since FLASH=YES is not allowed with BOA; generic FUV TIME-TAG setup; aperture change from BOA to WCA (10 s); exposure time; TIME-TAG memory readout.
FUV G160M at 1600 Å, TIME-TAG, BOA, FLASH=NO, FP-POS=2, 1100 s exposure	120 + 1100 = 1220	66 + 3 + 10 + 1100 + 114 = 1293	73 + 1100 + 114 = 1287	Generic FUV TIME-TAG setup; increment FP-POS (3 s); aperture change from WCA to BOA (10 s); exposure time; TIME-TAG memory readout.
FUV G160M at 1600 Å, TIME-TAG, AUTO WAVECAL, WCA, FP-POS=2, 12 s exposure	120 + 12 = 132	66 + 10 + 12 + 114 = 202	75 + 12 + 38 = 125	Another AUTO WAVECAL required as FP-POS has changed; generic FUV TIME-TAG setup; aperture change from BOA to WCA (10 s); exposure time; TIME-TAG memory readout.
Total science time in orbit 1	2200	2200	2200	
Total time used in orbit 1	3424	3684	3445	
Note: Two additional exposures, using FP-POS=3 and 4 in a second orbit, are not shown.				

¹ Periodic updates to APT may result in small discrepancies from the overheads shown here.

9.8 Visit Length Considerations

Visit lengths affect how programs are able to schedule, and thereby when they are executed. Visits of 3 orbits or fewer are easier to schedule than longer visits, and less observing time is lost in the event that an entire visit fails. In their Phase II proposals, it is recommended that proposers group observations into visits of 3 orbits or fewer to enable earlier scheduling. If at all possible, we recommend avoiding 4 orbit visits, since they are particularly difficult to schedule. As noted in the Call for Proposals, proposers must justify the use of visits longer than 6 orbits in the Description of Observations section of their Phase I proposals.

Chapter 10: Bright-Object Protection

Chapter Contents

- [10.1 Introduction](#)
- [10.2 Screening Limits](#)
- [10.3 Source V Magnitude Limits](#)
- [10.4 Tools for Bright-Object Screening](#)
- [10.5 Policies and Procedures](#)
- [10.6 On-Orbit Protection Procedures](#)
- [10.7 Bright Object Protection for Solar System Observations](#)
- [10.8 SNAP, TOO, and Unpredictable Sources Observations with COS](#)

10.1 Introduction

Both the FUV XDL and the NUV MAMA detectors are subject to damage or destruction by excessive illumination. An excessive local count rate can permanently reduce the sensitivity of the affected detector region. The most likely causes are a bright spectral emission line (XDL or MAMA) or a bright source observed in direct imaging (MAMA). A global over-illumination of the detector can result in its loss. To protect the detectors, onboard software monitors the local and global count rates. It shutsters the instrument in case of a local violation and lowers the high voltage if a global count-rate violation is detected. The local rate is checked before an exposure is begun, while the global rate is monitored continuously during the exposure. Under certain circumstances damage can result despite the onboard safety measures, and in any event lowering the high voltage will disrupt the HST schedule and operations. Therefore, all proposed COS observations must meet count-rate screening limits with safety margins to allow for uncertainties. COS is currently the only HST instrument to use UV detectors for target acquisitions. Such acquisitions must be screened, as well, including special procedures for imaging acquisitions of extended sources; see [Section 8.10.2](#). It is the responsibility of the observer to screen all proposed targets and fields during Phase II preparation, and of STScI to check and enforce these limits. The COS Bright Object Protection (BOP) policies and procedures are described in this chapter.

Table 10.1: COS Count-Rate Screening Limits.

Detector	Source type	Type of limit	Limiting count rate (counts/s)
FUV	predictable	global	15,000 per segment ¹
		local	0.67 per pixel ²
	irregular	global	6,000 per segment ¹
		local	0.67 per pixel ²
NUV	predictable	global	170,000 (imaging) or 30,000 per stripe (spectroscopic) ¹
		local	50 per pixel ³ (imaging) or 70 per pixel (spectroscopic)
	irregular	global	68,000 (imaging) or 12,000 per stripe (spectroscopic) ¹
		local	50 per pixel (imaging) or 70 per pixel (spectroscopic)

¹ The global data-rate limit for observations using `TIME-TAG` mode is 30,000 counts/s, as discussed in [Section 5.2.1](#).

² This local count-rate screening limit is not applicable to the 1055 and 1096 cenwaves of the COS G130M grating. For these modes the limiting count rate is 0.2 count/s/pixel for both source types.

³ For imaging acquisitions, a count rate of 360 count/s in the 9 × 9-pixel box surrounding the target (as computed by the COS Imaging Acquisition ETC) represents an equivalent safe upper limit.

10.2 Screening Limits

The global and local count-rate screening limits for each COS configuration are given in [Table 10.1](#). The limits are independent of observing mode (`TIME-TAG` or `ACCUM`). Compliance with these limits must be checked for all proposed COS targets by means of the [Exposure Time Calculator](#) (ETC), which issues warnings if they are exceeded. In Phase `I`, all proposed targets must be screened against these limits. In Phase `II`, the results of more detailed target and field checks must be submitted with the observing proposal; details are provided in [Section 10.6](#). Note that the local count-rate limits given in [Table 1.2](#) and the local count-rate screening limits given in [Table 10.1](#) are not applicable to the 1055 and 1096 cenwaves of the COS G130M grating. For those modes, the local limit is $0.2 \text{ count s}^{-1} \text{ pixel}^{-1}$ for both predictable and irregular sources.

It is also useful to note the distinction between the global count-rate screening limits and the data-rate limit on `TIME-TAG` exposures. While both limits may affect the feasibility of proposed observations, the global count-rate screening limits for each COS configuration are defined to protect the detectors and the data-rate limit on `TIME-TAG` exposures is defined to protect against the loss of data (as discussed in [Section 5.2.1](#)). In the FUV, a steep spectrum could exceed the global count-rate screening limit of $15,000 \text{ count s}^{-1}$ per detector segment without exceeding the $30,000 \text{ count s}^{-1}$ data-rate limit. In the NUV, the global count-rate screening limit is considerably higher at $30,000 \text{ count s}^{-1}$ per stripe, however, a target that is perfectly safe to observe could be far too bright to observe in `TIME-TAG` mode if it exceeds the $30,000 \text{ count s}^{-1}$ data-rate limit.

10.3 Source V Magnitude Limits

In the following tables, the screening limits in [Table 10.1](#) are converted into V magnitude limits for a variety of sources. These values are not meant to be a substitute for the [ETC](#), but rather an indication of whether a given object may be near the limit. The most sensitive spectroscopic setting and lowest rate limit (global or local) determine the listed values. Stellar spectra are assumed to be unreddened. [Table 10.2](#) corresponds to spectroscopy through the PSA, [Table 10.3](#) through the BOA, and [Table 10.4](#) to NUV imaging for both apertures.

These tables were calculated for the *Cycle 19 COS Instrument Handbook* (Version 3.0; December 2010). Due to the decline in the sensitivity of COS over time (TDS), targets that are brighter than the given values by up to 0.5 mag (4.0 to 4.5 mag for the G285M grating) may be within the spectroscopic screening limits. (Limits for imaging are not expected to differ.) Users are required to use the [ETC](#) for the final assessment of whether their targets violate the brightness limits.

Table 10.2: V Magnitude Limits for PSA Spectroscopy.

Spectral Class	FUV			NUV			
	G130M	G160M	G140L	G185M	G225M	G285M	G230L
O5 v	14.7	14.0	15.1	10.1	9.5	8.7	12.5
O7 v	14.5	13.8	14.9	10.0	9.5	8.6	12.4
O9 v	14.2	13.6	14.7	9.9	9.4	8.5	12.3
B0 v	14.2	13.5	14.6	9.8	9.3	8.4	12.2
B1 v	13.8	13.1	14.3	9.4	9.0	8.2	11.9
B3 v	12.8	12.5	13.4	8.8	8.4	7.7	11.3
B5 v	12.0	11.9	12.7	8.3	8.0	7.4	10.8
B8 v	10.9	11.0	11.5	7.5	7.2	6.7	10.0
A1 v	8.5	8.9	9.3	6.4	6.2	5.8	9.0
A3 v	6.4	7.8	8.3	6.1	6.0	5.6	8.7
A5 v	2.9	6.9	7.3	5.8	5.8	5.5	8.5
F0 v	-0.1	4.9	5.7	4.8	5.2	5.2	7.8
F2 v	-1.2	4.0	5.0	4.5	5.0	5.2	7.6
F5 v	-3.4	1.9	3.2	3.7	4.4	5.0	7.3
F8 v	-4.8	0.5	2.0	3.2	4.1	4.8	7.1
G2 v (Solar)	1.8	-0.5	3.4	1.4	2.7	4.4	6.8
G8 v (Tau Ceti)	3.0	-0.4	4.7	0.5	2.2	3.9	6.4

K2 v (Epsilon Eri)	4.0	-0.1	5.8	-0.8	1.1	3.2	6.1
KM III (Eta Ser)	-1.5	-1.4	0.2	-0.7	1.0	2.9	5.7
KM III (Alpha Boo)	-0.8	-2.3	0.9	-3.1	-1.1	0.9	4.7
KM III (Gamma Aql)	-2.3	-4.5	-0.5	-5.4	-3.9	-2.3	3.8
KM III (HD 146051)	-3.1	-5.0	-1.4	-7.0	-5.1	-3.1	3.3
KM III (Alpha Cet)	0.2	-1.5	1.9	-4.2	-1.9	-1.0	3.3
KM III (HD 123023)	0.0	-1.0	1.6	-3.2	-1.2	-0.3	3.7
KM III (Beta Gru)	-0.2	-0.6	1.5	-2.9	-1.0	0.7	3.4
T ~ 50,000 K Blackbody	14.6	14.0	15.0	10.1	9.5	8.6	12.5
$F_{\lambda} \sim \lambda^{-1}$	11.0	10.6	11.5	7.2	7.2	6.7	9.9
$F_{\lambda} = \text{const surface brightness}$	11.1	10.9	11.8	7.7	8.0	7.6	10.7
$F_{\lambda} = \text{const point source}$	9.3	9.2	10.0	6.0	6.3	5.9	9.0

Table 10.3: V Magnitude Limits for BOA Spectroscopy.

Spectral Class	FUV			NUV			
	G130M	G160M	G140L	G185M	G225M	G285M	G230L
O5 v	9.4	8.5	9.8	4.6	3.8	2.8	6.9
O7 v	9.2	8.4	9.6	4.4	3.7	2.7	6.8
O9 v	9.0	8.2	9.4	4.3	3.6	2.7	6.7
B0 v	8.9	8.0	9.3	4.2	3.5	2.6	6.6
B1 v	8.5	7.7	9.0	3.9	3.3	2.4	6.2
B3 v	7.5	7.0	8.1	3.2	2.7	1.9	5.6
B5 v	6.7	6.5	7.4	2.7	2.2	1.5	5.1
B8 v	5.5	5.5	6.2	1.9	1.5	0.8	4.3
A1 v	3.1	3.4	3.8	0.8	0.4	-0.1	3.3
A3 v	1.0	2.2	2.8	0.5	0.2	-0.3	3.0
A5 v	-2.5	1.4	1.8	0.2	0.0	-0.4	2.8
F0 v	-5.6	-0.7	0.1	-0.8	-0.6	-0.7	2.0

F2 v	-6.7	-1.6	-0.6	-1.2	-0.8	-0.8	1.7
F5 v	-8.8	-3.7	-2.4	-2.0	-1.4	-1.0	1.4
F8 v	-10.2	-5.0	-3.6	-2.5	-1.7	-1.1	1.2
G2 v (Solar)	-3.6	-6.1	-1.9	-4.3	-3.1	-1.5	0.8
G8 v (Tau Ceti)	-2.3	-5.9	-0.6	-5.2	-3.6	-2.0	0.3
K2 v (Epsilon Eri)	-1.2	-5.6	0.5	-6.4	-4.7	-2.7	0.1
KM III (Eta Ser)	-6.9	-6.9	-5.2	-6.3	-4.8	-3.1	-0.4
KM III (Alpha Boo)	-6.1	-7.8	-4.4	-8.7	-6.9	-5.1	-1.3
KM III (Gamma Aql)	-7.6	-10.0	-5.9	-11.1	-9.7	-8.2	-2.2
KM III (HD 146051)	-8.5	-10.5	-6.8	-12.6	-10.9	-9.0	-2.8
KM III (Alpha Cet)	-5.1	-7.0	-3.4	-9.7	-7.7	-7.0	-2.8
KM III (HD 123023)	-5.4	-6.5	-3.7	-8.8	-7.0	-6.4	-2.3
KM III (Beta Gru)	-5.6	-6.1	-3.8	-8.6	-6.8	-5.2	-2.6
T~50,000 K Blackbody	9.3	8.5	9.7	4.5	3.7	2.8	6.9
$F_{\lambda} \sim \lambda^{-1}$	5.7	5.1	6.2	1.6	1.4	0.8	4.2
$F_{\lambda} = \text{const surface brightness}$	5.8	5.4	6.4	2.2	2.2	1.7	5.0
$F_{\lambda} = \text{const point source}$	4.1	3.7	4.6	0.5	0.5	0.0	3.3

Table 10.4: V Magnitude Bright-Object Limits for Imaging.

Spectral Class	PSA+MirrorA	PSA+MirrorB	BOA+MirrorA	BOA+MirrorB
O5 v	19.2	16.3	13.5	10.7
O7 v	19.1	16.1	13.4	10.5
O9 v	19.0	16.0	13.3	10.4
B0 v	18.9	15.9	13.2	10.3
B1 v	18.6	15.6	12.9	10.0
B3 v	18.1	15.0	12.4	9.3
B5 v	17.6	14.5	11.9	8.9
B8 v	16.9	13.7	11.1	8.0

A1 v	15.8	12.6	10.1	6.9
A3 v	15.6	12.3	9.9	6.6
A5 v	15.3	12.0	9.6	6.2
F0 v	14.7	11.3	8.9	5.5
F2 v	14.4	11.0	8.6	5.2
F5 v	14.0	10.6	8.1	4.7
F8 v	13.7	10.3	7.8	4.4
G2 v (Solar)	13.0	9.6	7.1	3.7
G8 v (Tau Ceti)	12.6	9.1	6.6	3.2
K2 v (Epsilon Eri)	11.8	8.3	5.8	2.4
KM III (Eta Ser)	11.4	8.0	5.5	2.0
KM III (Alpha Boo)	9.6	6.1	3.6	0.2
KM III (Gamma Aql)	7.1	3.6	1.1	-2.3
KM III (HD 146051)	6.2	2.7	0.2	-3.3
KM III (Alpha Cet)	8.0	4.6	2.1	-1.3
KM III (HD 123023)	8.7	5.2	2.7	-0.7
KM III (Beta Gru)	8.9	5.5	3.0	-0.4
T~50,000 K Blackbody	19.2	16.2	13.5	10.6
$F_{\lambda} \sim \lambda^{-1}$	16.8	13.6	11.0	7.9
$F_{\lambda} =$ const surface brightness	10.9	8.0	5.1	2.3
$F_{\lambda} =$ const point source	15.8	12.6	10.1	6.9

10.4 Tools for Bright-Object Screening

[10.4.1 The Bright Object Tool \(BOT\)](#)

[10.4.2 The Exposure Time Calculator \(ETC\)](#)

10.4.1 The Bright Object Tool (BOT)

STScI has developed a Bright Object Tool (BOT) to facilitate field checking prior to COS program implementation. The BOT is implemented within [APT](#) (the [Astronomer's Proposal Tool](#)), using the Aladin interface, and reads target and exposure information from the Phase II proposal. Help files and training movies are available within [APT](#). The BOT is based on displays of the Digital Sky Survey (DSS) and on automated analysis of the field using data from two catalogs: the second Guide Star Catalog (GSC2) and the *GALEX* catalog.

GSC2 provides two magnitudes (photographic J and F), hence one color, for most fields down to about magnitude 22, which, combined with conservative assumptions about spectral type vs. color, allow expeditious target and field checks. In some cases, the GSC2 is inadequate because of crowding or the absence of one filter. The APT/BOT automatically clears stars with only a single GSC2 magnitude if they are safe based on the assumption that the target is an unreddened O5V star. Any other unknown targets must be cleared by hand.

Automated *GALEX* screening is now available within the APT/BOT. The AIS (all-sky) sources are screened as unreddened O5V stars and reported as either safe, unsafe, or unknown. Because it is based directly on UV fluxes, *GALEX* screening can reveal, for example, previously unknown hot companions to late-type stars. If the field passes the BOT check, it is safe; unsafe and unknown objects require further investigation. **Caveats:** (1) The *GALEX* catalog does not cover the whole sky, so PIs must check that their COS field is fully covered by *GALEX*. (2) *GALEX* fluxes represent upper limits in crowded regions because of the instrument's relatively low spatial resolution. (3) The *GALEX* detectors suffer local non-linear effects at high count rates. The fluxes and magnitudes in the current version of the *GALEX* catalog are not corrected for these effects and may be underestimated for the brightest stars. A preliminary correction is presented in Morrissey et al. (2007, [ApJS](#), 173, 682). The BOT now applies this correction to the *GALEX* catalog. As a result, it may report *GALEX* magnitudes that are brighter than those given in the *GALEX* catalog itself.

In general, a COS pointing with unconstrained telescope orientation requires the clearance of a field 43 arcsec in diameter. If any displacements from the default pointing (e.g., acquisition scans, POS TARGs, patterns, or mosaics) are specified, then the field to be cleared increases commensurately. Because both the PSA and BOA are exposed to the sky at all times, no unsafe or unknown star may fall within 7 arcsec of either aperture at any allowed orientation. The BOT automatically accounts for the reduced throughput of the BOA and `MIRRORB`. The BOT automatically creates a macro-aperture covering the expected field of view for an observation that accounts for a given combination of scans, POS-TARGs, patterns or mosaics. It also can account for the proper motion of the science target.

Note: Always check the science target with the [ETC](#), rather than relying on the BOT field report. When constructing your Phase II proposal within [APT](#), include the ETC exposure ID number to document your work and to facilitate the Phase II review.

10.4.2 The Exposure Time Calculator (ETC)

Should the tools available within the BOT be insufficient to clear a field object, its safety may be confirmed using the [ETC](#).

An existing UV spectrogram of the target or class may be imported directly into the [ETC](#). When using *IUE* data as input spectra in the [ETC](#), consider only low-resolution spectra taken through the large aperture. Note that the [ETC](#) does not convolve imported spectra to the COS resolution. To be conservative, one must assume that the entire flux of an emission line falls within a single COS resolution element. The [ETC](#) can also have emission lines of a given intensity and width included in a calculation.

If model spectra are used in the [ETC](#), the original Kurucz (not Castelli & Kurucz) models should be used for early-type stars. None of the provided models is adequate for late-type stars since the models lack chromospheric emission lines. Actual UV data must be used for late-type stars when possible. If a given star has only a *V* magnitude, it must be treated as an unreddened O5V star. If one color is available it may be processed as a reddened O5V star (which will always have a greater UV flux than an unreddened star of the same color).

If two colors are available, then the spectral type and reddening can be estimated separately. In some cases, the 2MASS *JHK* may be the only photometry available for an otherwise unknown star. The [ETC](#) supports direct entry of observed *J* and *H* magnitudes with E_{B-V} . It is also possible to estimate *V* and E_{B-V} from those data on the assumption of a reddened O5V star, and thus determine its count rates in the [ETC](#). Martins & Plez (2006, *A&A*, 457, 637) derive $(J - H)_0 = -0.11$ for all O stars, and $(V - J)_0 = -0.67$ and $(V - H)_0 = -0.79$ for early O types. (The *K* band should be avoided for BOP purposes because of various instrumental and astrophysical complications.) Bessell & Brett (1988, *PASP*, 100, 1134), Appendix B, give relationships between the NIR reddenings and E_{B-V}

V

10.5 Policies and Procedures

Bright Object Protection and target variability

All COS exposures, whether target-acquisition, spectroscopic, or imaging, must be checked for bright objects. Any COS targets or fields that cannot be demonstrated to be safe to a reasonable level of certainty in the judgment of the Contact Scientist (CS) will not be observed. In that case, it is possible that equivalent alternative targets may be approved upon request. Any observations that trigger the onboard safety mechanisms will not be rescheduled.

COS GOs *must* enter the [ETC](#) calculation number for each discrete exposure into the appropriate field of the [APT](#) when preparing their Phase [II](#) material. A GO *must* also report any unsafe or unknown stars from APT/BOT for each field, and either show that the observations are safe or document any unresolved issues. (An exception is moving-target fields, which cannot be cleared until the scheduling windows have been established.) It is not expected that all such issues will be resolved by the Phase [II](#) deadline, but they should at least be identified and have planned resolutions by then.

Light from a bright nearby source could scatter into the PSA. For example, a target that is safe for the BOA may scatter enough light into the PSA to violate our screening limits. The region of concern is an annulus extending 5 to 15 arcsec from the center of the PSA. Any field object falling in this annulus may not produce a global count rate in excess of 1×10^5 count s^{-1} per segment for the FUV channel or 2×10^5 count s^{-1} for the NUV, or a local count rate over 3.3 count s^{-1} pixel $^{-1}$ in the FUV or 250 count s^{-1} pixel $^{-1}$ in the NUV. **At present, the APT/BOT does not search for such objects, so they must be checked by hand.** In such cases, count rates must be estimated using the [ETC](#) as though the source were at the center of the PSA.

In worst cases, new ground-based data or HST CCD UV exposures may be required to clear the fields for BOP; in general, the latter must be covered by the existing Phase [I](#) time allocation.

For unsafe targets, one solution is to change to a less sensitive instrument configuration: one could use the BOA, [MIRRORB](#), or both (though the BOA is Available-but-Unsupported for science, see [Section 5.13](#)), a higher-resolution grating, or a less-sensitive wavelength setting. Note that the medium-resolution gratings actually have higher throughput than G140L when the data are rebinned, but are subject to brighter limits.

Use of ORIENT to reduce risk from nearby objects

For unsafe field objects that threaten to fall into the non-target aperture, an orientation restriction ([ORIENT](#)) may be used to constrain the spacecraft roll angle and thus the position of the non-target aperture, but such constraints will limit the scheduling of the observation and need to be requested under "Special Requirements" in the Phase [I](#) proposal document.

GOs planning COS observations of unpredictably variable targets should be aware of the special BOP procedures in effect for such cases. Observations of flare stars are allowed with COS (and STIS) only if the Contact Scientist is convinced that the targets would not violate BOP limits even in their brightest states. [COS ISR 2017-01](#) provides specific guidance for evaluating the suitability of M dwarfs for observation.

"STOP" procedure for highly variable targets

Targets that are known to vary on short timescales of days or more, such as cataclysmic variables, may require the Safe Target Offset Procedure (STOP). This procedure is described in detail in [ACS ISR 2006-04](#), and applies to all HST detectors subject to BOP; here we summarize it. In STOP visits, the proposers are required to provide photometric monitoring for at least seven consecutive nights leading up to the HST observation, with the latest observation happening within 24 hours of the target being observed by HST. The photometric monitoring may be done from the ground using optical bands, or may be coordinated with other space observatories. If the need to coordinate the photometric monitoring with other observatories imposes scheduling constraints, these constraints must be mentioned and justified in the Phase I proposal as a special requirement.

The Contact Scientist will make the final decision to observe the target if the photometric monitoring indicates that the target is stable and there is no danger to the health of the COS detectors. STOP visits are initially set up by STScI staff with a small offset that points the telescope at blank sky. If the Contact Scientist clears the visit to proceed, a command will be sent to remove the offset, and the observation will be executed normally. If the observation is not cleared, the observation will still be executed pointing at blank sky, since the offset will not be removed, and no light from the science target will enter the COS apertures.

It is expected that targets for which the STOP procedure is applied will usually be safe to observe. The intent of the procedure is to catch rare exceptions. If photometric monitoring indicates that the target is not safe to observe, the STOP observation will not be rescheduled, and the orbits for that observation will be charged against the program. Users who wish to observe targets that have a significant chance of being in an unsafe state should consider proposing those targets as Targets of Opportunity.

STScI reserves the right to limit the number of visits requiring quiescence observations within 20 days or less of an HST observation to no more than 12 such visits per Cycle, including all HST programs.

A pointing or configuration change after the targets and fields have been cleared by the STScI BOP review must be approved by the COS Team on the basis of a specific scientific justification and a new BOP review by the GO, which may be submitted via the CS.

Observers are expected to follow policies pertaining to values of `BUFFER-TIME` when proposals require a STOP procedure. For targets of variable brightness, the `BUFFER-TIME` should correspond to the maximum safe flux scenario, rather than the more likely scenario of a quiescent observation.

10.6 On-Orbit Protection Procedures

[10.6.1 FUV Bright Object Protection](#)
[10.6.2 NUV Bright Object Protection](#)

Should an overly bright object be observed with COS, on-board software will typically act to protect the instrument from damage. The most serious response is to reduce the high voltage of the affected detector; subsequent observations will not take place until COS undergoes a safe-mode recovery procedure that is run from the ground. Activating any of the instrument protection levels listed below is regarded as a serious breach of our health and safety screening procedures and is cause for an investigation. Observers are responsible for ensuring that their observations do not endanger the instrument.

10.6.1 FUV Bright Object Protection

There are five levels of protection for the COS FUV detector:

1. At the lowest level are the count-rate screening limits imposed on observers in order to provide a margin of safety for the instrument. The screening limits ([Table 10.1](#)) are set at a factor of two or more below actual risk levels, and we expect observers to work with us to ensure these limits are adhered to. They are determined by estimating the expected count rate from an object, both globally over the detector and locally in an emission line if appropriate. The COS [ETC](#) is the tool used for this check.
2. At the next level, within COS the "Take Data Flag" (TDF) is monitored during an exposure. If an event occurs that causes the TDF to drop (such as loss of lock on a guide star, which could lead to the telescope drifting), then the exposure will continue with the COS external shutter closed. Subsequent exposures in the visit may also be lost.
3. Next comes local rate monitoring. It is possible to permanently damage a localized region of the micro-channel plates without necessarily exceeding the global rate limits. This could occur if an object with bright emission lines were observed, for example. At the beginning of each exposure, the COS flight software bins the FUV spectrum by 4 pixels in x and 1024 in y ; if the count rate in any bin exceeds 1000 counts per 15 s, the external shutter is closed and the calibration lamps turned off. All subsequent exposures until the next grating change or target acquisition are lost.
4. Global rate monitoring is next. The COS flight software continuously monitors the total event rate for both FUV detector segments. If the rate for either segment exceeds 600,000 counts in 10 s, the high voltage to both segments is turned off. Special commanding is required to turn on the FUV detector high voltage, so subsequent FUV observations will be lost, and the HST schedule will be disrupted.
5. At the highest level, the instrument is protected by software that senses an over-current condition in the high-voltage power supply; if triggered, the software shuts down the high voltage.

10.6.2 NUV Bright Object Protection

Similar protections also apply to the NUV detector:

1. At the lowest level are the count-rate screening limits imposed on observers to provide a margin of safety for the instrument. The screening limits ([Table 10.1](#)) are set at a factor of two or more below actual risk levels, and we expect observers to work with us to ensure these

limits are adhered to. They are determined by estimating the expected count rate from an object, both globally over the detector, and locally in an emission line if appropriate. The [COS ETC](#) is the tool used for this check.

2. At the next level, within COS the "Take Data Flag" (TDF) is monitored during an exposure. If an event occurs that causes the TDF to drop (such as loss of lock on a guide star, which could lead to the telescope's drifting), then the exposure will continue with the COS external shutter closed. Subsequent exposures in the visit may also be lost.
3. Next comes local rate monitoring. It is possible to permanently damage a small region of a micro-channel plate without exceeding the global rate limits. This could occur if an object were imaged or had a spectrum with bright emission lines, for example. Before each observation, the flight software takes a 0.3 s exposure, bins it in "superpixels" of 4×4 pixels each, and analyzes it in two passes. During the first pass, the flight software checks that each superpixel does not exceed the threshold values of 225 counts and 390 counts for imaging and spectroscopic observations, respectively. During the second pass, the software steps a box (of 1×2 superpixels for spectroscopic exposures and 2×2 pixels for imaging exposures) across the image, checking that the same limits are not exceeded in the larger area. The purpose of the second pass is to ensure that bright sources at the edge of the superpixels are not missed. This 0.3 s exposure is not recorded. If the local rate limit is exceeded, the COS flight software closes the external shutter and all subsequent exposures until the next grating change or target acquisition are lost.
4. Global rate monitoring is next. The COS flight software continuously monitors the total event rate for the NUV MAMA. If the total count rate exceeds 20,000 in 0.1 s the high voltage to the MAMA is turned off, the external shutter is closed, and the calibration lamps are turned off. The NUV detector can resume operations only after a safe-mode recovery procedure, so subsequent NUV exposures will be lost, and the HST schedule disrupted.
5. At the highest level, the NUV MAMA is protected by the detector electronics. The Bright-Scene Detector (BSD) monitors the output of every 2 anode wires across the detector, corresponding to every 32nd row of pixels. The wires are parallel to the dispersion axis. If the total count rate exceeds 17,000 in 138 ms, then the high voltage is turned off. COS can resume operations only after a safe-mode recovery procedure. BSD differs from global-rate monitoring in two ways: it is done in hardware, not software, and what is measured is not a digitized count rate, but current in the anode grid wires.

10.7 Bright Object Protection for Solar System Observations

Observations of solar system objects with COS require particularly careful planning. To determine if a particular observation of a solar system target is safe, tables in [Section 10.3](#) can be used for an initial check. Ultimately, observers must use the COS [ETC](#). With a user-supplied input spectrum or assumptions about the spectral energy distribution of the target, the [ETC](#) will determine whether a specified observation violates any bright object limits. Generally speaking, for small ($< \sim 0.5 - 1$ arcsecond) solar system objects the local count-rate screening limit is the more restrictive constraint, while for large objects ($> \sim 1 - 2$ arcseconds) the global limit is much more restrictive. Imaging (including imaging acquisitions) is much more likely to violate count-rate screening limits than spectroscopy.

As a first approximation, small solar system targets can be regarded as point sources with a solar (G2 V) spectrum, and if the V magnitude is known, tables in [Section 10.3](#) can be used to estimate whether an observation with a particular COS grating and aperture is near the bright object limits. V magnitudes for the most common solar system targets (all planets and satellites, and the principal minor planets) can be found in the *Astronomical Almanac*. This approximation should provide a conservative estimate because it assumes that the flux is distributed over the minimum number of pixels, which is an overestimate, and because the albedos of solar system objects are almost always < 1 (meaning that the flux of the object will be less than that of the assumed solar spectrum at UV wavelengths where the bright object limits apply). If this simple estimate produces a number near the bright object limit, a more sophisticated estimate may be required to provide assurance that the object is not too bright to observe in a particular configuration.

For large solar system targets, checking of the bright object limits is most conveniently done by converting the integrated V magnitude (V_o , which can be found in the *Astronomical Almanac*) to V

magnitude/arcsec² as follows:

$$V / \text{arcsec}^2 = V_o - 2.5 \log (1 / \text{area}),$$

where $area$ is the area of the target in arcsec². This V/arcsec^2 and the diameter of the target in arcsec can then be input into the [ETC](#), using the Solar Spectrum template in the HST Standard Star menu for the spectral energy distribution, to test whether the bright object limits can be satisfied.

Alternatively, an observed spectrum obtained with a known slit or aperture size can be used as input to the [ETC](#). Most calibration techniques produce units of flux (e.g., ergs s⁻¹ cm⁻² Å⁻¹), even for extended targets. Such a calibration implicitly assumes a flux per solid angle (i.e., the angle subtended by the observing aperture or object, whichever is smaller), and it is more appropriate to convert to units of surface brightness (ergs s⁻¹ cm⁻² Å⁻¹ arcsec⁻²) by dividing the calibrated flux by the appropriate area (aperture size or object size, whichever is *smaller*). If such a spectrum is available, it can be passed to the [ETC](#) as a user-supplied spectrum. If the [ETC](#) result exceeds the local or global count-rate screening limit, the observation cannot be performed.

Field Safety Checks for Moving Targets

Multiple fields along the path of an object must be cleared for the safety of moving target observations. Of course, this cannot be accomplished until scheduling windows are assigned, and the fields may have to be checked again if the windows change. An automated capability to do that has been added to the **APT/BOT**. Your Contact Scientist will advise and assist with this procedure.

10.8 SNAP, TOO, and Unpredictable Sources Observations with COS

The COS photon-counting detectors can be harmed by exposure to bright light. Because all COS observations must be checked at STScI by a Contact Scientist to confirm that both the intended target and all nearby objects lie within safe-brightness limits, the total number of targets accepted for all COS and STIS MAMA SNAP programs will be limited to 150 per cycle.

For similar reasons, when planning Target of Opportunity (TOO) observations COS observers must ensure that sufficient time is available to allow for STScI screening of targets for compliance with safety limits. Ultra-rapid TOOs, (<2 days), are not allowed with COS. *No COS observations will be performed until the bright object screening has been completed.* This process can be greatly accelerated by preliminary discussions with the assigned Contact Scientist to clarify the information that the observer will need to provide to STScI and the criteria that will be used to determine if the target is safe to observe.

In the case of irregular variables that are either known to undergo unpredictable outbursts, or belong to classes of objects that are subject to outbursts, the proposer must determine whether the target will violate the bright object limits during outburst. Note that [COS ISR 2017-01](#) provides specific guidance for evaluating the suitability of M dwarfs for observation. If a violation is possible, the proposer must outline a strategy that will ensure that the target is safe to observe with COS. The observing strategy might include additional observations, obtained over a timescale appropriate to the particular type of variable object, with either HST or ground-based telescopes. If HST data are to be used for this purpose, the required orbits must be requested in Phase I (see [Call for Proposals](#)). STScI reserves the right to limit the number of visits requiring quiescence verification observations within 20 days or less of an HST observation to no more than 12 such visits per Cycle. Further details about these procedures are presented in [ACS ISR 2006-04](#). The general policies described there apply to the STIS/MAMA and COS detectors as well, with suitable scaling for the differences in the exact Bright Object Protection (BOP) limits for each detector and mode. These limits are described in the individual instrument handbooks.

For more information on these and other policies pertaining to HST observing, please see the [Call for Proposals](#).

Chapter 11: Data Products and Data Reduction

Chapter Contents

- [11.1 Overview](#)
- [11.2 COS Data Files](#)
- [11.3 Additional COS Files](#)

11.1 Overview

Raw COS data are processed through the STScI Data Processing pipeline. Data first undergo Generic Conversion, through which bits from individual exposures are unpacked and combined into files containing raw, uncalibrated data. Next, the raw files are processed through the COS calibration pipeline, **CaICOS**, which performs image and spectroscopic reduction to produce output files useful for scientific analysis. Finally, the data are ingested into the *Hubble* Data Archive through the Data Archive and Distribution System (DADS). This system populates a database containing header keywords that is accessible to users via the [Mikulski Archive for Space Telescopes](#) (MAST). Both calibrated and uncalibrated data are then available for distribution by [MAST](#) to the user.

11.2 COS Data Files

When data are taken in `TIME-TAG` mode (the default), the raw data are in the form of a table of photon events containing the arrival time, x and y pixel coordinates, and pulse height (for FUV data) for each photon detected. Raw `ACCUM` data are in the form of a 2-D image. For `ACCUM` FUV data, there will be two raw files for each exposure, one file for Segment A and one for Segment B. For `ACCUM` NUV data, there will be one raw file for each exposure.

The calibrated data have the same general format for both FUV and NUV, although there are differences in detail. There is a "corrtag" file (the file name contains the string "corrtag") containing a corrected events table. The `corrtag` table includes all of the columns from the raw data file, plus these additional columns: a weight that accounts for the flat-field and dead-time corrections, a data-quality column, and a column that gives the pulse-height amplitude of each event. ([Codes for the DQ flags are listed in the *COS Data Handbook*.](#)) The `corrtag` file provides several sets of corrected pixel coordinates for each event. These include `X[Y]CORR`, which are corrected for thermal drifts in the detector electronics, geometric distortions in the detector; and `Y` walk; `XDOPP`, which are the x coordinates corrected for orbital Doppler motions; `X[Y]FULL`, which are the `XDOPP` and `YCORR` coordinates corrected for OSM drift and recast into a coordinate system defined by the `WAVECAL` spectrum; and `WAVELENGTH`, which provides the wavelength corresponding to the `XFULL` coordinate. The `corrtag` file has a separate extension containing timeline information. It provides second-by-second values for the spacecraft position, solar and target altitude above the horizon, and count rates for the most prominent airglow lines and the background. The data in this extension can be useful when reprocessing `TIME-TAG` data, allowing the user to exclude, for example, data obtained during orbital day. The `costools` package offers a tool called `timefilter` for this purpose. For `ACCUM` data, the `corrtag` table has the same format, but all the values in the `TIME` column are a constant, half the exposure time. There is one row in this pseudo-`TIME-TAG` table for each count in the raw `ACCUM` image.

Additional calibrated files include the `flt` and counts images, which are created by binning the events in the `corrtag` table. Both images have units of counts/s, but the `flt` image is also corrected for flat-field and dead-time effects. For spectroscopic data, a 1-D extracted spectrum (or three spectra, for NUV exposures) will be written to an `x1d` file for each exposure. For data in an association (whereby multiple exposures are processed together—the usual case), the 1-D spectra for separate exposures will be averaged and written to an `x1dsum` table. If multiple `FP-POS` settings are used, there will be one `x1dsum` file for each `FP-POS` (`x1dsum[1,2,3,4]`), even if only one spectrum was obtained at each position. The distinction between the `x1d` and `x1dsum` files in such cases is that the `DQ_WGT` column of the `x1d` files (the data-quality weights) are used to eliminate bad or suspect data, such as detector dead spots. The `x1dsum` file without a number is the final sum of all of the exposures. It can be a weighted mean of all the `x1dsum[n]` files or, if a single exposure was obtained at a single `FP-POS` setting, a copy of the `x1d` file with the `DQ_WGTs` applied.

By default **CalCOS** will combine data taken at different `FP-POS` settings, but not at different central wavelengths. A new association is created when either the grating or central wavelength is changed, and **CalCOS** only combines data within an association.

Wavelength calibration can be performed in either of two ways. The default is to take line-lamp exposures ("wavecal" exposures) simultaneously with the science data (if performing observations at LP1-5) or via `SPLIT` wavecal exposures automatically inserted before and after the science exposures (if performing observations at LP6). In these cases, the wavecal spectra will be extracted and saved in lampflash tables. The alternative is to take separate wavecal exposures interspersed with the science exposures. These wavecals will be calibrated in the same way as science exposures, except that the calibrated wavecal data (`corrtag`, `flt`, `counts`, `x1d`) will not be corrected for the offset of the spectrum from the template, and no `x1dsum` file will be created for a wavecal.

11.3 Additional COS Files

Several additional files are used in the processing of COS data. These include association files (`asn`), which are used to control calibration processing; engineering support files (`spt`), which contain information used in the pipeline processing; and lampflash files (`lampflash`), which contain extracted wavelength calibration spectra used in the processing of `TIME-TAG` data with `FLASH=YES` or with `SPLIT` wavecal. For a full description of these and other files, see the [COS Data Handbook](#).

Chapter 12: The COS Calibration Program

Chapter Contents

- 12.1 Introduction
- 12.2 Ground Testing and Calibration
- 12.3 SMOV4 Testing and Calibration
- 12.4 COS Monitoring Programs
- 12.5 Cycle 17 Calibration Program
- 12.6 Cycle 18 Calibration Program
- 12.7 Cycle 19 Calibration Program
- 12.8 Cycle 20 Calibration Program
- 12.9 Cycle 21 Calibration Program
- 12.10 Cycle 22 Calibration Program
- 12.11 Cycle 23 Calibration Program
- 12.12 Cycle 24 Calibration Program
- 12.13 Cycle 25 Calibration Program
- 12.14 Cycle 26 Calibration Program
- 12.15 Cycle 27 Calibration Program
- 12.16 Cycle 28 Calibration Program
- 12.17 Cycle 29 Calibration Program
- 12.18 Cycle 30 Calibration Program
- 12.19 Cycle 31 Calibration Program

12.1 Introduction

In this chapter, we provide a brief overview of the calibration observations obtained during ground testing and on-orbit through Cycle 30. Potential Cycle 31 observers should assume that all of these calibrations will be completed by the time that Cycle 31 begins.

Observers who wish to use instrument configurations that are not addressed by these calibration plans should assess their specific calibration needs and include time in their Phase I proposal for any additional calibrations that are required.

12.2 Ground Testing and Calibration

The COS Investigation Definition Team (Principal Investigator, James Green, University of Colorado) was responsible for the ground testing and ground calibration of COS. Most of the ground test data was obtained in 2003 and 2006 during thermal vacuum testing at Ball Aerospace and Goddard Space Flight Center, respectively. These tests characterized the basic properties of the optics, the detectors, and the mechanisms. While some measurements (e.g., FUV full-detector flat-field images) cannot be repeated in orbit, most of the ground-test data have been superseded by on-orbit measurements obtained during SMOV4.

12.3 SMOV4 Testing and Calibration

The primary goal of the Observatory Verification program for Servicing Mission 4 (SMOV4) was the timely commissioning of HST for normal science operations. For the newly installed COS, this included testing the focus (internal and external), verifying the target-acquisition procedures, monitoring instrument stability (both in terms of image motions and sensitivity), and measuring plate scales, line-spread functions, and other instrument parameters. SMOV4 observations were completed in October 2009, and a series of Instrument Science Reports (ISRs) detailing the results of their analysis have been published. Those ISRs and the observing programs on which they are based are listed in [Table 12.1](#).

Table 12.1: COS ISRs Resulting from SMOV4 Calibration Programs.

Number	Title	Author(s)	Associated SMOV Programs
2009-01	Preliminary Characterization of the Post-Launch Line-Spread Function of COS	Ghavamian et al.	11489, 11476
2010-01	SMOV Absolute Flux Calibration of the COS NUV Modes	Massa et al.	11479
2010-02	SMOV Absolute Flux Calibration of the COS FUV Modes	Massa et al.	11492
2010-03	COS Near-UV Flat Fields and High S/N Determination from SMOV Data	Ake et al.	11478, 11481
2010-04	SMOV: COS NUV On-Orbit Optical Alignment	Hartig et al.	11468, 11469
2010-05	SMOV: COS NUV Wavelength Calibration	Oliveira et al.	11470, 11474, 11475
2010-06	SMOV: COS FUV Wavelength Calibration	Oliveira et al.	11485, 11488, 11487
2010-07	SMOV: COS FUV Focus Determination	Lennon et al.	11484
2010-08	NUV Spectroscopic Performance	Beland & Ghavamian	11476, 11477
2010-09	FUV Spectroscopic Performance	Ghavamian et al.	11489, 11490
2010-10	SMOV: COS NUV Imaging Performance	Goudfrooij et al.	11473
2010-11	FUV Darks	Sahnow et al.	11356, 11482, 11484
2010-12	NUV Darks	Sahnow et al.	11355, 11466,
2010-13	NUV/FUV Structural and Thermal Stability	Smith & Keyes	11480, 11493

2010-14	COS Target Acquisition Guidelines, Recommendations, and Interpretation	Keyes & Penton	11471, 11472, 11486
---------	--	----------------	---------------------

12.4 COS Monitoring Programs

An overview of the COS monitoring programs is given in [Table 12.2](#) along with the ID numbers of completed programs. [Table 12.3](#) lists COS contingency programs. Details on special calibration programs that were undertaken in a particular Cycle are given the appropriate subsection below. Instrument science reports (ISRs) detailing each cycle's calibration programs can be found on the [COS website](#).

Table 12.2: COS Monitoring Calibration Program.

Title			Accuracy Achieved	Program IDs	Products
NUV Monitors					
NUV Distribution	MAMA	Fold	<5% at the location of the peak of the fold distribution	11891 (Cycle 17) 12419 (Cycle 18) 12723 (Cycle 19) 13128 (Cycle 20) 13531 (Cycle 21) 13976 (Cycle 22) 14444 (Cycle 23) 14526 (Cycle 24) 14943 (Cycle 25) 15539 (Cycle 26) 15777 (Cycle 27) 16328 (Cycle 28) 16536 (Cycle 29) 16936 (Cycle 30) 17318 (Cycle 31)	ISR

NUV Dark Monitor	<0.2% in the global dark rate uncertainty	11894 (Cycle 17) 12420 (Cycle 18) 12720 (Cycle 19) 13126 (Cycle 20) 13528 (Cycle 21) 13974 (Cycle 22) 14442 (Cycle 23) 14521 (Cycle 24) 14942 (Cycle 25) 15538 (Cycle 26) 15776 (Cycle 27) 16327 (Cycle 28) 16535 (Cycle 29) 16935 (Cycle 30) 17317 (Cycle 31)	ISR Updated dark rates for the COS Exposure Time Calculator
------------------	---	---	--

NUV Spectroscopic Sensitivity Monitor	$S/N \sim 30$ at λ_{cen}	11896 (Cycle 17) 12421 (Cycle 18) 12719 (Cycle 19) 13125 (Cycle 20) 13527 (Cycle 21) 13973 (Cycle 22) 14441 (Cycle 23) 14858 (Cycle 24) 15387 (Cycle 25) 15540 (Cycle 26) 15778 (Cycle 27) 16329 (Cycle 28) 16537 (Cycle 29) 16937 (Cycle 30) 17319 (Cycle 31)	ISR Reference File
NUV Imaging Sensitivity	$S/N \sim 60$, observed to a predicted countrate accuracy of 0.1%	11899 (Cycle 17)	ISR Reference File

NUV Internal/External Wavelength Scale Monitor	1.7-3.7 pixels in wavelength scale accuracy	11900 (Cycle 17) 12422 (Cycle 18) 12722 (Cycle 19) 13127 (Cycle 20) 13529 (Cycle 21) 13975 (Cycle 22) 14443 (Cycle 23) 14859 (Cycle 24) 15388 (Cycle 25) 15541 (Cycle 26) 15779 (Cycle 27) 16330 (Cycle 28) 16538 (Cycle 29) 16938 (Cycle 30) 17320 (Cycle 31)	ISR Reference File
NUV Flat Monitor	$S/N = 20-25$ per 3.3 pixel element	12721 (Cycle 19)	ISR
COS ACQ/IMAGE Performance Monitoring	WCA-PSA offsets to <0.5 pixels	13124 (Cycle 20) 13526 (Cycle 21) 13972 (Cycle 22) 14440 (Cycle 23) 14857 (Cycle 24)	

NUV Target Acquisition Monitor	Offsets to <0.5 pixels	15389 (Cycle 25) 15542 (Cycle 26) 15780 (Cycle 27) 16331 (Cycle 28) 16539 (Cycle 29) 16939 (Cycle 30) 17321 (Cycle 31)	ISR
FUV Monitors			
FUV Detector Gain Maps	0.1 pulse height bin	13525 (Cycle 21) 13970 (Cycle 22) 14439 (Cycle 23) 14519 (Cycle 24) 14941 (Cycle 25) 15534 (Cycle 26) 15772 (Cycle 27) 16323 (Cycle 28) 16829 (Cycle 29) 17248 (Cycle 30) 17325 (Cycle 31)	ISR

FUV Dark Monitor	Rate < 10^{-6} count/pixel/s 0.1% in global dark rate uncertainty	11895 (Cycle 17) 12423 (Cycle 18) 12716 (Cycle 19) 13121 (Cycle 20) 13521 (Cycle 21) 13968 (Cycle 22) 14436 (Cycle 23) 14520 (Cycle 24) 14940 (Cycle 25) 15533 (Cycle 26) 15771 (Cycle 27) 16322 (Cycle 28) 16828 (Cycle 29) 17247 (Cycle 30) 17324 (Cycle 31)	ISR Updated dark rates for the COS Exposure Time Calculator
------------------	---	---	--

FUV Spectroscopic Sensitivity Monitor	$S/N = 30$ at λ_{cen}	11897 (Cycle 17) 12424 (Cycle 18) 12715 (Cycle 19) 13119 (Cycle 20) 13520 (Cycle 21) 13967 (Cycle 22) 14435 (Cycle 23) 14854 (Cycle 24) 15384 (Cycle 25) 15535 (Cycle 26) 15773 (Cycle 27) 16324 (Cycle 28) 16830 (Cycle 29) 17249 (Cycle 30) 17326 (Cycle 31)	ISR Reference File
--	--------------------------------------	---	-----------------------

<p>FUV Internal/External Wavelength Monitor</p>	<p>Wavelength zeropoint accuracies: G130M: 5.7-7.5 pixels G160M: 5.8-7.2 pixels G140L: 7.5-12.5 pixels</p>	<p>11997 (Cycle 17) 12425 (Cycle 18) 12717 (Cycle 19) 13122 (Cycle 20) 13522 (Cycle 21) 13969 (Cycle 22) 14437 (Cycle 23) 14855 (Cycle 24) 15385 (Cycle 25) 15536 (Cycle 26) 15774 (Cycle 27) 16325 (Cycle 28) 16534 (Cycle 29) 17250 (Cycle 30) 17327 (Cycle 31)</p>	<p>ISR Reference File</p>
<p>FUV Target Acquisition Monitor</p>	<p>Offsets to <0.5 pixels</p>	<p>15386 (Cycle 25) 15537 (Cycle 26) 15775 (Cycle 27) 16326 (Cycle 28) 16831 (Cycle 29) 16942 (Cycle 30) 17582 (Cycle 31)</p>	<p>ISR</p>

Table 12.3: COS Contingency Programs.

Title	Program IDs
-------	-------------

NUV Detector Recovery after Anomalous Shutdown	11892 (Cycle 17) 12430 (Cycle 18) 12724 (Cycle 19) 13129 (Cycle 20) 13533 (Cycle 21) 13978 (Cycle 22) 14446 (Cycle 23) 14523 (Cycle 24) 14945 (Cycle 25) 15544 (Cycle 26) 15782 (Cycle 27) 16335 (Cycle 28) 16541 (Cycle 29) 17323 (Cycle 31)
FUV Detector Recovery after Anomalous Shutdown	11893 (Cycle 17) 12431 (Cycle 18) 12718 (Cycle 19) 13123 (Cycle 20) 13532 (Cycle 21) 13977 (Cycle 22) 14445 (Cycle 23) 14522 (Cycle 24) 14944 (Cycle 25) 15543 (Cycle 26) 15781 (Cycle 27) 16334 (Cycle 28) 16540 (Cycle 29) 17322 (Cycle 31)
COS FUV Characterization of Modal Gain When Changing High Voltage	16333 (Cycle 28) 16833 (Cycle 29) 17252 (Cycle 30) 17329 (Cycle 31)
COS FUV Change in Spectroscopic Sensitivity Trends	16332 (Cycle 28) 16832 (Cycle 29) 17251 (Cycle 30) 17328 (Cycle 31)

12.5 Cycle 17 Calibration Program

The Cycle 17 calibration program continued the testing begun during SMOV. It included long-term programs to monitor the sensitivity and wavelength scale of both the NUV and FUV detectors. Midway through Cycle 17, additional calibration programs were added. Brief descriptions of these monitoring programs are presented in [Table 12.2](#). [Table 12.4](#) lists additional special calibration programs that were undertaken in Cycle 17. A comprehensive review of the Cycle 17 calibration program was published in [COS ISR 2012-02](#) (Osten et al. 2012).

Table 12.4: Cycle 17 Calibration Program.

Program ID	Title	Accuracy Achieved	Products
12010	COS FUV Line Spread Function Characterization	Continuum $S/N = 9.2$ near 1530 Å	COS ISR 2009-01, Tables of LSF models
12052	COS NUV Grating Efficiency Test	Few percent uncertainty in count-rate ratios	Calibration Workshop paper, ISR
12080	G140L Focus Sweep	30% uncertainty in autocorrelation FWHM of spectra	ISR
12081	COS Flux Calibration Below 1150 Å with G140L/1280	3% for 900–1150 Å, 10% for 300–700 Å	ISR, Reference file
12082	Extending COS/ G130M Coverage Down to 905 Å with Two New Central Wavelengths	wavelength scale: ± 0.5 Å, sensitivity: ± 5 –10%, resolution: 20–30%	ISR, Reference file
12083	G140L/1280 Wavecal Template	N/A	Reference file
12084	G140L/1280 Internal-to-External Wavelength Scales	7.5–12.5 pixel wavelength zero-point accuracy	Reference file
12085	STIS/E230M Data to Determine Internal-to-External Offsets in COS/G230L	Not evaluated yet	Reference file
12086	Generation of 1-D Fixed-Pattern Templates	2%	Reference file, ISR
12096	COS FUV Detector Lifetime Position Test	min S/N per resel of 30 at λ_{cen}	ISR

12.6 Cycle 18 Calibration Program

The Cycle 18 calibration program continued the calibration and monitoring observations performed in Cycle 17, including long-term programs to monitor the sensitivity and wavelength scale of both the NUV and FUV detectors. Brief descriptions of these monitoring programs are presented in [Table 12.2](#). [Table 12.5](#) lists additional special calibration programs that were undertaken in Cycle 18. A comprehensive review of the Cycle 18 calibration program was published in [COS ISR 2013-04](#) (Kriss et al. 2012).

Table 12.5: Cycle 18 Calibration Program FUV Lifetime Position Calibration Program.

Program ID	Title	Accuracy Achieved	Products
12414 ¹	COS Observations of Geocoronal Lyman- α Emission	G140L: $S/N = 2$ per pixel at 1200 Å, G130M: $S/N = 2$ per pixel at 1213 Å	List of exposures on the COS website ² that GOs may use to model and subtract Lyman α
12426	FUV Sensitivity Characterization	$S/N \sim 10/\text{pixel}$	ISR, Reference file
12432	COS FUV Detector Gain Sag vs. High Voltage	1% over 2 Å bands	Decision on change of voltage or lifetime position

¹ Coordinated parallel with STIS calibration program 12414.

² <http://www.stsci.edu/hst/instrumentation/cos/calibration/airglow>.

As described in [Section 4.1.7](#), gain sag affects spectra obtained with the FUV detector. To address this problem the COS team performed studies to move the Aperture Mechanism so that the FUV spectra fell on a different part of the detector, called a lifetime position. This work was divided into three phases. [Table 12.6](#) lists the programs that were used to determine the location of the new lifetime position, enable science at that location, and finally calibrate observations obtained there. The additional lifetime calibration program "Second COS FUV Lifetime Position: Wavelength Scales (FCAL1)" uses observations from programs 12805, 12806, and 12796.

Table 12.6: Lifetime Position 2 Calibration Program.

	I. Identify the New Lifetime Position
12676	COS/FUV Characterization of Detector Effects
12677	COS/FUV Mapping of the Stray PtNe Light through FCA
12678	COS/FUV Characterization of Optical Effects
	II. Enable Science at the New Lifetime Position

12793	Second COS FUV Lifetime Position: FUV Detector High Voltage Sweep (FENA1)
12795	Second COS FUV Lifetime Position: Verification of Aperture and FUV Spectrum Placement (FENA2)
12796	Second COS FUV Lifetime Position: Focus Sweep Enabling Program (FENA3)
12797	Second COS FUV Lifetime Position: FUV Target Acquisition Parameter Update (FENA4)
	III. Calibrate the New Lifetime Position
12805	Second COS FUV Lifetime Position: Wavelength and Resolution Calibration (FCAL2)
12806	Second COS FUV Lifetime Position: Flux and Flat-field Calibration and TDS Transfer (FCAL3)
12807	Second COS FUV Lifetime Position: Verification of FUV BOA Operations (FCAL4)

Phase I was part of Cycle 18. Phases II and III took place during Cycle 19.

12.7 Cycle 19 Calibration Program

The Cycle 19 calibration program continued the routine calibration and monitoring observations performed in Cycle 18, including long-term programs to monitor the sensitivity and wavelength scale of both the FUV and NUV detectors. Brief descriptions of these monitoring programs are presented in [Table 12.7](#). [Table 12.7](#) lists additional special calibration programs that were undertaken in Cycle 19. A comprehensive review of the Cycle 19 calibration programs is detailed in [COS ISR 2014-01](#) (Duval et al. 2014).

Table 12.7: Cycle 19 Calibration Program.

Program ID	Title	Accuracy Achieved	Products
12775 ¹	COS Observations of Geocoronal Lyman- α Emission	G140L: $S/N = 2$ per pixel at 1200 Å, G130M: $S/N = 2$ per pixel at 1213 Å	List of exposures on the COS website ² that GOs may use to model and subtract Lyman α
13070	Characterization of the Spatial Resolution and Wavelength Solution of the New FUV Modes (C1055, C1096, C1222)	10% in residual difference between model and observations	ISR, LSFs for C1055, C1096, C1222

¹ Coordinated parallel with STIS calibration program 12775.

² <http://www.stsci.edu/hst/instrumentation/cos/calibration/airglow>.

12.8 Cycle 20 Calibration Program

The Cycle 20 calibration program continued the routine calibration and monitoring observations performed in Cycle 19, including long-term programs to monitor the sensitivity and wavelength scale of both the FUV and NUV detectors. Brief descriptions of these monitoring programs are presented in [Table 12.2](#). [Table 12.8](#) lists additional special calibration programs that were undertaken in Cycle 20.

Table 12.8: Cycle 20 Calibration Program.

Program ID	Title	Accuracy Achieved	Products
13145 ¹	COS Observations of Geocoronal Lyman- α Emission	G140L: $S/N = 2$ per pixel at 1200 Å, G130M: $S/N = 2$ per pixel at 1213 Å	List of exposures on the COS website ² that GOs may use to model and subtract Lyman α

¹ Coordinated parallel with STIS calibration program 13145.

² <http://www.stsci.edu/hst/instrumentation/cos/calibration/airglow>

12.9 Cycle 21 Calibration Program

The Cycle 21 calibration program continued the routine calibration and monitoring observations performed in Cycle 20, including long-term programs to monitor the sensitivity and wavelength scale of both the FUV and NUV detectors. Brief descriptions of these monitoring programs are presented in [Table 12.2](#). [Table 12.9](#) lists additional special calibration programs that were undertaken in Cycle 21.

Table 12.9: Cycle 21 Calibration Program.

Program ID	Title	Accuracy Achieved	Products
13523	PtNe Lamp Cross Calibration	Lamp flash times to within 10%	ISR tables of lamp flash times for Lamp 2
13530	NUV Focus Sweep	Analysis in progress	ISR

12.10 Cycle 22 Calibration Program

The Cycle 22 calibration plans for COS (see [Table 12.10](#)) continued the routine calibration and monitoring observations performed in Cycles 17-21. Brief descriptions of these monitoring programs are presented in [Table 12.2](#).

The program also included enabling and calibration programs designed to facilitate the move to Lifetime Position 3 (LP3).

Table 12.10: Cycle 22 Calibration Program.

Program ID	Title	Accuracy Achieved	Products
13970	COS FUV Detector Gain Maps	NA	Gain maps of detector
13971	Characterization of HV change effect on sensitivity	NA	ISR

Table 12.11: Lifetime Position 3 Calibration Program.

I. Optimize New Lifetime Position	Program ID
Characterization of COS/FUV modal gain at lifetime position 3 {LOP1}	13617
Optimization of COS/FUV spectrum placement at lifetime position 3 {LOP2}	13618
II. Enable New Science at the New Lifetime Position	
Verification of Aperture and FUV Spectrum Placement for COS at LP3 {LENA1}	13634
FUV Focus Sweep Enabling Program for COS at LP3 (LENA2)	13635
Third COS FUV Lifetime Position: FUV Target Acquisition Parameter Update {LENA3}	13636
COS FUV Detector Response to New HV Management System at LP3 {LENA4}	13637
III. Calibrate the New Lifetime Position	
Third COS FUV Lifetime Position: Wavelength and Resolution Calibration (LCAL2)	13931
Third COS FUV Lifetime Position: Cross-Dispersion Profiles, Flux, and Flat-Field Calibration (LCAL3)	13932
Third COS FUV Lifetime Position: Verification of FUV BOA Operations (LCAL4)	13933

12.11 Cycle 23 Calibration Program

The Cycle 23 calibration plans for COS continued the routine calibration and monitoring programs performed in previous Cycles. Brief descriptions of the programs are listed in [Table 12.2](#). The full calibration plan for Cycle 23 is listed in [Table 12.12](#).

Table 12.12: Cycle 23 Calibration Programs.

Program Name	Program ID
NUV MAMA Fold Distribution	14444
NUV Detector Dark Monitor	14442
NUV Spectroscopic Sensitivity Monitor	14441
NUV Internal/External Wavelength Scale Monitor	14443
FUV Detector Dark Monitor	14436
FUV Spectroscopic Sensitivity Monitor	14435
FUV Internal/External Wavelength Scale Monitor	14437
COS FUV Detector Gain Maps	14439
COS Pure Parallel Observations of Geocoronal Ly alpha	14429
COS Target Acquisition Monitor	14440
Constraining the zero-points of the COS/NUV wavelength solution - G185M*	14503
Constraining the zero-points of the COS/NUV wavelength solution - G225M and G285M*	14504
STIS data of HD6655 to derive COS G285M/G230L wavelength zero-points*	14505

*non-routine program

12.12 Cycle 24 Calibration Program

The Cycle 24 calibration plans for COS continued the routine calibration and monitoring programs performed in previous Cycles. Brief descriptions of the programs are listed in [Table 12.2](#). The full calibration plan for Cycle 24 is listed in [Table 12.13](#).

The program also included enabling and calibration programs designed to facilitate the move to Lifetime Position 4 LP4); they are listed in [Table 12.14](#).

Table 12.13: Cycle 24 Calibration Programs.

Program Name	Program ID
COS NUV MAMA Fold Distribution	14526
NUV Detector Dark Monitor	14521
COS NUV Spectroscopic Sensitivity Monitor	14858
COS NUV Internal/External Wavelength Scale Monitor	14859
COS FUV Detector Dark Monitor	14520
COS FUV Spectroscopic Sensitivity Monitor	14854
COS FUV Internal/External Wavelength Scale Monitor	14855
COS FUV Detector Gain Maps	14519
COS Pure Parallel Observations of Geocoronal Ly alpha	14833
COS Target Acquisition Monitor	14857
COS/FUV Wavecal lamp template reference files at LP3*	14856
COS/FUV Wavelength Calibration at Lifetime Position 3*	14090

*non-routine program

Table 12.14: Lifetime Position 4 Calibration Program.

I. Optimize the New Lifetime Position	Program ID
Characterization of COS/FUV detector modal gain at Lifetime Position 4	14525
FUV Focus Sweep Exploratory Program for COS at LP4	14527
Optimization of COS/FUV spectrum placement at Lifetime Position 4	14841
Quick-check of the G130M Spectral Resolution at Lifetime Position 4 ¹	14842
COS/FUV Wavecorr at LP4	14869

II. Enable Science at the New Lifetime Position	
COS FUV Focus Sweep Program at LP4	14874
Verification of Aperture and FUV Spectrum Placement for COS at LP4	14875
COS LP4 FUV Target Acquisition Enabling and Verification	14907
COS/FUV LP4 Focus Sweep—New G130M/1223 Cenwave	14929
III. Calibrate the New Lifetime Position	
Fourth COS FUV Lifetime Position: Cross-Dispersion Profiles, Flux, and Flat-Field Calibration	14910
COS/FUV LP4: Spectral Resolution of G130M/1223	14935
COS FUV Dispersion Solutions at LP4	15365
COS FUV Spectral Resolution at LP4	15366
COS FUV Profile for 1223 cenwave at LP4	15367
COS FUV BOA performance at LP4	15368
COS FUV Lamp Templates at LP4	15369
COS FUV Gain Map at LP3/LP4	15370

¹ This and preceding programs are in Cycle 23; the rest are in Cycle 24.

12.13 Cycle 25 Calibration Program

The Cycle 25 calibration plans for COS continued the routine calibration and monitoring programs performed in previous Cycles. Brief descriptions of the programs are listed in [Table 12.2](#). The full calibration plan for Cycle 25 is listed in [Table 12.15](#). Programs were also included to calibrate cenwaves G140L/800 and G160M/1533; they are listed in [Table 12.16](#).

Table 12.15: Cycle 25 Calibration Programs.

Program Name	Program ID
COS NUV MAMA Fold Distribution	14943
COS NUV Detector Dark Monitor	14942
COS NUV Spectroscopic Sensitivity Monitor	15387
COS NUV Wavelength Scale Monitor	15388
COS NUV Target Acquisition Monitor	15389
COS FUV Detector Gain Maps	14941
COS FUV Detector Dark Monitor	14940
COS FUV Spectroscopic Sensitivity Monitor	15384
COS FUV Wavelength Scale Monitor	15385
COS FUV Target Acquisition Monitor	15386

Table 12.16: New Cenwave Calibration Programs.

I. Cenwave G140L/800	Program ID
COS FUV Focus Sweep for G140L/800 ¹	15451
COS FUV G140L/800 Flux Calibration and Cross-Dispersion Profile	15483
COS FUV G140L/800 Lamp Template	15484
II. Cenwave G160M/1533	
COS FUV Focus Sweep for G160M/1533	15452
COS/FUV/G160M/1533 Wavelength Calibration - Dispersion Solution	15457
COS/FUV/G160M/1533 Profiles and Fluxes	15458
FUV COS Lamp Templates for G160M/1533	15459

¹ This program was also used for the G140L/800 wavelength calibration.

12.14 Cycle 26 Calibration Program

The Cycle 26 calibration plans for COS continued the routine calibration and monitoring programs performed in previous Cycles. Brief descriptions of the programs are listed in [Table 12.2](#). The full calibration plan for Cycle 26 is listed in [Table 12.17](#).

Table 12.17: Cycle 26 Calibration Programs.

Program Name	Program ID
Cycle 26 NUV MAMA Fold Distribution	15539
Cycle 26 NUV Detector Dark Monitor	15538
Cycle 26 NUV Spectroscopic Sensitivity Monitor	15540
Cycle 26 NUV Wavelength Scale Monitor	15541
Cycle 26 NUV Target Acquisition Monitor	15542
Cycle 26 FUV Detector Gain Maps	15534
Cycle 26 FUV Detector Dark Monitor	15533
Cycle 26 FUV Spectroscopic Sensitivity Monitor	15535
Cycle 26 FUV Wavelength Scale Monitor	15536
Cycle 26 FUV Target Acquisition Monitor	15537
COS FUV Spectroscopic Sensitivity Monitor: One-Gyro Connection Program*	15680
COS Side 2 Initial NUV Checkout for Back-up Target in One-Gyro Mode*	15681
COS Side 2 Initial FUV Checkout for Back-up Target in One-Gyro Mode*	15682
COS/FUV Mapping of PtNe1 medium current to PtNe2 low current with G160M/1577 /4*	15983

*non-routine program

12.15 Cycle 27 Calibration Program

The Cycle 27 calibration plans for COS continued the routine calibration and monitoring programs performed in previous Cycles. Brief descriptions of the programs are listed in [Table 12.2](#). The full calibration plan for Cycle 27 is listed in [Table 12.18](#).

Table 12.18: Cycle 27 Calibration Programs.

Program Name	Program ID
Cycle 27 COS NUV MAMA Fold Distribution	15777
Cycle 27 COS NUV Detector Dark Monitor	15776
Cycle 27 COS NUV Spectroscopic Sensitivity Monitor	15778
Cycle 27 COS NUV Wavelength Scale Monitor	15779
Cycle 27 COS NUV Target Acquisition Monitor	15780
Cycle 27 COS FUV Detector Gain Maps	15772
Cycle 27 COS FUV Detector Dark Monitor	15771
Cycle 27 COS FUV Spectroscopic Sensitivity Monitor	15773
Cycle 27 COS FUV Wavelength Scale Monitor	15774
Cycle 27 COS FUV Target Acquisition Monitor	15775

12.16 Cycle 28 Calibration Program

The Cycle 28 calibration plans for COS continue the routine calibration and monitoring programs performed in previous Cycles. Brief descriptions of the programs are listed in [Table 12.2](#). The full calibration plan for Cycle 28 is listed in [Table 12.19](#). Two new contingency programs are introduced for this cycle and are included in the table below. The program COS FUV Change in Spectroscopic Sensitivity Trends is a supplement to the COS FUV Spectroscopic Sensitivity Monitor and is activated when the time-dependent sensitivity appears to be changing on short timescales. The COS FUV Characterization of Modal Gain When Changing High Voltage program is activated when the high voltage of the FUV detector is changed. In previous cycles, these contingency orbits were included in the COS FUV Spectroscopic Sensitivity Monitor and COS FUV Detector Gain Maps programs, respectively.

The program also included exploratory, enabling, and calibration programs designed to facilitate the move to Lifetime Position 5 (LP5); they are listed in [Table 12.20](#). In addition, this program also included exploratory programs designed to facilitate the move to Lifetime Position 6 (LP6); they are listed in [Table 12.21](#).

Table 12.19: Cycle 28 Calibration Programs.

Program Name	Program ID
Cycle 28 COS NUV MAMA Fold Distribution	16328
Cycle 28 COS NUV Detector Dark Monitor	16237
Cycle 28 COS NUV Spectroscopic Sensitivity Monitor	16329
Cycle 28 COS NUV Wavelength Scale Monitor	16330
Cycle 28 COS NUV Target Acquisition Monitor	16331
Cycle 28 COS FUV Detector Gain Maps	16323
Cycle 28 COS FUV Detector Dark Monitor	16322
Cycle 28 COS FUV Spectroscopic Sensitivity Monitor	16324
Cycle 28 COS FUV Wavelength Scale Monitor	16325
Cycle 28 COS FUV Target Acquisition Monitor	16326
Cycle 28 COS FUV Change in Spectroscopic Sensitivity Trends*	16332
Cycle 28 COS FUV Characterization of Modal Gain When Changing High Voltage*	16333

* contingency program

Table 12.20: Lifetime Position 5 Calibration Program.

I. Optimize the New Lifetime Position	Program ID
COS/FUV Mapping of FCA Light Leak Between +5" and +6" ^	15689
Testing for Systematics When Moving the COS Aperture Block*	16052
Initial Test of COS/FUV Spectrum Placement at Lifetime Position 5*	16106
II. Enable Science at the New Lifetime Position	
Verification of Target Placement for COS at LP5	16430
Focus Sweep Program for COS FUV Observations at LP5 and LP3	16431
COS LP5 FUV Target Acquisition Enabling and Verification	16432
III. Calibrate the New Lifetime Position	
COS FUV LP5 Calibration: Profiles, Traces, Sensitivities, Flat Fields and Spatial Resolution	16466
COS FUV LP5 Calibration: Spectral Resolution	16467
COS FUV LP5 Calibration: Dispersion Solutions	16468
COS FUV LP5 Calibration: Lamp Templates	16469
COS FUV LP5 Calibration: Bright Object Aperture Performance	16470
COS FUV LP5 Calibration: Gain Maps	16471

^program executed in Cycle 26

*program executed in Cycle 27

Table 12.21: Lifetime Position 6 Exploratory Program.

Program Name	Program ID
COS/FUV Gain Map and Aperture Placement at LP6	16472
FUV Focus Sweep Exploratory Program for COS at LP6	16491
FUV Exploratory Spectral Resolution Program at LP6	16495

i *If your program requires calibrations beyond those described here, then you should explicitly include this calibration in your Phase I proposal.*

12.17 Cycle 29 Calibration Program

The Cycle 29 calibration plans for COS continue the routine calibration and monitoring programs performed in previous Cycles. Brief descriptions of the programs are listed in [Table 12.2](#). The full calibration plan for Cycle 29 is listed in [Table 12.22](#). Two contingency programs introduced in Cycle 28 are included in this cycle as well. The program COS FUV Change in Spectroscopic Sensitivity Trends is a supplement to the COS FUV Spectroscopic Sensitivity Monitor and is activated when the time-dependent sensitivity appears to be changing on short timescales. The COS FUV Characterization of Modal Gain When Changing High Voltage program is activated when the high voltage of the FUV detector is changed.

The program also included enabling and calibration programs designed to facilitate the move to Lifetime Position 6 (LP6); they are listed in [Table 12.23](#).

Table 12.22: Cycle 29 Calibration Programs.

Program Name	Program ID	
Cycle 29 COS NUV MAMA Fold Distribution	16536	
Cycle 29 COS NUV Detector Dark Monitor	16535	
Cycle 29 COS NUV Spectroscopic Sensitivity Monitor	16537	
Cycle 29 COS NUV Wavelength Scale Monitor	16538	
Cycle 29 COS NUV Target Acquisition Monitor	16539	
Cycle 29 COS FUV Detector Gain Maps	16829	
Cycle 29 COS FUV Detector Dark Monitor	16828	
Cycle 29 COS FUV Spectroscopic Sensitivity Monitor	16830	
Cycle 29 COS FUV Wavelength Scale Monitor	16534	
Cycle 29 COS FUV Target Acquisition Monitor	16831	
Cycle 29 COS FUV Change in Spectroscopic Sensitivity Trends *	16832	
Cycle 29 COS FUV Characterization of Modal Gain When Changing High Voltage *	16833	

* contingency program

Table 12.23: Lifetime Position 6 Calibration Program.

I. Enable Science at the New Lifetime Position	Program ID

Verification of Target Placement for COS at LP6	16849
FUV Focus Sweep Enabling Program at LP6	16850
Verification and Update of TA Parameters at LP6	16851
II. Calibrate the New Lifetime Position	
COS FUV LP6 Calibration: Profiles, Traces, Sensitivities, Flat Fields, and Spatial Resolution	16906
Mapping the COS LP6 Spectral Resolution	16907
COS FUV LP6 Calibration: Dispersion Solutions	16908
COS FUV LP6 Calibration: Lamp Templates	16909
LP6 Gain Map Program	16910

i *If your program requires calibrations beyond those described here, then you should explicitly include this calibration in your Phase I proposal.*

12.18 Cycle 30 Calibration Program

The Cycle 30 calibration plans for COS continue the routine calibration and monitoring programs performed in previous Cycles. Brief descriptions of the programs are listed in [Table 12.2](#). The full calibration plan for Cycle 30 is listed in [Table 12.24](#). Two contingency programs introduced in Cycle 28 are included in this cycle as well. The program COS FUV Change in Spectroscopic Sensitivity Trends is a supplement to the COS FUV Spectroscopic Sensitivity Monitor and is activated when the time-dependent sensitivity appears to be changing on short timescales. The COS FUV Characterization of Modal Gain When Changing High Voltage program is activated when the high voltage of the FUV detector is changed.

Table 12.24: Cycle 30 Calibration Programs.

Program Name	Program ID	
Cycle 30 COS NUV MAMA Fold Distribution	16936	
Cycle 30 COS NUV Detector Dark Monitor	16935	
Cycle 30 COS NUV Spectroscopic Sensitivity Monitor	16937	
Cycle 30 COS NUV Wavelength Scale Monitor	16938	
Cycle 30 COS NUV Target Acquisition Monitor	16939	
Cycle 30 COS FUV Detector Gain Maps	17248	
Cycle 30 COS FUV Detector Dark Monitor	17247	
Cycle 30 COS FUV Spectroscopic Sensitivity Monitor	17249	
Cycle 30 COS FUV Wavelength Scale Monitor	17250	
Cycle 30 COS FUV Target Acquisition Monitor	16942	
Cycle 30 COS FUV Change in Spectroscopic Sensitivity Trends*	17251	
Cycle 30 COS FUV Characterization of Modal Gain When Changing High Voltage*	17252	

*contingency program

i *If your program requires calibrations beyond those described here, then you should explicitly include this calibration in your Phase I proposal.*

12.19 Cycle 31 Calibration Program

The Cycle 31 calibration plans for COS continue the routine calibration and monitoring programs performed in previous Cycles. Brief descriptions of the programs are listed in [Table 12.2](#). The full calibration plan for Cycle 31 is listed in [Table 12.25](#). Two contingency programs introduced in Cycle 17 are included in this cycle; both FUV and NUV [Detector Recovery After Anomalous Shutdown](#). Two contingency programs introduced in Cycle 28 are included in this cycle as well. The program COS FUV Change in Spectroscopic Sensitivity Trends is a supplement to the COS FUV Spectroscopic Sensitivity Monitor and is activated when the time-dependent sensitivity appears to be changing on short timescales. The COS FUV Characterization of Modal Gain When Changing High Voltage program is activated when the high voltage of the FUV detector is changed.

Table 12.25: Cycle 31 Calibration Programs.

Program Name	Program ID	
Cycle 31 COS NUV MAMA Fold Distribution	17318	
Cycle 31 COS NUV Detector Dark Monitor	17317	
Cycle 31 COS NUV Spectroscopic Sensitivity Monitor	17319	
Cycle 31 COS NUV Wavelength Scale Monitor	17320	
Cycle 31 COS NUV Target Acquisition Monitor	17321	
Cycle 31 COS FUV Detector Gain Maps	17325	
Cycle 31 COS FUV Detector Dark Monitor	17324	
Cycle 31 COS FUV Spectroscopic Sensitivity Monitor	17326	
Cycle 31 COS FUV Wavelength Scale Monitor	17327	
Cycle 31 COS FUV Target Acquisition Monitor	17582	
Cycle 31 COS FUV Detector Recovery After Anomalous Shutdown*	17322	
Cycle 31 COS NUV Detector Recovery After Anomalous Shutdown*	17323	
Cycle 31 COS FUV Change in Spectroscopic Sensitivity Trends*	17328	
Cycle 31 COS FUV Characterization of Modal Gain When Changing High Voltage *	17329	

* contingency program

i *If your program requires calibrations beyond those described here, then you should explicitly include this calibration in your Phase I proposal.*

Chapter 13: COS Reference Material

Chapter Contents

- 13.1 Introduction
- 13.2 Using the Information in this Chapter
- 13.3 Gratings
 - FUV Grating G130M
 - FUV Grating G130M with CENWAVE=1222
 - FUV Grating G130M with CENWAVE=1055 or 1096
 - FUV Grating G160M
 - FUV Grating G140L
 - NUV Grating G185M
 - NUV Grating G225M
 - NUV Grating G285M
 - NUV Grating G230L
- 13.4 Spectrograph Design Parameters
- 13.5 The Location of COS in the HST Focal Plane
- 13.6 The COS User Coordinate System

13.1 Introduction

The information in this chapter will help you to select a detector, grating configuration, and observing aperture, and to develop your observing plan. For each grating, the following information is provided:

- A brief description of the grating, with special considerations for its use.
- Grating parameters, including the dispersion and plate scale.
- Plots showing the available central-wavelength settings and the range of wavelengths covered by each setting and (for the FUV gratings) $FP-POS$ position.
- Plots and tables of sensitivities and effective areas as a function of wavelength.
- Plots of signal-to-noise ratio as a function of $STMAG$, F_{λ} , and exposure time.

Note that the quoted sensitivities are estimates for mid-Cycle 23 (April 2016). The [COS Exposure Time Calculator](#) (ETC) will be updated as the instrument's sensitivity continues to evolve. See the [COS website](#) for the latest information.

13.2 Using the Information in this Chapter

- [13.2.1 Grating Parameters](#)
- [13.2.2 Wavelength Ranges](#)
- [13.2.3 Grating Sensitivities and Effective Areas](#)
- [13.2.4 Signal-to-Noise Plots](#)

13.2.1 Grating Parameters

For each grating, the resolving power and dispersion are taken from [Table 5.1](#). Plate scales are derived from data obtained during SMOV.

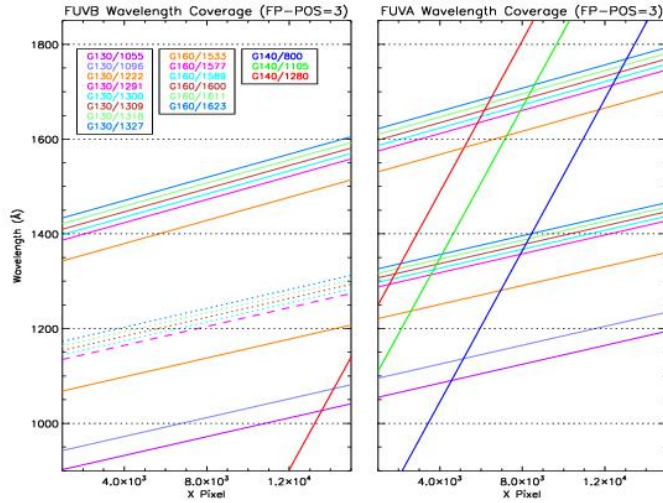
13.2.2 Wavelength Ranges

For each grating, we plot the wavelengths sampled by each central-wavelength setting. For the NUV gratings, the central wavelength is the approximate midpoint of Stripe B. For the FUV gratings, the central wavelength is (approximately) the shortest wavelength recorded on Segment A. Wavelength ranges for each central wavelength at $FP-POS=3$ are provided in tabular format in [Table 5.3](#) and [Table 5.4](#).

For the FUV gratings, the wavelength ranges sampled at each $FP-POS$ position are plotted separately. For the NUV gratings, the total wavelength range sampled by all $FP-POS$ positions is plotted for each central-wavelength setting.

[Figure 13.1](#) shows how some wavelengths are covered by multiple modes, but on different parts of the FUV detectors. At LP4 and LP5, the FUVB cenwaves shown with dotted lines are unavailable, while the one shown with a dashed line (1291) is available only at $FP-POS=3$ and 4.

Figure 13.1: Wavelength Coverage of the COS FUV Gratings.



13.2.3 Grating Sensitivities and Effective Areas

This section presents sensitivities and effective areas as a function of wavelength for each grating. The target is assumed to be a point source centered in the PSA. For both the FUV and NUV detectors,

the total systemic¹ *spectroscopic point-source sensitivity*, S_{λ}^p , has units of counts $\text{pix}_{\lambda}^{-1} \text{s}^{-1}$ per incident $\text{erg cm}^{-2} \text{s}^{-1} \text{\AA}^{-1}$, where:

- pix_{λ} = a pixel in the dispersion direction, and
- counts refer to the total counts from a point source integrated over the PSF in the direction perpendicular to the dispersion.

The count rate per pixel is simply the product of the target flux and the point-source sensitivity at a given wavelength. To estimate the signal-to-noise ratio (S/N) achieved at a given count rate and exposure time, follow the directions in [Section 7.3](#) or use the S/N plots in this chapter.

The effective area has units of cm^2 .

13.2.4 Signal-to-Noise Plots

For each grating, a plot is provided to help you estimate the S/N that can be achieved from a point source observed at a fiducial wavelength near the peak of the effective-area curve. The fiducial wavelength is indicated in the ordinate label of each plot. To estimate the S/N at other wavelengths, scale your source flux or magnitude by the relative sensitivities at the wavelength of interest and at the fiducial. The plots show S/N as a function of F_λ and of STMAG for a range of exposure times. $STMAG_\lambda$ is the color-dependent correction from V magnitude to STMAG at wavelength λ . Values of $STMAG_\lambda$ for various stellar and extragalactic sources are presented in [Table 13.1](#) and [Table 13.2](#), respectively. In producing these plots, we assumed an average sky background (as described in [Chapter 7](#)) and the dark current appropriate for each detector. These plots should be used only for rough estimates of exposure times. When constructing your proposal, use the [COS ETC](#) to estimate S/N values.

Note the following:

- The point source S/N has been calculated per resolution element and has been integrated over the PSF to contain all of the flux in the cross-dispersion direction.
- The symbols in the S/N figures delineate regions of parameter space where the dark current contributes more than half the source counts.
- The vertical shaded area indicates the bright-object screening limit given in [Table 10.1](#).

Follow these steps to use the S/N plots.

1. Look up, in [Table 13.1](#), the effective temperature and wavelength region of interest (e.g., 5000 K at 2000 Å). Interpolate in the table to get $STMAG_\lambda$.
2. Add the V magnitude of the target to get STMAG.
3. Find the appropriate plot for the desired grating and locate STMAG on the horizontal axis. Read off the S/N for the desired exposure time, or vice-versa. Alternatively, use F_λ directly on the horizontal axis.
4. To get accurate values for repeated, or $FP-POS$, exposures use the sub-exposure time when

consulting the plot, and then multiply the resulting S/N by \sqrt{N} , where N is the number of sub-exposures to be averaged.

For example, consider a $V = 15$ mag star of spectral type B0V, for which we want to derive the S/N achieved in a 100 s exposure using the NUV grating G230L. The S/N calculations for G230L are presented in [Figure 13.28](#), where we learn that the fiducial wavelength for this grating is 3001 Å. Assuming an effective temperature of 30,000 K, we obtain $STMAG_\lambda \sim -2.1$ at 3000 Å from [Table 13.1](#), making $STMAG = 12.9$. Returning to [Figure 13.28](#), we find this value on the horizontal axis. For an exposure time of 100 s, we find $S/N \sim 9.5$.

Table 13.1: $STMAG_\lambda$ as a Function of Wavelength for Stellar Objects.

Temp (K)	Wavelength (Å)
----------	----------------

	1000	1200	1500	2000	2500	3000	3500	4000	4500	5000
45000	-5.87	-5.46	-4.79	-3.87	-3.02	-2.36	-1.76	-1.27	-0.79	-0.37
30000	-5.38	-4.92	-4.37	-3.50	-2.70	-2.13	-1.56	-1.23	-0.76	-0.35
20000	-3.90	-3.38	-3.45	-2.73	-2.14	-1.66	-1.18	-1.13	-0.72	-0.33
15000	-1.68	-1.24	-2.68	-2.08	-1.53	-1.21	-0.83	-1.05	-0.68	-0.31
10000	9.18	6.27	-0.72	-0.68	-0.26	-0.21	-0.03	-0.88	-0.62	-0.29
9000	12.84	8.67	1.81	-0.19	0.15	0.05	0.16	-0.75	-0.58	-0.26
8000	17.10	11.79	6.33	0.51	0.58	0.21	0.24	-0.56	-0.46	-0.20
7000	20.97	15.07	9.29	1.86	1.26	0.36	0.24	-0.34	-0.32	-0.12
6000	N/A	19.44	14.17	5.50	2.92	0.94	0.47	0.02	-0.15	-0.04
5000	N/A	N/A	20.15	9.80	6.24	2.74	1.24	0.50	0.04	0.10
4000	N/A	N/A	N/A	14.74	9.70	5.53	2.37	0.97	0.24	0.58
3000	N/A	N/A	N/A	17.85	11.46	5.69	2.22	0.71	0.25	0.82

Table 13.2: $STMAG_{\lambda}$ as a Function of Wavelength for Non-Stellar Objects.

Spectrum	Wavelength (\AA)							
	1500	2000	2500	3000	3500	4000	4500	5000
Elliptical	3.35	3.19	4.17	2.92	1.60	0.70	0.17	0.15
S0	4.63	3.95	3.27	2.23	1.61	0.71	0.18	0.13
Sa	2.64	2.27	2.39	1.78	1.31	0.36	0.12	0.07
Sb	1.70	2.59	2.04	1.32	1.12	0.43	0.17	0.10
Sc	-0.18	0.44	-0.17	-0.68	-0.67	-0.51	-0.44	-1.25
Starburst, $E(B-V) < 0.1$	-1.71	-1.15	-0.68	-0.43	-0.13	-0.42	-0.23	-1.24
Starburst, $0.25 < E(B-V) < 0.35$	-0.95	-0.87	-0.33	-0.10	0.08	-0.19	-0.19	-0.28
Starburst, $0.51 < E(B-V) < 0.60$	-0.40	-0.18	0.01	0.23	0.03	-0.14	-0.12	-0.36
Starburst, $0.61 < E(B-V) < 0.70$	0.05	0.31	0.31	0.15	0.27	-0.17	-0.13	-0.11

The $STMAG_{\lambda}$ values of Table 13.1 are derived from the stellar models of Castelli and Kurucz (2003, 2004), assuming solar metallicity ($[Fe/H] = 0.0$) and a surface gravity of $\log(g) = 4.5$. The $STMAG_{\lambda}$ values of Table 13.2 are based on observed spectra of each object type.

¹ COS plus HST Optical Telescope Assembly (OTA).

13.3 Gratings

For each COS grating, we present the resolving power, dispersion, plate scale, the wavelength range covered at each central wavelength setting and `FP-POS` position, sensitivities, effective areas, and a tool for estimating S/N . Advice on use is provided where appropriate.

Note that the quoted sensitivities are estimates for mid-Cycle 23 (April 2016). The [COS ETC](#) will be updated as the instrumental sensitivity evolves. Users should be aware that the BOA is not well calibrated below 1200 Å, and is an Available-but-Unsupported mode (See [Section 5.13](#)).

Wavelengths in this handbook, and in COS data products, are always measured in vacuum.

Gratings:

- [FUV Grating G130M](#)
- [FUV Grating G130M with CENWAVE=1222](#)
- [FUV Grating G130M with CENWAVE=1055 or 1096](#)
- [FUV Grating G160M](#)
- [FUV Grating G140L](#)
- [NUV Grating G185M](#)
- [NUV Grating G225M](#)
- [NUV Grating G285M](#)
- [NUV Grating G230L](#)

FUV Grating G130M

Description

The G130M grating samples wavelengths between about 900 and 1450 Å. (Its use at shorter wavelengths is discussed below.) It offers higher resolution and effective area than the G140L grating, but less spectral coverage. Note that the [COS 2025 policy](#) limits the use of Segment B for this grating at LP4 and LP5; the settings shown with a dashed line in [Figure 13.2](#) are not available.

If observing with the G130M grating for values of central wavelength (CENWAVE) equal to [1222](#), [1055](#), or [1096](#), please consult the linked pages for special consideration of these settings.

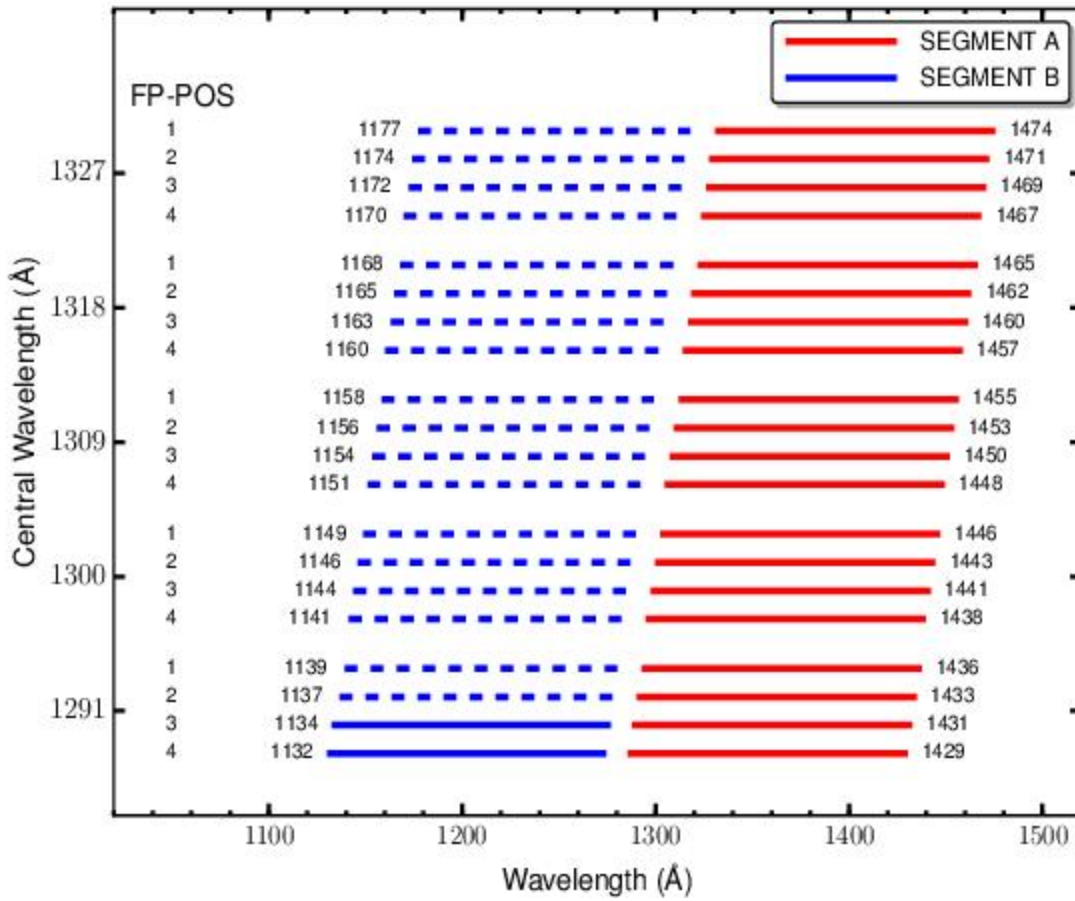
Special Considerations

The gap between Segments A and B spans 14.3 Å. To fill this gap requires exposures separated by two central-wavelength settings.

Grating	Resolving Power R $= \lambda/\Delta\lambda$	Dispersion (mÅ pixel ⁻¹)	Plate Scale (milliarcsec pixel ⁻¹)		FP-POS Step (Å step ⁻¹)
			Disp. Axis	Cross-Disp. Axis	
G130M	12,000–16,000 ¹	9.97	22.9	100	2.5

¹ See below for the 1055, 1096, and 1222 settings, which have $R < 13,000$.

Figure 13.2: Wavelength Ranges for the G130M Grating.



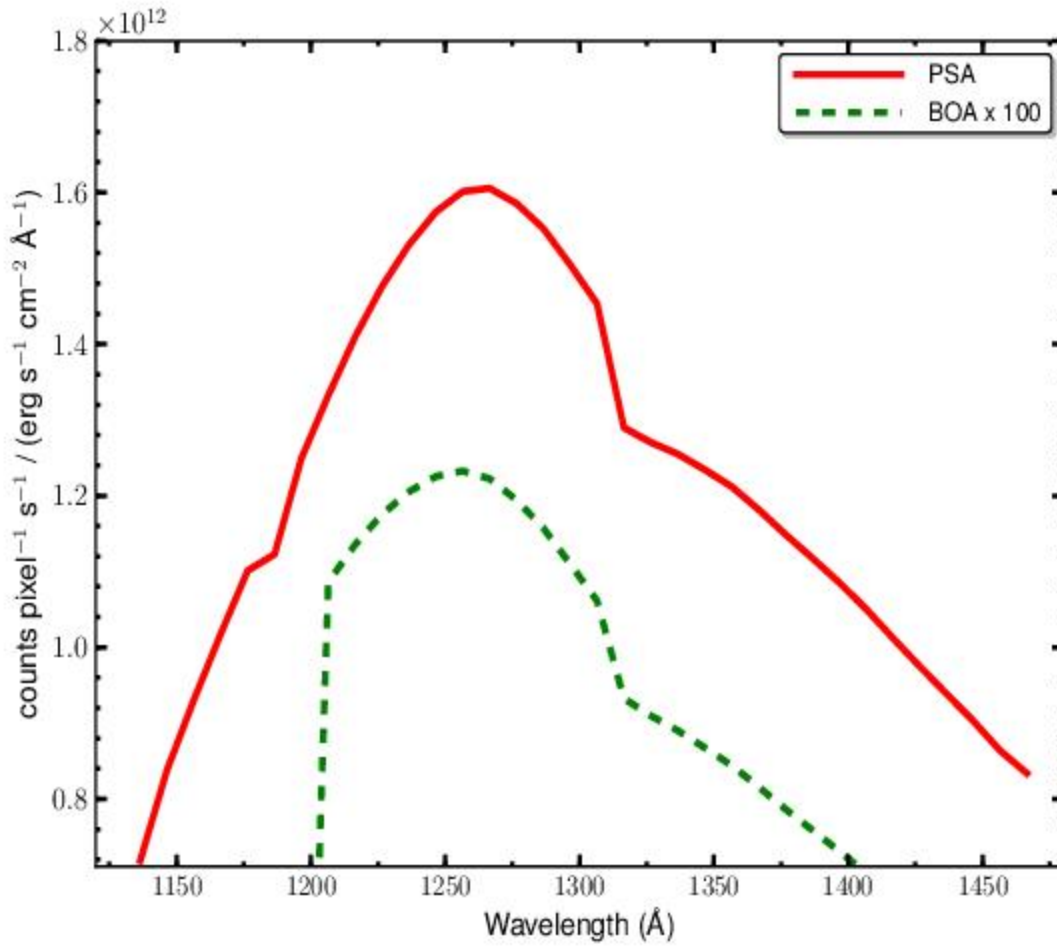
G130M Point-Source Sensitivity

Table 13.3: G130M Point-Source Sensitivity for PSA.

Wavelength (Å)	Throughput	Sensitivity (counts pixel ⁻¹ sec ⁻¹ per erg cm ⁻² sec ⁻¹ Å ⁻¹)	Effective Area (cm ²)
1136	2.757e-02	7.1e+11	1.25e+03
1150	3.336e-02	8.7e+11	1.51e+03
1200	4.695e-02	1.3e+12	2.12e+03
1250	5.588e-02	1.6e+12	2.53e+03
1300	5.041e-02	1.5e+12	2.28e+03
1350	4.008e-02	1.2e+12	1.81e+03
1400	3.382e-02	1.1e+12	1.53e+03

1450	2.702e-02	8.9e+11	1.22e+03
1469	2.477e-02	8.3e+11	1.12e+03

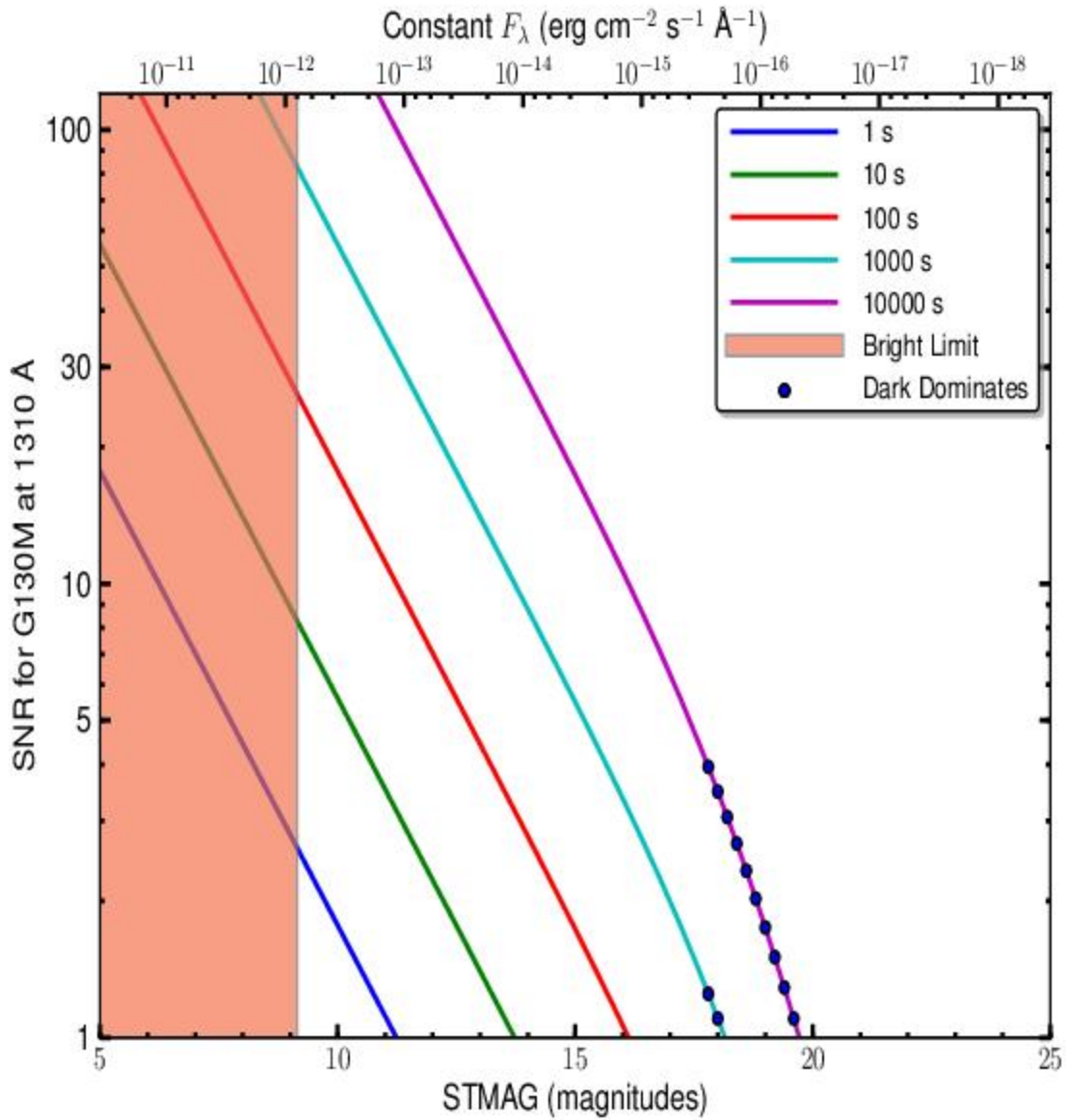
Figure 13.3: G130M Point-Source Sensitivity for PSA and BOA.



The throughput of the BOA is poorly characterized below 1200 Å and close to zero below 1150 Å.

G130M Signal-to-Noise Ratio

Figure 13.4: Point-Source Signal-to-Noise as a Function of STMAG for G130M at 1310 Å.



The top axis displays constant F_λ values corresponding to the STMAG units ($V+STMAG_\lambda$) on the bottom axis. Recall that $STMAG = 0$ is equivalent to $F_\lambda = 3.63E-9$ erg cm⁻² s⁻¹ Å⁻¹. Colors refer to exposure times in seconds. The edge of the shaded area corresponds to the bright-object screening limit. Use of the PSA is assumed.

FUV Grating G130M with CENWAVE=1222

Description

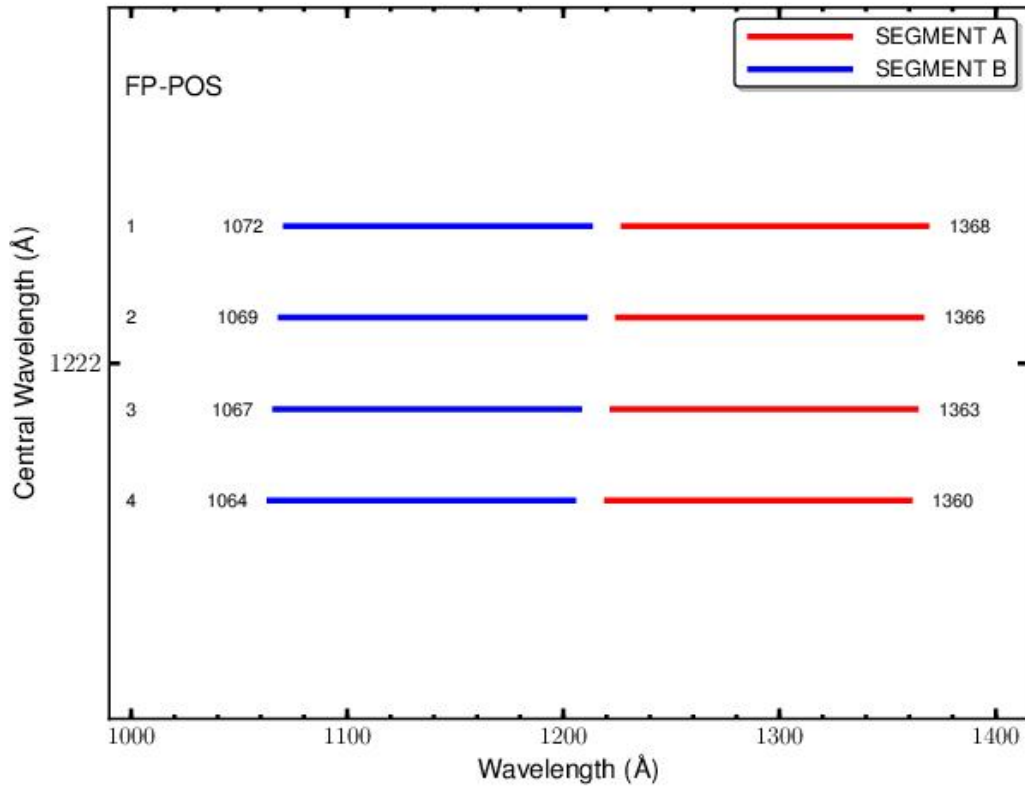
When used with a central wavelength of 1222 Å, grating G130M samples wavelengths between about 1065 and 1365 Å with a resolving power $R > 10,000$. Its sensitivity is comparable to that of other G130M modes and considerably higher than G140L. The resolving power of this mode is $R > 10,000$ at 1135 Å and $R > 12,000$ at 1340 Å.

Special Considerations

A key advantage of this observing mode is that it places the Lyman- α airglow line in the gap between detector Segments A and B, eliminating this source of damaging high-intensity flux.

Grating	Resolving Power R $= \lambda/\Delta\lambda$	Dispersion (mÅ pixel ⁻¹)	Plate Scale (milliarcsec pixel ⁻¹)		FP-POS Step (Å step ⁻¹)
			Disp. Axis	Cross-Disp. Axis	
G130M	10,000-15,000	9.97	22.9	100	2.5

Figure 13.5: Wavelength Ranges for the G130M/1222 Mode.



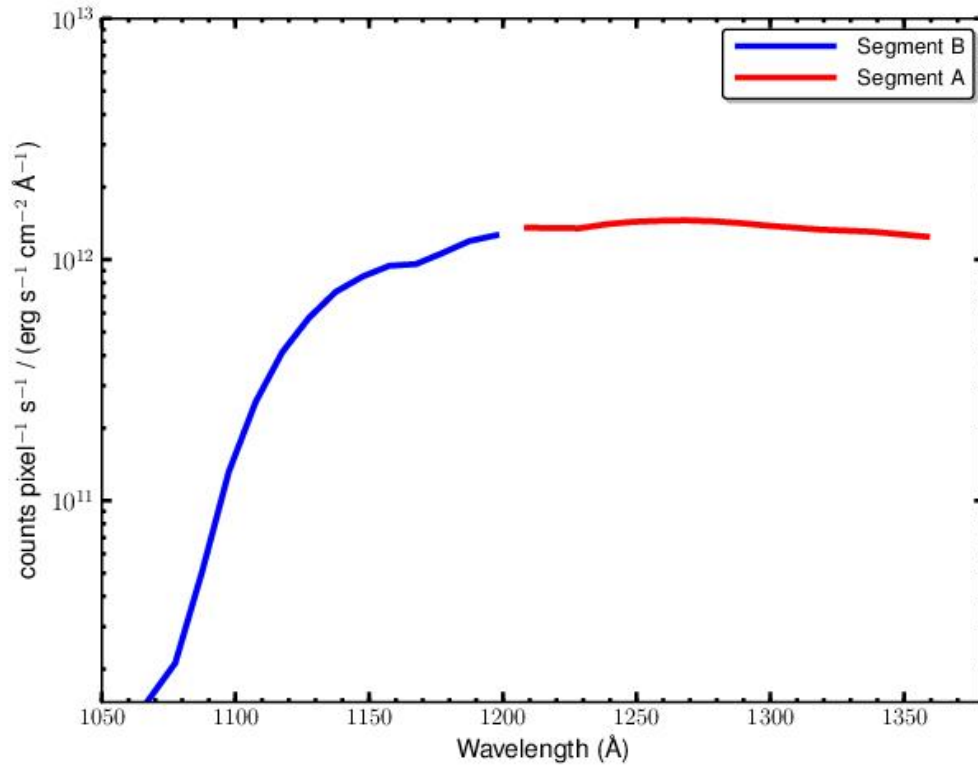
G130M/1222 Point-Source Sensitivity

Table 13.4: G130M/1222 Point-Source Sensitivity for PSA.

Wavelength (Å)	Throughput	Sensitivity (counts pixel ⁻¹ sec ⁻¹ per erg cm ⁻² sec ⁻¹ Å ⁻¹)	Effective Area (cm ²)
1066	6.028e-04	1.5e+10	2.73e+01
1100	6.219e-04	1.6e+11	2.81e+02
1150	3.337e-02	8.7e+11	1.51e+03
1200	4.698e-02	1.3e+12	2.13e+03
1250	5.059e-02	1.4e+12	2.29e+03
1300	4.672e-02	1.4e+12	2.11e+03
1350	4.137e-02	1.3e+12	1.87e+03

1363	3.979e-02	1.2e+12	1.80e+03
------	-----------	---------	----------

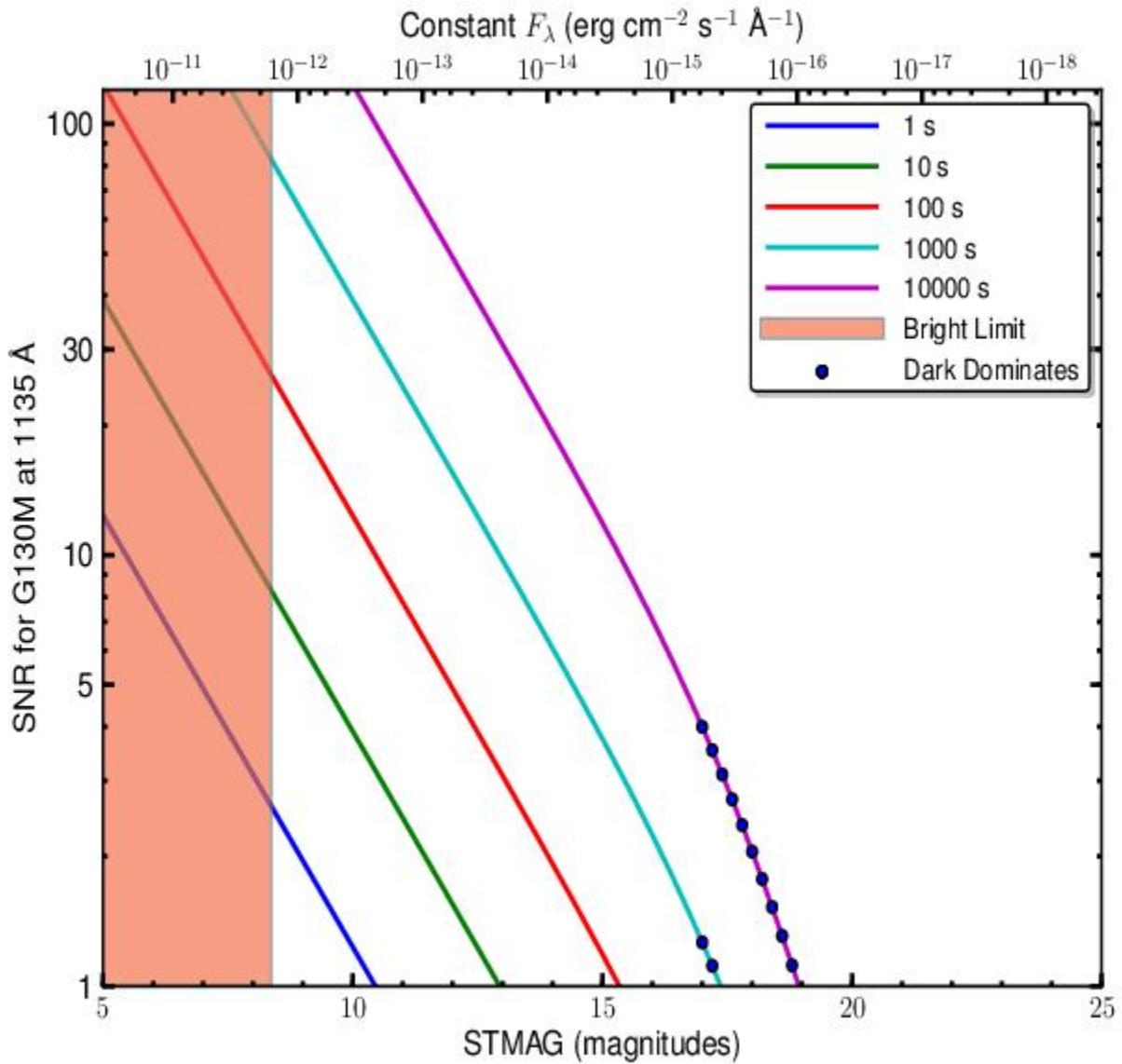
Figure 13.6: G130M/1222 Point-Source Sensitivity for PSA.



The sensitivity through the BOA is not shown, as its MgF₂ filter is very low at wavelengths $\lambda < 1150$ Å.

G130M Signal-to-Noise Ratio

Figure 13.7: Point-Source Signal-to-Noise as a Function of STMAG for G130M at 1135 Å.



The top axis displays constant F_λ values corresponding to the STMAG units ($V+STMAG_\lambda$) on the bottom axis. Recall that $STMAG = 0$ is equivalent to $F_\lambda = 3.63E-9$ erg cm⁻² s⁻¹ Å⁻¹. Colors refer to exposure times in seconds. The edge of the shaded area corresponds to the bright-object screening limit. Use of the PSA is assumed.

FUV Grating G130M with CENWAVE=1055 or 1096

Description

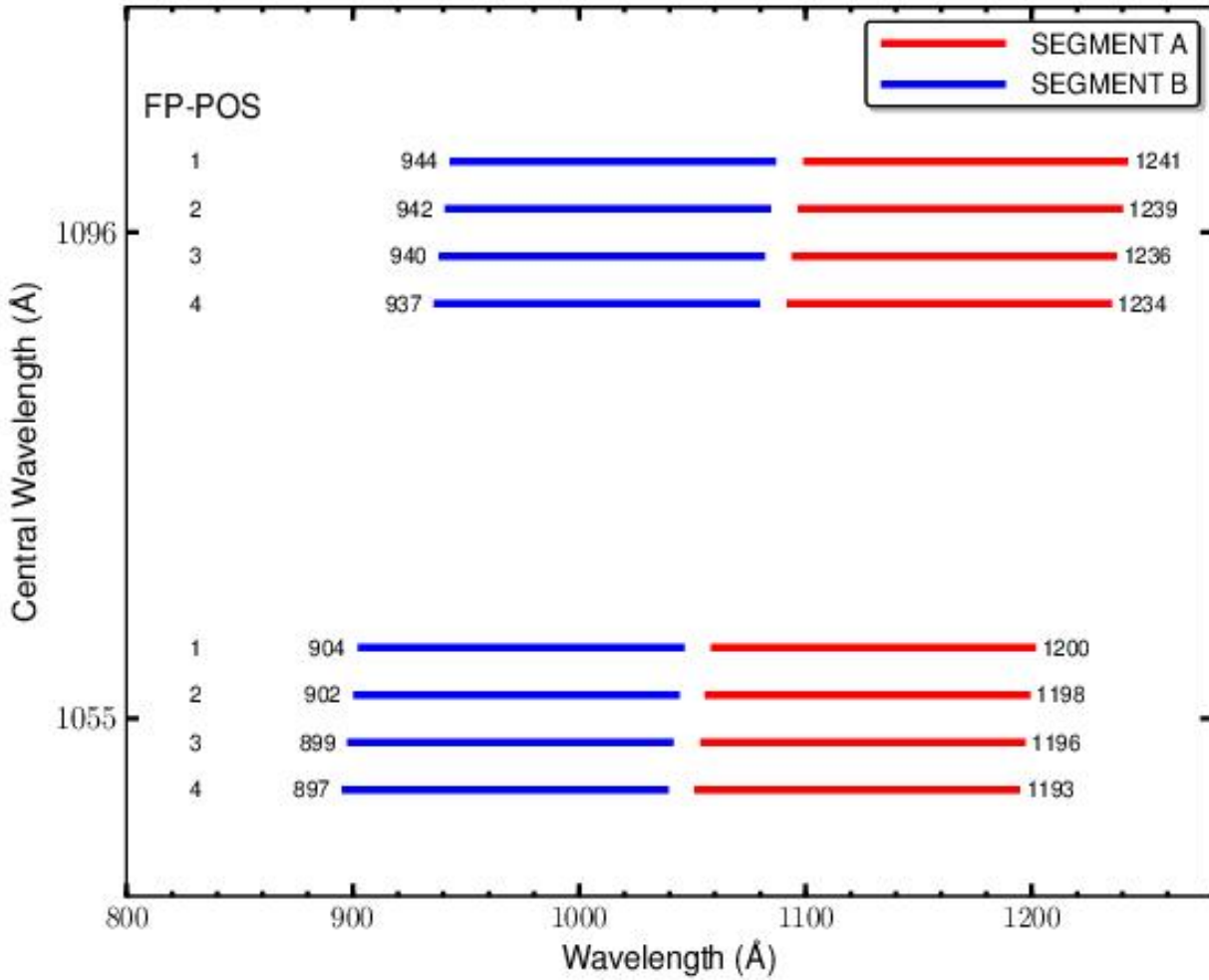
When used with a central wavelength of 1055 or 1096 Å, grating G130M samples wavelengths between about 900 and 1200 Å. Its resolution and effective area are higher than those of the G140L grating, but lower than those of G130M when used at longer central wavelengths.

Special Considerations

The COS sensitivity rises steeply between 1070 and 1150 Å. To observe bright targets near the Lyman limit, turn off detector Segment A and use only Segment B.

Grating	Resolving Power $R = \lambda/\Delta\lambda$	Dispersion (mÅ pixel ⁻¹)	Plate Scale (milliarcsec pixel ⁻¹)		FP-POS Step (Å step ⁻¹)
			Disp. Axis	Cross-Disp. Axis	
G130M Segment A	3,000–8,000	9.97	22.9	100	2.5
G130M Segment B	5,000–12,000	9.97	22.9	100	2.5

Figure 13.8: Wavelength Ranges for the G130M/1055 and 1096 Modes.



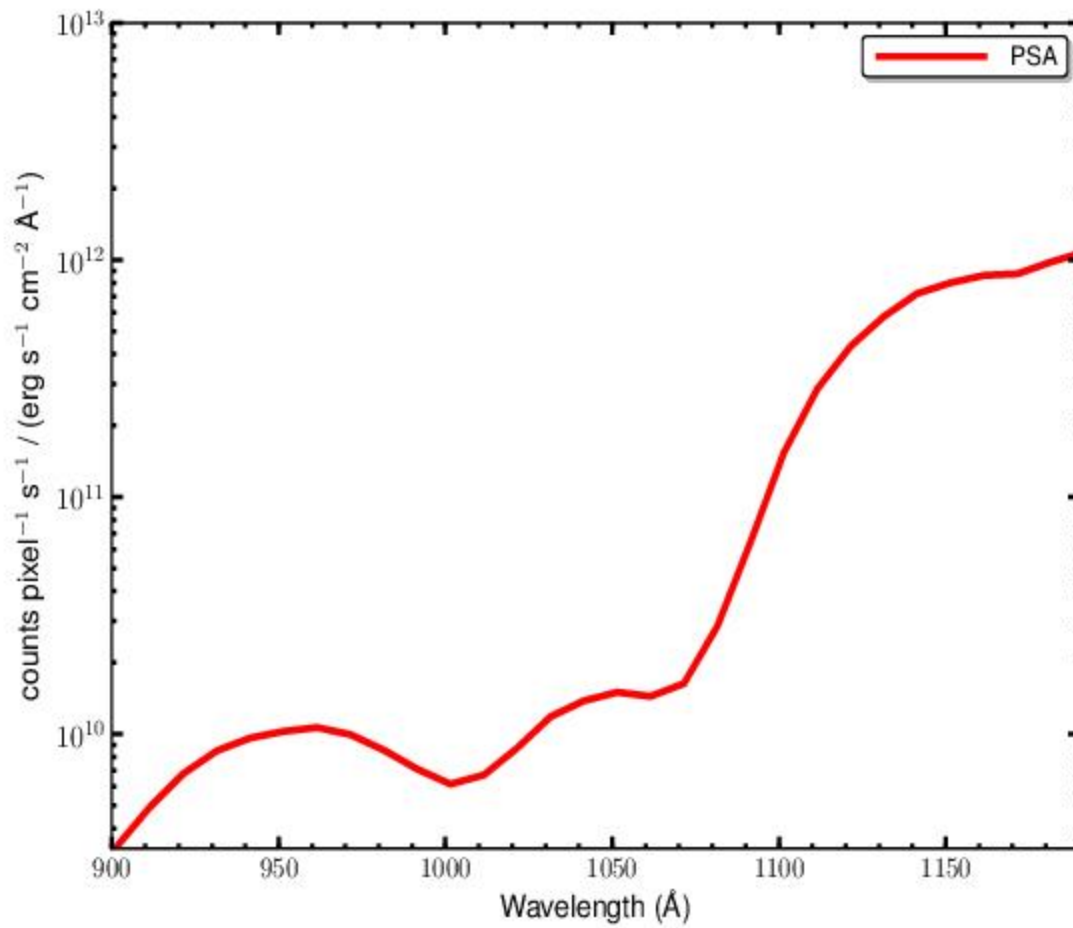
G130M/1055 and 1096 Point-Source Sensitivity

Table 13.5: G130M/1055 and 1096 Point-Source Sensitivity for PSA.

Wavelength (Å)	Throughput	Sensitivity (counts pixel ⁻¹ sec ⁻¹ per erg cm ⁻² sec ⁻¹ Å ⁻¹)	Effective Area (cm ²)
901	1.611e-04	3.3e+09	7.29e+00
950	4.736e-04	1.0e+10	2.14e+01
1000	2.709e-04	6.1e+09	1.23e+01
1050	6.355e-04	1.5e+10	2.87e+01
1100	5.538e-03	1.4e+11	2.51e+02

1150	3.076e-02	8.0e+11	1.39e+03
1200	4.216e-02	1.1e+12	1.91e+03
1237	4.389e-02	1.2e+12	1.99e+03

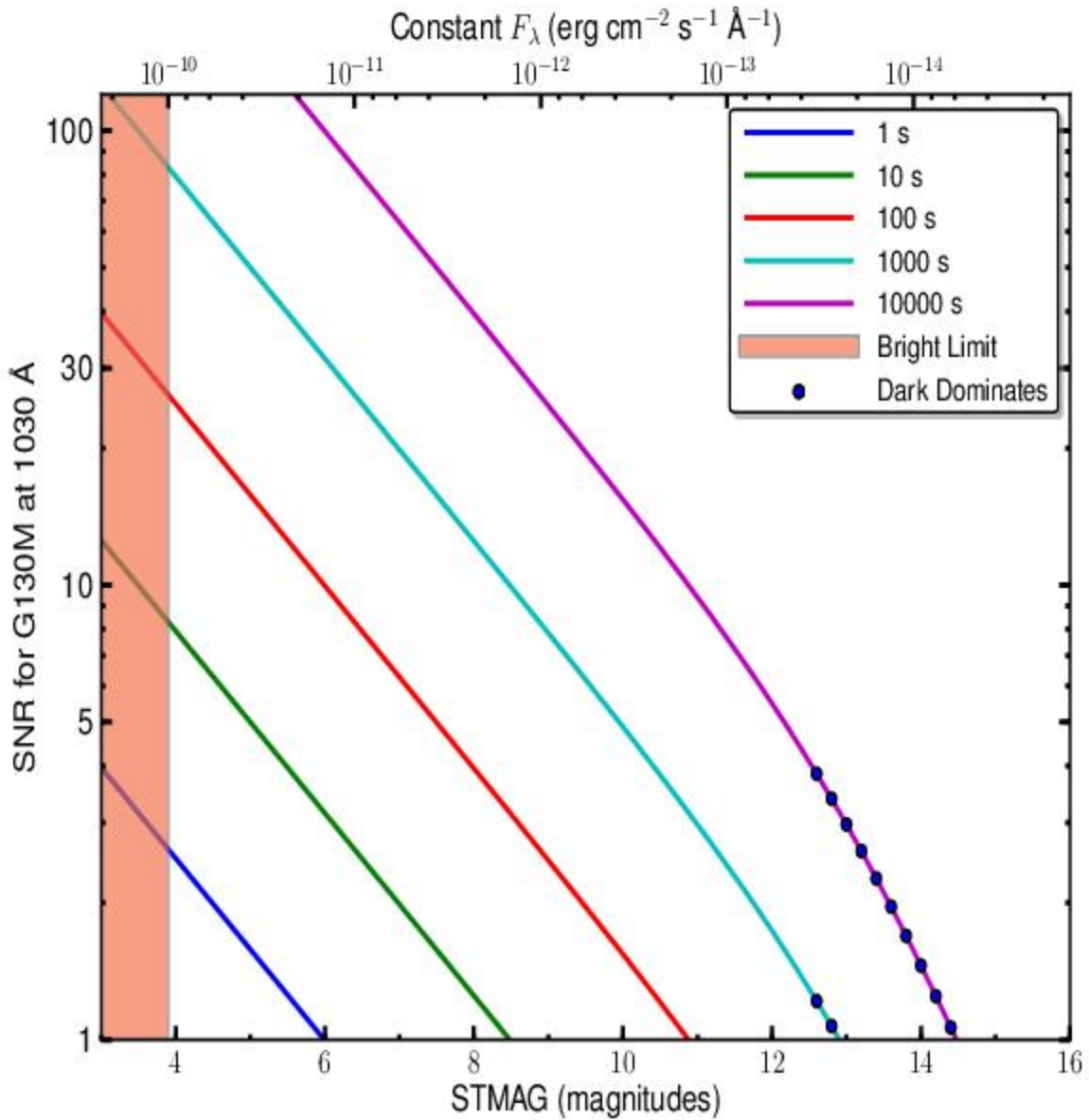
Figure 13.9: G130M/1055 and 1096 Point-Source Sensitivity for PSA.



The sensitivity through the BOA is not shown, as its MgF₂ filter is very low at these wavelengths.

G130M/1055 and 1096 Signal-to-Noise Ratio

Figure 13.10: Point-Source Signal-to-Noise as a Function of STMAG for G130M at 1030 Å.



The top axis displays constant F_λ values corresponding to the STMAG units ($V+STMAG_\lambda$) on the bottom axis. Recall that $STMAG = 0$ is equivalent to $F_\lambda = 3.63E-9$ erg cm⁻² s⁻¹ Å⁻¹. Colors refer to exposure times in seconds. The edge of the shaded area corresponds to the bright-object screening limit. Use of the PSA is assumed.

FUV Grating G160M

Description

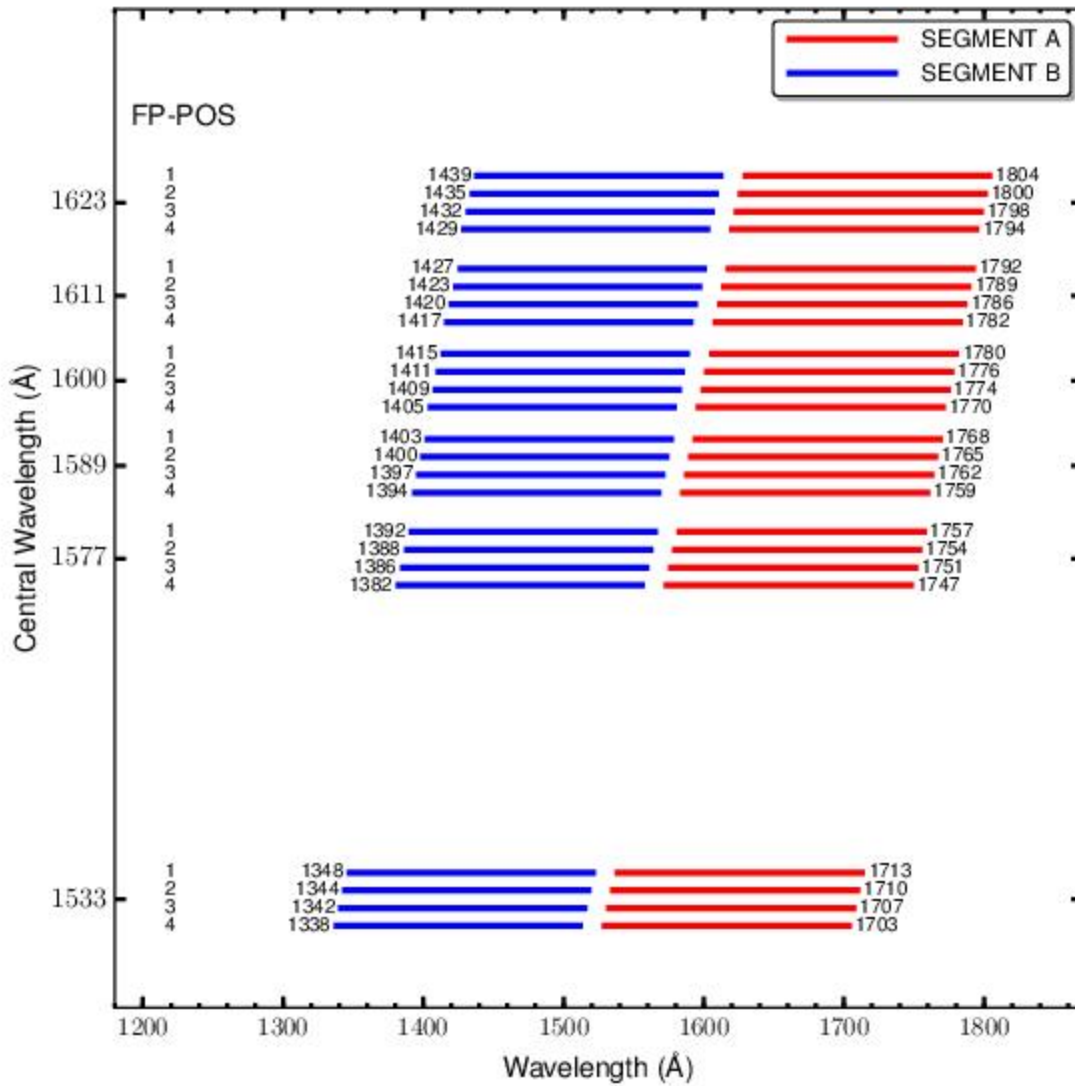
The G160M grating samples wavelengths between about 1360 and 1775 Å. It offers higher resolution and effective area than the G140L grating, but less spectral coverage.

Special Considerations

The gap between Segments A and B spans 18.1 Å. To fill this gap requires exposures separated by two central-wavelength settings.

Grating	Resolving Power R $= \lambda/\Delta\lambda$	Dispersion (mÅ pixel ⁻¹)	Plate Scale (milliarcsec pixel ⁻¹)		FP-POS Step (Å step ⁻¹)
			Disp. Axis	Cross-Disp. Axis	
G160M	13,000-20,000	12.23	24.3	90	3.1

Figure 13.11: Wavelength Ranges for the G160M Grating.



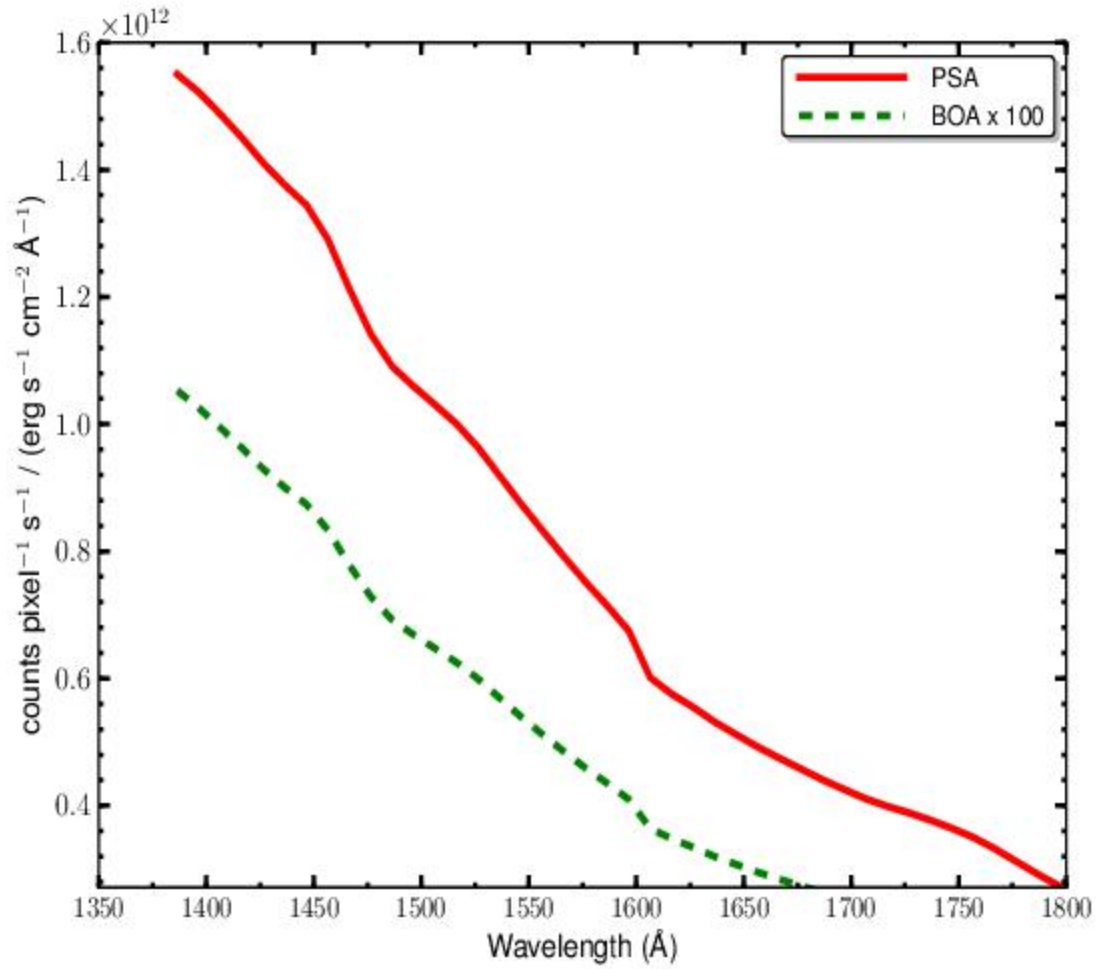
G160M Point-Source Sensitivity

Table 13.6: G160M Point-Source Sensitivity for PSA.

Wavelength (Å)	Throughput	Sensitivity (counts pixel ⁻¹ sec ⁻¹ per erg cm ⁻² sec ⁻¹ Å ⁻¹)	Effective Area (cm ²)
1386	4.015e-02	1.6e+12	1.82e+03
1400	3.867e-02	1.5e+12	1.75e+03
1450	3.287e-02	1.3e+12	1.49e+03
1500	2.512e-02	1.1e+12	1.14e+03

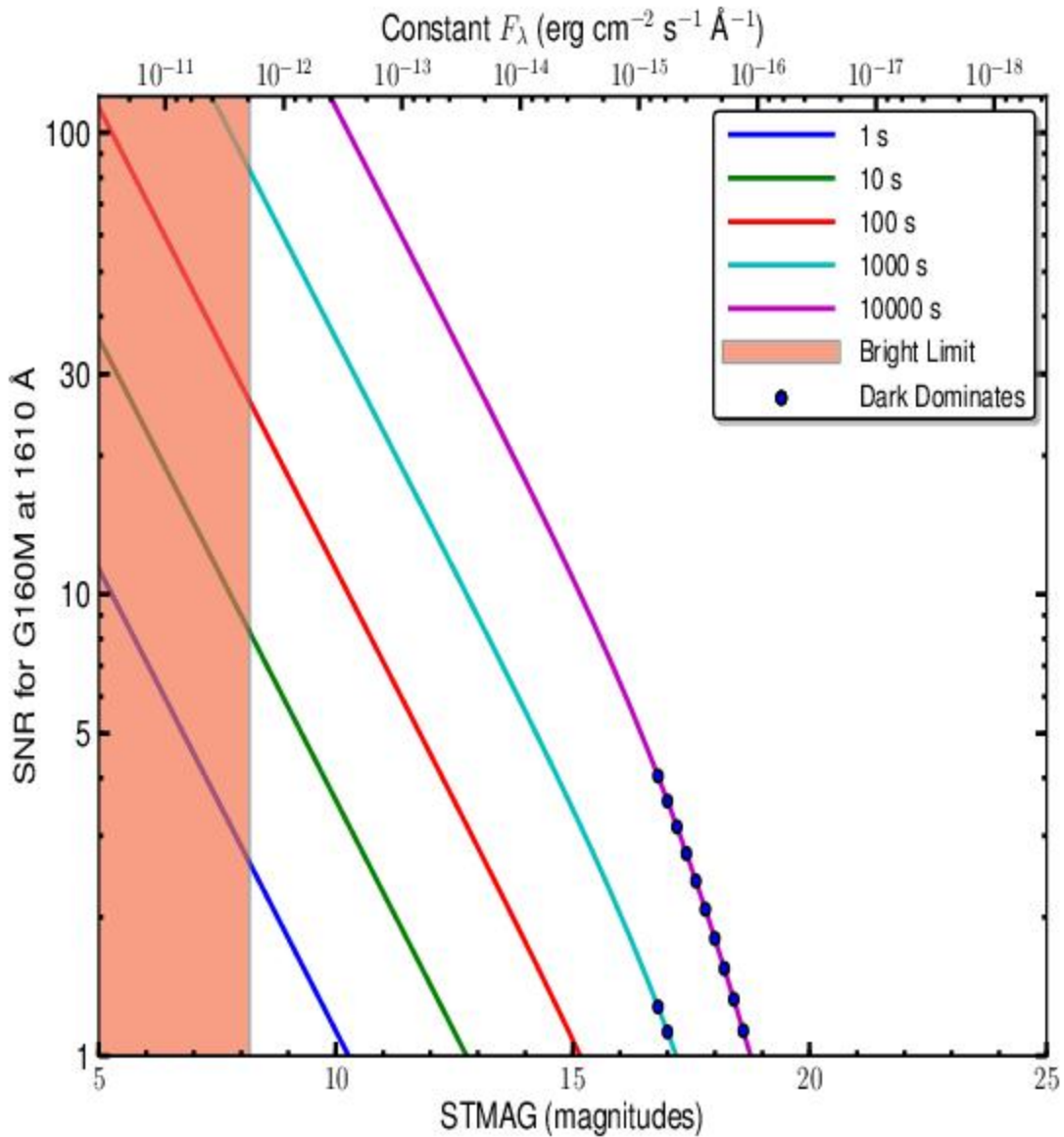
1550	1.989e-02	8.6e+11	9.00e+02
1600	1.482e-02	6.6e+11	6.70e+02
1650	1.098e-02	5.0e+11	4.97e+02
1700	8.872e-03	4.2e+11	4.01e+02
1750	7.378e-03	3.6e+11	3.34e+02
1798	5.413e-03	2.7e+11	2.45e+02

Figure 13.12: G160M Point-Source Sensitivity for PSA and BOA.



G160M Signal-to-Noise Ratio

Figure 13.13: Point-Source Signal-to-Noise as a Function of STMAG for G160M at 1610 Å.



The top axis displays constant F_λ values corresponding to the STMAG units ($V+STMAG_\lambda$) on the bottom axis. Recall that $STMAG = 0$ is equivalent to $F_\lambda = 3.63E-9 \text{ erg cm}^{-2} \text{ s}^{-1} \text{ \AA}^{-1}$. Colors refer to exposure times in seconds. The edge of the shaded area corresponds to the bright-object screening limit. Use of the PSA is assumed.

FUV Grating G140L

Description

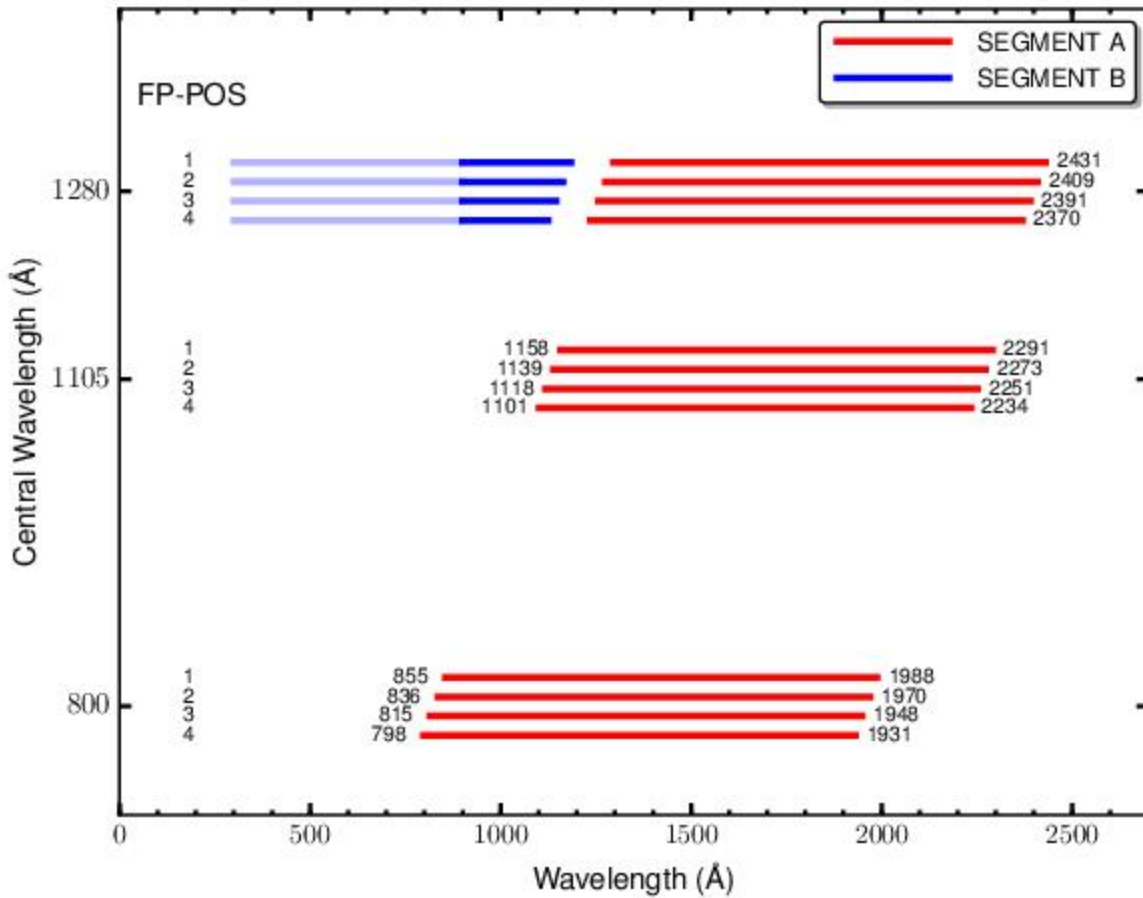
G140L is a low-resolution grating ($R \sim 2000$) with wavelength coverage extending to 900 Å, and perhaps below. Its sensitivity at EUV wavelengths, marked in light blue in [Figure 13.14](#), has not been calibrated. The grating has three central-wavelength settings: 800, 1105, and 1280 Å.

Special Considerations

The gap between Segments A and B spans 105 Å. When settings 800 or 1105 are used, the high voltage on Segment B must be lowered to avoid a dangerously high count rate from zero-order light. Wavelengths longer than 2150 Å may be contaminated by second-order light.

Grating	Resolving Power R $= \lambda/\Delta\lambda$	Dispersion (mÅ pixel ⁻¹)	Plate Scale (milliarcsec pixel ⁻¹)		FP-POS Step (Å step ⁻¹)
			Disp. Axis	Cross-Disp. Axis	
G140L	1,500–4,000	80.3	23.0	90	20.1

Figure 13.14: Wavelength Ranges for the G140L Grating.



The COS sensitivity at EUV wavelengths (marked in light blue) is not known.

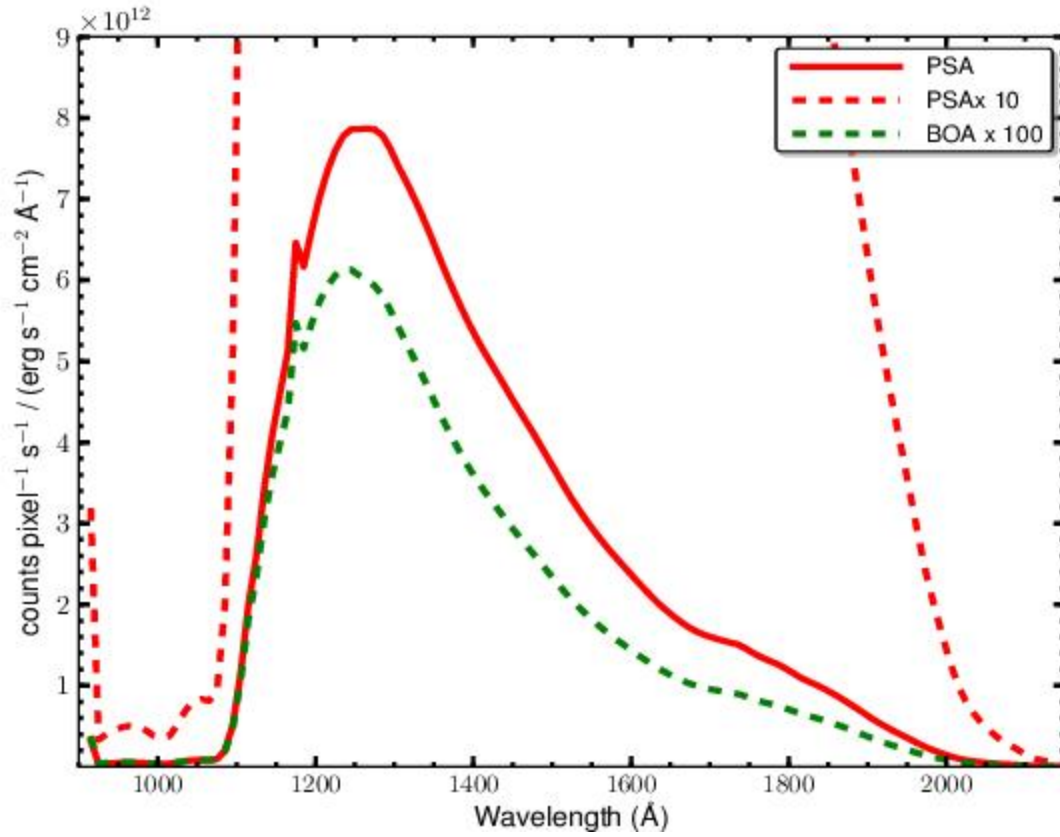
G140L Point-Source Sensitivity

Table 13.7: G140L Point-Source Sensitivity for PSA.

Wavelength (Å)	Throughput	Sensitivity (counts pixel ⁻¹ sec ⁻¹ per erg cm ⁻² sec ⁻¹ Å ⁻¹)	Effective Area (cm ²)
914	1.907e-02	1.6e+12	1.82e+03
950	2.701e-04	1.5e+12	1.75e+03
1000	2.025e-04	1.3e+12	1.49e+03
1050	4.370e-04	1.1e+12	1.14e+03
1100	3.869e-02	8.6e+11	9.00e+02
1150	2.098e-02	6.6e+11	6.70e+02

1200	3.143e-02	5.0e+11	4.97e+02
1250	3.481e-02	4.2e+11	4.01e+02
1300	3.191e-02	3.6e+11	3.34e+02
1350	2.642e-02	2.7e+11	2.45e+02
1400	2.117e-02	5.4e+12	9.58e+02
1450	1.726e-02	4.5e+12	7.81e+02
1500	1.369e-02	3.7e+12	6.19e+02
1550	1.052e-02	2.9e+12	4.76e+02
1600	8.191e-03	2.4e+12	3.71e+02
1650	6.315e-03	1.9e+12	2.86e+02
1700	5.209e-03	1.6e+12	2.36e+02
1750	4.523e-03	1.4e+12	2.05e+02
1800	3.648e-03	1.2e+12	1.65e+02
1850	2.789e-03	9.3e+11	1.26e+02
1900	1.829e-03	6.3e+11	8.27e+01
1950	1.012e-03	3.6e+11	4.58e+01
2000	3.978e-04	1.4e+11	1.80e+01
2050	1.308e-04	4.9e+10	5.92e+00
2100	4.006e-05	1.5e+10	1.81e+00
2148	5.357e-06	2.1e+09	2.42e-01

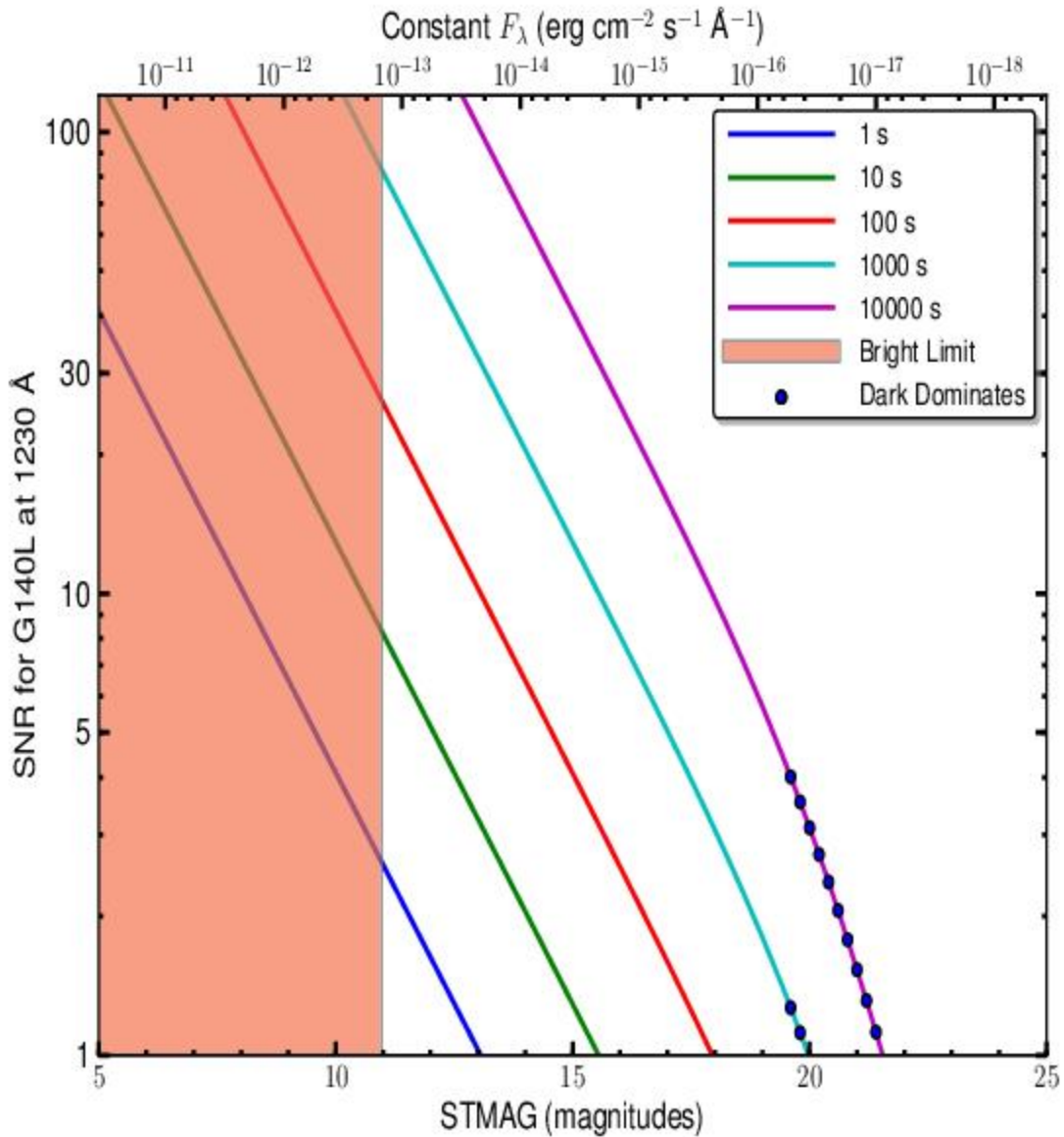
Figure 13.15: G140L Point-Source Sensitivity for PSA and BOA.



PSA \times 10 is plotted to show sensitivity below 1100 \AA .

G140L Signal-to-Noise Ratio

Figure 13.16: Point-Source Signal-to-Noise as a Function of STMAG for G140L.



The top axis displays constant F_λ values corresponding to the STMAG units ($V+STMAG_\lambda$) on the bottom axis. Recall that $STMAG = 0$ is equivalent to $F_\lambda = 3.63E-9$ erg cm⁻² s⁻¹ Å⁻¹. Colors refer to exposure times in seconds. The edge of the shaded area corresponds to the bright-object screening limit. Use of the PSA is assumed.

NUV Grating G185M

Description

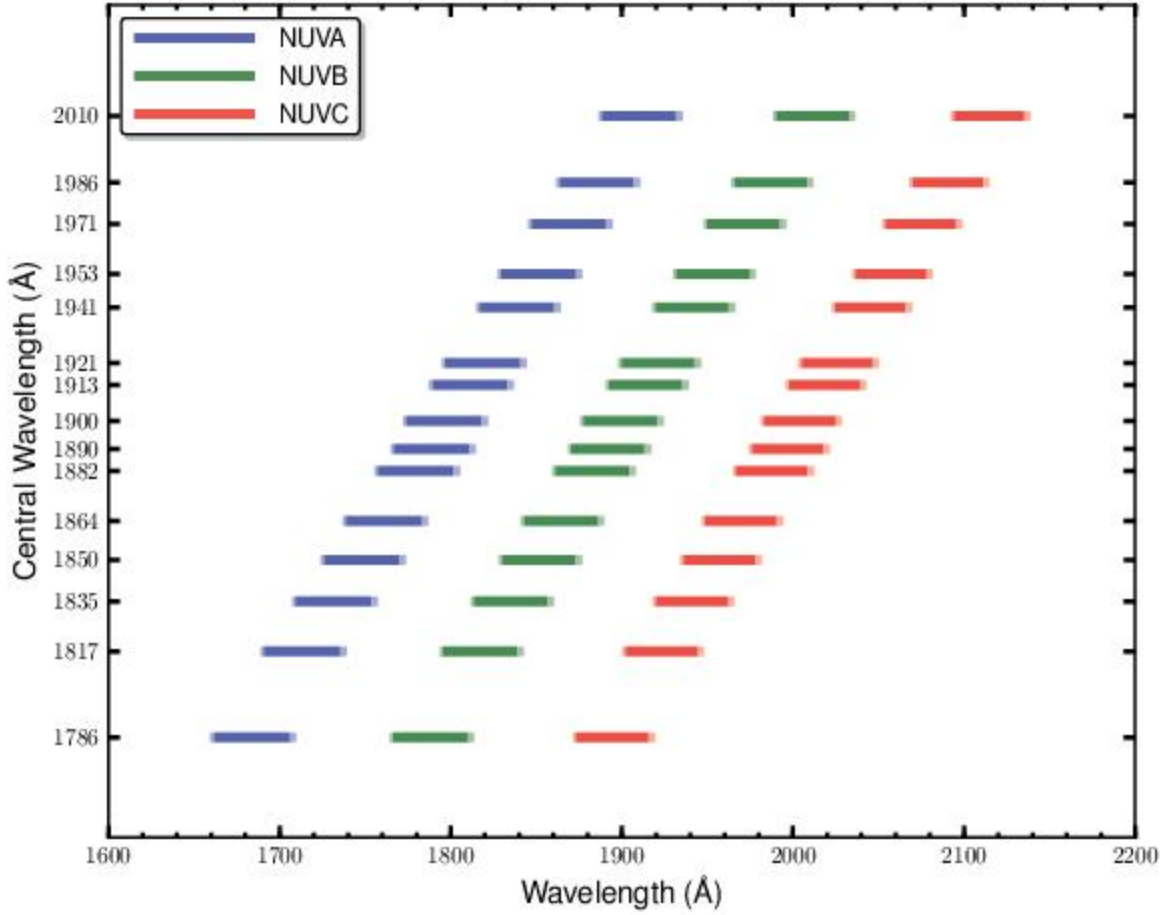
The G185M grating samples wavelengths between about 1700 and 2100 Å. The grating has 15 central wavelength settings.

Special Considerations

G185M spectra consist of three 35 Å stripes separated by two 64 Å gaps. To acquire a complete spectrum requires the use of six central-wavelength settings.

Grating	Resolving Power $R = \lambda / \Delta\lambda$	Dispersion (mÅ pixel ⁻¹)	Spatial Resolution (milliarcsec pixel ⁻¹)	Plate Scale (milliarcsec pixel ⁻¹)		FP-POS Step (Å step ⁻¹)
				Disp. Axis	Cross-Disp. Axis	
G185M	16,000–20,000	37	75 ± 4	24.3	23.8	1.9

Figure 13.17: Wavelength Ranges for the G185M Grating.



Dark lines represent wavelengths sampled by all four FP-POS positions.

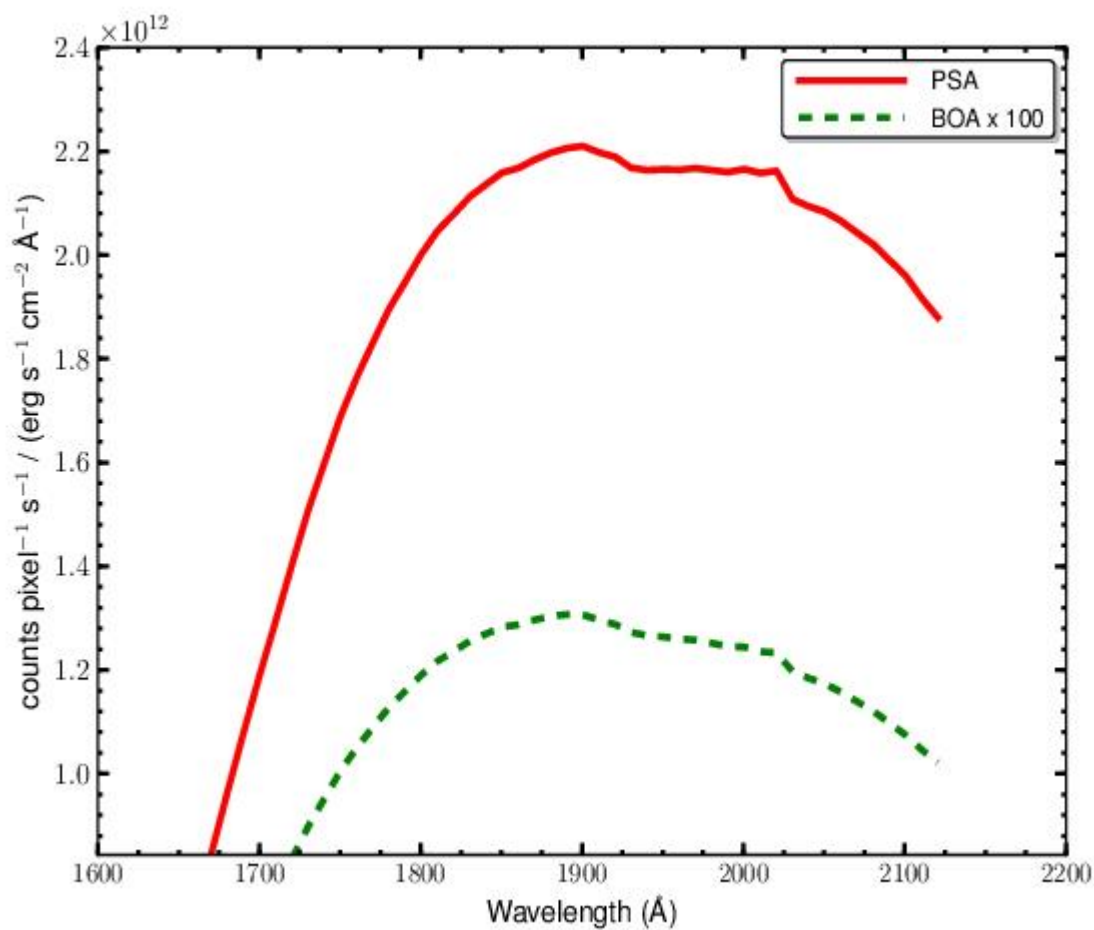
G185M Point-Source Sensitivity

Table 13.8: G185M Point-Source Sensitivity for PSA.

Wavelength (Å)	Throughput	Sensitivity (counts pixel ⁻¹ sec ⁻¹ per erg cm ⁻² sec ⁻¹ Å ⁻¹)	Effective Area (cm ²)
1670	6.068e-03	8.4e+11	2.75e+02
1700	8.398e-03	1.2e+12	3.80e+02
1750	1.158e-02	1.7e+12	5.24e+02
1800	1.335e-02	2.0e+12	6.04e+02
1850	1.401e-02	2.2e+12	6.34e+02
1900	1.397e-02	2.2e+12	6.32e+02
1950	1.334e-02	2.2e+12	6.03e+02

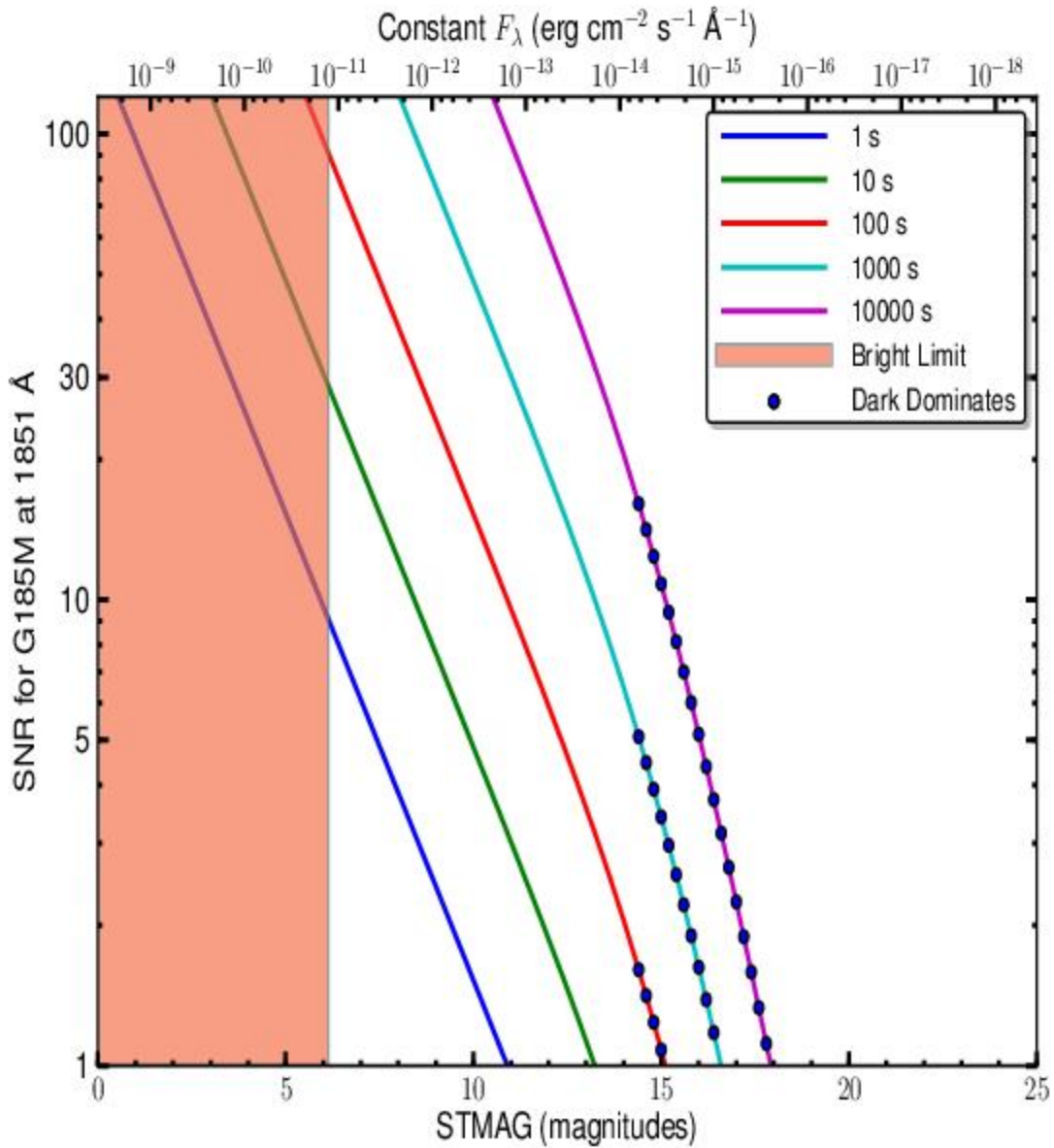
2000	1.301e-02	2.2e+12	5.88e+02
2050	1.221e-02	2.1e+12	5.53e+02
2100	1.122e-02	2.0e+12	5.08e+02
2127	1.047e-02	1.9e+12	4.74e+02

Figure 13.18: G185M Point-Source Sensitivity for PSA and BOA.



G185M Signal-to-Noise Ratio

Figure 13.19: Point-Source Signal-to-Noise as a Function of STMAG for G185M.



The top axis displays constant F_λ values corresponding to the STMAG units ($V+STMAG_\lambda$) on the bottom axis. Recall that $STMAG = 0$ is equivalent to $F_\lambda = 3.63E-9 \text{ erg cm}^{-2} \text{ s}^{-1} \text{ \AA}^{-1}$. Colors refer to exposure times in seconds. The edge of the shaded area corresponds to the bright-object screening limit. Use of the PSA is assumed.

NUV Grating G225M

Description

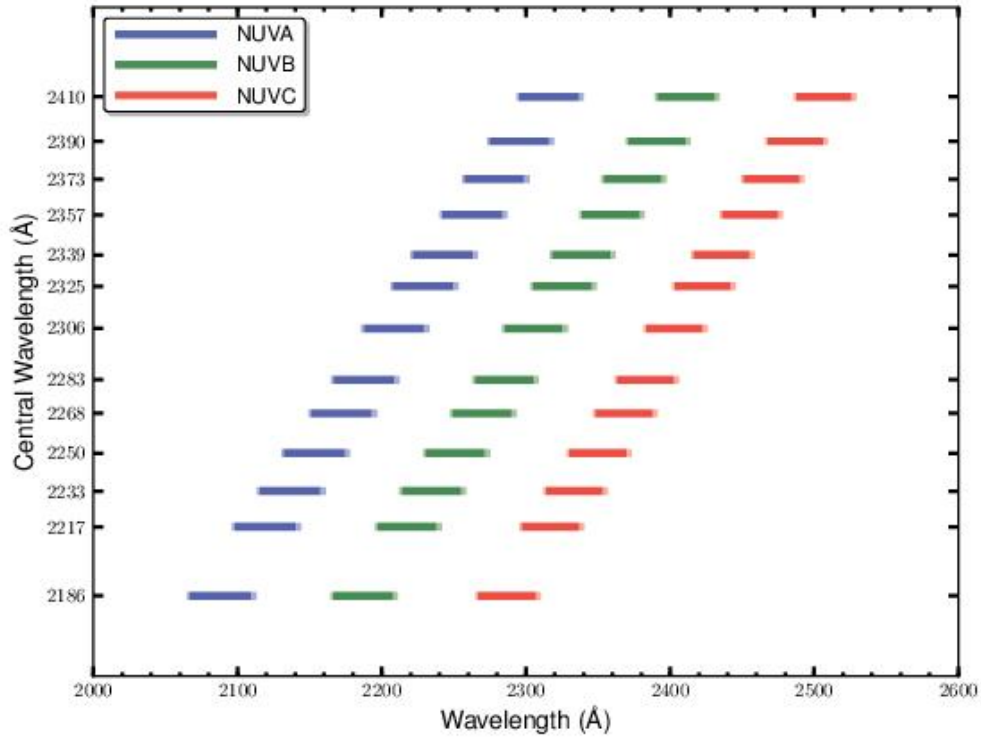
The G225M grating samples wavelengths between about 2100 and 2500 Å. The grating has 13 central wavelength settings.

Special Considerations

G225M spectra consist of three 35 Å stripes separated by two 64 Å gaps. To acquire a complete spectrum requires the use of six central-wavelength settings.

Grating	Resolving Power $R = \lambda / \Delta\lambda$	Dispersion (mÅ pixel ⁻¹)	Spatial Resolution (milliarcsec pixel ⁻¹)	Plate Scale (milliarcsec pixel ⁻¹)		FP-POS Step (Å step ⁻¹)
				Disp. Axis	Cross-Disp. Axis	
G225M	20,000–24,000	33	58 ± 2	24.3	23.1	1.7

Figure 13.20: Wavelength Ranges for the G225M Grating.



Dark lines represent wavelengths sampled by all four FP-POS positions.

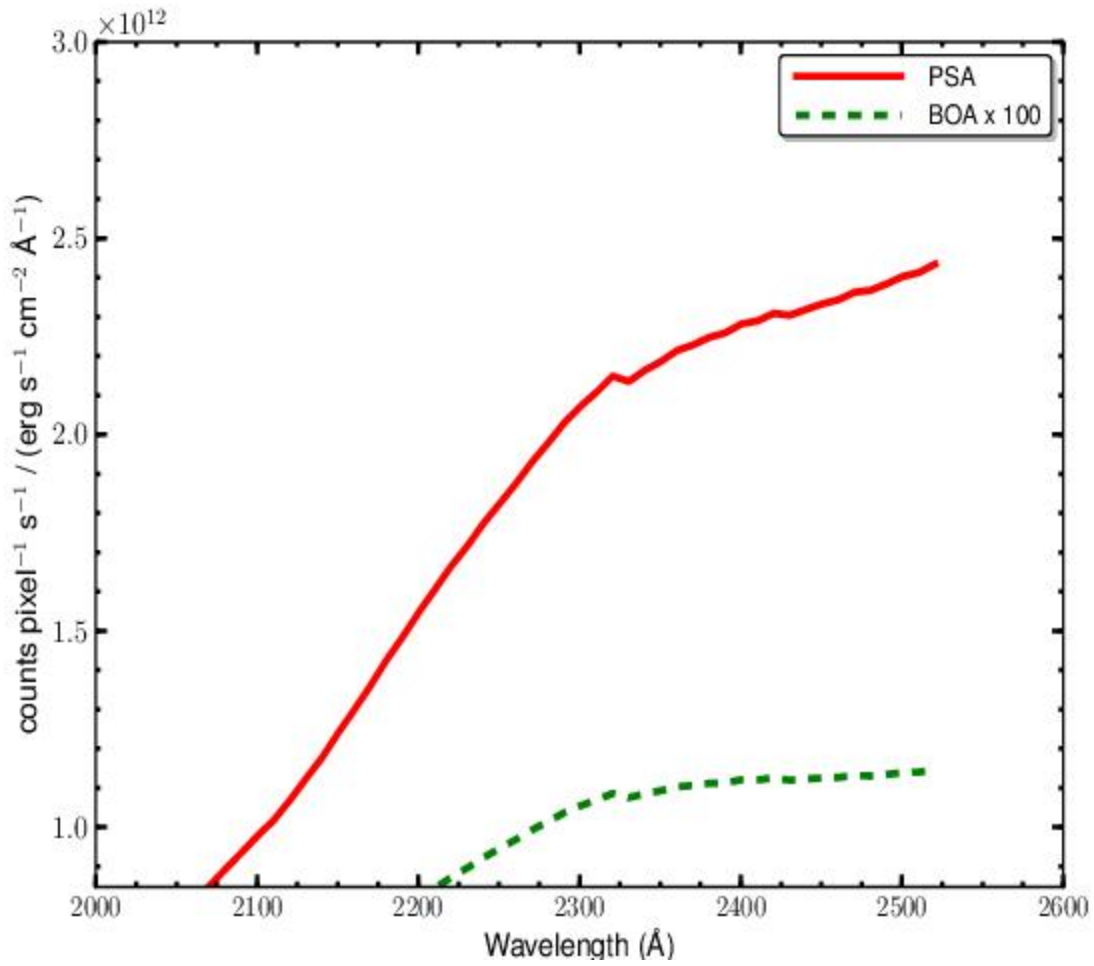
G225M Point-Source Sensitivity

Table 13.9: G225M Point-Source Sensitivity for PSA.

Wavelength (Å)	Throughput	Sensitivity (counts pixel ⁻¹ sec ⁻¹ per erg cm ⁻² sec ⁻¹ Å ⁻¹)	Effective Area (cm ²)
2070	5.242e-03	8.5e+11	2.37e+02
2100	5.949e-03	9.8e+11	2.69e+02
2150	7.366e-03	1.2e+12	3.33e+02
2200	8.986e-03	1.5e+12	4.07e+02
2250	1.036e-02	1.8e+12	4.68e+02
2300	1.151e-02	2.1e+12	5.21e+02
2350	1.189e-02	2.2e+12	5.38e+02
2400	1.215e-02	2.3e+12	5.50e+02
2450	1.217e-02	2.3e+12	5.51e+02
2500	1.129e-02	2.4e+12	5.56e+02

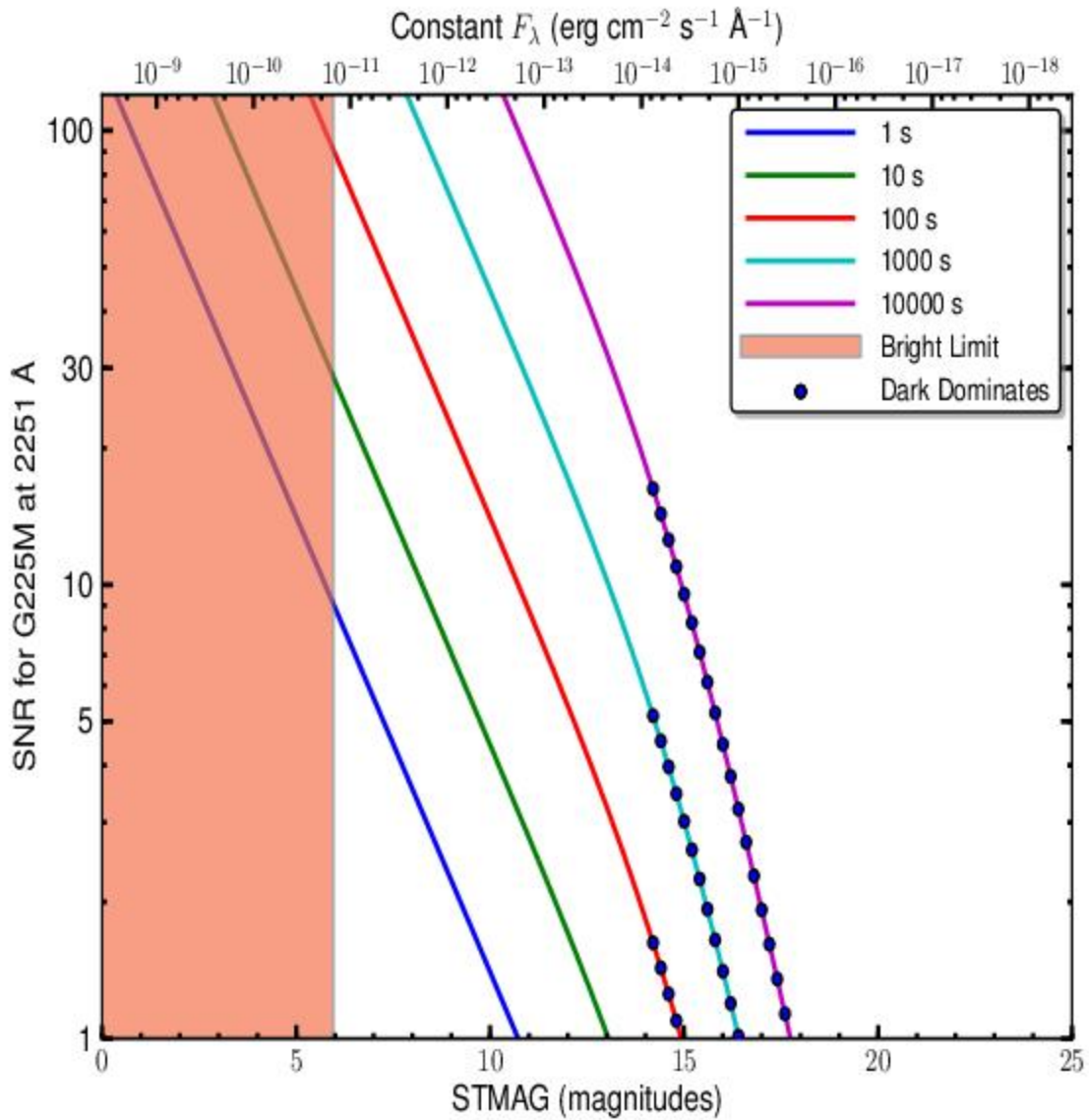
2527	1.238e-02	2.4e+12	5.60e+02
------	-----------	---------	----------

Figure 13.21: G225M Point-Source Sensitivity for PSA and BOA.



G225M Signal-to-Noise Ratio

Figure 13.22: Point-Source Signal-to-Noise as a Function of STMAG for G225M.



The top axis displays constant F_λ values corresponding to the STMAG units ($V+STMAG_\lambda$) on the bottom axis. Recall that STMAG = 0 is equivalent to $F_\lambda = 3.63E-9$ erg cm⁻² s⁻¹ Å⁻¹. Colors refer to exposure times in seconds. The edge of the shaded area corresponds to the bright-object screening limit. Use of the PSA is assumed.

NUV Grating G285M

Description

The G285M grating samples wavelengths between about 2500 and 3200 Å. The grating has 17 central-wavelength settings.

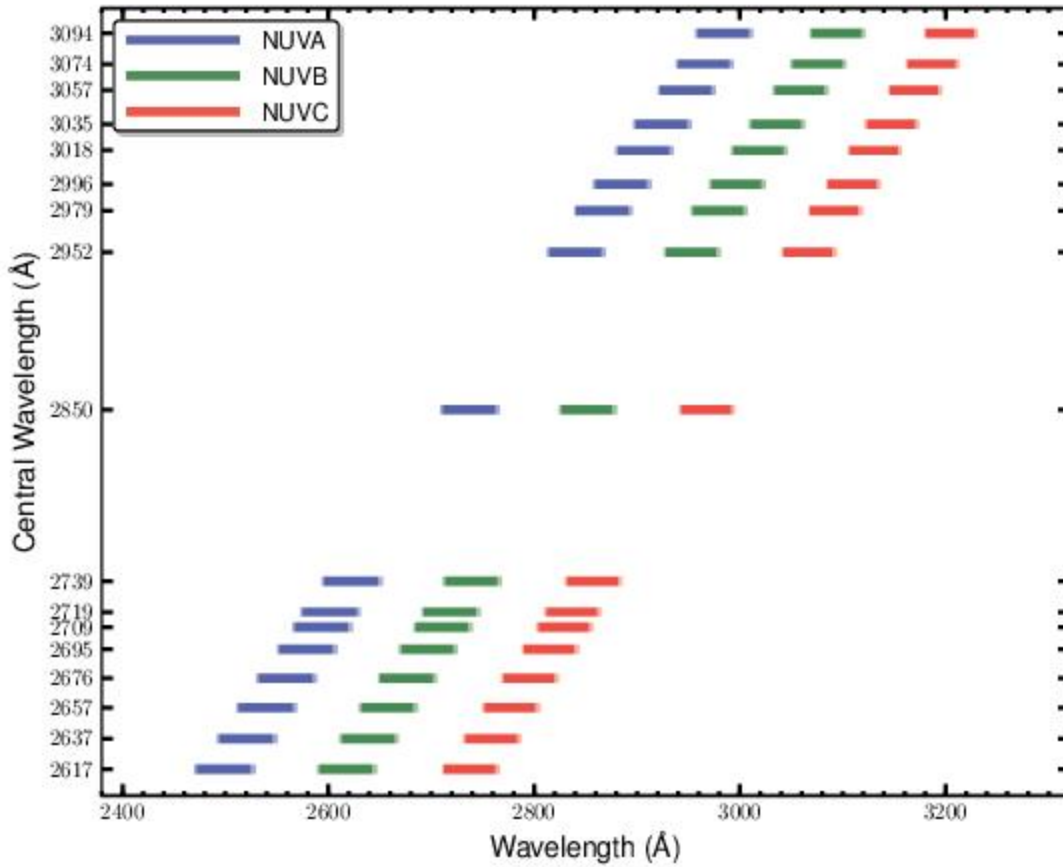
Special Considerations

G285M spectra consist of three 41 Å stripes separated by two 74 Å gaps. To acquire a complete spectrum requires the use of eight central-wavelength settings.

Because of declining throughput, NUV observations with the G285M grating are available but unsupported (See [Section 5.11](#)). Users interested in medium-resolution spectroscopic coverage of the wavelength region from 2500 to 3200 Å are encouraged to use STIS instead. The material in this section demonstrates the sensitivity of G285M in 2016, when it was much greater.

Grating	Resolving Power $R = \lambda / \Delta\lambda$	Dispersion (mÅ pixel ⁻¹)	Spatial Resolution (milliarcsec pixel ⁻¹)	Plate Scale (milliarcsec pixel ⁻¹)		FP-POS Step (Å step ⁻¹)
				Disp. Axis	Cross-Disp. Axis	
G285M	20,000–24,000	40	56 ± 1	24.3	24.4	2.1

Figure 13.23: Wavelength Ranges for the G285M Grating.



Dark lines represent wavelengths sampled by all four FP-POS positions.

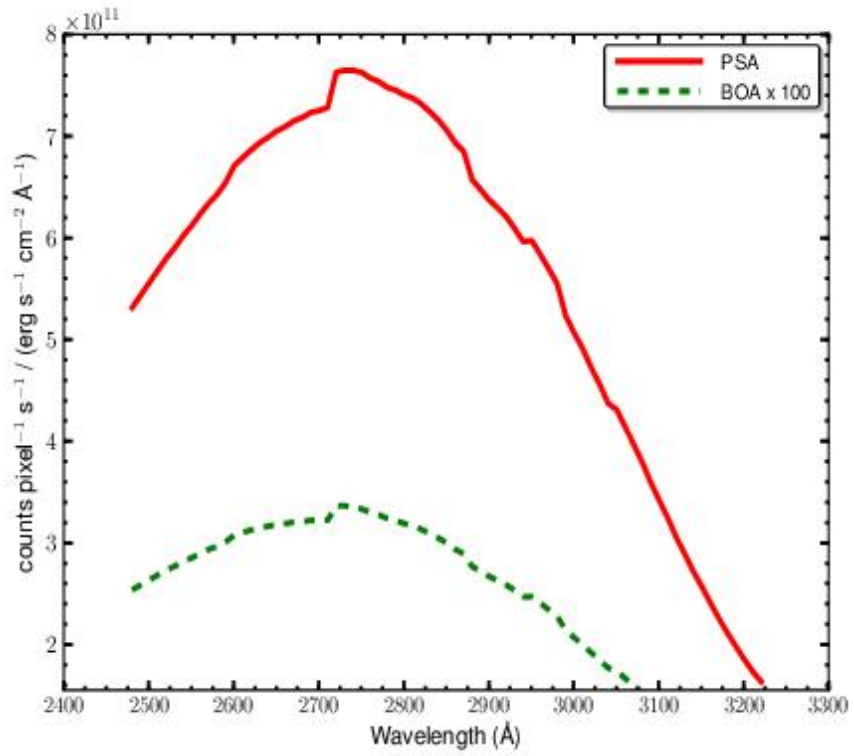
G285M Point-Source Sensitivity

Table 13.10: G285M Point-Source Sensitivity for PSA.

Wavelength (Å)	Throughput	Sensitivity (counts pixel ⁻¹ sec ⁻¹ per erg cm ⁻² sec ⁻¹ Å ⁻¹)	Effective Area (cm ²)
2480	2.316e-03	5.3e+11	1.05e+02
2500	2.403e-03	5.6e+11	1.09e+02
2550	2.595e-03	6.1e+11	1.17e+02
2600	2.791e-03	6.7e+11	1.26e+02
2650	2.878e-03	7.0e+11	1.30e+02
2700	2.906e-03	7.2e+11	1.31e+02
2750	3.002e-03	7.6e+11	1.36e+02
2800	2.863e-03	7.4e+11	1.30e+02

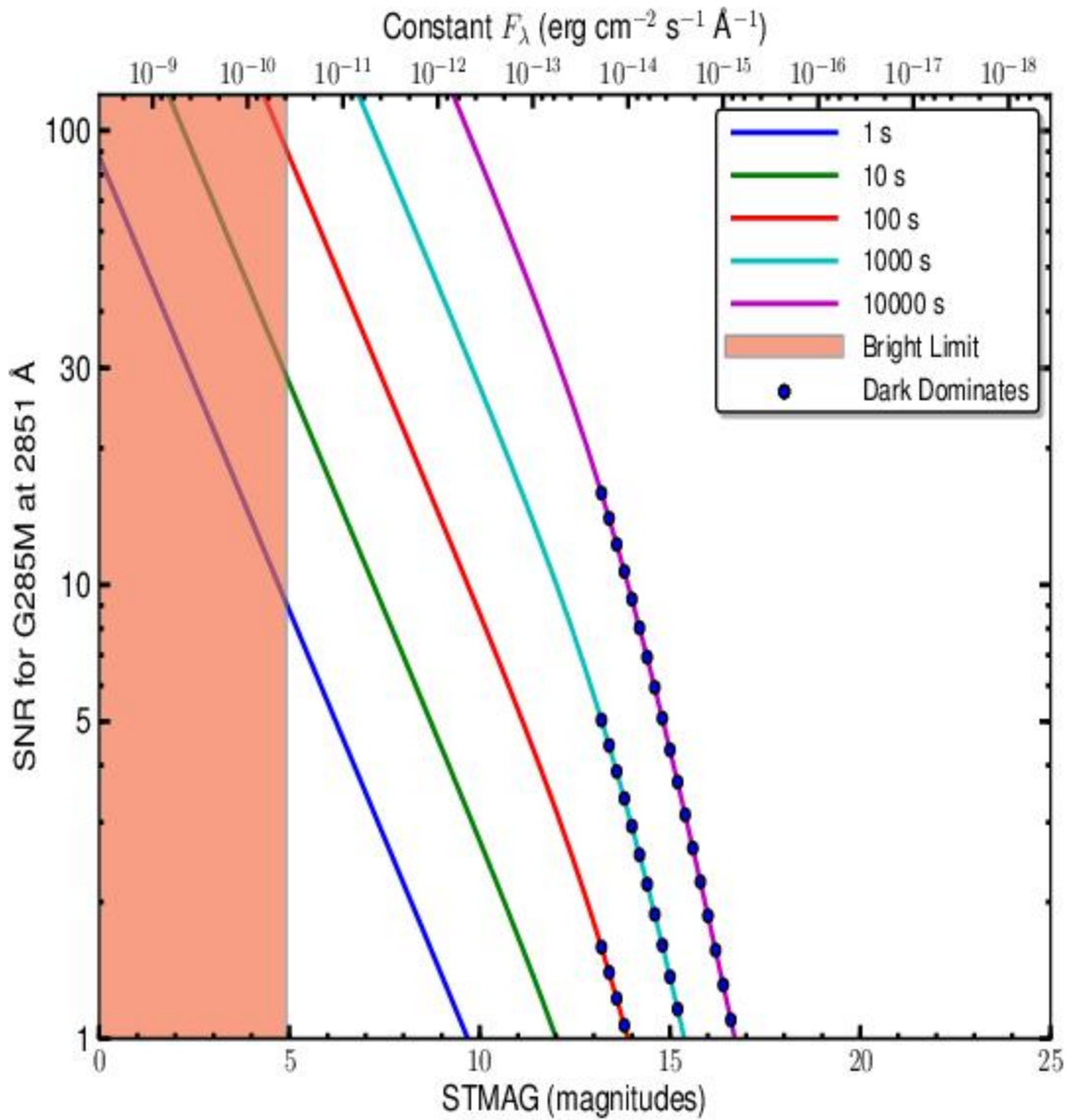
2850	2.682e-03	7.1e+11	1.21e+02
2900	2.390e-03	6.4e+11	1.08e+02
2950	2.194e-03	6.0e+11	9.92e+01
3000	1.829e-03	5.1e+11	8.28e+01
3050	1.532e-03	4.3e+11	6.93e+01
3100	1.197e-03	3.4e+11	5.42e+01
3150	8.866e-04	2.6e+11	4.01e+01
3200	6.297e-04	1.9e+11	2.85e+01
3229	5.211e-04	1.6e+11	2.36e+01

Figure 13.24: G285M Point-Source Sensitivity for PSA and BOA.



G285M Signal-to-Noise Ratio

Figure 13.25: Point-Source Signal-to-Noise as a Function of STMAG for G285M.



The top axis displays constant F_λ values corresponding to the STMAG units ($V+STMAG_\lambda$) on the bottom axis. Recall that $STMAG = 0$ is equivalent to $F_\lambda = 3.63E-9$ erg cm⁻² s⁻¹ Å⁻¹. Colors refer to exposure times in seconds. The edge of the shaded area corresponds to the bright-object screening limit. Use of the PSA is assumed.

NUV Grating G230L

Description

G230L is a low-resolution grating ($R \sim 3000$) with wavelength coverage extending from about 1650 to 3200 Å. The grating has four central-wavelength settings.

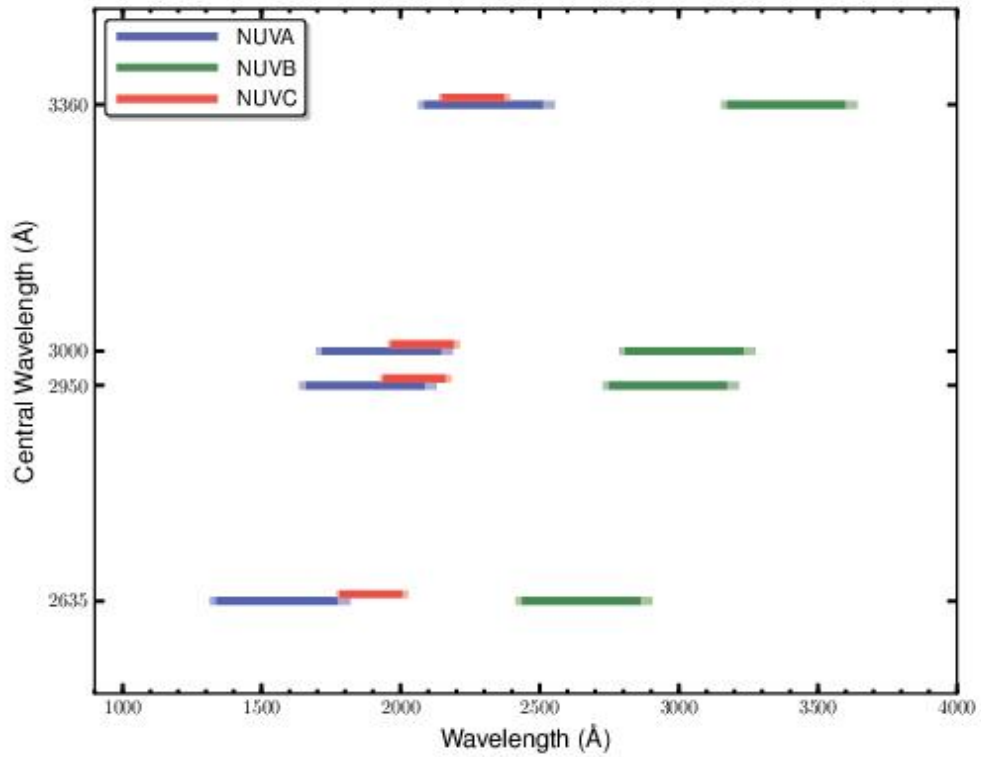
Special Considerations

G230L spectra consist of three 400 Å stripes separated by two 700 Å gaps. To acquire a complete spectrum requires the use of all four central-wavelength settings.

Only stripes A and B record first-order light, and even they may be contaminated by second-order light when central wavelength 3360 is used. See [Table 5.4](#).

Grating	Resolving Power $R = \lambda / \Delta\lambda$	Dispersion (mÅ pixel ⁻¹)	Spatial Resolution (milliarcsec pixel ⁻¹)	Plate Scale (milliarcsec pixel ⁻¹)		FP-POS Step (Å step ⁻¹)
				Disp. Axis	Cross-Disp. Axis	
G230L	2,100–3,900	390	81 ± 1	24.3	24.0	20.3

Figure 13.26: Wavelength Ranges for the G230L Grating.



Dark lines represent wavelengths sampled by all four FP-POS positions. Wavelengths above 3200 Å may be contaminated by second-order light.

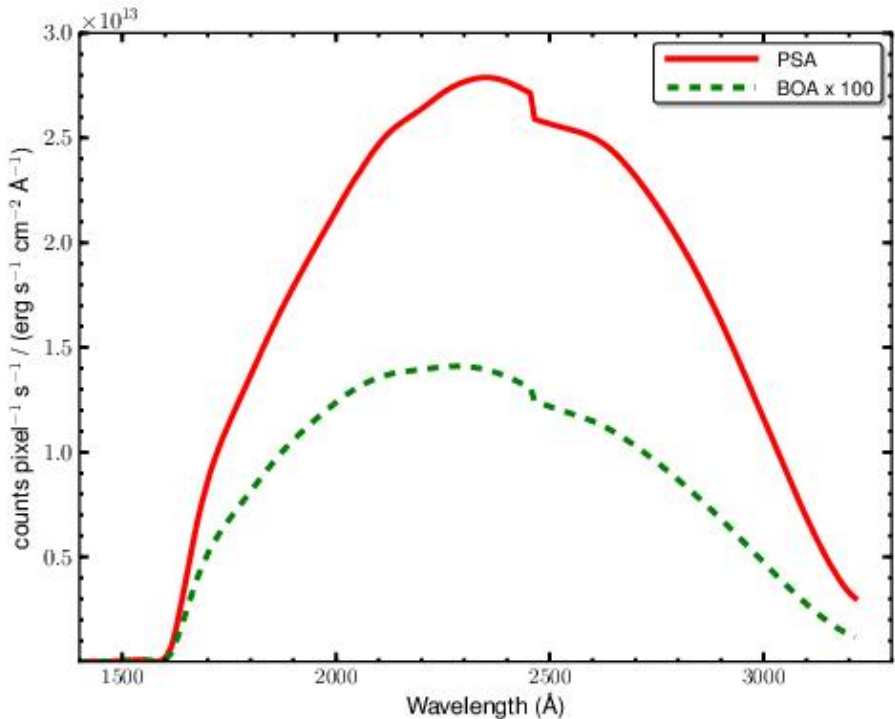
G230L Point-Source Sensitivity

Table 13.11: G230L Point-Source Sensitivity for PSA.

Wavelength (Å)	Throughput	Sensitivity (counts pixel ⁻¹ sec ⁻¹ per erg cm ⁻² sec ⁻¹ Å ⁻¹)	Effective Area (cm ²)
1400	7.061e-09	7.4e+06	3.19e-04
1600	1.419e-04	1.7e+11	6.42e+00
1800	1.020e-02	1.4e+13	4.61e+02
2000	1.447e-02	2.2e+13	6.55e+02
2200	1.612e-02	2.6e+13	7.29e+02
2400	1.550e-02	2.8e+13	7.01e+02
2600	1.294e-02	2.5e+13	5.85e+02
2800	9.680e-03	2.0e+13	4.38e+02
3000	5.195e-03	1.2e+13	2.35e+02

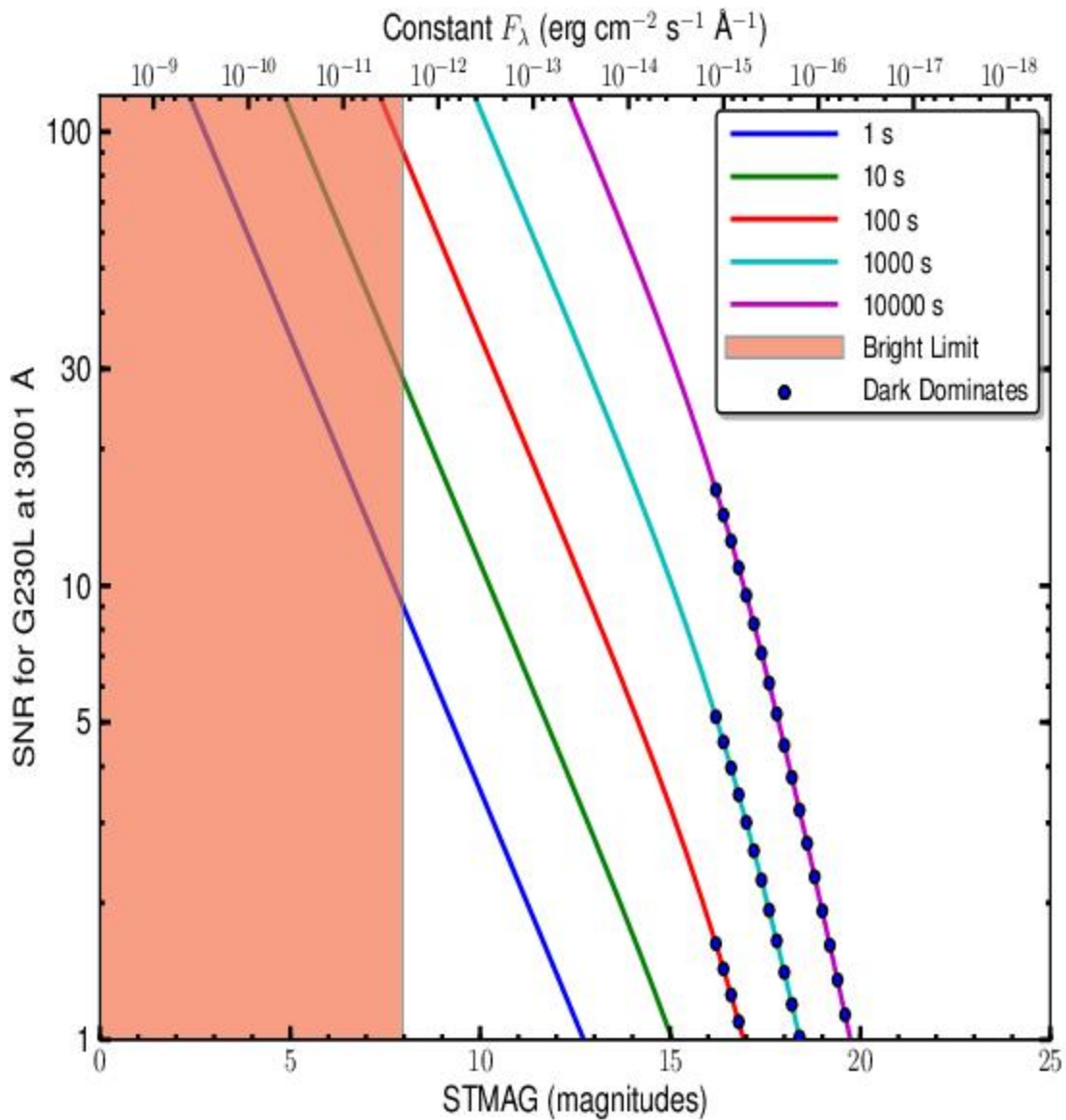
3200	1.389e-03	3.3e+12	6.29e+01
3400	3.252e-03	8.2e+12	1.47e+02

Figure 13.27: G230L Point-Source Sensitivity for PSA and BOA.



G230L Signal-to-Noise Ratio

Figure 13.28: Point-Source Signal-to-Noise as a Function of STMAG for G230L.



The top axis displays constant F_λ values corresponding to the STMAG units ($V+STMAG_\lambda$) on the bottom axis. Recall that $STMAG = 0$ is equivalent to $F_\lambda = 3.63E-9$ erg cm⁻² s⁻¹ Å⁻¹. Colors refer to exposure times in seconds. The edge of the shaded area corresponds to the bright-object screening limit. Use of the PSA is assumed.

13.4 Spectrograph Design Parameters

- 13.4.1 FUV Channel
- 13.4.2 NUV Gratings

13.4.1 FUV Channel

Table 13.12 presents design parameters of the FUV spectrograph and gratings. The FUV gratings are concave and have holographically generated grooves to provide dispersion and correct for astigmatism. The gratings have aspherical surfaces to correct for HST's spherical aberration. The FUV "M" gratings have been ion etched to produce triangular groove profiles for better efficiency. The G140L grating has grooves with a laminar profile. All FUV gratings are coated with MgF₂ over aluminum.

The surface of the optic is a sphere of the quoted radius, but with a deviation of $\Delta z = a_4 r^4 + a_6 r^6$, where z is measured along the vertex normal. The quantities γ , δ , r_c , and r_d are the standard positions of the recording sources as defined in Noda, Namioka, and Seya (1974, J. Opt. Soc. Amer., 64, 1031).

Table 13.12: Design Parameters for the FUV Spectrograph and Gratings.

Dimension	G130M	G160M	G140L
secondary mirror vertex to aperture (z, mm)	6414.4		
V ₁ axis to aperture (mm)	90.49		
aperture to grating (mm)	1626.57		
α (degrees)	20.1	20.1	7.40745
β (degrees)	8.6466	8.6466	-4.04595
α - β (degrees)	11.4534		
grating to detector (mm)	1541.25		
detector normal vs. central ray (degrees)	9.04664		
nominal groove density (lines mm ⁻¹)	3800	3093.3	480
radius of curvature (mm)	1652	1652	1613.87
a ₄	1.45789 × 10 ⁻⁹	1.45789 × 10 ⁻⁹	1.33939 × 10 ⁻⁹
a ₆	-4.85338 × 10 ⁻¹⁵	-4.85338 × 10 ⁻¹⁵	1.4885 × 10 ⁻¹³

γ (degrees)	-71.0	-62.5	10.0
d (degrees)	65.3512	38.5004	24.0722
r_c (mm)	-4813.92	-4363.6	3674.09
r_d (mm)	5238.29	4180.27	3305.19
recording wavelength (Å)	4880		

13.4.2 NUV Gratings

Table 13.13 presents design parameters of the NUV gratings. The NUV gratings are flat and were not constructed holographically. The NUV MAMA has low but measurable sensitivity at FUV wavelengths, and with some gratings second-order light could contaminate the spectrum. To minimize this effect, the coated optics are optimized for wavelengths above 1600 Å. Given the four reflections used in the NUV channel, wavelengths below 1600 Å, including geocoronal Lyman α , are effectively eliminated. In addition, gratings G230L and G285M have order-blocking filters mounted directly on them to block the second-order spectra below 1700 Å. Even with these filters, it is possible for second-order light to appear on the NUV MAMA when G230L is used, especially in the long-wavelength stripe.

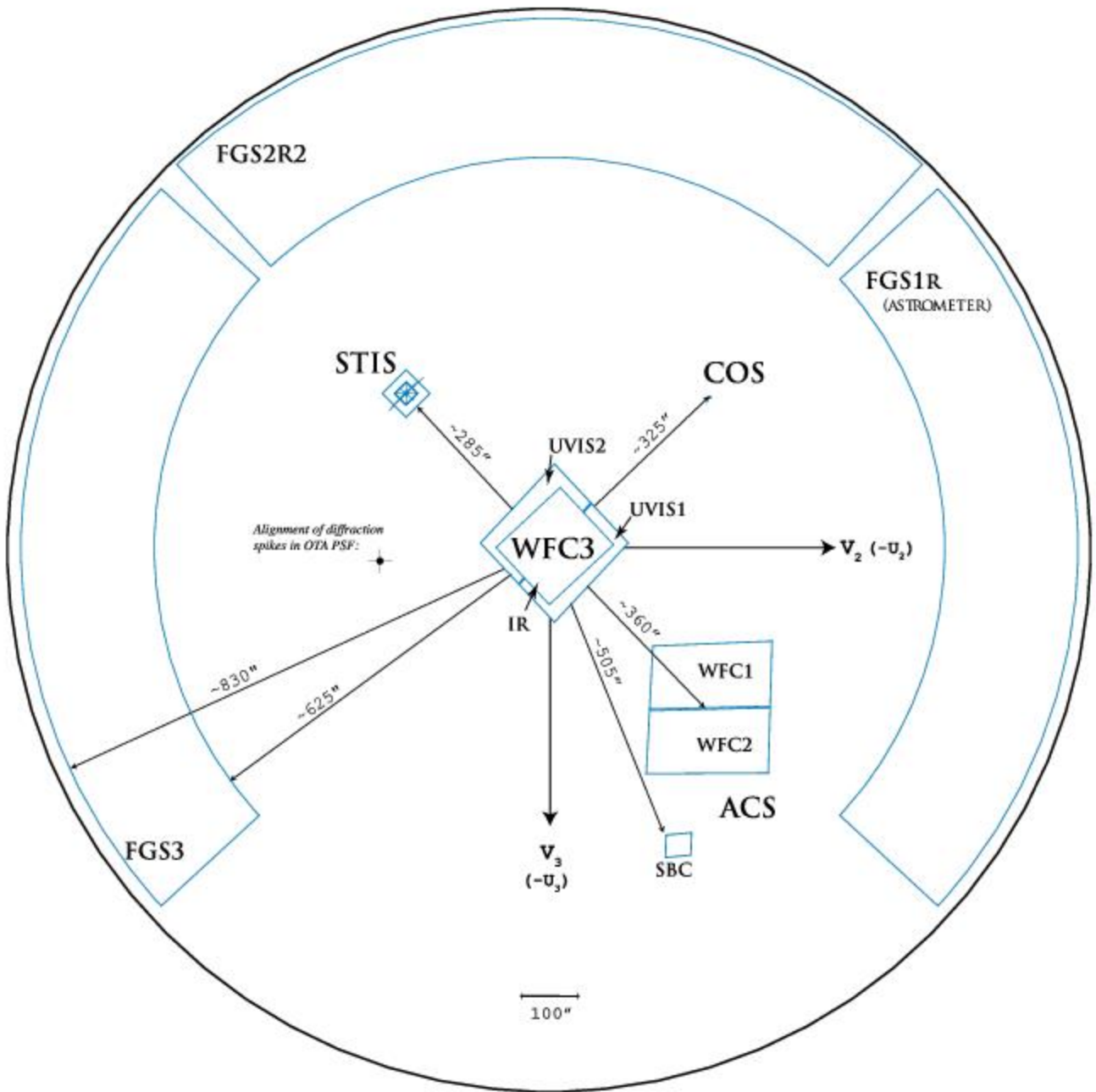
Table 13.13: Design Parameters for the NUV Gratings.

Dimension	G185M	G225M	G285M	G230L
groove density (mm^{-1})	4800	4800	4000	500
α (degrees)	27.24	33.621	35.707	5.565
β (degrees)	25.85	32.23	34.32	1.088
coating	Al + MgF ₂	Al only	Al only	Al + MgF ₂

13.5 The Location of COS in the HST Focal Plane

The location of the COS aperture in the HST focal plane is shown in [Figure 13.29](#). Note the relative orientation of the HST V_2 and V_3 axes (the V_1 axis is along HST's optical axis), as well as the relative locations and orientations of the other instruments. The COS aperture lies ~ 325 arcsec from the V_1 axis in the $+V_2, -V_3$ quadrant.

Figure 13.29: A Schematic View of the HST Focal Plane.

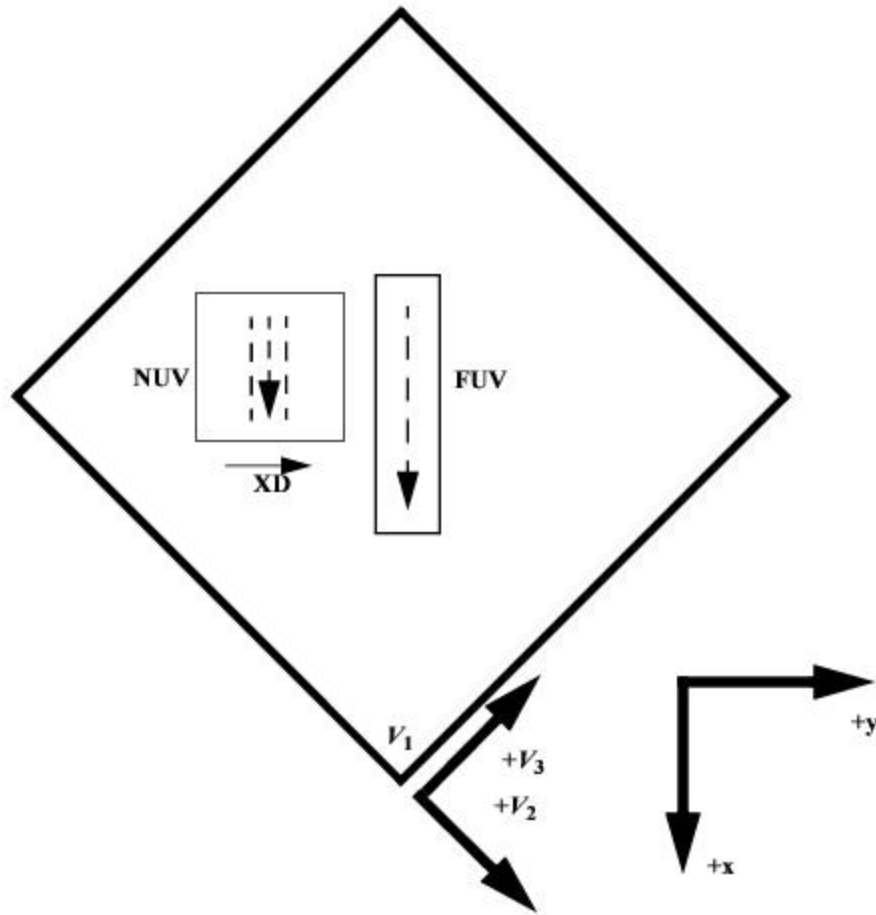


This drawing shows the entire HST focal plane and the apertures of the scientific instruments. The view is from the rear of the telescope looking forward toward the sky, the opposite of the sense of [Figure 13.30](#).

13.6 The COS User Coordinate System

Figure 13.30 presents a schematic layout of the COS focal plane. In this figure, the x and y axes denote the COS user coordinate system. In this system, x lies along the wavelength (dispersion) axis and increases with increasing wavelength for both the FUV and NUV channels. For the NUV channel, y increases with increasing wavelength in the cross-dispersion (XD) direction. All references to COS (including `POS TARG` specifications in APT, the [Astronomer's Proposal Tool](#), detector pixel coordinates, and science header keywords) employ the user coordinate system.

Figure 13.30: Schematic Layout of the COS Detectors.



This view is from the front of the telescope looking aft. The dashed arrows show the direction of increasing wavelength for the two detectors, and "XD" indicates the direction of increasing wavelength for the NUV cross-dispersion direction. The x and y axes denote the COS user coordinate system. For both the FUV and NUV channels, wavelength increases in the $+x$ or $(+V_2, -V_3)$ direction. Note that this diagram is purely schematic and it is intended to show only relative directions. This diagram does not show the locations of apertures. The bottom corner of this square (at V_1) corresponds to the center of the WF3 camera (see [Figure 13.29](#)).

Glossary

The following terms and acronyms are used in this Handbook.

Term	Definition
ACCUM	Operating mode for COS in which only the locations of detected photons are recorded; no time information is recorded. ACCUM mode is designed for bright objects with high count rates. See also TIME-TAG.
Along Dispersion (AD)	The dispersion direction, corresponding to the long/major axis on both the FUV and NUV detectors.
Aperture Mechanism (ApM)	The Aperture Mechanism is used to place either the BOA or PSA into position as the science aperture. The ApM is also moved to place the FCA into position if a flat-field exposure is to be taken.
APT	The Astronomer's Proposal Tool, software provided by STScI for writing Phase I proposals and Phase II programs. The use of APT is encouraged in all cases, even for Phase I proposals, because it provides an accurate estimate of the actual time needed to obtain an observation. For more information, go to http://apt.stsci.edu .
BOA	The Bright Object Aperture is 2.5 arcsec in diameter with a neutral-density filter that attenuates flux by a factor of about 200.
CalCOS	The COS calibration pipeline, a software package that performs image and spectroscopic data reduction to produce output files useful for scientific analysis.
central wavelength	For the NUV gratings, the central wavelength is the approximate midpoint of the stripe B spectrum. For the FUV gratings, the central wavelength refers approximately to the shortest wavelength recorded on Segment A. This is frequently referred to as "cenwave" throughout this handbook.
channel (FUV or NUV)	One of the two COS optical systems, FUV and NUV, including mirrors, gratings, and detectors.
COS 2025	A policy that took effect at the beginning of Cycle 25 with the goal of retaining full science capability of the COS/FUV channel until 2025. It places restrictions on the use of particular G130M cenwaves at Lifetime Position 4 in order to reduce gain sag due to geocoronal Lyman α .
CVZ	The Continuous Viewing Zones are regions of the sky where HST can observe without interruptions caused by target occultation by the Earth. These zones are approximately 24 degrees in size centered on the orbital poles, which are 28.5 degrees from the celestial poles.

ETC	Exposure Time Calculator, software provided by STScI to estimate exposure times needed to achieve, say, a given signal-to-noise level on a source. Although information is provided in this handbook on exposure estimation, the ETC provides the most accurate way to determine the exposure times required to acquire or observe an object. The ETC is used together with the APT to plan HST observations. For more information, go to http://www.stsci.edu/hst/cos/software/planning/etc .
FCA	Flat-field Calibration Aperture, the aperture through which the on-board deuterium lamps illuminate the COS optical system.
FGS	Fine Guidance Sensor. By tracking guide stars, the three FGSs can maintain the pointing stability of HST with a precision of 2 mas or less.
FP-POS	A command used to move the spectrum on the detector (in the dispersion direction) to reduce the effects of fixed-pattern noise.
FUSE	<i>Far Ultraviolet Spectroscopic Explorer</i> , a moderate-resolution ($R \sim 15,000$), far-UV spectrograph that used micro-channel plate detectors similar to those employed by the FUV channel of COS.
FUV	The far-ultraviolet channel of COS can observe wavelengths from less than 900 to 1800 Å.
gain sag	A reduction in the efficiency of the COS FUV micro-channel plate detector at converting incoming photons into detectable events. It is a consequence of detector use.
GALEX	<i>Galaxy Evolution Explorer</i> , a NASA mission observing the sky in two ultraviolet bandpasses. <i>GALEX</i> data are useful for determining the UV fluxes of COS targets. For more information, go to http://www.galex.caltech.edu .
GSC2/ICRS	Guide Star Catalog II/International Celestial Reference System. The GSC2 is an all-sky optical catalog based on 1" resolution scans of the photographic Sky Survey plates from the Polomar and UK Schmidt telescopes. The ICRS is the fundamental celestial reference system adopted by the International Astronomical Union for high-precision astrometry. Uncertainties in this system are dominated by the 0.3" uncertainty of the GSC2.
GTO	Guaranteed Time Observer, a member of the COS science team who has been granted a share of telescope time as part of their involvement in designing and building COS.
home position	The default position for a mechanism. COS is reconfigured at the start of each visit, and mechanisms are returned to their home positions. For the ApM, the home is the PSA; for OSM1, home is G130M, CENWAVE=1222; and for OSM2, home is MIRRORA.
IDT	Investigation Definition Team, NASA's term for the group that proposed and built COS.
lifetime position	A region on which a spectrum illuminates the FUV detector. Due to the onset of gain sag, the lifetime position has been changed four times since the beginning of COS operations. Starting in Cycle 29, COS began using multiple lifetime positions at the same time. The most recently commissioned lifetime position was LP5, which took place on October 4, 2021. The next lifetime position will be LP6, which will be commissioned at the beginning of Cycle 30.

LSF	Line Spread Function, the shape of a spectral feature emitted by a monochromatic point source.
MAMA	Multi-Anode Micro-channel Array, a photon-counting UV detector, used in the NUV channel.
MAST	The Mikulski Archive for Space Telescopes, which makes available data from a number of NASA missions, including HST. Go to http://archive.stsci.edu .
MCP	Micro-Channel Plate, a resistive glass plate with 10–15 micron-sized holes used within both the XDL and MAMA detectors to amplify photo-electrons into charge pulses large enough for electronic processing.
MIRRORA, MIRRORB	MIRRORA and MIRRORB are internal flat mirrors used for NUV imaging in COS. MIRRORA provides the highest throughput. MIRRORB uses a reflection off of the order-sorting filter of MIRRORA to get lower throughput, which can be helpful when observing bright targets.
NUV	The near-ultraviolet channel of COS can observe wavelengths from ~1650 to 3200 Å.
OSM1, OSM2	The Optics Select Mechanisms place gratings or mirrors in the optical path.
OTA	Optical Telescope Assembly, HST's optical system of primary and secondary mirrors, plus the structure that holds them and maintains alignment.
pixel	The basic stored unit of data. In the NUV channel, MAMA pixels correspond to physical portions of the detector. In the FUV channel, the position of a detected event is assigned to a pixel based on calculations, but there are no physical pixels as such.
PHD	Pulse-Height Distribution, a histogram of the charge cloud sizes collected in a particular exposure or portion thereof. The PHD is a useful measure of data quality and is recorded as a data product for FUV exposures. PHD data are not available for NUV exposures or in ACCUM mode.
POS TARG	The "POS TARG X, Y," special requirement is used to request a target offset in APT. POS TARG offsets are specified in the COS user coordinate system, which is used in all COS data products (Section 13.6). Note that the POS TARG coordinates represent motion of the target in the aperture; the telescope moves in the opposite direction.
PSA	Primary Science Aperture, a circular aperture 2.5 arcsec in diameter and completely open.
PSF	Point Spread Function, the two-dimensional distribution of light at the detector plane produced by the HST+COS optics.

resel	Resolution element of a spectrum or image. For spectra, a resel corresponds to the FWHM of a narrow emission line. Using pre-flight data, resels were determined to be roughly 6 pixels wide (dispersion direction) by 10 tall for the FUV channel and 3 × 3 pixels for the NUV. On-orbit data suggests that the FUV resel is somewhat larger than this, while the NUV resel is somewhat smaller. Note that spectra are recorded in pixel units and that any rebinning into resels is performed on the ground during data reduction.
segment	The COS FUV detector consists of two independent segments. In all spectroscopic modes, the long-wavelength end of the spectrum falls on Segment A, and the short-wavelength end on Segment B.
SMOV	Servicing Mission Observatory Verification, the period immediately following a servicing mission in which HST's instruments are activated, tested, and made ready for science observing. Only a minimal set of calibrations are done in SMOV to confirm instrument performance; more detailed calibrations are performed in the ensuing cycle.
stim pulse	Artificially induced events on each segment of the FUV detector. The stim pulses allow for the correction of thermal distortion and aid in determining the dead-time correction.
STMAG	In this system, the flux density is expressed per unit wavelength, and the reference spectrum is flat in F_λ . $STMAG = -2.5 \log F_\lambda - 21.10$.
stripe	To accommodate the NUV detector format, COS NUV spectra are split into three non-contiguous stripes, each of which covers a relatively small range in wavelength.
TAGFLASH	Use of TIME-TAG mode with FLASH=YES selected. In this mode, wavelength-calibration spectra are obtained at periodic intervals during a PSA TIME-TAG observation so that any drifts of the spectrum due to residual motion of the optics can be removed.
TIME-TAG	A COS observing mode in which the locations (pixels) and times (to the nearest 32 msec) are recorded for each detected photon. Doing this consumes memory but allows great flexibility in reducing and analyzing the data.
wavecal	A wavelength calibration exposure; i.e., an exposure of the Pt-Ne wavelength calibration lamp through the WCA.
WCA	Wavelength Calibration Aperture, which is illuminated by a Pt-Ne wavelength calibration lamp.
XD	Cross-dispersion direction, corresponding to the Y axis on both the FUV and NUV detectors.
XDL	Cross Delay Line, the type of detector used in the FUV channel of COS.